Durham E-Theses

Ultrasound propagation in the sodium borosilicate glass system

Maynell, Coin, A.

ULTRASOUND   PROPAGATION   IN   THE   SODIUM
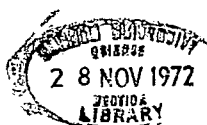
BOROSILICATE   GLASS   SYSTEM

A thesis submitted to the University of

Durham in candidature for the Degree of

Doctor of Philosophy

by

Colin A. Maynell, B.Sc. (Dunelm)

Department of Applied Physics and Electronics,

Science Laboratories, South Road, Durham City.

October   1972

Abstract

Measurements of ultrasound wave velocity and attenuation are used to investigate the structure of Na_2O-B_2O_3-SiO_2 glasses. The propagation characteristics of longitudinal and shear waves between $1.3^{\circ}K$ and $400^{\circ}K$ at frequencies between 12 MHz and 60 MHz are dominated by a broad and intense acoustic loss peak whose height and position are frequency sensitive. Of the previously proposed models for the mechanism of the acoustic loss, which also occurs in other inorganic glasses, the ultrasound absorption is most consistent with a thermally activated structural relaxation involving the transverse vibration of an oxygen atom between two potential wells of equal or nearly equal depth in the plane of a non-linear cation-oxygen-cation bond. An Akhieser type acoustic phonon-thermal phonon interaction is shown not to be responsible for the observed loss. An attempt frequency of 10^{13}Hz and a distribution of activation energies out to 12 K cal/mole but with a mean value of about 3 K cal/mole are found for the relaxation mechanism in the Na_2O-B_2O_3-SiO_2 glasses.

The absolute value and the temperature coefficient of ultrasound velocity, and the maximum acoustic loss are strongly dependent on the total Na_2O content of the glasses. Ultrasound propagation characteristics are also affected by phase-separation inducing heat treatment: the steady rise in the height of the loss peak and the complex behaviour of the ultrasound velocity with time

of treatment suggest that structural rearrangement is still taking place in the individual glassy phases even after long periods of heat treatment.

Also reported is the existence of a small acoustic loss peak at liquid helium temperatures in the $Na_2O-B_2O_3-SiO_2$ glasses. This feature of the ultrasound absorption spectrum is characteristic of many tetrahedrally coordinated inorganic glasses. On the assumption of an Arrhenius activation process for this loss peak, an activation energy of 60 ± 15 cal/mole and an attempt frequency of 10^{10} to 10^{12} Hz is indicated.

Acknowledgements

Primarily I must express my sincere gratitude to Dr. G.A. Saunders, without whose supervision, encouragement and interest, this work would not have been possible. Working in Dr. Saunders' research group at Durham has provided me with experience from which I will continue to benefit for many years to come.

I am indebted to many others for their help in the execution of this work; Professor D.A. Wright for use of the facilities in the Department of Applied Physics and Electronics; Mrs. J. Henderson for her careful typing of the manuscript; Mrs. C. Pennington for her advice on the preparation of the diagrams; Mr. F. Spence and all the technical staff, especially Mr. R. Waite, for constructing much of the apparatus used in these experiments.

My thanks are also extended to the staff of the Advanced Research Unit of James A. Jobling at Brancepeth Castle, Co. Durham for their co-operation in this study; in particular I would like to acknowledge the invaluable advice and assistance of Mr. S. Scholes.

My appreciation would not be complete without reference to the patience and understanding of my wife, Celia, whose support for the inner man has greatly increased the impetus of the outer during the course of this study.

I am grateful to the Science Research Council for the sponsorship of this work.

CONTENTS

Chapter 7 (Continued)

CHAPTER   ONE

INTRODUCTION

Introduction

The elasticity and anelasticity are basic properties of any solid. Ultrasound velocity and attenuation measurements provide basic knowledge of these properties and hence furnish much information on the structure and interatomic binding in materials. As the phonons emitted from an ultrasound source are both coherent and monochromatic they are of particular value in experimental determinations of lattice processes and interactions. These phonons are of much lower frequency than those involved in the conduction of heat. Thermal conductivity too can provide a great deal of information about lattice processes, but the phonons involved are incoherent and because of their wide range of frequencies they are affected by a larger variety of scattering processes than the ultrasound phonons.

As yet ultrasonic studies in glasses have been limited to one or two component systems and few details are available for multicomponent or phase separated glasses, many of which are of technological importance. The present concern has been a study of the elastic and anelastic behaviour of $Na_2O-B_2O_3-SiO_2$ ternary glasses with the object of gaining information on the intrinsic properties of the materials and on the effects of glass-in-glass phase separation. An attempt is also made to clarify the basic absorption mechanism in inorganic glasses about which there is at present much controversy. Before a detailed discussion of the propagation of elastic

waves in a disordered system can be undertaken it is
pertinent to discuss the term 'glass' and to mention the
incidence of glass-in-glass phase separation and its
consequences.

1.1   What is a glass?

The vitreous or glassy state is characterized
by the absence of both structural periodicity and symmetry.
One widely accepted opinion is that a glass is a super-
cooled liquid;   although one method of preparation of a
glass is to cool a liquid through its freezing point
without the occurrence of crystallization, and this
behaviour conforms to such a description,   glasses such
as gels dried by evaporation, copolymers prepared by
chemical reaction or evaporated films should also be
included. Structural models for glasses fall roughly
into two categories;   those which regard glasses as highly
defect crystals and those which are based on statistical
concepts peculiar to the liquid or gaseous state. X-ray
diffraction from polycrystals with increasingly small
grain size becomes progressively very much like that from
glasses, which could on one hand indicate that glasses
are in fact crystalline materials with very small grain
sizes. However, Bell and Dean (1968), on the other hand,
have shown that ball and spoke models of vitreous SiO_2
constructed on the random network theory of Zachariasen
(1932) show a theoretical radial distribution function
and configurational entropy in very good agreement with

experimentally determined values. Thus many difficulties
arise in the comparison between the two main structural
classifications even for glasses which are simple in
terms of chemical composition. It would be limited
value to discuss here the merits of the various models
within each classification as only a minimal amount of
inference can be drawn as to the likely structure of
the multicomponent glasses of this present study. A
better starting point for an understanding of the term
'glass' is through the preparation and properties of
such materials.

1.2   Under what conditions can a glass be formed?

Liquids solidify into the glassy state, if they
can be cooled through the crystallization temperature
range rapidly enough to exclude the formation of crystal
nuclei. A glass is to be distinguished from a material
formed by discontinuous solidification in which the solid
mass grows in the parent liquid at the solid-liquid
interface. Formation of a glass occurs rather by a
continuous increase in viscosity on the lowering of the
liquid temperature.

There is a stage in the cooling process, called
the glass transition range, where the viscosity may
increase by several orders of magnitude over about $10^{\circ}K$.
The glass transition temperature T_g is itself determined
by the cooling rate; Figure 1.1 shows the effect of
different cooling rates on the specific volume $\bar{V}$ of a
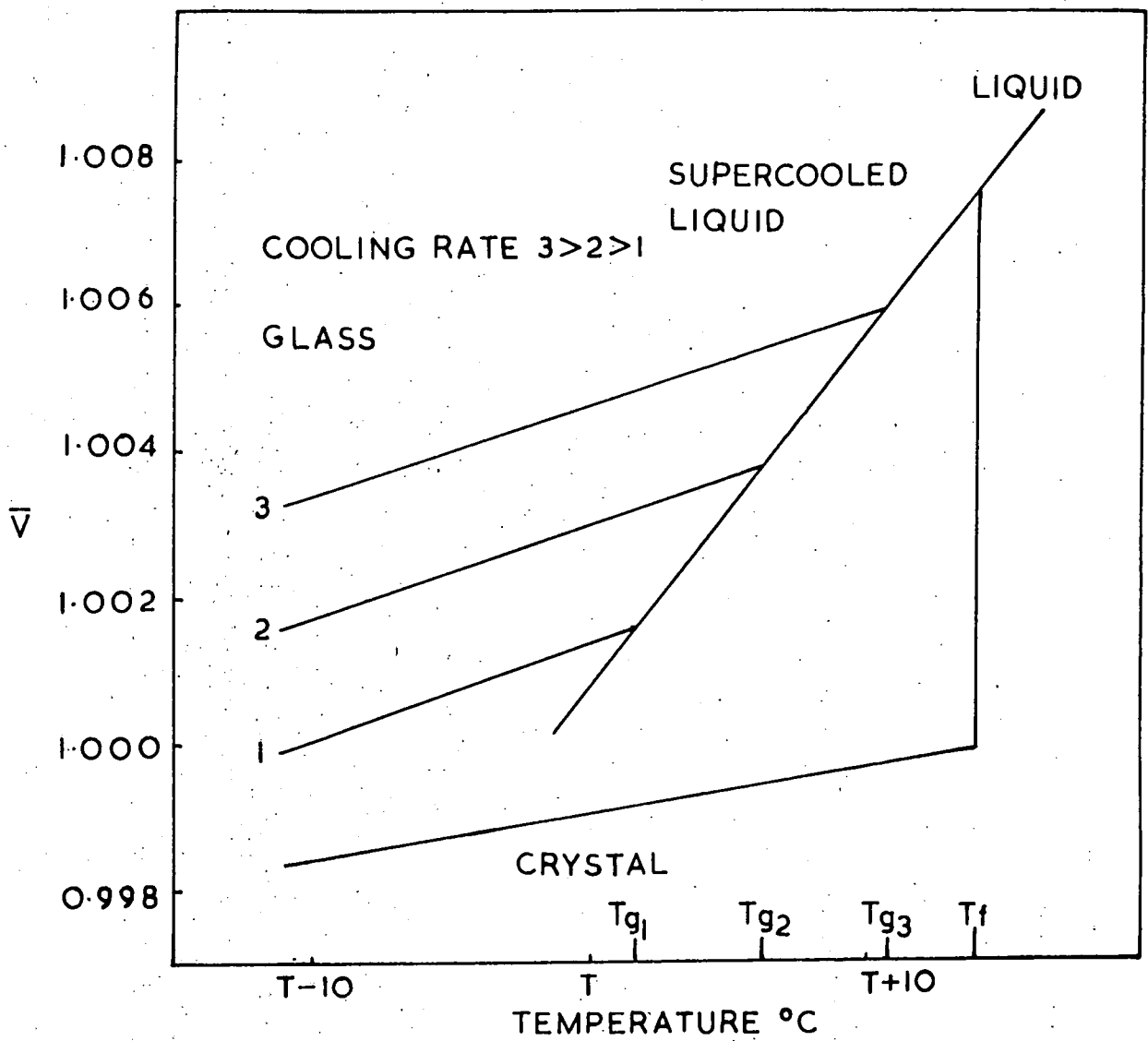
Figure 1.1 The formation of a glass and the effect of cooling rate on sample density.

glass forming liquid and illustrates the different Tg's of the final glasses. Different cooling rates result in different glass densities and hence by implication structures; thus the cooling rate can effect any physical property of a glass which is density or structure sensitive. Another concept connected with the thermal history of a glass, which is met with in the course of this thesis, is that of the fictive temperature $\bar{T}$ at which the internal structure of a glass sample would be at equilibrium. On cooling a glass below its Tg point the internal structure is frozen in as structural relaxation times sharply increase with the rise in viscosity; in general $\bar{T}$ is equal to Tg. The fictive temperature of a glass may be changed by annealing at the required temperature for a time long enough for structural re-arrangement to occur.

1.3   Phase separation in glasses

During recent years it has become increasingly evident that many glasses originally thought to be homogeneous in character are in fact separated on a submicroscopic scale into two or more distinct but still glassy phases. Even visibly clear glasses like Pyrex - itself a sodium borosilicate glass - are thought to be heterogeneous in character, as well as the opalescent glasses produced by heat treatment of certain compositions in, for example, the soda-lime-silica and alkali borosilicate systems. Techniques used to reveal the phase separated nature of various glasses have been

electrical conduction and dielectric loss (Charles, 1964), electron microscopy (Vogel and Gerth, 1962) and small angle X-ray diffraction (Porai-Koshits and Andreyev, 1958). Any experimental method which is able to assist in the elucidation of the structures of such glasses and the mechanisms involved in the separation processes will be a valuable technique in the rapidly expanding field of glass physics.

The morphologies of phase separated glasses are of two types: droplets of a second phase dispersed in a matrix of the complementary composition, and a structure where the two phases are completely interconnected. Factors such as thermal history and composition decide which morphology a glass will take and also determine the scale of the separation which may be anywhere between about 50 $\overset{o}{A}$ and 10 μ. A more detailed description of glass-in-glass separation will be found in Chapter 4.

The $Na_2O-B_2O_3-SiO_2$ glass system forms the basis for many commercial materials of technological importance. Over a region of the ternary diagram along the $B_2O_3-SiO_2$ edge, with low and restricted values of Na_2O content, metastable immiscibility is exhibited. If the ratio of SiO_2 to B_2O_3 is high, chemically durable glasses of low coefficient of thermal expansion result, and it is in this area of composition that glasses with the trade names of Pyrex, Simax and Phoenix reside. As the ratio is lowered past unity, glasses result from which the high B_2O_3 phase can be reached, providing that this phase is

continuous. Such glasses form the starting composition
for the high SiO_2 (about 96wt%) porous and consolidated
Vycor material. It is well known that careful control
on both Na_2O content and thermal history is essential to
achieve the desired result in the production of this
latter glass; this fact itself suggests that a particular
phase separated structure is prerequisite for the final
product and that the chemical and physical processes
involved must be terminated before equilibrium is
reached.

Many important properties of a glass are structure
sensitive and are dependent on the phase-separation which
is itself a microscopic structure-forming process. A
knowledge of the mechanisms involved in glass-in-glass
separation is thus of direct technological interest. A
primary purpose of this present work is to assess if
ultrasound propagation is a useful tool in the study of
glassy phase separation phenomena and to report on the
effects in the mechanical properties due to phase
separation in the glasses.

1.4   Vibrations in crystals and glasses

A consequence of the absence of adequate models
for the structure of glasses is that the theoretical
treatment of vibrations in such disordered systems is
made difficult. The absence of periodicity precludes
the use of the mathematical procedures available for
crystal lattices; this lack of quantitative knowledge

is a recurrent problem throughout the field of glass physics. A brief comparison will be made here between the salient features of the wave propagation characteristics in crystalline solids and the more scant details of those in glassy materials to identify the most important differences and similarities relevant to the present study.

For a solid which contains N atoms the vibrations may be considered as the superposition of 3N independent normal modes. In a crystal system, which exhibits periodicity in the lattice, these normal modes are plane waves and are characterized by a frequency ω, a wave vector q and a polarization. Where there are C atoms in the primitive cell of the lattice there are 3 acoustic branches to the phonon spectrum, where the atoms vibrate in phase, and 3C-3 optical branches, where the atoms vibrate out of phase. The frequency of a particular mode depends on the wave vector; a typical plot of this relationship for a crystal with 2 atoms per primitive cell is shown in Figure 1.2. In the long wavelength limit, where the crystal behaves as an elastic continuum, the phase velocity ω/q and the group velocity $d\omega/dq$ are equal. A decrease in the group velocity of the acoustic modes occurs as the value of q approaches its maximum value, a phenomenon known as dispersion. The maximum value of q is defined by the lattice parameter.

A glass however has no long-range order. As a result of this non-periodicity the normal modes are in
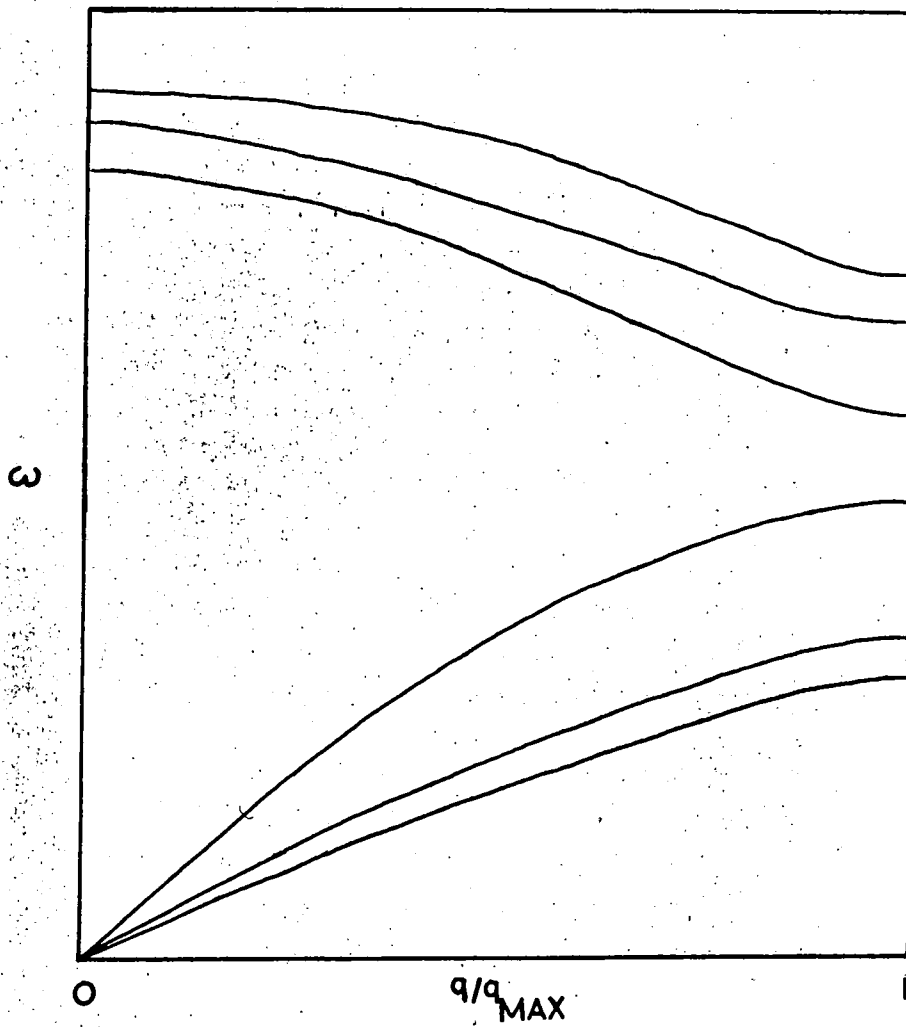
Figure 1.2 Schematic plot of frequency against wave number for lattice waves in a crystal with two atoms per primitive cell.

general not plane waves. Theoretical calculations of one
dimensional models of a glass (Dean, 1964; Anderson, 1965)
suggest that away from the long wavelength limit the
ω-q relationship loses its basic simplicity. There exists
an increasingly wide range of frequencies for each wave
vector and at very short wavelengths the distinction
between acoustical and optical phonon modes is not well
defined. However, in the long wavelength limit, a glass
still behaves as an elastic continuum and the normal
waves are essentially plane waves. The wavelengths of
ultrasound at 10MHz are typically about 5.10^{-2} cm and
consequently see little of the non-periodicity of the
structure. Ultrasonic stress waves may be treated as
long wavelength normal modes of a glass and their
propagation characteristics of velocity and attenuation
are isotropic.

C H A P T E R   T W O

ELASTICITY AND ANELASTICITY OF

SOLIDS

Introduction

A body is deformed under the action of external forces. It is said to be elastic if it returns to its original dimensions after the removal of these forces, and the subject of elasticity is the discussion of the relationship between applied stress and resultant stain.

If, however, the stress and strain are not single-valued functions of each other, the solid is said to be anelastic. Such a property is observed in a solid where stress and/or strain time derivatives are present in the equation relating stress and strain. In this type of solid, there is a hysterisis effect when the stress is oscillatory. Energy dissipation will occur over the range of frequencies where the strain cannot keep up with the alternation in stress.

This chapter is concerned with the equation of motion for both elastically anisotropic and isotropic solids, and the velocity of high-frequency ultrasonic stress waves are obtained as a solution to this equation. Also discussed is the standard linear anelastic solid model of Zener (1947). The rate of dissipation of energy of the stress wave as a function of frequency is deduced for anelastic materials which exhibit stress-strain relationships characteristic of this type of solid. The last section deals with the various methods of expressing the rate of energy dissipation, or attenuation, of an ultrasound wave, and relates these quantities to the internal friction manifested in a solid.

2.1.1 Definition of Stress

The stress tensor σ_{ij} represents the components of force acting on an elemental area of the solid, and denotes the force per unit area in the i direction on the plane normal to the j direction.

2.1.2 Definition of Strain

The idea of strain is connected with the displacement of a point in a body. If, as a result of deformation, the cordinates of a point $\underline{x}$ (x_1, x_2, x_3) are moved to x_1+u_1, x_2+u_2, x_3+u_3, the u quantities are the displacement vectors and the strains are defined by (e.g. Nye, 1957)

$$\varepsilon_{ij} = \frac{1}{2}\left(\frac{\partial u_i}{\partial x_j} + \frac{\partial u_j}{\partial x_i}\right) \qquad 2.1$$

For example,

$$\varepsilon_{11} = \frac{\partial u_1}{\partial x_i} \qquad 2.2$$

$$\varepsilon_{12} = \frac{1}{2}\left(\frac{\partial u_1}{\partial x_2} + \frac{\partial u_2}{\partial x_1}\right) \qquad 2.3$$

This second rank tensor is the symmetrical part of the Cartesian tensor describing the point displacement in a body; the anti-symmetrical part

$$\omega_{ij} = \frac{1}{2}\left(\frac{\partial u_i}{\partial x_j} - \frac{\partial u_j}{\partial x_i}\right) \qquad 2.4$$

is concerned with rotational movement with which we are not concerned here. The simple physical meaning of the

components of the strain tensor ε_{ij} is that with i equal to j, the component represents the fractional change in length of a line parallel to the x_i direction, and with i not equal to j, it is twice the change in the angle originally defined by the x_i and x_j directions.

2.1.3   Hookes Law

This law states that the strain in a body is proportional to the stress acting upon it. Thus, relationships involving the fourth rank tensors C_{ijkl}, known as the elastic stiffness constants of the solid, may be written

$$\sigma_{ij} = C_{ijkl}\,\varepsilon_{kl} \qquad \qquad 2.5$$

This is the most general linear stress-strain relationship which indicates zero strain under conditions of zero stress, and results in 81 elastic stiffness constants in the equations of type

$$\sigma_{11} = C_{1111}\varepsilon_{11} + C_{1112}\varepsilon_{12} + C_{1123}\varepsilon_{13} + C_{1121}\varepsilon_{21} + C_{1122}\varepsilon_{22}$$

$$+ C_{1123}\varepsilon_{23} + C_{1131}\varepsilon_{31} + C_{1132}\varepsilon_{32} + C_{1133}\varepsilon_{33} \qquad 2.6$$

From the symmetry of stress and strain, we obtain

$$C_{ijkl} = C_{kijl} = C_{iklj} = C_{kilj} \qquad \qquad 2.7$$

which reduces the number of independent elastic constants to 36. A further condition that the elastic potential is

a function of state, and is independent of the path by
which it is reached gives

$$C_{ijkl} = C_{jlik} \qquad 2.8$$

leaving a total of 21 independent constants, which is the
number associated with the crystal class of lowest
symmetry, the triclinic system.

For ease of writing the fourth rank tensor
C_{ijkl}, a condensed matrix notation is used as follows:

Tensor Notation   11   22   33   23,32   13,31   12,21
Matrix Notation   1   2   3   4   5   6

For example, C_{1112} is written C_{16}, and C_{2332} as C_{44}.

2.1.4   Adiabatic and Isothermal Elastic Constants

As the entropy is effectively constant under
the conditions of an ultrasonic measurement, the
adiabatic elastic constants are obtained. The difference
between the adiabatic constants, C^{σ}_{ijkl}, and isothermal
constants C^{θ}_{ijkl} is given by the equation (Nye 1957)

$$C^{\sigma}_{ijkl} = C^{\theta}_{ijkl} + \lambda_{ij}\lambda_{kl}\, T/C_v \qquad 2.9$$

where λ_{ij} and λ_{kl} are the temperature coefficients of
stress at constant strain, T is the absolute temperature,
and C_v is the specific heat at constant volume. This
gives rise to a difference between the adiabatic and
isothermal elastic constants no greater than 1%.

2.1.5   Crystalline and Isotropic Systems

Writing the complete set of stress-strain relationships in matrix notation, we obtain

$$
\begin{vmatrix} \sigma_{11} \\ \sigma_{22} \\ \sigma_{33} \\ \sigma_{23} \\ \sigma_{31} \\ \sigma_{12} \end{vmatrix}
=
\begin{vmatrix}
C_{11} & C_{12} & C_{13} & C_{14} & C_{15} & C_{16} \\
C_{12} & C_{22} & C_{23} & C_{24} & C_{25} & C_{26} \\
C_{13} & C_{23} & C_{33} & C_{34} & C_{35} & C_{36} \\
C_{14} & C_{24} & C_{34} & C_{44} & C_{45} & C_{46} \\
C_{15} & C_{25} & C_{35} & C_{45} & C_{55} & C_{56} \\
C_{16} & C_{26} & C_{36} & C_{46} & C_{56} & C_{66}
\end{vmatrix}
\begin{vmatrix} \varepsilon_{11} \\ \varepsilon_{22} \\ \varepsilon_{33} \\ \varepsilon_{23} \\ \varepsilon_{31} \\ \varepsilon_{12} \end{vmatrix}
\qquad 2.10
$$

Crystalline symmetry of a solid reduces the number of independent elastic constants needed to describe completely the stress-strain relationship in a solid from 21 for the triclinic system to 3 for the cubic system, where the C_{ikjl} matrix becomes

$$
\begin{matrix}
C_{11} & C_{12} & C_{12} & 0 & 0 & 0 \\
C_{12} & C_{11} & C_{12} & 0 & 0 & 0 \\
C_{12} & C_{12} & C_{11} & 0 & 0 & 0 \\
0 & 0 & 0 & C_{44} & 0 & 0 \\
0 & 0 & 0 & 0 & C_{44} & 0 \\
0 & 0 & 0 & 0 & 0 & \tfrac{1}{2}(C_{11}-C_{12})
\end{matrix}
$$

For an isotropic solid, the coefficients must be independent of the rectangular axes chosen, which produces the conditions

$$C_{12} = C_{13} = C_{23} \; , \quad C_{44} = C_{55} = C_{66} \qquad 2.11$$

$$C_{11} = C_{22} = C_{33} \; , \quad C_{44} = (C_{11}-C_{12})/2$$

Thus, for an isotropic system, two independent elastic constants, λ and μ, known as the Lamé constants may be defined such that

$$C_{12} = \lambda \; , \quad C_{11} = \lambda+2\mu \; , \quad C_{44} = \mu \qquad 2.12$$

In this situation, the stress-strain law may be written

$$\sigma_{ij} = \lambda \delta_{ij} \varepsilon_{kk} + 2\mu \varepsilon_{ij} \qquad 2.13$$

where δ is the Kronecker delta function which has the properties:

$$\delta_{ij} = 1 \quad \text{for } i = j \qquad 2.14$$

$$\delta_{ij} = 0 \quad \text{for } i \neq j$$

2.1.6   The Equation of Motion

To derive the equation of motion for a stress wave in an elastic contimum, the forces acting on an elemental volume are considered. On examination of the forces on opposite pairs of faces of a small parallelopiped, the components of the forces resulting from the differences between these pairs of forces are obtained.

From Newton's equation of motion is found the relationship

$$\frac{\partial \sigma_{ij}}{\partial x_j} = \rho \frac{\partial^2 s}{\partial t^2} \qquad \text{2.15}$$

where ρ is the density of the medium, and $\underline{s}$ is the displacement vector. Hence

$$C_{ijkl} \frac{\partial \varepsilon_{kl}}{\partial x_j} = \rho \frac{\partial^2 s_i}{\partial t^2} \qquad i = 1,2,3 \qquad \text{2.16}$$

and from equation 2.1

$$\frac{\partial \varepsilon_{kl}}{\partial x_j} = \frac{1}{2} \frac{\partial^2 s_l}{\partial x_k \partial x_j} + \frac{\partial^2 s_k}{\partial x_l \partial x_j} \qquad \text{2.17}$$

Combination of equations 2.5 and 2.17 gives

$$C_{ijkl} \frac{\partial^2 s_l}{\partial x_k \partial x_j} + \frac{\partial^2 s_k}{\partial x_i \partial x_j} = 2\rho \ddot{s}_i \qquad \text{2.18}$$

As $C_{ijkl} = C_{ijlk}$, we can rewrite this as

$$C_{ijkl} \frac{\partial^2 s_l}{\partial x_j \partial x_k} = \rho \ddot{s}_l \qquad \text{2.19}$$

The problem is now to solve this equation for a plane wave of the type

$$s_l = s_{ol} e^{i(wt - \underline{k} \cdot \underline{x})} \qquad (l = 1,2,3) \qquad \text{2.20}$$

where $\underline{k}$ (k_1, k_2, k_3) is a wave vector normal to the planes of constant phase, and is equal to $(w/v) \cdot \underline{n}$, $\underline{n}$ (n_1, n_2, n_3) is a unit vector normal to the wave front, w is the wave angular frequency, and v is the

phase velocity. The particle displacement vector $\underline{s}$ is in general not parallel to the wave vector $\underline{k}$.

Substituting equation 2.20 into equation 2.19 produces

$$\frac{\partial^2 s_\ell}{\partial x_k \partial x_j} = -n_k n_j S_{o_\ell} (w^2/v^2) e^{i(wt - \underline{k} \underline{x})} \qquad 2.21$$

and combining this with the equation of motion 2.15 we obtain

$$C_{ijk\ell} S_{o_\ell} n_k n_j = \rho v^2 S_{o_i} \qquad 2.22$$

Expansion of these relationships leads to the Christoffel equations:

$$(C_{1j1\ell} n_j n_\ell - \rho v^2) S_{o_1} + C_{1j2\ell} n_j n_i S_{o_2} + C_{1j3\ell} n_j n_\ell S_{o_3} = 0$$

$$C_{2j1\ell} + (C_{2j2\ell} n_j n_\ell - \rho v^2) S_{o_2} + C_{2j3\ell} n_j n_\ell S_{o_3} = 0 \qquad 2.23$$

$$C_{3j1\ell} + C_{3j2\ell} n_j n_\ell S_{o_2} + (C_{3j3\ell} n_j n_\ell - \rho v^2) S_{o_3} = 0$$

For these equations to be satisfied for all S_{o_i}, the determinant of the coefficients must be equal to zero, yielding a cubic equation in v^2. These three roots represent the velocities of three different waves with mutually orthogonal displacement vectors but with parallel propagation directions. In general, these displacements are neither perpendicular nor parallel to the propagation direction.

To find these three solutions, an expansion of equation 2.23 for all j and ℓ values is undertaken. This produces a determinant of the form

$$
\begin{vmatrix}
L_{11} - \rho v^2 & L_{12} & L_{13} \\
L_{12} & L_{22} - \rho v^2 & L_{23} \\
L_{13} & L_{23} & L_{33} - \rho v^2
\end{vmatrix} = 0 \qquad 2.24
$$

where

$$L_{11} = n_1^2 C_{11} + n_2^2 C_{66} + n_3^2 C_{55} + 2n_2 n_3 C_{55} + 2n_3 n_1 C_{15} + 2n_1 n_2 C_{16} \qquad 2.25$$

$$L_{12} = n_1^2 C_{16} + n_2^2 C_{26} + n_3^2 C_{45} + n_2 n_3 (C_{46} + C_{25}) + n_3 n_1 (C_{14} + C_{56})$$
$$+ n_1 n_2 (C_{12} + C_{66})$$

$$L_{13} = n_1^2 C_{15} + n_2^2 C_{46} + n_3^2 C_{35} + n_2 n_3 (C_{45} + C_{36}) + n_3 n_1 (C_{13} + C_{55})$$
$$+ n_1 n_2 (C_{14} + C_{56})$$

$$L_{22} = n_1^2 C_{66} + n_2^2 C_{22} + n_3^2 C_{44} + 2n_2 n_3 C_{24} + 2n_3 n_1 C_{46} + 2n_1 n_2 C_{26}$$

$$L_{23} = n_1^2 C_{56} + n_2^2 C_{24} + n_3^2 C_{24} + n_2 n_3 (C_{44} + C_{23}) + n_3 n_1 (C_{36} + C_{45})$$

$$L_{33} = n_1^2 C_{55} + n_2^2 C_{44} + n_3^2 C_{33} + 2n_2 n_3 C_{34} + 2n_3 n_1 C_{35} + 2n_1 n_2 C_{45}$$

The unit vectors $C n_1$, n_2, n_3) are then substituted for the propagation direction required, as are the $C_{ijk\ell}$ values according to the symmetry of the solid under consideration. For example, for plane wave

propagation in a cubic crystal in the <100>, the
determinant is reduced to

$$
\begin{vmatrix}
C_{44} - \rho v^2 & 0 & 0 \\
0 & C_{44} \pm \rho v^2 & 0 \\
0 & 0 & C_{11} - \rho v^2
\end{vmatrix} = 0 \qquad 2.26
$$

indicating two waves of velocity $(C_{44}/\rho)^{\frac{1}{2}}$ and one wave
of velocity $(C_{11}/\rho)^{\frac{1}{2}}$.

Determination of the mode of the plane wave is
carried out by substituting these velocities back into
the Christoffel equations 2.23 and calculating the
particle displacement vectors S_{o_i} for each velocity;
the relationship $n_1^2 + n_2^2 + n_3^2 = 1$ exists as $\underline{n}$ is a unit vector,
and is used in this calculation. The combination of
particle displacement vector and propagation direction
describes the mode as either longitudinal or shear. In
the above example, one longitudinal wave of velocity
$(C_{11}/\rho)^{\frac{1}{2}}$ and two shear waves of velocity $(C_{44}/\rho)^{\frac{1}{2}}$ are
obtained.

Isotropy of the elastic constants, where all
directions are equivalent, reduces equation 2.26 to

$$
\begin{vmatrix}
\mu - \rho v^2 & 0 & 0 \\
0 & \mu - \rho v^2 & 0 \\
0 & 0 & (\lambda + 2\mu) - \rho v^2
\end{vmatrix} = 0 \qquad 2.27
$$

indicating a longitudinal wave of velocity $(\lambda + 2\mu/\rho)^{\frac{1}{2}}$
and a shear wave of velocity $(\mu/\rho)^{\frac{1}{2}}$. These different
modes of propagation are always pure modes for an
isotropic solid; the particle displacement vector is
parallel to the direction of propagation for the
longitudinal or compressional mode, and perpendicular
to the direction of propagation for the shear or transverse
mode. The energy flux vector, which defines the direction
of flow of acoustic energy is also parallel to the
direction of propagation of the wave, not usually the
case for a crystalline anisotropic solid.

Thus the second order elastic constants, com-
ponents of the fourth rank tensor, may be calculated
in an isotropic solid from measurements of the longitudinal
and shear wave ultrasound velocities. From these con-
stants the Young's modulus E, Poissons ratio ν, Shear
modulus μ, and Bulk modulus κ, may be found the
relationships:

$$E = \rho V_S^2 \; (3V_L^2 - 4V_S^2)/(V_L^2 - V_S^2) \qquad\qquad 2.28$$

$$\nu = (V_L^2 - 2V_S^2)/(2(V_L^2 - V_S^2)) \qquad\qquad 2.29$$

$$\mu = \rho V_S^2 \qquad\qquad 2.30$$

$$\kappa = \rho(3V_L^2 - 4V_S^2)/3 \qquad\qquad 2.31$$

2.2.1 Anelasticity of solids

The property of a solid whereby the stress and
strain are not uniquely related in the pre-plastic range
is called anelasticity. Early attempts were made by

Meyer (1874) and Voigt (1892) to generalize the equations
of classical elasticity theory to include an account
of anelastic phenomena. These accounts were based on
the assumption that the stress components are a linear
function of both strain and strain rate, and were of the
form

$$\sigma = a\,\varepsilon + b\,\dot{\varepsilon} \qquad\qquad 2.32$$

where the dot indicates differentiation with respect to
time. Solids obeying this law are called Voigt solids
and manifest after-elasticity. These solids do not
exhibit instantaneous strain. A mechanical analogue with
the stress-strain relationship is illustrated in Figure 2.1.

However, most solids do show an instantaneous
strain, and the model of Voigt has been modified by
Zener (1947) to include this behaviour. The model for
this type of solid, known as the 'standard linear solid,'
is also shown in Figure 2.1.

The standard linear solid suffers an instantaneous
displacement when a stress is applied. The magnitude of
this displacement is governed by the elastic constants of
the springs. During the time that the stress is applied,
the dashpot relaxes to produce a gradual increase in
deformation of the solid. Conversely, if the strain is
suddenly removed, the structure suffers an instantaneous
expansion followed by a more gradual release of energy
in the springs as the force relaxes across the dashpot.
Thus, this model illustrates all the after-elastic
properties of a real solid.

VOIGT SOLID
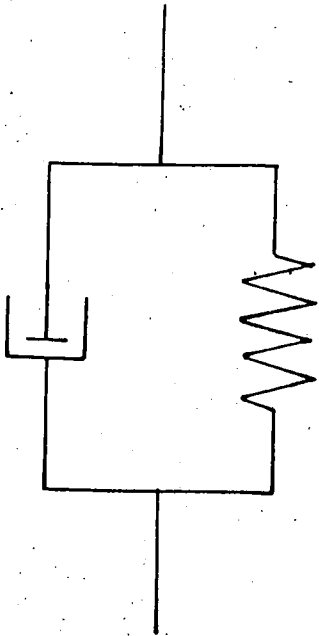
DEFORMATION
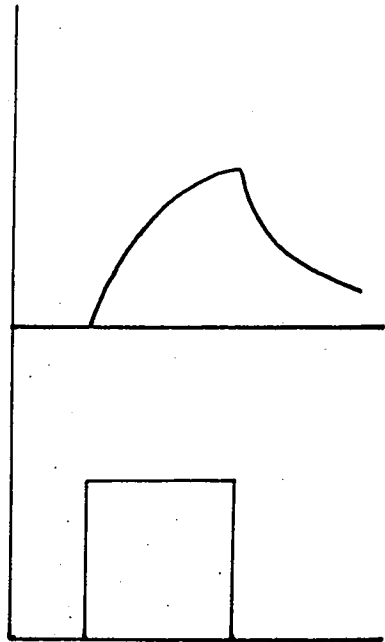
FORCE

TIME

STANDARD LINEAR SOLID
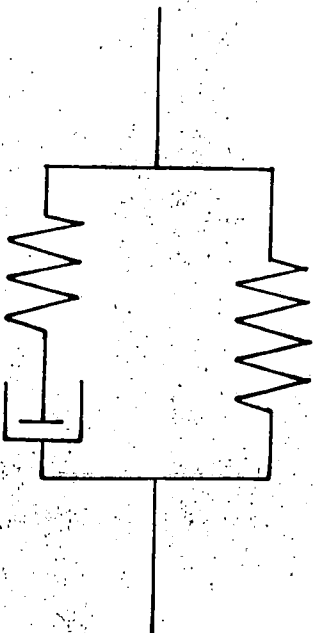
DEFORMATION

FORCE
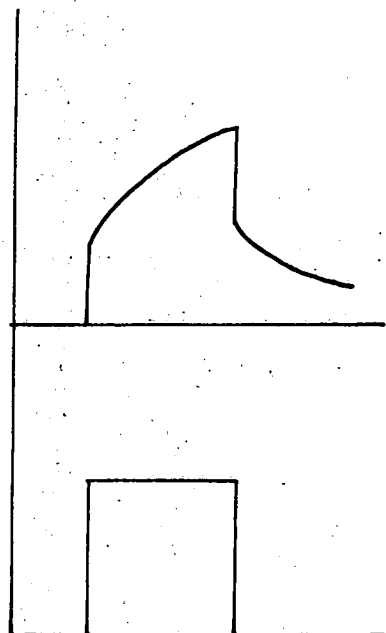
TIME

Figure 2.1   A comparison of the Voigt and Standard Linear
Solid models and their mechanical behaviour.

A further merit of the standard linear model is
that the rate of energy dissipation does not increase
rapidly as the frequency of the applied stress increases,
in contrast to the Voigt model which shows frequency-
squared dependence for the rate of energy dissipation.
At high frequencies, this rate becomes independent of
the frequency for the standard linear model.

If the stress and strain are not single valued
functions of one another over a complete cycle of vibration,
dissipation of energy will occur. Consequently, the
presence of time derivatives in the stress-strain relation-
ship will assure an attenuation of a periodic stress
wave such as an ultrasonic wave.

2.2.2   Calculation of the energy dissipation versus frequency relationship for the standard linear solid

The equation governing the stress-strain relation-
ship for the standard linear solid is

$$\sigma + \tau_\varepsilon \dot{\sigma} = M_R (\varepsilon + \tau_\sigma \dot{\varepsilon}) \qquad 2.33$$

where τ_ε is the relaxation time of the stress under
conditions of constant strain, and τ_σ is the relaxation
time of the strain under conditions of constant stress.
M_R is a modulus of elasticity to be fully explained later.

When ε and $\dot{\varepsilon}$ are both zero, equation 2.33 has
the form

$$\sigma + \tau_\varepsilon \dot{\sigma} = 0 \qquad 2.34$$

which has the solution

$$\sigma(t) = \sigma(o) e^{-t/\tau_\varepsilon} \qquad 2.35$$

On imposition of an instantaneous strain ε_0 applied at
t = 0, the stress relaxes to its equilibrium $M_R \varepsilon_0$. Thus
the solution to equation 2.33 becomes

$$\sigma(t) = M_R \varepsilon_0 + (\sigma_0 - M_R \varepsilon_0)e^{-t/\tau_\varepsilon} \qquad 2.36$$

Therefore the final or relaxed value of elastic modulus
is equal to M_R. Suppose now that in a very short time
δt the stress received a finite increment $\Delta\sigma$. Integration
of equation 2.33 with respect to time as $\delta t \rightarrow 0$ reduces
to

$$\tau_\varepsilon \Delta\sigma = M_R \tau_\varepsilon \Delta_\varepsilon \qquad 2.37$$

If now is introduced an instantaneous or 'unrelaxed'
modulus M_u such that

$$\Delta_\sigma = M_u \Delta\varepsilon \qquad 2.38$$

the relationship between M_R and M_u becomes

$$\frac{M_u}{M_R} = \frac{\tau_\sigma}{\tau_\varepsilon} \qquad 2.39$$

It is now of interest to find the relationship between
stress and strain when these quantities are periodic.
The solution $\sigma(t) = \sigma_0 e^{i\omega t}$ and $\varepsilon(t) = \varepsilon_0 e^{i\omega t}$ are sub-
stituted in equation 2.33, and we obtain

$$(1+i\omega\tau_\varepsilon)\,\sigma_0 = M_R(1+i\omega\tau_\sigma)\varepsilon_0 \qquad 2.40$$

and hence

$$\sigma_0 = M_R \frac{(1+i\omega\tau_\sigma)\varepsilon_0}{(1+i\omega\tau_\varepsilon)} \qquad 2.41$$

$$= M_\omega \varepsilon_0 \qquad 2.42$$

To calculate the angle, θ, by which the strain lags behind the stress, the imaginary and real parts of the elastic modulus at angular frequency ω are compared. Energy dissipation is usually expressed in terms of logarithmic decrement δ, fractional loss of energy per cycle $\Delta W/W$, or quality factor Q. This latter quantity is defined as the ratio of reactance to resistance of an element, and is equal to $\tan\theta$. It may be shown, that for relatively small energy losses

$$\frac{1}{Q} = \frac{\delta}{\pi} = \frac{1}{2\pi} \cdot \frac{\Delta W}{W} \qquad 2.43$$

Thus, from equation 2.41

$$Q^{-1} = \tan\theta = \frac{\omega(\tau_\sigma - \tau_\varepsilon)}{1 + \omega^2 \tau_\sigma \tau_\varepsilon} \qquad 2.44$$

This quantity is known as the internal friction. Introduction of the geometric mean of τ_σ and τ_ε, equal to $\bar{\tau}$, and combination of equations 2.39 and 2.44 leads to

$$Q^{-1} = \frac{M_u - M_R}{(M_u M_R)^{\frac{1}{2}}} \cdot \frac{\omega\bar{\tau}}{1 + (\omega\bar{\tau})^2} \qquad 2.45$$

If now a further quantity Δ equal to $(M_u - M_R)/(M_u M_R)^{\frac{1}{2}}$ is defined, then

$$Q^{-1} = \frac{\Delta\omega\bar{\tau}}{1 + (\omega\bar{\tau})^2} \qquad 2.46$$

Thus, when $M_u \simeq M_R$, Δ is the relative difference between the unrelaxed and relaxed moduli or the 'relaxation strength' of the system.

It is also of interest to find the effective elastic modulus at angular frequency ω. This is given by the ratio of the stress to that part of the strain which is in phase with the stress.

From equation 2.41 we find

$$\varepsilon_o = \frac{\sigma_o}{M_R} \cdot \frac{(1+i\omega\tau_\varepsilon)}{(1+i\omega\tau_\sigma)} \qquad 2.47$$

or

$$\varepsilon_o = \frac{\sigma_o}{M_R} \cdot \frac{(1+\omega^2\tau_\varepsilon\tau_\sigma+i\omega(\tau_\sigma-\tau_\varepsilon))}{(1+\omega^2\tau_\sigma^2)} \qquad 2.48$$

The part of the strain in phase with the stress is the real part of equation 2.48, therefore

$$M_\omega = \frac{1+(\omega\tau_\sigma)^2}{1+(\omega\bar{\tau})^2} \cdot M_R \qquad 2.49$$

and the fractional difference between the elastic modulus at angular frequency ω and the modulus when $M_u \simeq M_R$ is given by

$$\frac{M_u - M_\omega}{M_u} = \Delta \frac{1}{1+(\omega\bar{\tau})^2} \qquad 2.50$$

The variation of M_ω and $\tan\theta$ with angular frequency is shown in Figure 2.2. The internal friction reaches a maximum when $\omega\bar{\tau}$ is unity, and the modulus increases from the relaxed value M_R to the unrelaxed value M_u. It may be seen that the elastic modulus has reached its two extreme values while $\tan\theta$ is still appreciable; the transition range in elastic modulus is narrower than that in internal friction.
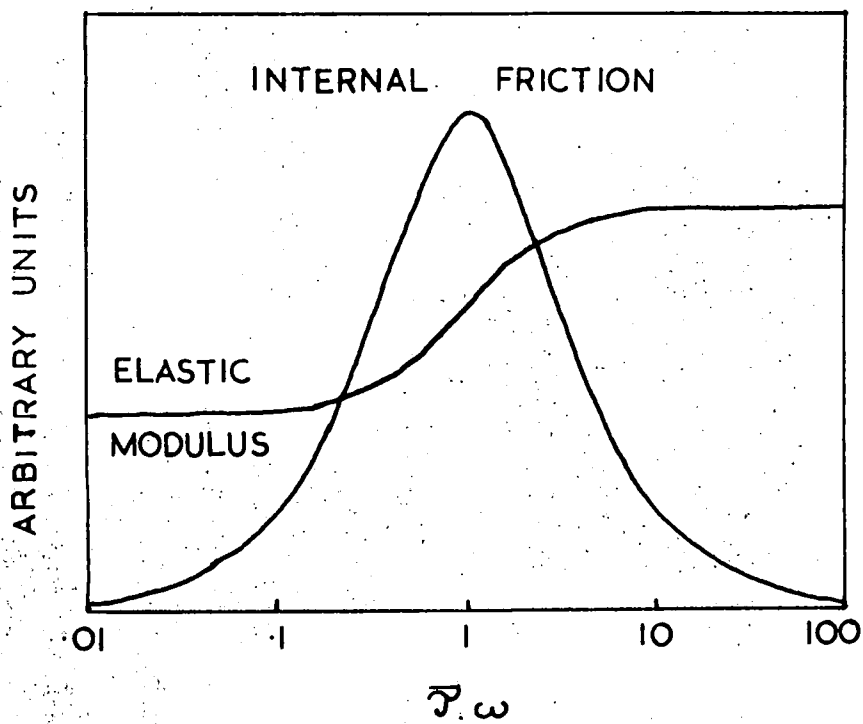
Figure 2.2 The frequency dependence of the internal friction and elastic modulus in the Standard Linear Model.

2.2.3 Attenuation of ultrasound waves

This section is devoted to a description of the various methods of expressing the attenuation of an ultrasound wave, their interconnection, and their relation to internal friction.

A plane stress wave, such as that introduced into a material in an ultrasonic experiment, may be represented by

$$\sigma(x,t) = \sigma_o e^{i(\omega t - 1x)} \qquad 2.51$$

Assumption of a complex velocity and propagation constant, such that

$$v = v_1 + iv_2 \quad , \quad k = k_1 - i\alpha \qquad 2.52$$

when combined with equation 2.51 gives

$$\sigma(x,t) = \sigma_o e^{-\alpha x} e^{i(\omega t - kx)} \qquad 2.53$$

The attenuation coefficient α is thus described as the imaginary part of the complex propagation constant, and has the units of reciprocal length.

Another approach is by assuming a complex velocity and complex angular wave frequency,

$$v = v_1 + i\alpha \quad , \quad \omega = \omega_1 + i\alpha_1 \qquad 2.54$$

which leads to

$$\sigma(x,t) = \sigma_o e^{-\alpha_1 t} e^{i(\omega t - kx)} \qquad 2.55$$

where the attenuation coefficient is now defined as the complex part of the frequency, and has the dimensions of reciprocal time.

Since the attenuation is determined by the envelope of the high frequency wave, one can use the expression

$$\sigma(x) = \sigma_o e^{-\alpha x} \qquad 2.56$$

to represent the amplitude of the stress wave with distance travelled in the elastic medium. Taking logarithms of both sides of this equation,

$$\log_e \sigma(x) = \log_e \sigma_o - \alpha x \qquad 2.57$$

Thus at two different points, x_1 and x_2, along the propagation direction of the wave, the attenuation of the wave amplitude is

$$\alpha = \frac{1}{x_2 - x_1} \log_e \frac{\sigma(x_1)}{\sigma(x_2)} \quad \text{nepers/unit length} \qquad 2.58$$

or $\quad \alpha = 20 \log_{10} \dfrac{\sigma(x_1)}{\sigma(x_2)} \quad \text{db} \qquad 2.59$

or $\quad = \dfrac{1}{x_2 - x_1} 20\log_{10} \dfrac{\sigma(x_1)}{\sigma(x_2)} \quad \text{db/unit length} \qquad 2.60$

and the relationship between attenuation in db and nepers becomes

$$\alpha \text{ (db/unit length)} = 8.686 \, \alpha \text{ (nepers/unit length)} \quad 2.61$$

A further method of expressing the attenuation, as outlined in Section 2.2.2 is in terms of the logarithmic decrement, δ, defined for a harmonic oscillator in free decay with small damping as the natural logarithm of the ratio of the energy dissipated per unit cycle of vibration

to twice the total stored energy. As the energy of a harmonic oscillator is given by the square of the amplitude of vibration,

$$\delta = \log_e \frac{\sigma n}{\sigma n+1} \qquad 2.62$$

and hence, from equation 2.58

$$\delta = \frac{\alpha(\text{nepers/cm}) \cdot v(\text{cm/sec})}{(\omega/2\pi) \quad (\text{sec}^{-1})} \qquad 2.63$$

The dissipation or quality factor, Q, has equivalent definitions

$$Q = \omega/\Delta\omega \qquad 2.64$$

known as the bandwidth half width definition,

$$\text{or} \qquad Q = \omega \cdot \frac{\text{instantaneous energy in system}}{\text{energy dissipated per unit time}} \qquad 2.65$$

$$\text{Therefore} \qquad Q^{-1} = \pi \cdot \delta \qquad 2.66$$

$$\text{or} \qquad Q^{-1} = \frac{\alpha(\text{db/sec})}{8.686 \, \omega \, (\text{sec}^{-1})} \qquad 2.67$$

Ultrasonic experiments are concerned with the measurement of the decay in amplitude of forced vibrations in a material, and the attenuation, α, is usually measured directly in units of db/μsec. Thus, by using equation 2.67, the conversion from attenuation to internal friction may be made.

C H A P T E R   T H R E E

A REVIEW OF THE ACOUSTIC PROPERTIES OF

INORGANIC GLASSES

Introduction

This chapter has been included to form a background to the ultrasonic investigation of the $Na_2O-B_2O_3-SiO_2$ glasses in this present work, and takes the form of a review concerned with the acoustic properties of glasses over the frequency range 0.25 Hz to 27.5 GHz. This survey commences with a review of previous studies at frequencies in the high KHz, MHz and GHz ranges, firstly in the temperature region between $4.2^{O}K$ and $400^{O}K$, and then at temperatures below $4.2^{O}K$. A short section is then devoted to the effects of hydroxyl ion content and fictive temperature on the ultrasound propagation in glasses. A further section which details results of internal friction and elastic moduli determinations at lower frequencies has been added to complete the survey of the acoustic properties of glasses over a wide frequency range. The review then proceeds with a discussion of the inter-relation between ultrasound velocity and thermal capacity in the context of the vibrational character of the glassy state. Some results of the comparison between acoustic and thermal properties of glasses are included. The last section of this chapter is devoted to a discussion of the mechanism which influences the ultrasound propagation characteristics of many inorganic glasses, including the $Na_2O-B_2O_3-SiO_2$ glasses, in the frequency and temperature range of this present concern. An attempt is made to isolate the most likely model for the loss mechanism.

3.1.1 Ultrasound propagation in glasses between 4.2°K and 400°K

The majority of ultrasonic studies of glassy systems have been concerned with vitreous SiO_2 at kilohertz (e.g. Marx and Sivertsen, 1953) and megahertz (e.g. McSkimin, 1953; Jones et al, 1964) frequencies, and also in the higher gigahertz region by Brillouin scattering techniques (Flubacher et al, 1960; Pine, 1969). The acoustic properties of vitreous SiO_2 below room temperature are dominated by a large and broad attenuation peak with a corresponding activation energy $\bar{H}$ of 1030 cal/mole (Anderson and Bömmel, 1955) and an attempt or characteristic vibrational frequency ω_o of 5.10^{13} Hz on the assumption of an Arrhenius type of activation process for the loss

$$\omega = \omega_o \exp(-\bar{H}/RT) \qquad 3.1$$

Work on other glassy systems such as GeO_2 and $Na_2O\text{-}GeO_2$ (Krause and Kurkjian, 1966), B_2O_3 and As_2O_3 (Strakna and Savage, 1964) and BeF_2 (Krause, 1968) show the presence of a similar large acoustic attenuation peak, the intensity and position of which is dependent on both the glass composition and the acoustic frequency. A summary of these results is shown graphically in Figure 3.1. The acoustic attenuation peak has been found to have approximately the same order of magnitude of attempt frequency for all the glasses studied; the varying temperatures of the loss maxima are explained by different activation energies for the different glass compositions.

Figure 3.1 The temperature dependence of acoustic loss in inorganic glasses. Dashed lines are for $Na_2O-B_2O_3-SiO_2$ glasses of this present study.
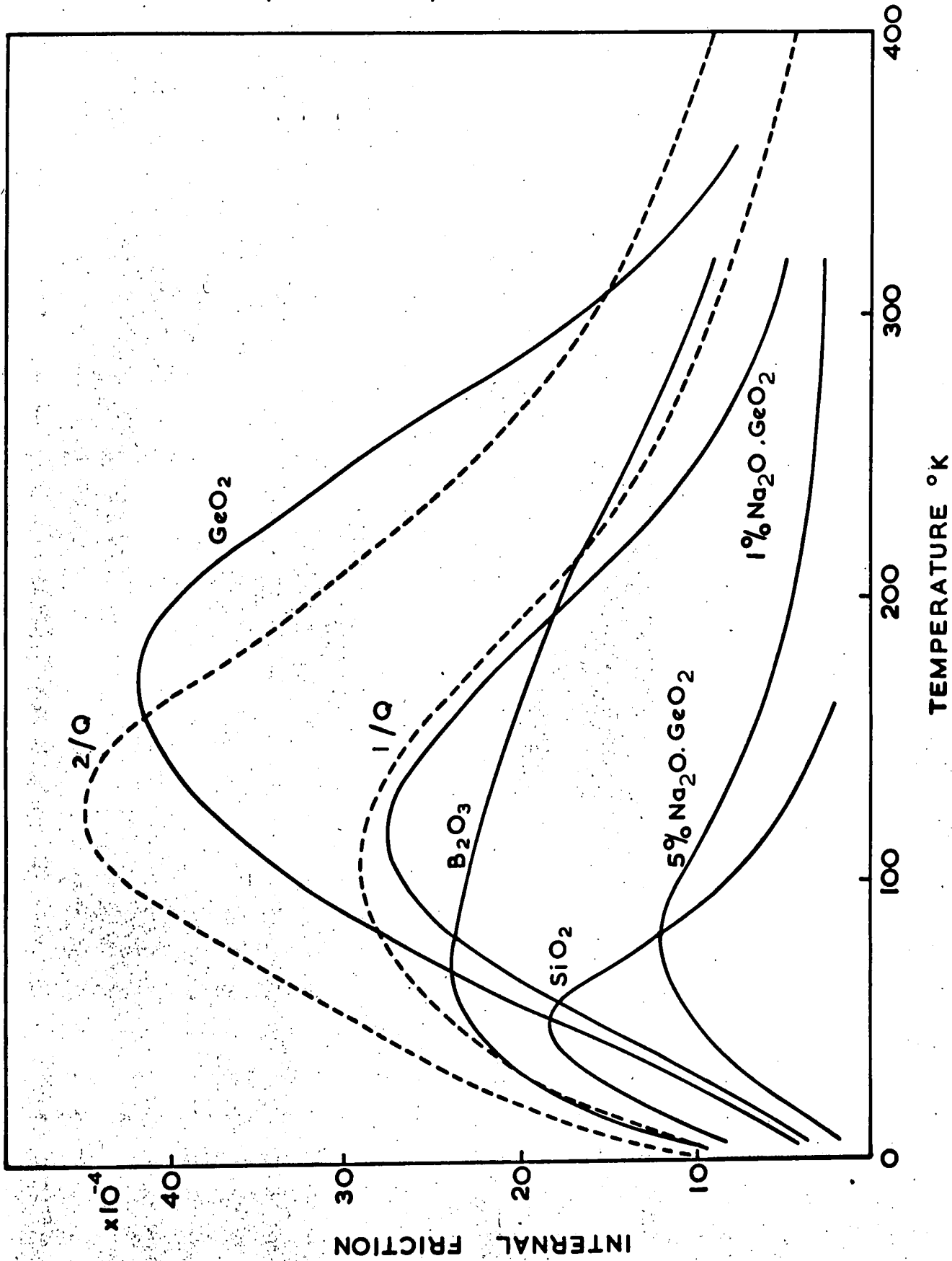
The compositional dependence of this acoustic loss in the Na_2O-GeO_2 system has been reported in some detail by Krause and Kurkjian (1966). Addition of 1 mole% Na_2O to GeO_2 reduces the peak height by 50% and decreases the temperature of the maximum observed acoustic loss from $170^{\circ}K$ to $120^{\circ}K$ at 20 MHz acoustic frequency. Further addition reduces the peak height and again decreases the peak temperature, but beyond 10 mole% Na_2O little extra effect is noticed.

This large acoustic loss peak has also been found in the Na_2O-B_2O_3-SiO_2 glasses reported in the present study. Discussion of the compositional dependence of this acoustic loss will form an important part of this thesis.

In attempts to understand the interatomic binding and structure of glasses, many workers have measured elastic wave velocities as a function of glass composition. Murthy and Aguayo (1964) have proposed that the addition of Na_2O to vitreous GeO_2 results in the increase of the coordination number of the germanium atoms from 4 to 6, and a strengthened cross linking of the structure is expected. The ultrasound velocity composition in the Na_2O-GeO_2 system shows a maximum at about 20% Na_2O, in accord with this theory (Krause and Kurkjian, 1966); the decrease in ultrasound velocity beyond the maximum is most probably due to the production of singly bonded oxygen atoms.

A similar maximum in acoustic velocity has been observed in the $Na_2O-B_2O_3$ system at about 30 mole% Na_2O (Gladkov and Tarasov, 1960) where the initial increase has been attributed to the change in coordination number of the boron from 3 to 4. In contrast, a continuous decrease in acoustic velocity is reported by the same authors on addition of Na_2O to vitreous SiO_2, and is interpreted on the basis of the continuous production of singly bonded oxygen atoms with no corresponding increase in the coordination number of the silicon atoms beyond 4.

The effect of composition upon the longitudinal acoustic velocities in $Na_2O-B_2O_3-SiO_2$ glasses has been studied by Gladkov and Tarasov (1960). No acoustic attenuation results are reported. In place of the original graphs presented by Gladkov and Tarasov of velocity versus percentage B_2O_3 in $B_2O_3-(Na_2O:SiO_2)$ for various mole ratios of Na_2O to SiO_2, Figure 3.2. shows contour lines of equal longitudinal velocity on the ternary phase diagram, which is a much more convenient method of presentation. Thermal histories are not quoted for the glasses of this study which makes phase separation characteristics impossible to assess. The acoustic velocities quoted by these workers for unannealed vitreous SiO_2 ($5.60.10^5$ cm/sec) and annealed vitreous SiO_2 ($5.72.10^5$ cm/sec) seem rather low in comparison to those of various vitreous SiO_2 samples reported in the comprehensive study of Fraser (1968). This latter author reports the lowest longitudinal velocity
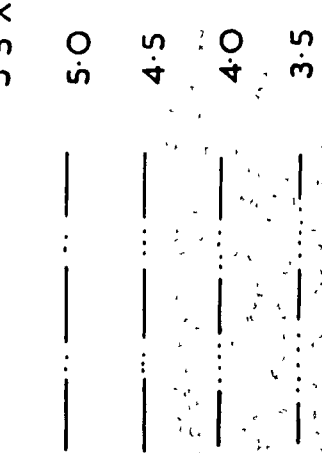
Figure 3.2 Lines of equal longitudinal velocity redrawn from results of Gladkov and Tarasov (1960). Actual glasses studied are denoted thus· ⊙
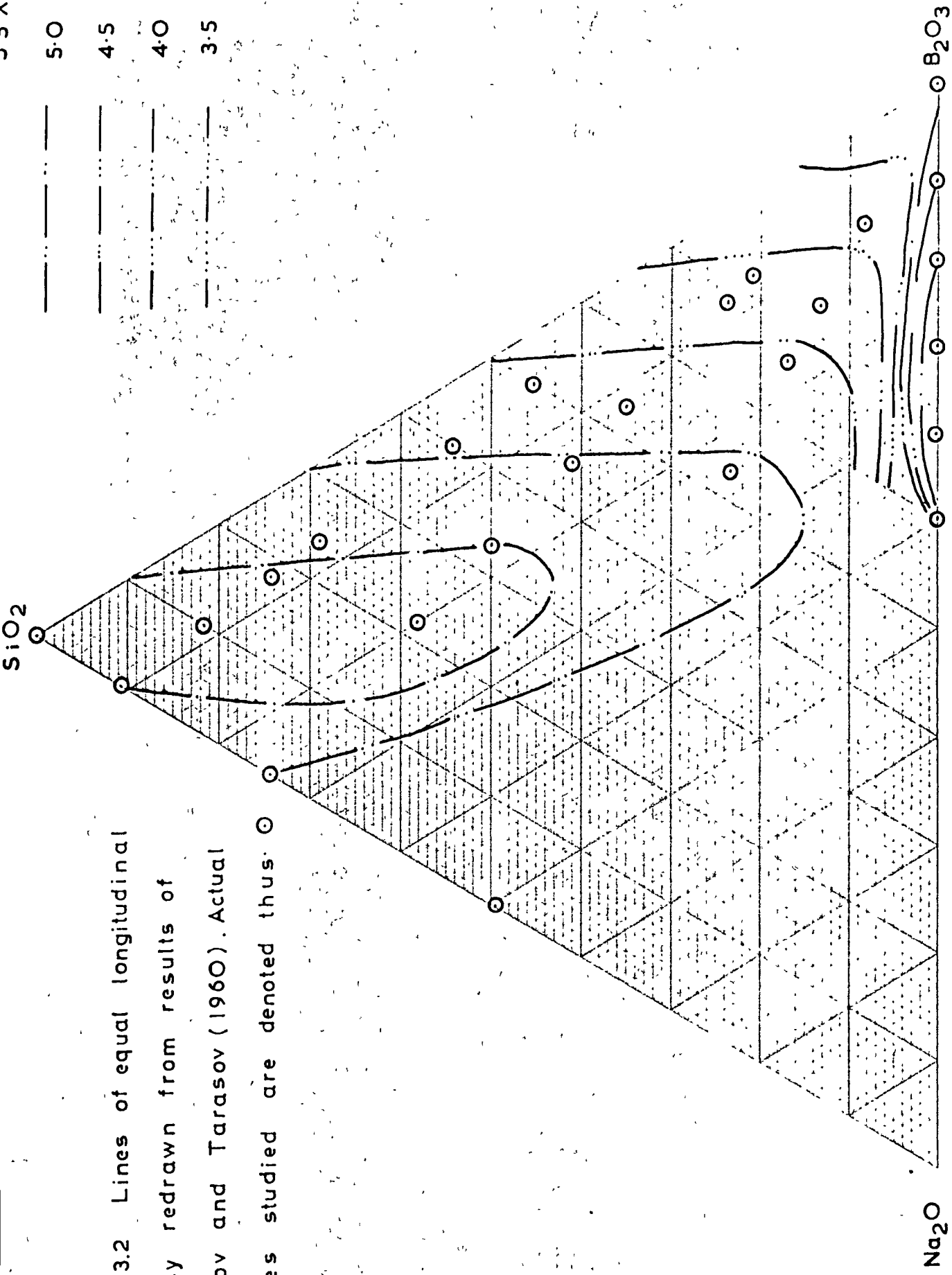
Ternary wt% diagram of $Na_2O-B_2O_3-SiO_2$ system

SiO_2

Na_2O

B_2O_3

5·0
4·5
4·0
3·5

as $5.936.10^5$ cm/sec for Spectrosil of 900°C fictive
temperature, and the highest as $5.992.10^5$ cm/sec for
I.R. Vitreosil of 1400°C fictive temperature. A
considerable discrepancy also exists between the value
of Gladkov and Tarasov for the velocity in pure B_2O_3
glass ($3.05.10^5$ cm/sec) and the value of Uhlmann and
Shaw (1971) ($3.40.10^5$ cm/sec).

The reason for the discrepancy between the
reported ultrasound velocities in the pure vitreous
SiO_2 and B_2O_3 cannot be ascertained as no details of
the method of measurement are included in the paper by
Gladkov and Tarasov, except that it was by an unspecified
ultrasonic technique. It is useful to look at their
work in the light of this present study. However, it
will be seen that it is vital in comparison of results
on glassy systems to have formal details of sample
preparation and characterization; such details are not
reported by Gladkov and Tarasov.

The important question of the behaviour of the
elastic constants in systems where phase separation is
exhibited, as well as their dependence on composition,
has been studied by Uhlmann and Shaw (1971) for various
PbO- and alkali oxide silicates and borates. They have
shown that the theoretical formulae (see Chapter 7) for
the elastic constants of a two phase material derived
by Hashin and Shtrikman (1963) fit the experimental
data fairly well. However, details of phase morphology
and thermal history of the glasses are not included;

these factors will be shown to have a profound effect on the ultrasound velocities of the Na_2O-B_2O_3-SiO_2 glasses of this present work.

Temperature dependences of ultrasound velocity below room temperature for SiO_2, GeO_2, BeF_2, $Zn(PO_3)_2$ and B_2O_3 glasses are reported by Krause and Kurkjian (1968). All evidence a relaxation in elastic modulus associated with the large acoustic attenuation peak. With the exception of B_2O_3, they also all have a positive temperature coefficient of ultrasound velocity at higher temperatures than the relaxation minimum. However, addition of as little as 1 mole% Na_2O to GeO_2 has the effect of changing the temperature coefficient of acoustic velocity from positive to negative; addition of further Na_2O serves to increase the now negative coefficient (Krause and Kurkjian, 1966).

3.1.2 Ultrasound propagation in glasses below $4.2^O K$

A low temperature loss peak of relatively small intensity has been observed at about $4^O K$ at 20MHz acoustic frequency in vitreous SiO_2 (Krause, 1964) and also in vitreous GeO_2, BeF_2 and $Zn(PO_3)_2$ (Krause and Kurkjian, 1968). There remain many difficulties associated with the understanding of the nature of the effects which cause this acoustic loss peak. This peak has been shown to be of equal intensity in both Suprasil synthetic fused SiO_2 which contains 1000 p.p.m. OH ions and Infrasil which is virtually water-free. A similar peak

in the dielectric loss occurs at about 2^OK at 100 KHz (Jaeger, 1968) and which has, on the assumption of an Arrhenius type activation process, a similar attempt frequency ($1.4.10^{11}$Hz) and activation energy (60 cal/mole) to the acoustic peak found by Krause. This suggests a common cause for both the acoustic and the dielectric loss. However, Jaeger has shown that the intensity of the dielectric loss is dependent on the OH content of the vitreous SiO_2, and furthermore has demonstrated that this loss is absent in certain samples where the acoustic loss is present. No satisfactory explanation for this point of apparent contradiction has yet been found.

Krause and Kurkjian (1968) have noted that this very low temperature acoustic attenuation peak occurs in glasses with an open tetrahedrally coordinated structure, but not in the planar triangular B_2O_3 glass. They have also drawn attention to the positive temperature coefficient of ultrasound velocity at 300^OK and the 10^OK to 20^OK negative coefficient of thermal expansion of open tetrahedrally coordinated glasses while the converse of these properties is apparent in glassy B_2O_3. Thus, it appears that the low temperature acoustic attenuation peak and the other low temperature anomalies of these glasses may have a common origin in their similar vibrational states. Indeed White and Birch (1965) have suggested that low frequency optical modes of vibration can exist in such a structure, and may be responsible for the low temperature anomalies in thermal properties.

Krause (1964) has investigated the possibility that a thermal phonon process is the cause of this low temperature attenuation peak. Measurements on samples of different cross section showed identical results, and as Krause considered that at these low temperatures the thermal phonon mean free path was of the order of the sample size he concluded that such a process is not responsible. However, Zeller and Pohl (1971) have shown that the mean free path of a thermal phonon in vitreous SiO_2 at $4^{\circ}K$ is approximately 10^{-4} cms. In the light of this recent result we can conclude that any size dependent effect is negligible and therefore Krause's argument is not correct. However, additional evidence that the process responsible for the low temperature peak is not a phonon-phonon interaction will be presented in the discussion of this work.

Krause subjected selected samples of vitreous SiO_2 to an electric field of 6 KV/cm at $700^{\circ}C$ for 2 days, but they exhibited an unchanged attenuation peak at $4^{\circ}K$. Thus it seems that an impurity cation is not associated with the loss mechanism.

3.1.3 The effect on acoustic propagation characteristics of the hydroxyl ion content and fictive temperature

Two factors which have been found to have an effect on the acoustic properties of glasses are (i) water or hydroxyl ion content and (ii) fictive temperature. To gain an insight into the precautions necessary in the

manufacture of glass samples for acoustic studies it is of use to review the effects of these two factors.

Hydroxyl ion content has been shown by Kurkjian and Krause (1966) to have a profound effect on the large acoustic absorption peak in vitreous B_2O_3. 'Wet' and 'dry' specimens of B_2O_3 were prepared; the former was melted in air at 950^OC and the latter was melted at 1150^OC and bubbled for 10 hours with dry nitrogen to remove any water present. Infra-red transmission spectroscopy evidenced that the dry specimen contained only 5% of the OH ion concentration of the wet specimen. The wet specimen exhibited a large acoustic loss peak centred at 300^OK at 20 MHz and a smaller peak at 50^OK, while the dry specimen showed a much enlarged peak at 50^OK and only a small peak at 300^OK. The reduction in size of the 300^OK peak was consistent with the fractional reduction in the OH concentration. These authors have also found that addition of Na_2O removed the 300^OK peak of the wet specimen, but beyond 15 mole% Na_2O, a new loss at 150^OK was observed.

Both hydroxyl ion content and fictive temperature have been shown to exert small but significant effects on the acoustic properties (Krause, 1971; Fraser, 1968) and also the dielectric properties (Jaeger, 1968) of vitreous SiO_2. Comparisons by Krause of the ultrasound velocity and attenuation in Corning 7940 SiO_2 samples with 850 p.p.m. OH and fictive temperature of 980^OC and 1400^OC, and Suprasil samples with 17 p.p.m. OH and fictive

temperature $1000^O C$ and $1200^O C$ show that the higher the OH content the higher the $50^O K$ acoustic loss peak and the greater the temperature coefficient of velocity at $300^O K$. An increase in fictive temperature lowers the acoustic loss. These results are in general agreement with those of Fraser, who has studied many different SiO_2 specimens by a resonant sphere technique. Jaeger has shown that there is a correlation between the height of the analogous large peak in dielectric loss and the fictive temperature, in general agreement with the findings in the acoustic properties of vitreous SiO_2.

The conclusion to be drawn here is that knowledge of the OH or water content and thermal history of a glass sample is necessary when interpreting the acoustic properties. These two factors are vital in the full characterisation of a glass specimen, and should always be included in the description of the state of a glass sample.

3.1.4 Internal friction and elastic moduli at low frequencies

Many measurements of the internal friction and elastic constants of glasses have been made by both resonance and torsional vibration techniques. Experiments have included the measurement of anelastic and elastic properties as a function of both composition and phase separation characteristics, with a view to a greater understanding of the structure of glasses.

An abbreviated review of the important studies to date
is included here, together with the general conclusions
from the results obtained.

Frequencies below 1Hz

Measurements of the internal friction of both
quenched and droplet structured phase separated samples
of a glass of mole% $3.9Na_2O-31.2B_2O_3-64.9$ SiO_2 have been
made by Mazurin (1968). The method involved measurements
of the damping of torsional vibrations of a fibre of the
glass. This author reports a peak in the internal
friction at $470^{O}C$ at an oscillation frequency of 0.25 Hz,
unique to the phase separated sample, which moved to higher
temperatures at higher frequencies. The magnitude of this
shift is quoted to correlate with the temperature dependence
of the viscosity of the sample which indicates an activa-
tion energy for the loss process of about 20 Kcal/mole.
Assuming an Arrhenius activation process, one may calculate
that this peak would occur at approximately $5000^{O}C$ in
the low MHz acoustic frequency range, making observation
of this peak by the pulse-echo technique used in this work
impossible.

Frequencies in the low KHz range

Experiments in the low KHz region have been
executed up to the Tg point of various glasses by
monitoring the resonant frequency and damping of
flexural vibrations of bars of the glass suspended from

their nodal points. A typical alkali silicate vibrating at 1 KHz to 10 KHz exhibits a broad loss at about 250°K to 450°K, interpreted as an alkali ion diffusion process, and a further loss at 500°K to 700°K attributed to a non-bridging oxygen ion diffusion process. Silicate glasses containing two different alkali ions show a third peak which is usually known as the 'mixed alkali peak.'

Taylor and Day (1970) have measured the internal friction in the $Li_2O-Na_2O-SiO_2$, $Li_2O-Na_2O-B_2O_3-SiO_2$ and $Na_2O-B_2O_3-SiO_2$ glass systems. Heat treatments produced phase separation directly observable by direct transmission electron microscopy. Measurements of the internal friction of samples between 170°K and 700°K evidenced that the mechanism responsible for the 'mixed alkali' diffusion peak is unaffected by advancing phase separation. However, they found that the alkali ion diffusion peak in the $Na_2O-B_2O_3-SiO_2$ glass is reduced in magnitude as phase separation proceeds, in agreement with the findings of Day and Rindone (1961). These latter authors also report that the alkali ion and non-bridging oxygen ion diffusion peaks of a $Li_2O-2.75 SiO_2$ glass are unaffected by phase separation until crystallization in the glass commences.

These somewhat negative findings are further substantiated by Redwine and Field (1969) who have observed that the ionic diffusion peaks in Na_2O-SiO_2 glasses are largely unaffected by phase separation.

However, they conclude from an earlier study of the same system (1968), that for glasses with an inter-connected phase separation morphology, the elastic moduli are linearly dependent on the total amount of soda present, and are larger than for a quenched glass of the same composition. In the metastable droplet structured region of phase separation, the mechanical properties of the glass are reported to behave as a homogeneous material having the same structure as the continuous phase. The dispersed phase exerts only second order effects on the elastic moduli.

The absence of any significantly large effect of phase separation on the ionic diffusion phenomena, with the exception of glasses in the $Na_2O-B_2O_3-SiO_2$ system, is perhaps to be expected; the movement of the ions under the conditions of alternating stress is only of the order of the interatomic spacing while the phase separation boundaries are typically thousands of atoms apart. The activation energies of these ionic diffusion processes are in the range 20 to 40 K cal/mole, and temperatures around and above the Tg point would be necessary to render these peaks observable at MHz acoustic frequencies. The difficulties of such an experiment are large as sample geometry and phase separation morphology would be constantly changing at these elevated temperatures; ionic diffusion phenomena are best studied by low frequency techniques.

3.2.1 The interrelation between thermal capacity and ultrasound velocity and attenuation

The information about the vibrational states of a solid is contained in the frequency distribution of $G(\omega)$, the number of vibrational modes with frequencies between ω and $\omega + d\omega$. In the harmonic approximation constant volume heat capacities are related to this distribution by

$$Cv = k \int_{o}^{\omega_{max}} G(\omega) \frac{e^{-\frac{\hbar\omega}{kT}} (\hbar\omega/kT)^2}{\left(e^{\frac{\hbar\omega}{kT}} - 1\right)^2} d\omega \qquad 3.2$$

where ω_{max} is the cut-off of the Debye distribution $G(\omega) = \alpha\omega^2$, and is related to the Debye temperature through

$$\theta_D = \frac{\hbar \, \omega_{max}}{k} \qquad 3.3$$

Even in the simplest crystal, the true shape of $G(\omega)$ is complex, and the usefulness of heat capacity data in examining the shape of $G(\omega)$ is limited as C_v is determined by the integral over the whole spectrum. Plots of θ_D from heat capacity measurements against temperature to show any deviation from the Debye theory behaviour can indicate the approximate size and position of the first peak in $G(\omega)$, but no details of the high frequency part of the spectrum are obtainable.

As the temperature approaches $0°K$, the Debye continuum hypothesis approaches reality and all solids, including glasses, behave as an elastic continuum. Discussions of results from heat capacity data can be

undertaken in terms of deviation from this limiting

behaviour;   data is usually analysed by use of a

C/T^3 versus T^2 plot which shows any deviation from the

Debye limiting solution to the equation for specific

heat given by Blackman (1955) to account for dispersion

as

$$C_v = AT^3 + BT^5 + CT^7 + \dots \tag{3.4}$$

Here, A tends to C_v/T^3 as T tends to zero.   In the low

temperature limit

$$A = \frac{12\,\pi^4\,N\,k}{5\theta_D^3} \tag{3.5}$$

Ultrasound waves have the advantage that

their velocities may be measured very accurately.

Extrapolation of velocities to $0^\circ K$ may easily be made

and the Debye temperature can then be calculated from

the equation (e.g. Anderson, 1959)

$$\theta_D = \frac{h}{k}\,(N/4\pi)^{1/3}\,v_m \tag{3.6}$$

where the mean sound velocity v_m is, for a glass with

longitudinal velocity v_ℓ and shear velocity v_s,

$$v_m = \left[\frac{1}{3}\left(\frac{2}{v_s^3} + \frac{1}{v_\ell^3}\right)\right]^{-\frac{1}{3}} \tag{3.7}$$

Comparison of the thermal and acoustic properties is thus

made through the parameter A of equation 3.5.

It should be noted that the Debye temperature

θ_D is not uniquely defined for a glass (Anderson, 1959)

and is dependent on and defined by the choice of N, the volume density of primitive vibrational units which is somewhat arbitrary for a glass with more than one component. Thus the choice of the density of fundamental vibrational units is important; if it is taken as the number of atoms per unit volume, the resulting θ_D is the Debye temperature for the density of states distribution containing all the modes of the solid. This convention is most useful for comparison with specific heat data as the latter does not distinguish between the acoustic and optic branches of the phonon spectrum.

Thermal and elastic properties must agree in the low temperature limit and many interesting points arise from their comparison as that limit is approached. Figure 3.3 shows the behaviour of C_v/T^3 with T^2, normalized to the elastic wave value of C/T^3 at T=0, of vitreous GeO_2 and vitreous SiO_2. The results of Antoniou and Morrison (1965) show that vitreous GeO_2 behaves normally with C/T^3 approaching the elastic wave value in the $0^{\circ}K$ limit, but some 'excess' specific heat is present above this limit. However, for vitreous SiO_2, the value of C/T^3 is somewhat higher than expected and at $2^{\circ}K$ is about twice the limiting value calculated from the acoustic velocities (McSkimin, 1953; White, 1965).

Recent measurements of the heat capacity in vitreous SiO_2 (White and Birch, 1965), GeO_2 (Zeller and Pohl, 1971), BeF_2 (Leadbetter and Wycherley, 1971) and glycerol (Craig, Massena and Mallya, 1965) have shown
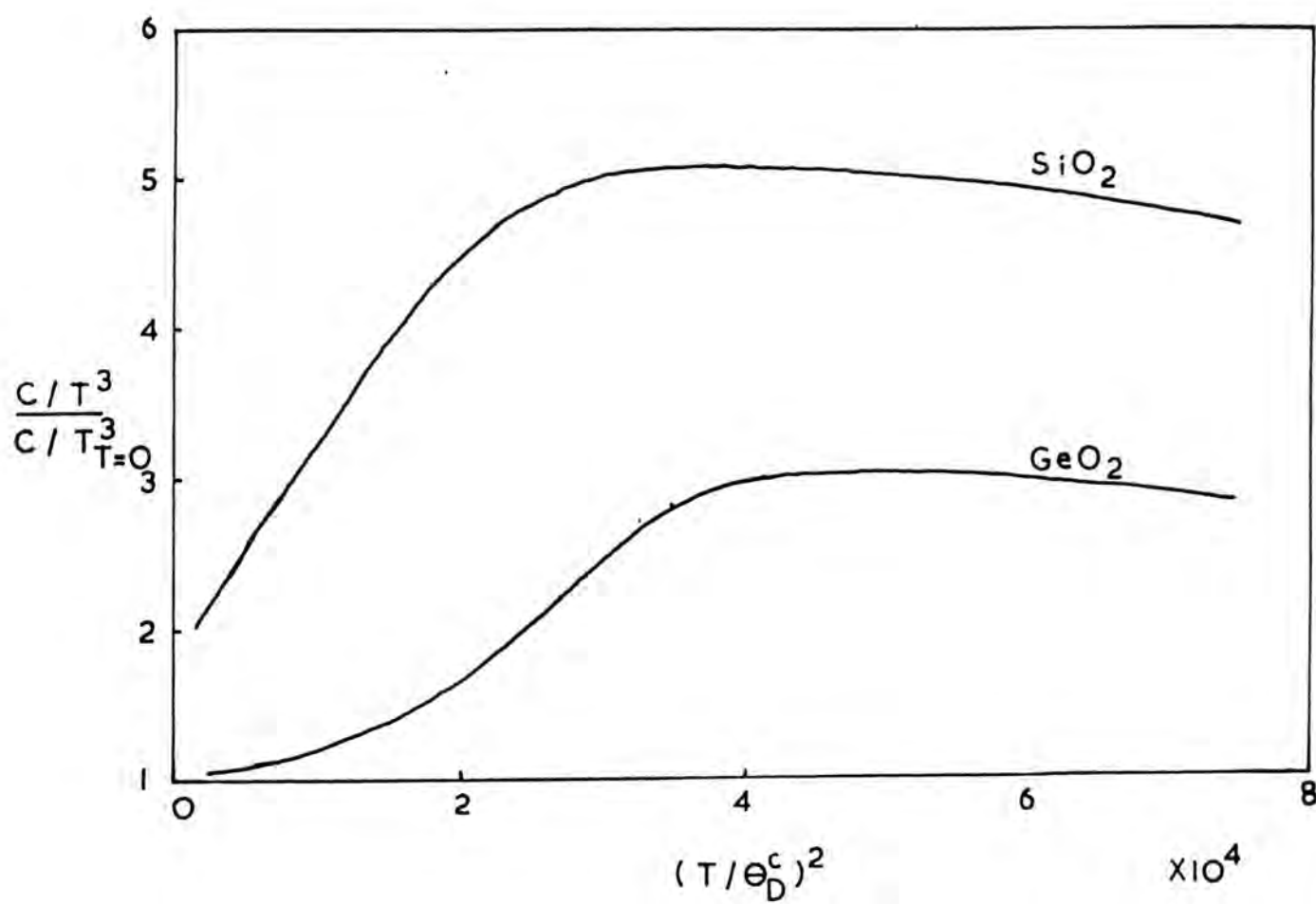
Figure 3.3 Reduced C/T^3 plot for vitreous SiO_2 and GeO_2

an increase in C/T^3 below about $2^\circ K$. This parameter is observed to be still increasing even at the lowest temperatures at which the thermal capacity has been measured ($0.1^\circ K$).

It is tempting to associate the excess specific heat in vitreous SiO_2 and GeO_2 with the mechanism responsible for the acoustic absorption peak. However, there is no simple correlation between the reduction in excess specific heat and ultrasonic absorption upon neutron irradiation of SiO_2 and GeO_2 (Leadbetter and Morrison, 1963) and furthermore, while the acoustic absorption peak is present in Pyrex, there is no excess specific heat (Marx and Sivertsen, 1953).

3.3.1   Ultrasound attenuation : the large acoustic loss peak

Before any conclusions may be drawn from the compositional dependence of the characteristics of the large acoustic attenuation peak (see Figure 3.1) that occurs in most, if not all, the inorganic glasses studied to date, an attempt must be made to understand the underlying mechanism. Three models have been proposed by different workers; two are similar and involve atomic motions in a variety of local environments within the glass structure, and the third involves a phonon-phonon interaction between the ultrasound wave and the phonon spectrum of the glass lattice. These models will now be discussed in turn and a conclusion

will be drawn as to the most likely mechanism responsible.

Model of Anderson and Bömmel

Anderson and Bömmel (1955) have interpreted the attempt frequency and activation energy of the large acoustic loss peak in vitreous SiO_2 as that of a structural relaxation. The vibrational period has an order of magnitude consistent with the shortest period of the lattice vibration that contributes to the specific heat: the loss mechanism seems to be connected with the vibration of a small structural unit. An activation energy of 1030 cal/mole is too small for an atomic diffusion process and also for a molecular rotation. It is, however, of the correct magnitude for a small change in bond angle.

The model for the acoustic loss mechanism proposed by Anderson and Bömmel is an oxygen atom vibrating between two potential wells of equal energy perpendicular to a non-linear Si-O-Si bond, shown pictorially in Figure 3.4. A stress wave biases one of the potential wells with respect to the other, and the equilibrium distribution of oxygen atoms is disturbed. The relaxation back to the initial state takes place in a time characteristic of the vibrational period of the oxygen atom. When this time is of the order of the ultrasonic stress wave period, energy is returned to the stress wave out of phase and attenuation results. A particular feature of this model is that the mechanism is only effective in attenuating a longitudinal wave

• Silicon   O Oxygen
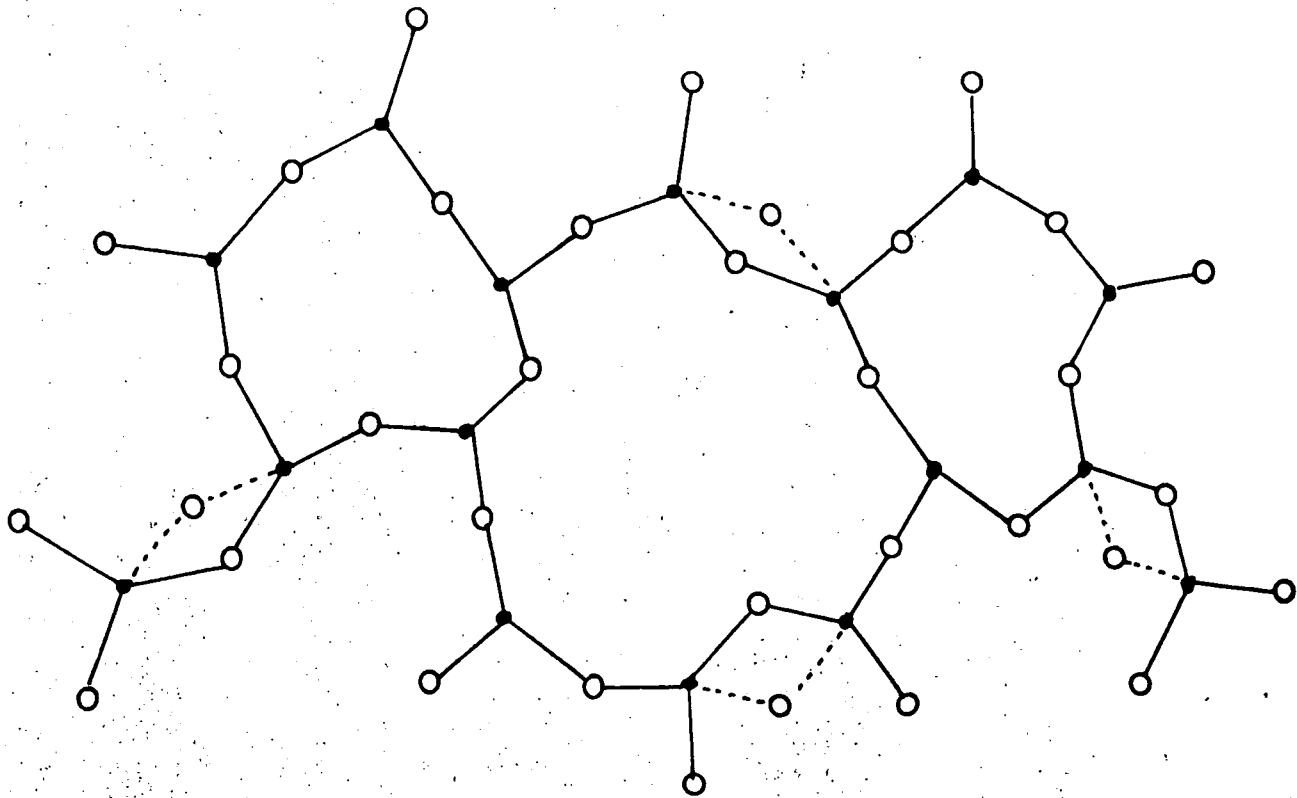
i ANDERSON AND BÖMMEL
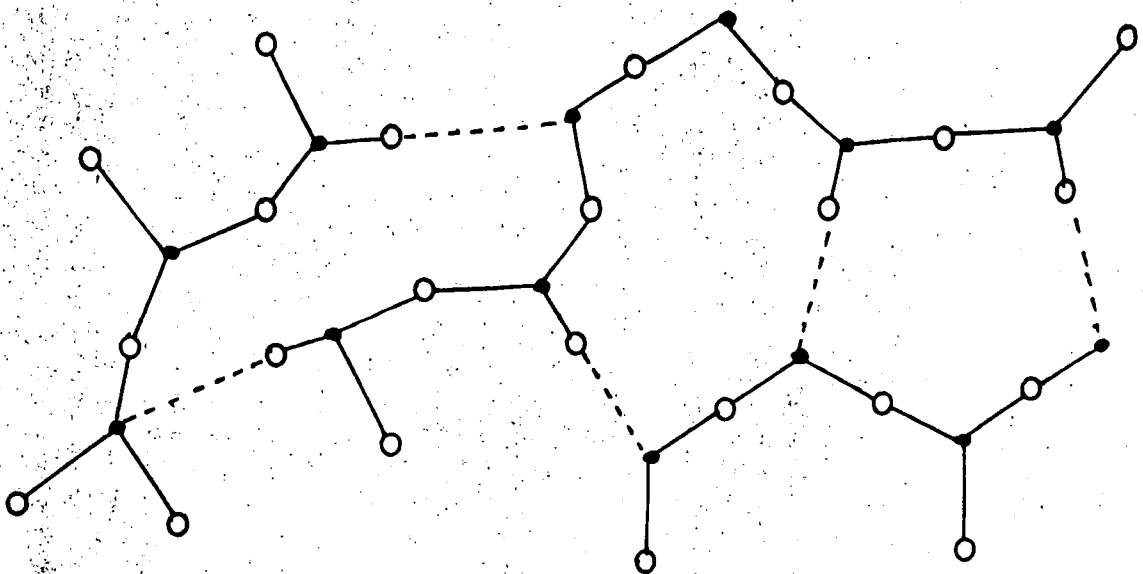
ii STRAKNA

Figure 3.4 Comparison of the structural relaxation models.

if the potential wells are originally of unequal depth; results indeed show that a greater loss peak is exhibited for a shear wave than for a longitudinal ultrasound wave in vitreous SiO_2. A calculation of the elastic energy required to force apart the two Si atoms as the oxygen atom passes between is obtained from a multiplication of the elastic constant $(\lambda + 2\mu)$ by the distance through which the Si atoms must move; this shows that a Si-O-Si bond angle of 4° to 5° is necessary to produce an activation energy of 1030 cal/mole. This angle agrees with results from x-ray studies of the bond angles in vitreous SiO_2 which indicate an Si-O-Si bond divergence of at least 5° (Stevels, 1953).

To account for the width of the attenuation peak, which is broader than that for a process with a single relaxation time τ, a distribution of activation energies for the movement of the oxygen atoms has to be invoked. The anomalously large width of the peak is demonstrated in the loss versus reciprocal temperature plot of Figure 3.5; this choice of axes eliminates thermal broadening effects.

The equation describing the internal friction is the sum over the complete range of activation energies of contributions from many equations of type 2.46, and is thus

$$Q^{-1} = \sum_i \Delta i \frac{\omega \tau_i}{1 + \omega^2 \tau_i^2} \qquad 3.8$$
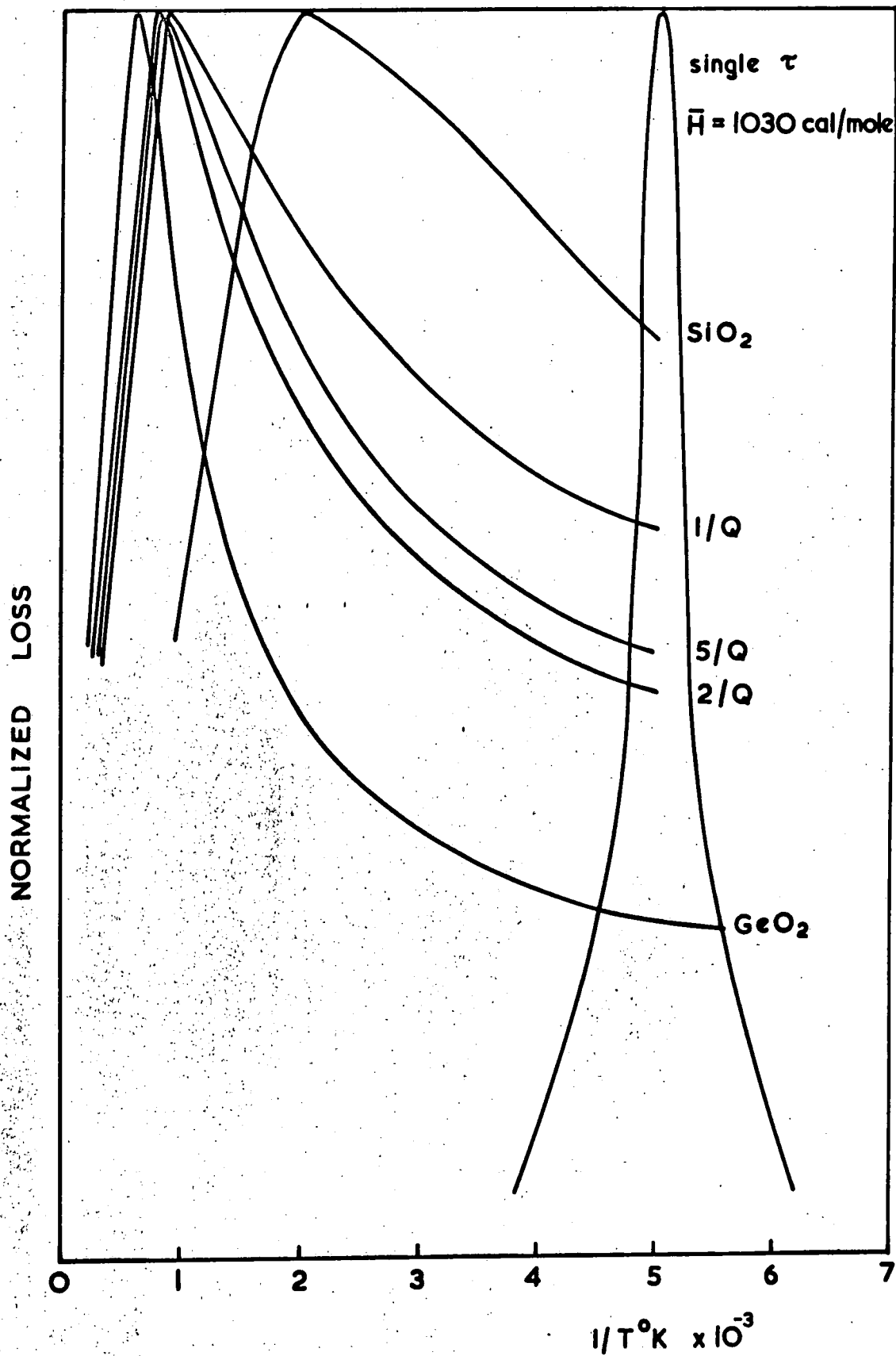
Figure 3.5 Normalised loss versus reciprocal temperature for some selected glasses in comparison to a single τ relaxation peak.

where $\qquad \tau_i = \tau_o \exp(-Hi/RT)$ $\qquad$ 3.9

Using this equation, Anderson and Bömmel have calculated the shape of the distribution in activation energies needed to account for the observed experimental attenuation. This distribution, which is in the form of Δi versus Hi, is shown in Figure 3.6. Also accounted for by the shape of this distribution is the variation with frequency experimentally observed internal friction at the peak maximum which rises from $8.3.10^{-4}$ at 66KHz to $1.88.10^{-3}$ at 20MHz and eventually to $7.2.10^{-3}$ at 27.5GHz.

Model of Strakna

A second, very similar model has been proposed for the loss mechanism in vitreous SiO_2 by Strakna (1961) in which the oxygen atom is considered to vibrate between two equi-potential wells in the direction of an elongated Si-O-Si bond, also shown schematically in Figure 3.4. Strakna has measured the characteristics of the $50^{O}K$ absorption peak in vitreous SiO_2 before and after fast neutron irradiation, and cites the results in evidence for his model as opposed to that of Anderson and Bömmel. The shape of the distribution of activation energies for movement of the oxygen atoms is unchanged by neutron irradiation although the intensity of the absorption peak is reduced, a fact which suggests that the centres responsible for the loss are either completely eliminated or left unchanged. Damage due to either thermal spikes or displacement collisions is considered by Strakna to
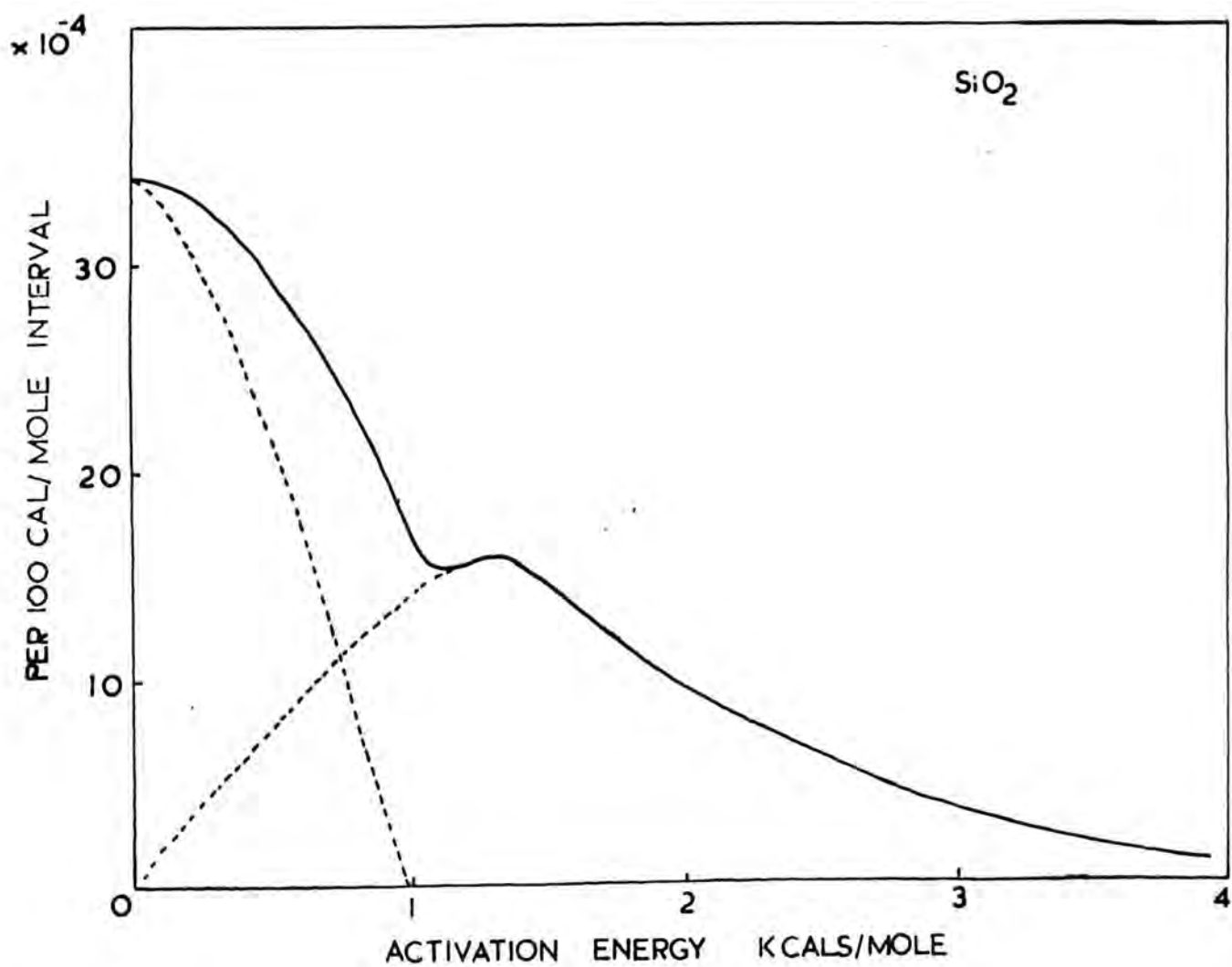
Figure 3.6   The activation energy distribution of the loss mechanism
in vitreous SiO_2.

be likely to change the relative orientation of the SiO_4 tetrahedra and thus perturb the Si-O-Si bond angle distribution. If Anderson and Bömmel's model is correct, this would lead to an alteration in the activation energy distribution which is in fact not seen.

To identify the anomalous Si-O distances for the elongated Si-O-Si bond model, Strakna separates the activation energy distribution, which is identical to that for the Anderson and Bömmel model, into two parts as seen in Figure 3.6. An identical pair of distributions can be calculated by using a one dimensional Morse function and Gaussian distributions of Si-Si bond lengths centred around 3.83 Å and 3.89 Å. From these lengths, the anomalous Si-O distances are shown to be centred at 1.74 Å and 2.12 Å. The validity of the model is then somewhat substantiated by peaks corresponding to Si-O distances at 2.12Å and an Si-Si distance at 3.86 Å which occur in x-ray electron density plots (Richter, Breitung and Herre, 1953). Strakna also concludes from the size of the x-ray peaks that 20% to 30% of the Si-O-Si bonds are elongated.

Model of Pine

Another interpretation of the large acoustic attenuation peak in vitreous SiO_2 is that of Pine (1969) who suggests that it is the result of an interaction between the ultrasound phonons and the phonon spectrum of the lattice. Pine has measured the attenuation of 27.5GHz longitudinal hypersonic waves by a Brillouin

scattering technique and has fitted his theory to the experimental results using some arbitrary parameters but which find some justification in the Raman spectra of vitreous SiO_2 of Flubacher et al (1960).

When the product of the acoustic angular frequency ω and the thermal phonon mode relaxation time τ is less than unity, the ultrasound phonon can only interact with the phonon population as a whole and not with individual phonons. The treatment of Akhieser (1939) and simplifications by Bommel and Dransfeld (1960) and Woodruff and Ehrenreich (1961) consider the phonon population as a 'gas' whose macroscopic parameters are periodically varied by the ultrasound wave. The results of these derivations take the form of

$$\alpha = \frac{8.686 \; \gamma^2 \omega T C_v}{2 \; \rho V_m^3} \cdot \frac{\omega \tau}{1 + \omega^2 \tau^2} \; db/cm \qquad 3.10$$

where γ is an averaged dimensionless Grüneisen constant of the order of unity, C_v is the thermal mode specific heat per unit volume, ρ is the density and V_m is the mean sound velocity.

Pine obtains the thermal mode lifetime from theoretical considerations of the decay and scattering of the thermal phonons, using the anharmonic theory of Maradudin and Fein (1962); a vibrational frequency ω_o is broadened by decay into two other phonons such that $\omega' + \omega'' = \omega_o$, and by scattering one mode into another such that $\omega' - \omega'' = \omega_o$. For the decay process, the

thermal lifetime is given by

$$\tau^{-1} = (n' + n'' + 1) A \qquad 3.11$$

and for the scattering process by

$$\tau^{-1} = (n'' - n') B \qquad 3.12$$

where A and B are complex functions of the anharmonic selection rules and the joint densities of states of ω' and ω'', and the constants n' and n" are the Bose-Einstein functions

$$n = \left(e^{\frac{\hbar\omega}{kT}} - 1 \right)^{-1} \qquad 3.13$$

Pine obtains the thermal mode specific heat from the Einstein model for which

$$C_v = 3Nk \left(\frac{\hbar\omega}{kT} \right)^2 \cdot \frac{e^{\frac{\hbar\omega}{kT}}}{\left(e^{\frac{\hbar\omega}{kT}} - 1 \right)^2} \qquad 3.14$$

with the usual notation.

To fit the theoretical to the experimental attenuation, Pine has to choose values for the several variables; one example of a fit is given by

$$\omega_O = 100 cm^{-1} \ , \quad \omega' = 500 cm^{-1} \ , \quad \omega'' = 400 \ cm^{-1}$$

$$B = 3.10^{13} \qquad A = 0$$

while another slightly better one by

$$\omega_O = 50 cm^{-1} \ , \quad \omega' = 450 cm^{-1} \ , \quad \omega'' = 400 cm^{-1}$$

$$B = 10^{14} sec^{-1}, \qquad A = 0$$

Pine finds some justification for these arbitrary choices

of phonon frequencies and constants A and B in the Raman

spectra of vitreous SiO_2, but why the thermal phonon mode

at ω_o is only scattered by the phonons at $400 cm^{-1}$ to

$500 cm^{-1}$ is unexplained.

However, recent measurements of the thermal con-

ductivity κ and specific heat by Zeller and Pohl (1971)

allow access to experimental values for the thermal phonon

lifetime and specific heat of vitreous SiO_2, and we will

now re-examine Pine's theory in the light of these new

results. In the dominant phonon approximation, the mean

lifetime of the thermal phonons can be obtained through

the relationship

$$\tau = \frac{3\kappa}{C_v \, v_m^2} \qquad\qquad 3.15$$

Thus, from knowledge of the thermal conductivity and

specific heat of vitreous SiO_2, the thermal phonon lifetime

can be calculated. The use of such a lifetime for a

phonon-phonon calculation of acoustic attenuation is

standard practice; for example good agreement is found

between theoretical and experimental attenuation in

crystalline quartz (Bömmel and Dransfeld, 1959). For

direct comparison with experimental results of the

acoustic attenuation in vitreous SiO_2, the phonon-phonon

acoustic loss has been calculated at the peak temperatures

of the experimental loss at 20MHz, 330MHz, 930MHz and

27.5GHz, namely $46^{O}K$, $60^{O}K$, $67^{O}K$ and $130^{O}K$. Table 3.1

lists the values of thermal conductivity, specific heat,

Peak Temperature $^{\circ}K$	Acoustic Frequency MHz	Thermal Conductivity ergs/cm$^{\circ}$K	Specific Heat ergs/g$^{\circ}$K	Phonon Mean Free Path cm	Phonon Relaxation Time secs	Attenuation db/cm	
						Calculated	Measured
46	20	2×10^4	1×10^6	1.1×10^{-7}	2.7×10^{-13}	1.3×10^{-5}	1.35
60	330	2×10^4	1.1×10^6	1.1×10^{-7}	2.7×10^{-13}	3.3×10^{-3}	36
67	930	2×10^4	1.1×10^6	1.1×10^{-7}	2.7×10^{-13}	3.0×10^{-2}	113
130	27,500	4×10^4	5×10^6	1×10^{-7}	2.4×10^{-13}	6.7×10^{1}	9,200

Table 3.1

Comparison between the measured attenuation and that calculated

for the Akhieser mechanism for vitreous SiO_2

thermal phonon mean free path and thermal phonon lifetime, and compares the values of experimental and calculated acoustic attenuation. The mean sound velocity of vitreous SiO_2 is taken as $4.11.10^5$ cm/sec at all temperatures; the variation with temperature is small (Anderson, 1959). A constant Grüneisen parameter of unity and a sample density of $2.2023g/cm^3$ has been assumed.

It can be seen from these results in Table 3.1 that the theoretical acoustic attenuation is many orders of magnitude lower than the experimental attenuation over the whole of the frequency range covered. Thus, a phonon-phonon type of interaction cannot be held responsible for the large acoustic attenuation peak in vitreous SiO_2. It is also of interest to compare the magnitude of the acoustic attenuation in crystalline quartz at 100^OK and 1GHz (Bömmel and Dransfeld, 1959) which has been attributed to a phonon-phonon interaction similar to that invoked by Pine, to that in vitreous SiO_2 at 930MHz (Jones et al, 1964). The acoustic attenuation in vitreous SiO_2 is a factor 30 times larger than that in crystalline quartz. Yet both materials exhibit a very similar specific heat, and the thermal conductivity, and hence thermal phonon relaxation time, is approximately 50 times smaller in the vitreous material. From this comparison alone it is clear that the large peak in vitreous SiO_2 is unlikely to be the result of a thermal phonon process.

3.3.2   Comparison of the models

It has been shown that it is very unlikely that a phonon-phonon interaction is responsible for the large acoustic loss peak in vitreous SiO_2, and this proposal will now be disregarded. This leaves the structural relaxation models as the two most likely explanations for the loss. Deduction of the correct model from the ultrasonic data alone is difficult as the equations which govern the ultrasound wave propagation characteristics are identical for both mechanisms.

The attempt frequency of 10^{13} Hz is approximately equal to the frequency associated with the motion of an oxygen atom along an Si-O-Si band of $3.30.10^{13}$ Hz (Lippincott et al, 1958) and also the Si-O-Si bending mode frequency of $2.40.10^{13}$ Hz (Bell et al, 1968) which provides a good phenomenological basis for both models. Corresponding cation-oxygen-cation vibrational modes in other glasses would be expected to have similar frequencies, explaining the common value for ω_0 amongst inorganic glasses. However, this order of magnitude of vibrational frequency is characteristic of many vibrational modes, as can be seen in the Raman spectrum of vitreous SiO_2 (Flubacher, 1959) which shows many features between $600 cm^{-1}$ and $1200 cm^{-1}$. Thus, purely from the attempt frequency alone, the vibrational mode and relaxing unit responsible for the acoustic loss is almost impossible to identify.

Supporting evidence for the validity of both models is also found in results of X-ray diffraction studies. Let us re-examine the structure of the radial distribution function of vitreous SiO_2 in the light of more recent studies to gain more information on the features considered by Strakna to favour the elongated bond model. A physical model of vitreous SiO_2 has been constructed by Bell and Dean (1967). The theoretical radial distribution function computed from the model compares very well with that obtained from X-ray studies, both contain the features referred to by Strakna. However, on inspection of the theoretical distribution function the anomalous Si-Si distance at 3.86 $\overset{o}{A}$ appears to have some origin in Si-O as well as Si-Si bond lengths. The anomalous Si-O distance at 2.12 $\overset{o}{A}$ is seemingly an O-O distance which occurs at 2.3 $\overset{o}{A}$ in the experimental plot. No Si-O contribution to the radial distribution function is expected between 1.6 $\overset{o}{A}$ and 3.0 $\overset{o}{A}$. Furthermore, the conclusion of Strakna that 20% to 30% of the Si-O-Si bonds are elongated implies that the relaxation in elastic modulus would be 10% to 15%, whereas the observed relaxation is only about 2%.

More recent and very accurate studies of the X-ray scattering in vitreous SiO_2 (Warren and Mozzi, 1969) indicate that the structure is basically a disordered arrangement of essentially undistorted SiO_4 tetrahedra.

The Si-O-Si bonds are found to range from 120° to 180°, with the most probable angle at 144°. These results are in general agreement with Stevels (1953) but do not include any evidence for the elongated bond model of Strakna. The Si-O distances are found to be close to 1.62 $\overset{\text{o}}{\text{A}}$; a double minimum in the potential along an elongated Si-O-Si bond does not develop until each cation oxygen distance is 1.90 $\overset{\text{o}}{\text{A}}$. It thus seems that, in the light of this present result, the anomalously long Si-O-Si bond proposed by Strakna to be the mechanism causing the ultrasound absorption in vitreous SiO_2 is a feature which is in fact not seen in the structure of the glass. On the other hand, the existence of the non-linear Si-O-Si bond is well proved.

In conclusion, it seems that while the model of Anderson and Bömmel, which involves the transverse motion of oxygen atoms in a non-linear cation-oxygen-cation bond, is not unique in describing the loss mechanism responsible for the large attenuation peak in inorganic glasses, it is the most feasible alternative. As such, this mechanism will be treated as the cause of the acoustic loss in the discussion of this work. However, many of the arguments centred around this consideration can apply equally well to the elongated bond model and where appropriate any feature which can help to distinguish the correct model will be noted when met with.

C H A P T E R   F O U R

PHASE-SEPARATION, THE $Na_2O-B_2O_3-SiO_2$

SYSTEM, AND THE SAMPLE PREPARATION AND

CHARACTERIZATION

Introduction

Chapter 4 commences with a detailed discussion of the phenomenon of glass-in-glass phase-separation and of the contemporary theories on the processes involved in metastable and unstable unmixing. Some observations are made on the contention between workers about the mechanisms of glassy phase-separation. Details of previous studies of the $Na_2O-B_2O_3-SiO_2$ system, in particular those concerning the metastability dome and the tie line directions are found in Section 4.1.8. Precise details of the thermal history of the glasses of this study are included in the sections on sample manufacture, preparation and heat treatment, and to complete the characterization, the determinations of the physical properties of density and water or OH content are described in full. The chapter terminates with a description of electron micrographs which were taken to determine the degree and morphology of the phase-separation exhibited by the $Na_2O-B_2O_3-SiO_2$ samples of this study.

4.1.1   Thermodynamics of phase separation in glasses

The thermodynamics of the metastability of a
phase is best understood through the approach of Gibbs (1948)
who formulated the requirements for the existence of a
metastable equilibrium. This approach considers two types
of infinitesimal fluctuation; an infinitesimal portion of
a new and stabler phase, and an infinitesimal compositional
or density fluctuation. Metastability to the former
fluctuation occurs if the interfacial testion is positive,
and a finite fluctuation, or nucleus, is required to render
the phase unstable. For a phase to be stable with respect
to an infinitesimal compositional or density fluctuation
it is necessary that the chemical potential of the components
increase with increasing density of the component. In
some systems there exists a temperature, dependent on com-
position, at which this criterion is no longer valid, which
is called the spinodal. Below this temperature the phase
is unstable to infinitesimal compositional changes and
spontaneously separates into two different but related
phases. Above the spinodal, but below the limit where
phase separation will still reduce the free energy of the
system, the phase is metastable to separation. Thus,
Gibb's formulation for metastability within the two phase
region reduces to

$$\frac{\partial^2 F}{\partial c^2} > 0$$

where F is the molar free energy, and c is the mole
fraction.

A spinodal is most commonly expected in systems
which have an upper consulate temperature Tc to the
boundary of the two phase region defined by the coexistence
curve. Figure 4.1 shows diagrammatically a hypothetical
phase diagram for a binary system, and also shows the
variation in free energy with composition at temperatures
above and below the consulate temperature. At temperatures
above the consulate the free energy must curve upwards
everywhere or separation would reduce the free energy.
At temperatures below the consulate the free energy still
curves upwards except between the limits defined by the
spinodal where $\partial^2 F/\partial c^2 < 0$. Between the limits of the
two phase region, the free energy is still reduced by
phase separation, but in the metastable region separation
will only occur if one phase can nucleate. New phases
produced by phase separation are themselves subject to the
same criteria for metastability, and may themselves suffer
further decomposition.

4.1.2   Metastable phase separation

To create the finite nucleus necessary for
phase separation to occur in the metastable region, energy
must be expended at the interface between a small droplet
of the new phase and the original matrix. The work required
to form this droplet decreases as $1/\Delta T_b^2$, where ΔT_b is the
undercooling below the two-phase boundary, and thus under-
cooling is necessary before a nucleus can appear. This
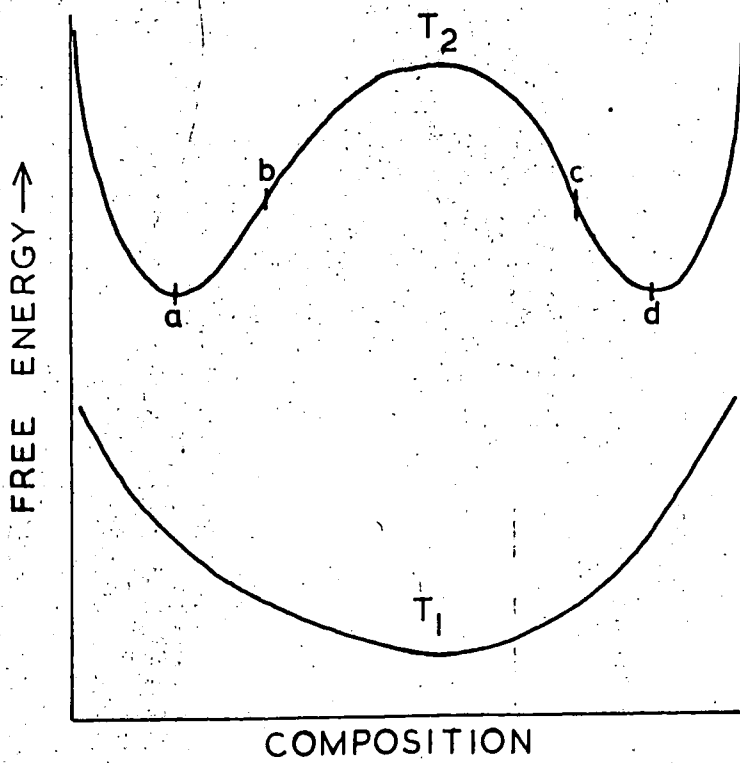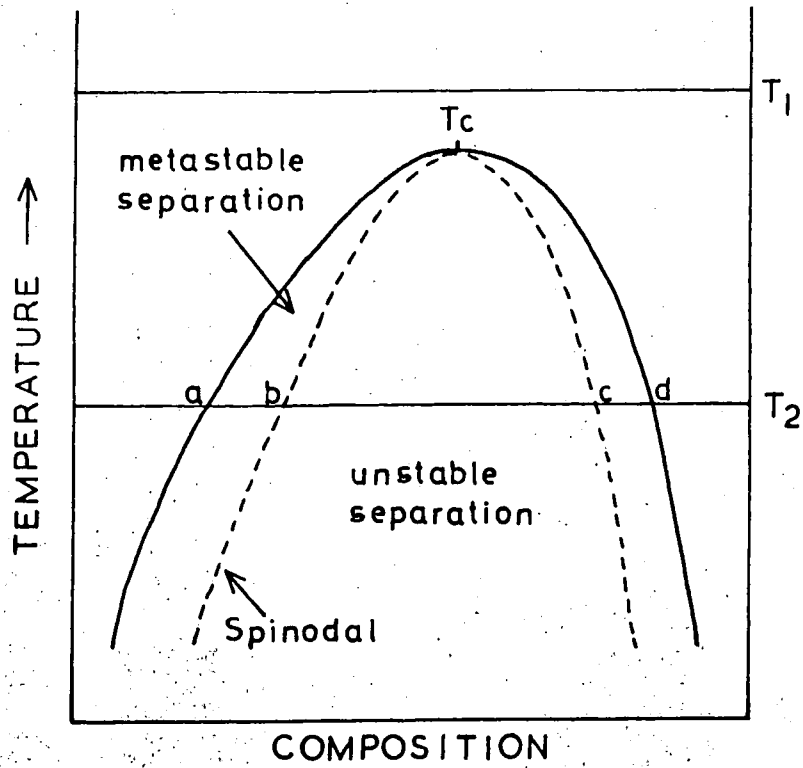process is called homogeneous nucleation.

Figure 4.1   Phase and free energy diagrams for a hypothetical binary system

Heterogeneous nucleation can occur at container walls, or on particles of a foreign nature such as dust. The work of forming a heterogeneous nucleus at a surface is still proportional to $1/\Delta T_b^2$, but the proportionality constant is reduced. Thus metastable separation will more readily occur by heterogeneous nucleation. Caution must be observed to keep any glass melt under study free from contamination, and interpretation of results for glasses cooling at surfaces must be treated with care.

Just above the spinodal, the work needed to form the droplet is proportional to $\Delta T_s^{3/2}$ where ΔT_s is the temperature of the phase above the value at the spinodal. At the spinodal this work is reduced to zero.

After nucleation in the metastable region of phase separation, the rate of separation is dependent on the number of nuclei formed. This type of separation is characterised by a distinct new unconnected phase growing in a matrix of the original phase. These droplets may in time grow and coalesce. The second phase is thought to be invariant in composition with time of heat treatment at constant temperature, and exhibits a sharp boundary with the matrix. Second phase droplet sizes show a tendency towards a random distribution, and no ordering is noticed in their position in the homogeneous matrix.

4.1.3   Spinodal phase separation

While the kinetics of phase separation of compositions which lie between the spinodal and the line

defining the region metastable to phase separation are
generally agreed to be nucleation and growth, there is
still much contention about the kinetics involved for
compositions which lie below the spinodal. Two main
theories have been proposed by Cahn (1961) and Haller (1965)
which will be discussed in turn.

4.1.4   Theory of Cahn

When a single phase liquid is cooled rapidly
enough through the region metastable to phase separation
so that appreciable decomposition does not occur, the theory
of Cahn maintains that the kinetics of phase separation
change after the spinodal has been crossed. In this theory
it is proposed that growth of the nuclei ceases, and
stationary compositional waves form in the matrix which
reduce the free energy, and initially grow in amplitude
only. Two completely interpenetrating phases result whose
mutual boundaries are at first quite diffuse, but as further
separation reduces the free energy the phases move further
apart in composition and become better defined. The inter-
connectivity of the phases is initially at a maximum and
decreases with time; long heat treatments can actually
result in the minor phase becoming disconnected to form
droplets in the matrix of the complementary phase.

Cahn (1965) has developed a mathematical analysis
for his theory. He has shown that the time constant τ
for the increase in amplitude of the compositional
fluctuations is inversely proportional to the square of

the undercooling below the spinodal ΔT_s, and is also inversely proportional to the mobility of the migrating species. Thus τ, which is infinite at the spinodal, decreases to a minimum with undercooling, but increases again as the diffusional mobility decreases with decreasing temperature. Cahn and Charles (1965) have shown that the minimum value of τ occurs when $\Delta T_s \simeq 10\%$ of the spinodal temperature. They have derived a formula for calculating τ,

$$\tau \simeq \frac{\lambda^2}{8\pi^2 D} \cdot \frac{T}{\Delta T_s}$$

where λ is the wavelength of the compositional fluctuations, and D is the diffusion coefficient, in this case defined as the ratio of diffusional flux to the partial molar free energy gradient. Typically in a $Na_2O-B_2O_3-SiO_2$ glass melt, $T = 1000°K$, $\Delta T_s = 100°K$ (for a minimum τ), $\lambda = 100\text{Å}$, hence $\tau = 10^{-13}/D$. The diffusional coefficient may be anywhere in the region 10^{-13} to 10^{-5}, showing that τ is usually less than 1 sec and may be as small as 1 μsec. Thus, isothermal spinodal decomposition is difficult to observe during its initial stages due to the rapidity of the unmixing.

To calculate the cooling rate $\frac{dT}{dt}$ necessary to avoid phase separation, the time required to pass the temperature $T - \Delta T_s$ is equated to the minimum value of τ. This time is of the order of $T_s/(dT/dt)$. Thus

$$\frac{dT}{dt} \simeq \frac{8\pi^2 D \Delta T_s}{\lambda^2 T} \quad \text{to avoid phase separation. Substituting}$$

values as before it may be seen that cooling rates of $1^{\circ}C$/sec are needed if D is very small at 10^{-15} cm^2/sec, and rates of $10^{3\circ}C$/sec are necessary if D is 10^{-12} cm^2/sec. With diffusional constants any larger than this, spinodal decomposition is almost unavoidable, though some hope may be offered in systems where the spinodal lies near or below the glass transition temperature and the mobility of the migrating species is extremely small.

4.1.5   Theory of Haller

Haller has shown that spherical growth from randomly emplaced nuclei can lead to an interconnected phase separation morphology provided that the volume fraction of the nucleated phase is sufficiently high. The interconnection arises from the lumping together of the individual spherical second phase droplets. Haller has theoretically determined the dependence of the interfacial area with time for various simplified transport models, and has found that this area is proportional to $t^{-\frac{1}{2}}$. Experimental observations of the advancement of phase separation in the Na_2O-SiO_2 system show good agreement with this dependence, and Haller concludes that an interfacial controlled bulk diffusion process is operative during the growth of the droplets.

A feature of Haller's interconnecting growth theory is that the degree of interconnectivity will increase with time, whereas Cahn's theory predicts that the interconnectivity of the structure decreases from a

maximum as the degree of phase separation increases.
Experimental observation of interconnectivity behaviour
in the initial stage of phase separation should distinguish
between the proposed mechanisms.

4.1.6 The opposing theories of spinodal decomposition; a comparison

A large number of investigators have undertaken
experiments to determine which of the two mechanisms is
applicable to spinodal phase separation in glass forming
liquids, but no general agreement, as yet, has been
reached. The rapidity of spinodal phase separation is
an obstacle in the course of isothermal phase separation
observations; knowledge of the phase morphology in the
early stages of separation is essential in distinguishing
between the two theories. Zarzycki and Naudin (1967)
have examined the decomposition of $PbO-B_2O_3$ glasses by
an X-ray scattering technique; the addition of Al_2O_3
in small amounts was made to slow the phase separation
procedure without disturbing the basic features of the
miscibility gap. Their results favoured the theory of
Cahn, but some discrepancy in the observed value of the
spinodal temperature casts some doubt upon the validity
of their work. Seward et al (1968) have shown that
vapour deposited films of $BaO-SiO_2$ glass heated in the
beam of an electron microscope produced an inter-
connected structure from the growth and lumping of
individual particles, but as the temperature could not

be ascertained, it is impossible to say in which
temperature range this mechanism is more favourable
than that of Cahn. However, as the compositions were
at the centre of the miscibility gap, they would most
likely have been in the spinodal region of phase separa-
tion if a spinodal exists for this system. Srinivasan
et al (1971) have made observations on the time dependence
of the connectivity of a sample of $Na_2O-B_2O_3-SiO_2$ glass
in the centre of the miscibility gap of this system,
and have suggested that their results are consistent
with the mechanism proposed by Haller. They also noted
that for three samples of identical composition, heat
treated at 748°C, 720°C and 650°C, the degree of
connectivity of the second phase particles is strongly
dependent upon the volume fraction of the phase, in
keeping with the theory of Haller.

However, to further complicate the issue over
the mechanisms of phase separation below the spinodal,
Simmons, Macedo et al (1968, 1970; 1971,a.b) have
found that for many inorganic oxide melts, including
$Na_2O-B_2O-SiO_2$ glasses well away in composition from
the region of liquid immiscibility, there is an 'excess'
viscosity. They have evolved a model to predict the
correct activation energy distribution for viscous
flow in these glasses whose physical significance is
the presence of microstructure in the melt. The size
of this microstructure is about 50Å in radius, in a
$Na_2O-B_2O_3-SiO_2$ glass, suggesting that the glass is in

fact heterogeneous in the melt. The sizes of the
regions of microstructure vary with melt temperature,
and thus it is expected and indeed observed that the
phase separation shown by a glass sample upon heat
treatment in the subliquidus region is in fact dependent
upon the melt temperature at manufacture. This is again
a firm reason why the thermal history of a glass must
be known before the structural characterisation is
complete, and is a detail unrecognized by many investi-
gators of phase-separation phenomena. So if in fact the
glasses are heterogeneous in the melt, what is the
significance of the coexistence curve defining the limit
to metastable immiscibility? It is of more than
philosophical value to conject that any two phase system
can be anything but phase separated on a molecular scale;
the definition of phase separation must depend upon the
scale in question. This leads us to a further look at
subliquidus immiscibility, and the question of the
determination of the position of the two phase boundary
for a glassy system.

4.1.7   The coexistence curve and subliquidus immiscibility

Just as any two liquids may show partial
immiscibility, so may two solids. True subliquidus
immiscibility occurs when the coexistence curve does
not intersect the liquidus. Thus, there are regions
on the phase diagram where a single-phase binary solid
is stable at one temperature, but on cooling the

single-phase will first become metastable and then unstable to decomposition.

The method used by investigators of the coexistence curve, which is the boundary of two-phase metastability, is normally to heat treat a glass for a considerable length of time and then decide from the absence or presence of opalicity whether the glass composition at that temperature lies above or below the coexistence curve. A blue-white hazy appearance results from the scattering of light at the interphase boundaries, and is evidence of phase-separation. Transparent glasses thus fall into the category of homogeneity and are considered to be single-phase.

In the well-known paper by Rockett et al (1965) the coexistence curve in the system $SiO_4-Na_2B_8O_{13}$ has been determined by such a method. However, electron microscopy (Scholes, private communication) has revealed that glasses in the same system which appear transparent and have been placed in the region above the coexistence curve actually have a two-phase structure on a very small scale. It thus appears that the experimental position of the curve depends on the method used to determine it. We can thus pose the question of whether the coexistence curve determined by opalicity and clearning experiments defines the limit to metastable immiscibility. Such a definition is reliant on a size effect; that is the glass is considered as

homogeneous when the phase-separated regions are too small to scatter visible light. Although this must be regarded as a major criticism of this method of investigating the coexistence curve, the results obtained through such a convenient method are not too much in disagreement with those obtained using electron microscopy. As we shall see in the next section, the metastability dome for the $Na_2O-B_2O_3-SiO_2$ system determined by opalicity and clearing experiments is in good agreement with answers obtained from direct analyses of the phases of separated glasses.

It must be stressed that glasses which are optically clear must not be regarded as necessarily single phase; the more sensitive method of the determination of the phase-separation chatacteristics by electron microscopy provides a better criterion for distinguishing between heterogeneity and homogeneity.

4.1.8   Ternary systems : $Na_2O-B_2O_3-SiO_2$

A three-component system may be treated thermo-dynamically in a very similar way to a binary system. If two legs of a ternary exhibit metastable immiscibility, then a region of metastable immiscibility is expected in the area between them. Given metastable immiscibility along the $Na_2O-B_2O_3$ and Na_2O-SiO_2 edges of the $Na_2O-B_2O_3-SiO_2$ system, (Skatulla, 1958), and true liquid immiscibility along the $SiO_2-B_2O_3$ edge at low concentrations of B_2O_3, metastable immiscibility is expected over a large portion of the diagram.

Figure4.2 Metastability surface of $Na_2O-B_2O_3-SiO_2$ (Charles,1970)
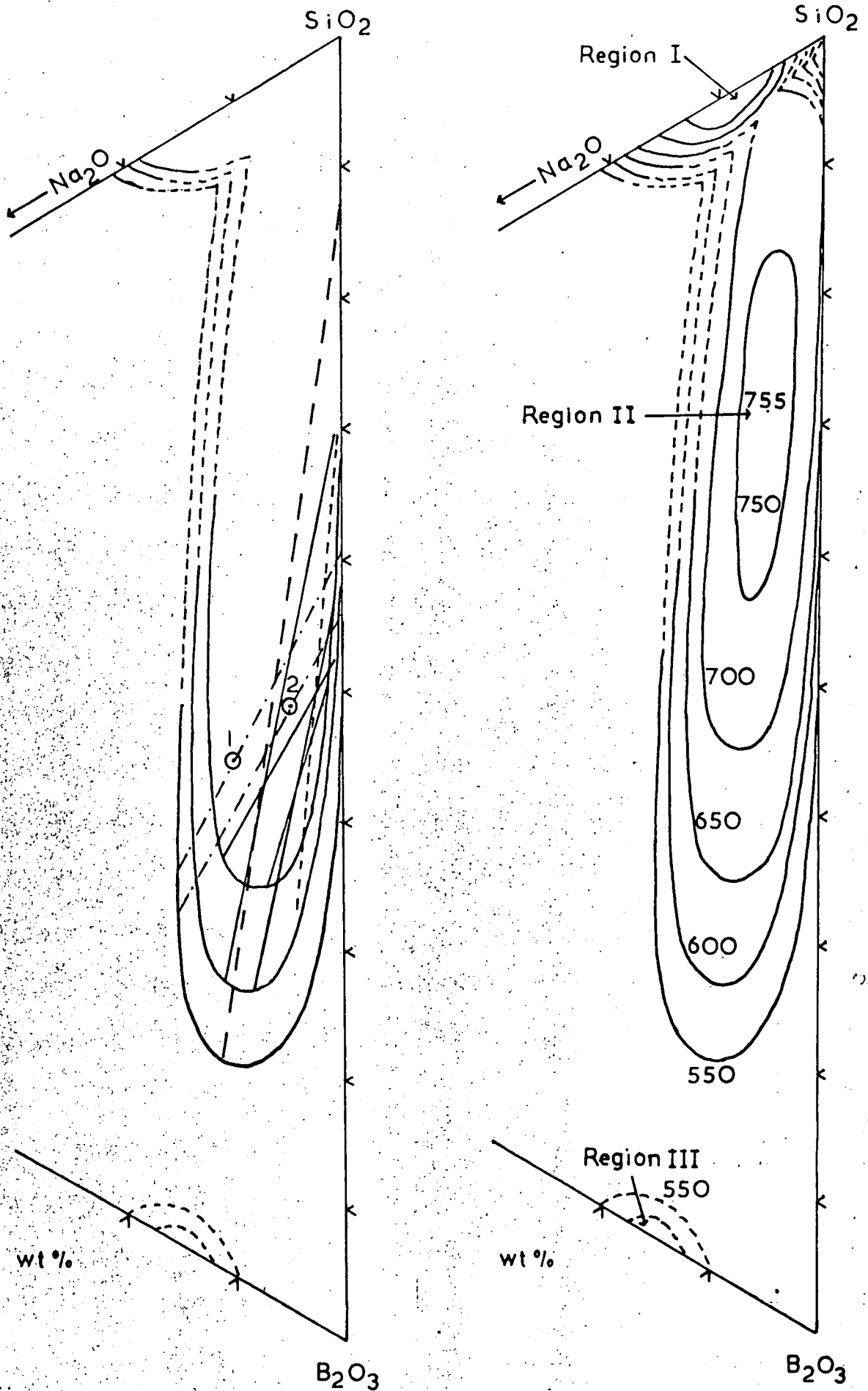
Tie lines:

—·—·— this work, from volume fractions of electron micrographs

——— Scholes (1970), — — — Charles (1970), — — — — Tran(1965)

Figure 4.2 shows the ternary diagram of Charles et al (1970), who determined the isotherms by opalicity and clearing experiments of about 100 different glass compositions. These isotherms are estimated to be correct to $\pm 10^{\circ}C$. This diagram is in general agreement with results of similar studies of Galakhov (1969), except that this author does not accept that the region I near the SiO_2-Na_2O edge intersects the main region II, due to a lowering of the Tg surface below the coexistence boundary. The consulate temperature of region II is estimated to be $755^{\circ}C$. Although the region of metastability is restricted to a region of relatively low Na_2O content along the SiO_2-B_2O_3 edge, glass formation is observed over a large portion of the diagram.

To fully exploit the usefulness of this diagram, it is desirable to draw in tie lines. The difficulty here lies in determining the composition of the phases after separation has taken place. Analysis of electron micrographs of phase separated glasses should provide volume ratios at the phases present, and thus by the application of the lever rule it should be possible to draw in tie lines. However, Burnett (1968) has shown that this method is prone to inaccuracy as the leaching of the phases in a direction perpendicular to the plane of the electronmicrograph has the effect of slightly exaggerating the volume fraction of the phase most resistant to the etch, usually the silica rich phase.

Tie-lines based on analyses of glasses leached in HCl
to remove the continuous B_2O_3 rich phase in spinodally
decomposed glasses also suffer from the error that SiO_2
is precipitated in the pores after leaching (Mazurin 1969),
and it is also possible that Na^+ ions can diffuse out
from the silica rich remaining phase (Charles 1965).
Scholes and Wilkinson (1970) have heat treated
$Na_2O-B_2O_3-SiO_2$ glasses until the separation is of the
order of 5 to 10μ in size, and have investigated the
phase composition by electron probe microanalysis.
These are the first tie lines to be drawn from experiments
made by direct analysis of the phases in situo. Although
their tie lines lie in the general direction of those
suggested by the former workers, they do expose certain
differences in their directions. Figure 4.2 shows the
various tie lines for Charles (1970), Tran (1965) and
Scholes and Wilkinson for a temperature of 600°C, and
the latter authors also for the tie line at 650°C.
However there is general agreement between workers for
the sense of rotation of the tie lines with increasing
temperature. It is also of note that the tie-lines of
Scholes and Wilkinson terminate on the isotherms of
metastability found by Charles (1970) appropriate to
the temperature of heat treatment. From this we must
conclude that despite the various limitations to the
method of determining the metastability dome by
opalescence and clearing, it yields a good result at
least for the glass compositions in the area of the
ternary diagram in question.

Figure 4.3   Na$_2$O–B$_2$O$_3$–SiO$_2$ glass
compositions
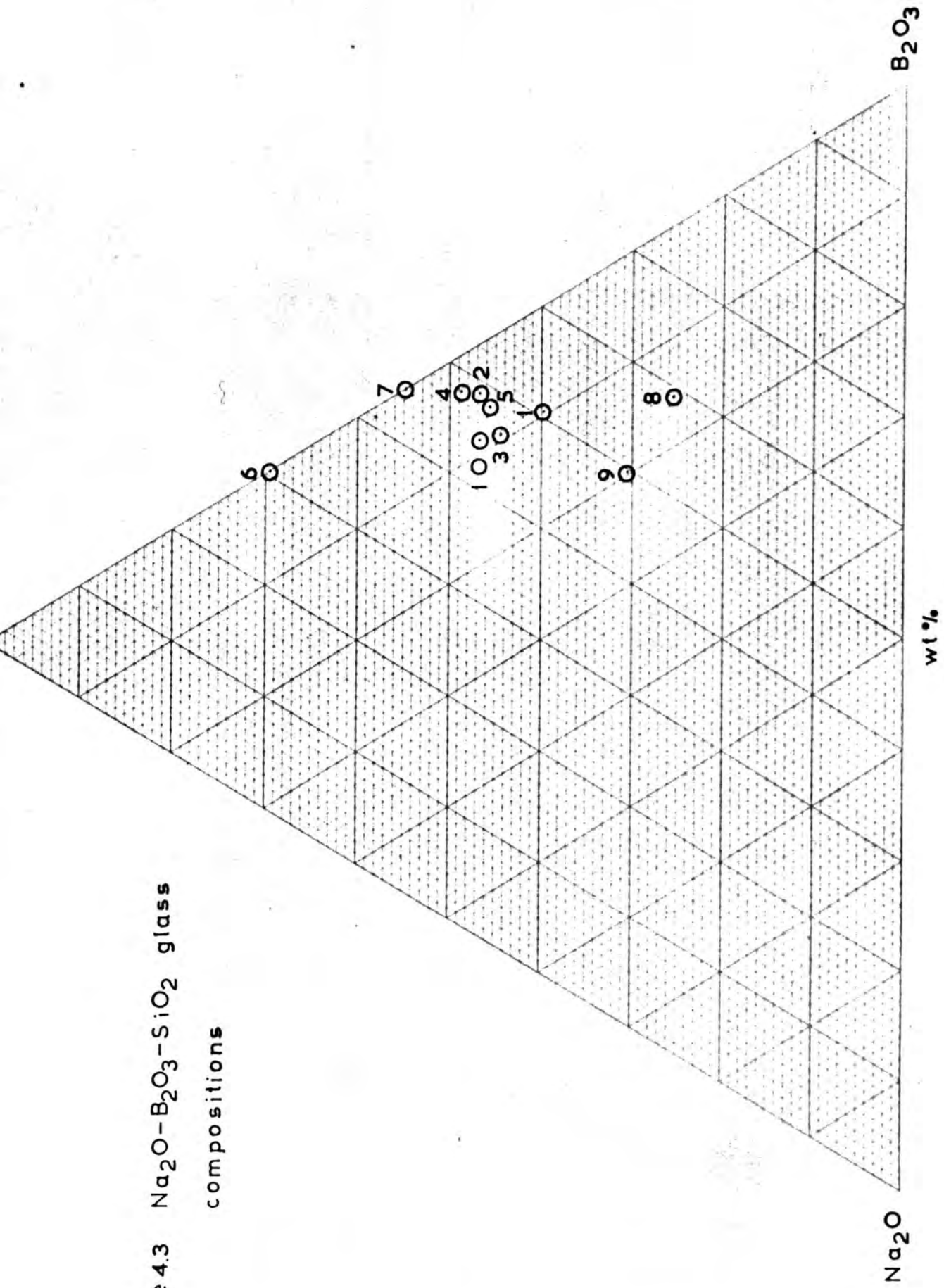
Charles and Turkalo (1969) have investigated the question of three-liquid immiscibility in the $Na_2O-B_2O_3-SiO_2$ system, the possibility of which was suggested by Vogel (1965) and Kuhne and Skatulla (1959). They found no evidence to support this possibility, which was also partly based on directions and end-points of tie lines proposed by Charles et al (1970) which are now thought to be incorrect.

Preparation and characterisation of the glass samples

4.2.1   Manufacture

Glass compositions for study in this work were chosen to lie in and around that region of the ternary phase diagram of the $Na_2O-B_2O_3-SiO_2$ system where sub-liquidus immiscibility occurs, and are plotted on the ternary diagram in Figure 4.3, and are also given in Table 4.1.   The compositions of glasses 1 and 2 were selected such that heat treatment at $550^{O}C$ would result in interconnected and droplet structures respectively.   The glass batches were prepared from 120 mesh Brazilian quartz, and analytical grade B_2O_3 and Na_2CO_3.   About 1 wt.% of $NaNO_3$ was included to oxidise any metallic ions present and thus prevent the platinum crucible, in which the batches were melted, from attack.   Platinum ions are known to be strong nucleating agents in inorganic glass systems and their presence would lead to anomalous phase separation (Rindone and Ryder, 1957).

Glass Batch No.	wt%			mole%			$Tg\,^{\circ}C$	$Mg\,^{\circ}C$	$\times10^{-7}/^{\circ}C$
	Na_2O	B_2O_3	SiO_2	Na_2O	B_2O_3	SiO_2			
1	10.0	50.5	39.7	10.4	46.9	42.7	453	495	65.1
2	4.4	48.9	46.6	4.6	45.3	50.1	392	460	54.8
3	8.8	44.5	6.7	9.1	41.0	49.9		(495)	
4	3.3	48.7	48.0	3.4	45.1	51.5		(460)	
5	6.2	48.1	45.7	6.4	44.5	49.0		(480)	
6	0	30.5	69.5	0	27.2	72.8		(450)	
7	0	45.3	54.7	0	41.7	58.3	351	431	49.7
8	15.1	59.1	25.6	16.0	55.9	28.1	469	504	80.0
9	19.8	49.7	30.3	20.8	46.4	32.8	500	529	98.9
10	9.6	46.1	44.4	9.9	42.6	47.5		(495)	

Table 4.1

$Na_2O-B_2O_3-SiO_2$ glass compositions obtained from chemical analysis, Tg and Mg points, and coefficients of thermal expansion.

After the appropriate amounts of each constituent had been weighed out they were crushed in an agate mill and agitated in an automatic mixer for fifteen minutes to form a homogeneous powder. Each glass was melted in the platinum crucible complete with lid in an electric furnace. Founding temperatures and times were such as to ensure that the final products were seen and batch free; glasses 1 to 5 and 10 were successfully melted at $1450^{\circ}C$ for $3\frac{1}{2}$ hours, glasses 6 and 7 at $1600^{\circ}C$ for 8 hours, and glasses 8 and 9 at $1200^{\circ}C$ for $3\frac{1}{2}$ hours. Two binary B_2O_3-SiO_2 glasses of lower mole fraction B_2O_3 than glasses 6 and 7 were prepared but not successfully melted; only a sintered powder resulted as the high melting temperature required could not be attained in the available furnace.

To see if a reduction in OH content has any large effect on the propagation characteristics of ultrasound in the Na_2O-B_2O_3-SiO_2 system, glasses 3, 5, 8 and 9 were bubbled with dry nitrogen for 10 minutes immediately before the end of the found. This procedure has the effect of reducing the water content. Glasses 6 and 7 could not be bubbled due to their high viscosity. All glasses were stirred occasionally to improve their homogeneity.

The molten glass batches were poured into cold, steel button moulds of diameter $1\frac{1}{2}$ inches and thickness $\frac{1}{2}$ inch. Specimens any larger than this cooled too slowly and developed the hazy blue appearance character-istic of large scale phase separation. On removal from

the mould the samples were wrapped in asbestos cloth and left to cool further on top of a warm furnace.

Internal strain was seen in all samples when viewed between crossed polaroids. It was necessary to remove this strain or the resultant elastic inhomo- geneities would give spurious results in the ultrasonic velocity and attenuation measurements. To assess the temperatures required for strain annealing, the Tg and Mg points of several of the samples were determined from plots of the temperature dependence of the thermal expansion. Figure 4.4 shows a typical plot, and indicates the position of the Tg and Mg points. Table 4.1 gives the Tg and Mg points for the glass samples for which they were determined; the figures in brackets indicate estimated Tg and Mg points. To remove the internal strain, the glass samples were heated to $20^{\circ}C$ below their Mg points, held steady for 10 minutes, and then slowly cooled by switching off the power to the furnace. Figure 4.5 shows a typical cooling curve for this procedure. All glasses showed relief of the internal strain after annealing except those from batch 2 which had to be heated to $410^{\circ}C$ to produce an effective anneal. Glasses which were studied in their quenched state were annealed immediately after manufacture; those which were heat treated to enhance phase separation were annealed after this treatment.

4.2.2. Heat treatment

To produce phase separation in certain batches in the $Na_2O-B_2O_3-SiO_2$ system, subsequent heat treatment was
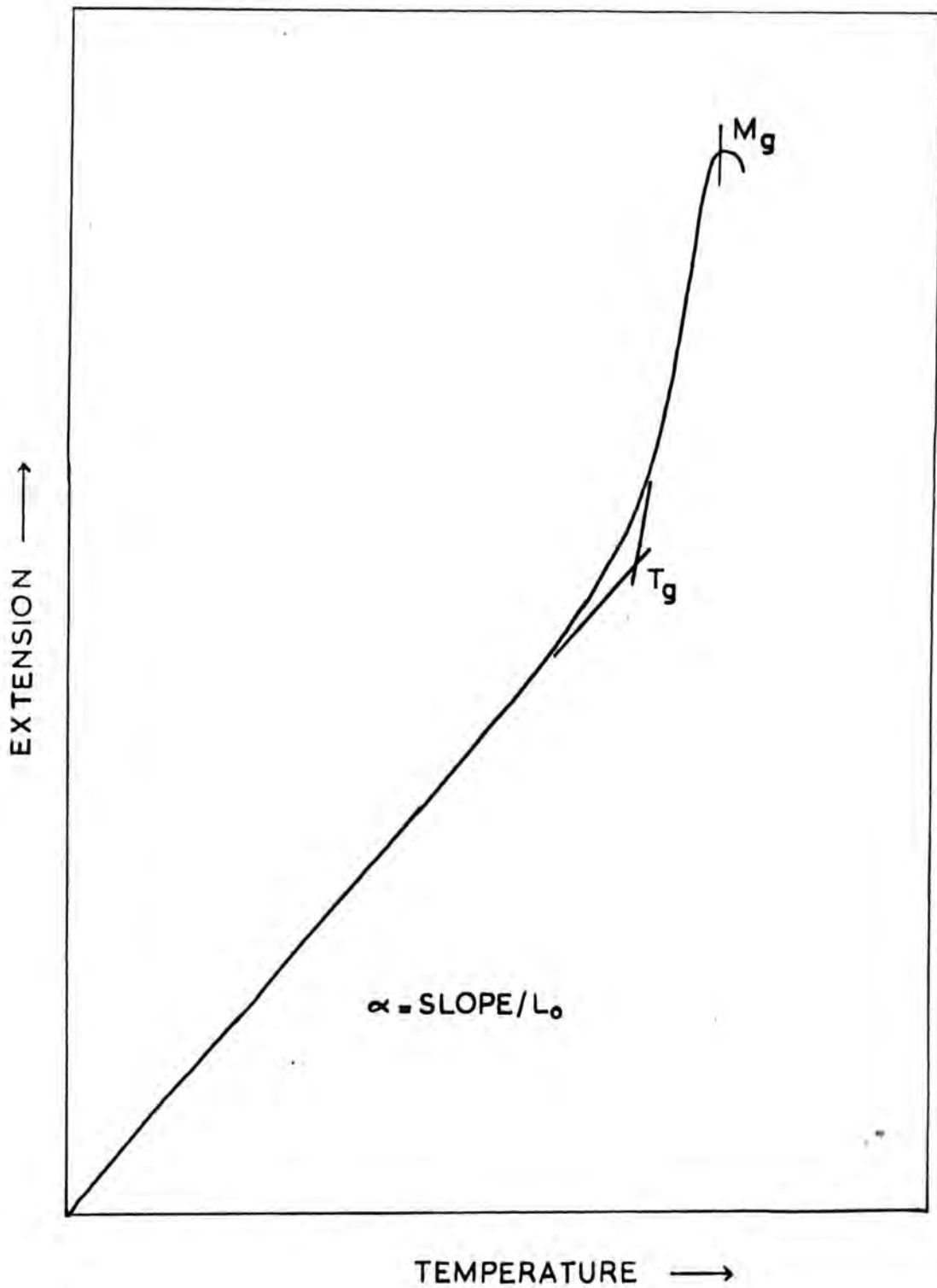
Figure 4.4   Estimation of Tg and Mg points from the thermal expansion curve.
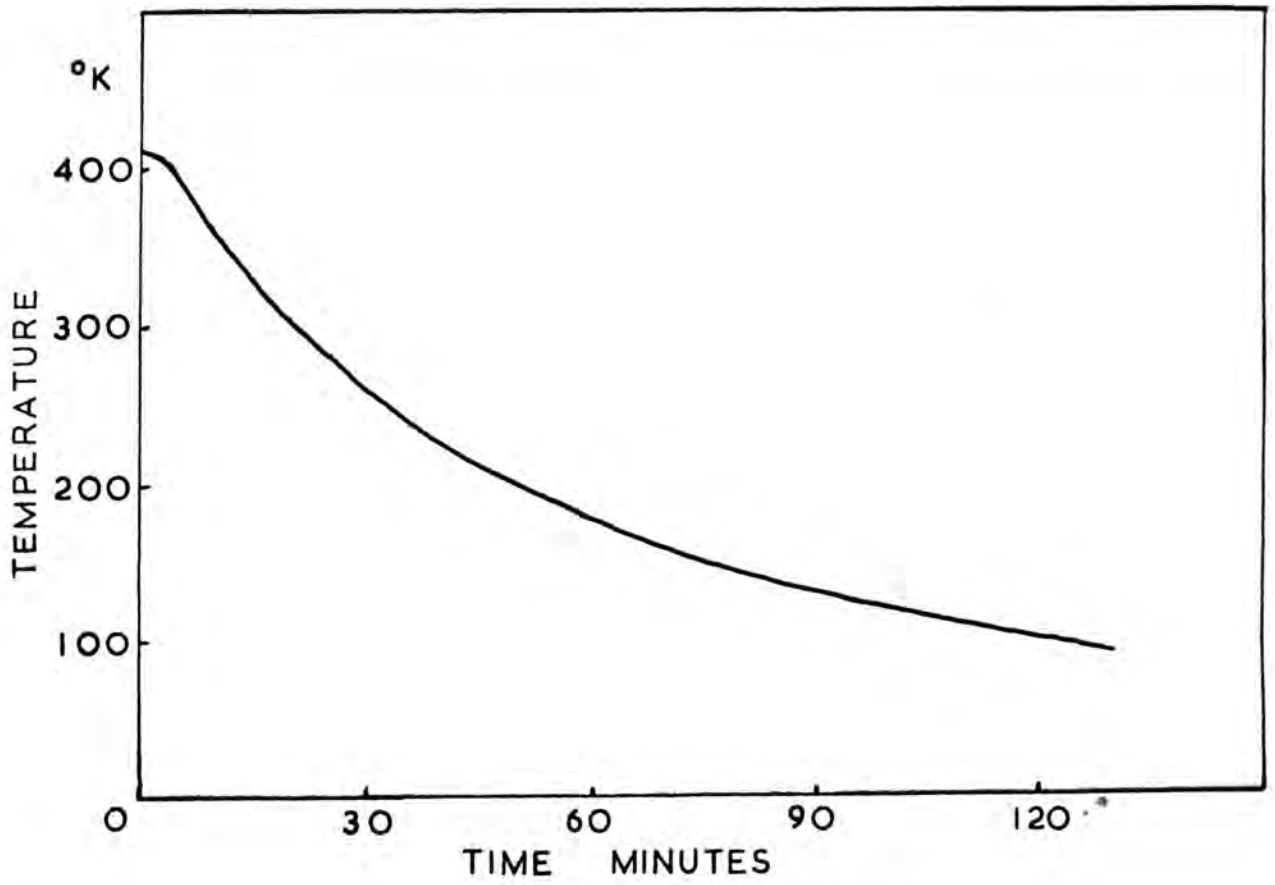
Figure 4.5 Typical cooling curve after strain annealing.

carried out at the appropriate temperature of 550°C.
Separate samples from batches 1 and 2 were heat treated
for 24, 48, 96, 168 and 504 hours, and from batches 4
and 5 for 48 hours. Heat treatment was terminated by
quenching in air, and the samples were subsequently
placed in a dessicator to cool.

For easy identification of the various glass
samples in the text to follow, the sample is represented
by its batch or composition number, and its time of heat
treatment at 550°C. For example, sample 2/48 is a glass
sample from batch 2 which has been heat treated for
48 hours at 550°C. An anteceding Q indicates that the
glass is quenched, and has received no heat treatment.

4.2.3 Cutting and polishing

The shape, size and finish of a sample for ultra-
sound measurements is dictated by the maximum tolerable
error in acoustic velocity and attenuation. Exact
details of the errors arising in the determination of
ultrasound velocity and attenuation are postponed until
Chapter 5. For the levels of attenuation in the samples
of glass of this study, parallelopipeds of dimension
13 x 13 x approximately 6 mm are required with a
parallelism between the faces perpendicular to the 6 mm
direction of better than 10^{-4} radians of arc, and with
a corresponding flatness so that the condition of
parallelism is maintained over the entire area of the
face.

Approximately sized specimens were cut from the button-shaped samples with a diamond wheel, and the two appropriate faces were polished on a Logitech semi-automatic lapping and polishing machine. A vacuum chuck is integral with the polishing apparatus to hold the sample during polishing, thus excluding the use of an adhesive which can cause non-parallelism in the final product. By careful adjustment of the polishing rig, and abrading the sample on a solder plate with successive sizes of diamond paste from 25μ down to $\frac{1}{4}\mu$, the desired parallelicity together with a flatness of a $\frac{1}{4}$ wavelength of light was attained. Measurements of these tolerances were made by observing the white-light fringes generated between the sample faces and an optical flat set up on the polishing stage of the Logitech machine. Visual examination evidenced the absence of scratches on the polished faces. A dial gauge was used to measure the sample thickness.

4.2.4. Density measurements

Sample densities were measured by an Archimedes principle method, using analytical grade methanol of previously determined density. The specimen was suspended by a nylon thread, and the volume of submerged thread was ascertained and used as a correction to the upthrust. During the experiment the methanol temperature was measured, and the density of $0.7915 g/cm^3$ at $19.8^{\circ}C$ was corrected for thermal expansion through the coefficient 3α equal to $119 \times 10^{-5}/^{\circ}C$

The choice of methanol was made for two reasons. Firstly, the low surface tension discourages bubbles of air from adhering to the sample during immersion, and also allows a fine balance to be obtained while the sample is submerged in the liquid as only a small surface tension force is exerted at the air-methanol interface. Secondly, methanol is not absorbed by and does not react with the glass compositions of this study, as evidenced by specimen weighing before and after immersion in methanol for 24 hours.

Results of the density determinations are shown in Table 6.1. Densities of different specimens of the same composition and heat treatment were found to be equal within experimental error evidencing good macroscopic homogeneity of the batch glasses; the quoted densities are for the specimens used in the ultrasound propagation experiments.

4.2.5 Estimation of the water or OH content

An efficient method of estimation of the water or OH content of a glass is by measurement of the infrared absorption or transmission spectrum. The effect of the OH or water content on the acoustic properties of glasses has been stressed in Chapter 3, and thus it is necessary to make a quantitative measurement of this content in the $Na_2O-B_2O_3-SiO_2$ glasses of this work for their full characterisation.

Samples of the quenched glasses were ground flat and parallel to a width of approximately 1 mm, and were stored in dry machine oil which was removed prior to experiment. Infra-red absorption spectra between 1μ and 2.5μ were measured with a Pye-Unicam spectrometer, and transmission spectra between 2.5μ and 5μ were measured with a Beckmann spectrometer. The absorption spectra measured with the former instrument were not intense enough for detailed resolution, so the measurements were repeated using the ultrasound specimens of thickness approximately 6 mm. The final spectra observed are shown in Figure 4.6

The dominant features of all the infra-red spectra of the $Na_2O-B_2O_3-SiO_2$ glasses of this present study are a large absorption band at approximately 2.8μ, and a smaller but quite distinctive band at about 1.4μ. These results are very similar to those of Adams (1961) who has demonstrated the effect of water content upon the infra-red spectra of B_2O_3 and SiO_2 glasses. He has shown that in these two glasses the fundamental OH vibration is observed at 2.79μ and 2.73μ, and the first overtone band of the unassociated OH ion at 1.40μ and 1.38μ respectively. Further evidence for the identification of the absorption bands in the $Na_2O-B_2O_3-SiO_2$ is found in the work of Franz (1966), who has observed the fundamental stretching frequency of OH ions in Li, Na and K borate glasses in a similar position in the infra-red spectrum.
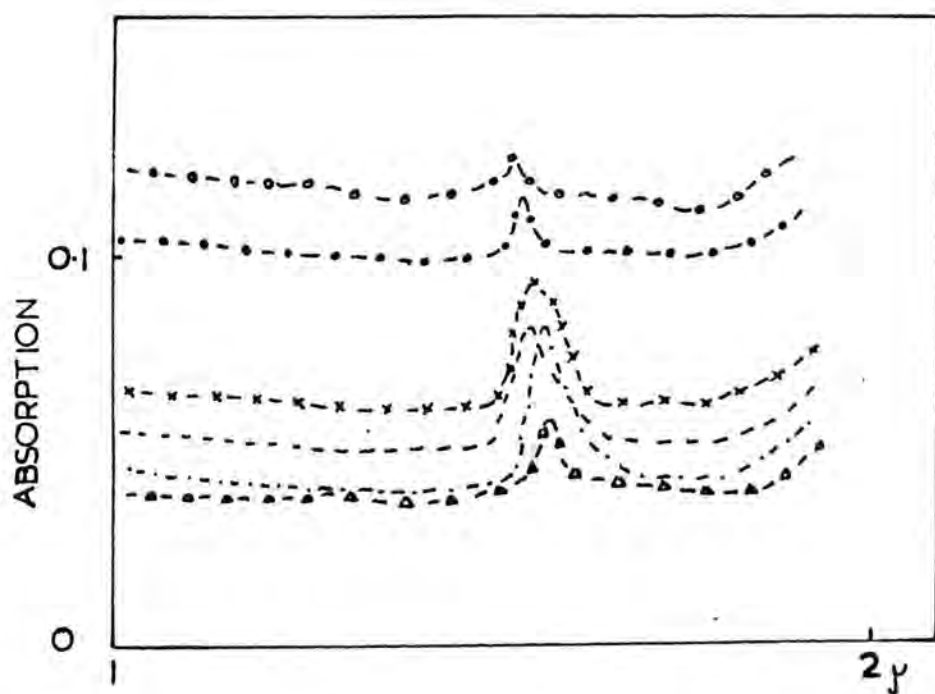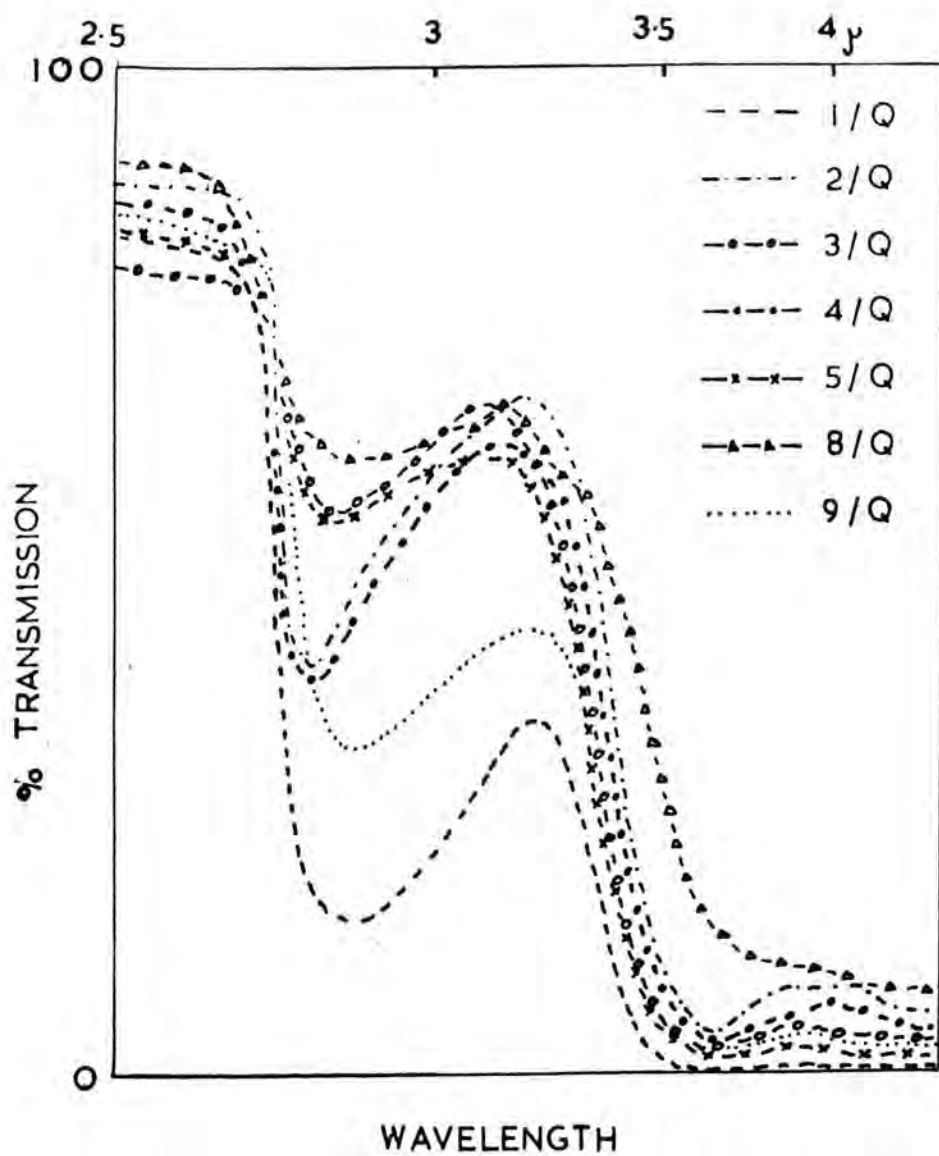
Figure 4.6 Infra-red spectra of $Na_2O - B_2O_3 - SiO_2$ glasses.

The problem in making a quantitative determination of OH content from the infra-red spectra is choosing the extinction coefficient α for the glass to use in the Lambert-Beer equation. This equation takes the form

$$E = \alpha C = \frac{1}{d} \log_e \frac{1}{D}$$

where E is the extinction of the spectrum at the peak, C is the concentration of the absorbing species, (in this case OH), d is the sample thickness and D is the fraction of the infra-red radiation transmitted. Nemec and Götz (1969) report an experimentally determined value for α of 49.1 ℓ/mole-cm for the fundamental OH vibration peak in a glass of composition SiO_2 50.86, Al_2O_3 14.84, B_2O_3 10.5, CaO 17.95, MgO 4.79, Na_2O 0.98, BaO 0.17 wt %. A comparison with the experimental values for the extinction coefficient found by Franz (1966) for Na_2O-B_2O_3 glasses containing 10-20 wt % Na_2O, suggests that a value for α of about 50 ℓ/mole-cm would not be too much in error for a Na_2O-B_2O_3-SiO_2 glass. This latter figure has been used to calculate the OH or water content of the glasses in this present study from the intensity of the infra-red absorption peak at 2.8μ; the results of these calculations are given in Table 4.2

No data on the extinction coefficient of the overtone band at 1.4μ is available to date. However, it is interesting to compare their relative intensities; these peaks are of size in approximate proportion to the OH concentration calculated from the fundamental

Table 4.2

OH or water content of $Na_2O-B_2O_3-SiO_2$ glasses calculated from the infra-red spectra

Glass Batch No.	Path Length cms	Calculated OH content p.p.m. (wt)
1	0.093	2,800
2	0.037	3,500
3	0.063	800
4	0.042	3,000
5	0.058	980
8	0.061	780
9	0.101	1,200

vibration peak at 2.8μ. More significantly, they are smaller than the corresponding absorption peak in the 'wet' B_2O_3 glass which showed anomalous acoustic attenuation (see Chapter 3) and are of the same order of magnitude for those of the 'dry' B_2O_3 glass (Kurkjian and Krause, 1966).

4.2.6   Electron microscopy

To determine the degree of morphology of the phase separation of both quenched and heat treated samples of the Na_2O-B_2O_3-SiO_2 glasses, transmission electron micrographs have been made of carbon replicas from freshly broken surfaces of each sample. Good definition of the separation structure has been obtained by etching the broken surface with water for 10 seconds, and pre-shadowing with platinum. Prints from samples of these micrographs are shown in Figures 4.7 to 4.10. Volume fractions of the individual glassy phases have been estimated where possible by lineal analysis of micrographs representing total areas of 5000 square microns. The features of the phase separation of each glass composition will now be discussed in turn.

Composition 1

Sample 1/Q is seen to be heterogeneous on a fine scale at high magnification though transparent and clear to the eye. The sample must then be considered as phase separated though the morphology is not

distinguishable. The micrographs of the samples that
have been heat treated at 550°C evidence that the
morphology is of the interconnected type and is thus
typical of glasses which have undergone unstable spinodal
decomposition. Mutual phase boundaries are sharp for all
the heat treated samples of this composition, and the
scale of the separation is approximately 3000Å. There
appears to be a little tendency for the minor phase to
break up even after 504 hours of treatment at 550°C but
there is no evidence of crystallisation in the bulk of
the glass although a little surface de-vitrification
was observed after the longest period of treatment.

The volume fractions of the SiO_2-rich B_2O_3-poor
unetched phase for the various samples are as follows:
1/24 0.38;   1/48 0.36;   1/96 0.38;   1/168 0.36;
1/504 0.37.   Thus, the constant value for the volume
fraction indicates that the phase separation is complete
in less than 24 hours of heat treatment and that the
phases are undergoing the ripening process consecutive
to the initial unmixing. This we also expect from
consideration of the cooling rates necessary to avoid
separation which were discussed in Section 4.1.4 of
this chapter. The slight variation in the figures for
the volume fraction of the individual phases is most
likely the result of over-etching of the water soluble
phase.

Assuming equal density for the two phases, the
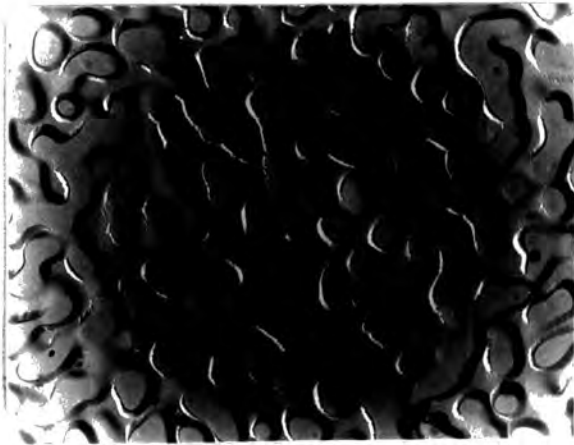tie-line for this glass has been drawn on the diagram
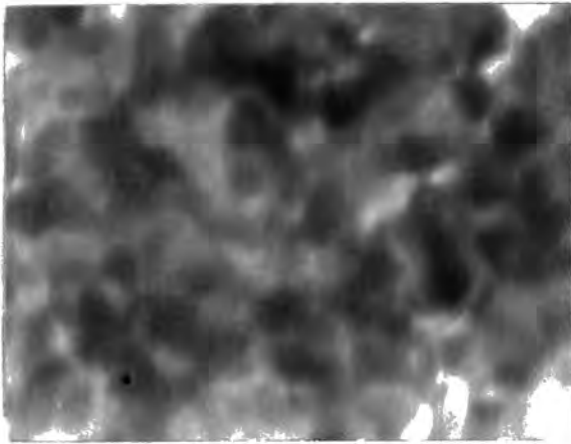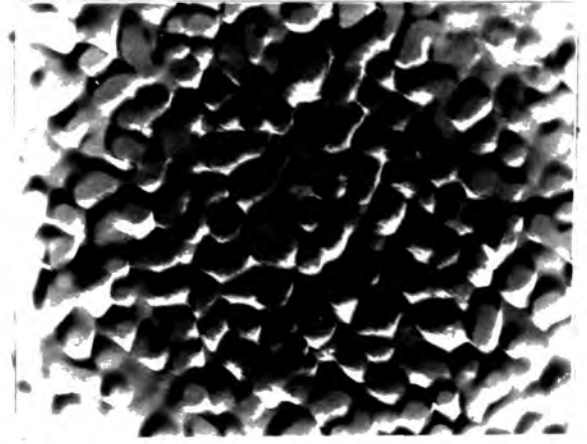
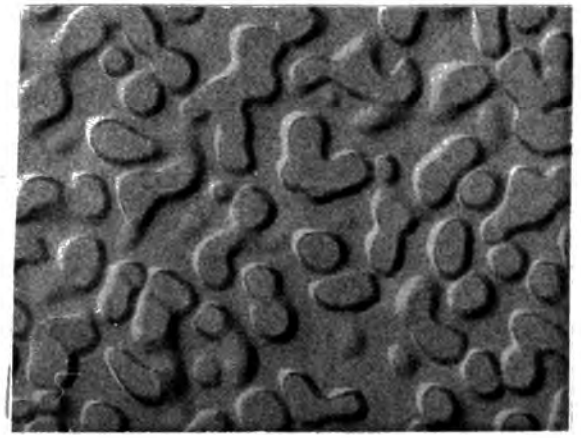|			
1/Q	X185,000	1/24	X 29,500
1/48	X 29,500	1/96	X29,500
1/168	X 29,500	1/504	X 29,500

Figure 4.7 Electron micrographs of glasses in batch I.

of Charles in Figure 4.3. The direction for this tie-
line agrees with those of previous workers and confirms
the assignation of an SiO_2-rich B_2O_3-poor composition
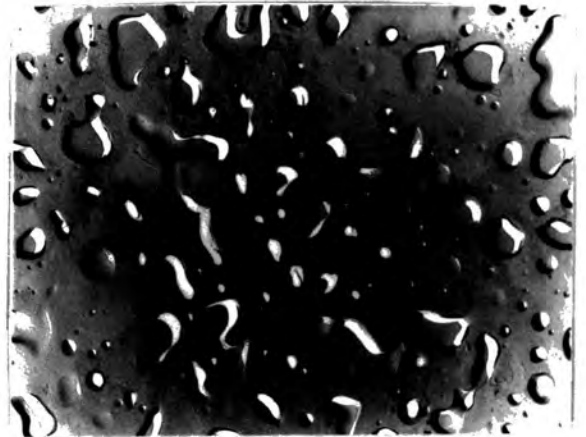to the minor phase.

Composition 2

The quenched sample of this composition shows
quite distinct phase separation in the form of droplets
of maximum diameter about 500 $\overset{o}{A}$, dispersed in the
complementary phase. A variation in the shape and size
of these droplets is apparent though the mutual phase
boundaries are not well defined. This glass shows no
opalescence, but too must be regarded as phase separated.
Heat treatment at 550°C reveals a droplet structured
minor phase which is shown by differential etching to be
the B_2O_3-rich phase. This is typical morphology for a
glass undergoing metastable decomposition. The droplets
are randomly positioned in the structure and grown in
maximum linear dimension of about 7000 $\overset{o}{A}$ after 24 hours
of heat treatment to about 5µ after 504 hours. Minimisa-
tion of the interfacial energy causes the spheroidation
of the nucleated phase as the separation proceeds. No
crystallisation is apparent in any of the glass samples.

Nucleated phase volume fractions are estimated
as: 2/24 0.28; 2/48 0.29; 2/96 0.28; 2/168 0.28;
2/504 0.29. Once again the constant volume for this
value evidences that the individual phases have reached
their final compositions before 24 hours of heat
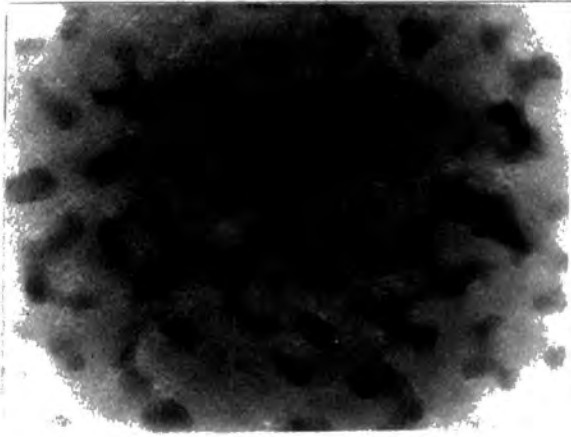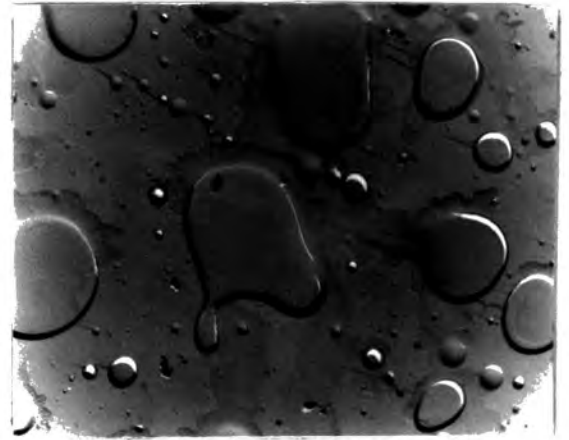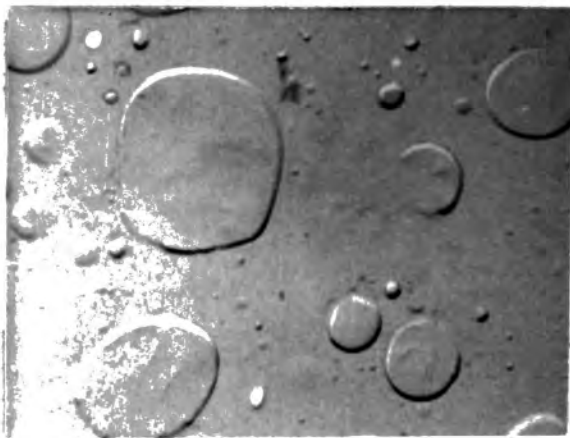
| 2/Q | X 185,000 | 2/24 | X 7,300 |

| 2/48 | X 7,300 | 2/96 | X 7,300 |

| 2/168 | X 7,300 | 2/504 | X 7,300 |

Figure 4.8   Electron micrographs of glasses in batch 2

treatment and that the glasses in this series represent various stages of coalescence of the minor phase.

Figure 4.3 shows the tie-line for this glass on the assumption of equal densities of the phases; its direction is nearly parallel to that for composition 1, and supports the contention that the minor phase is B_2O_3, Na_2O-rich and SiO_2-poor.

Composition 3

Glass 3/Q is seen to be heterogeneous, with separation occurring on a scale between 500 Å and 1000 Å. This sample shows no blue hazy appearance typical of phase separation but must be regarded as separated.

Composition 4

The quenched sample of composition 4 is separated on a scale of 1000 Å to 3000 Å but is optically quite clear. After 48 hours of treatment at $550^{\circ}C$ this glass shows a phase separation of size 1μ to 3μ. The morphology is difficult to determine; boundaries are sharp yet no large distribution in second phase particle size is evident. This second phase appears to be undergoing a transition between an inter-connected and a droplet structure, and has a volume fraction of 0.37. A B_2O_3-rich SiO_2-poor composition is evident for this phase.
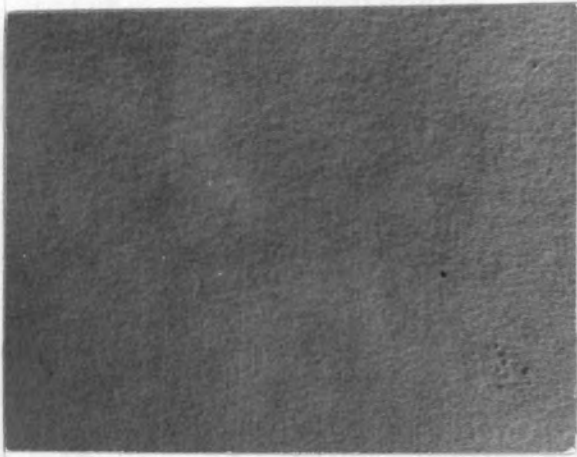
3 / Q   X 13,500
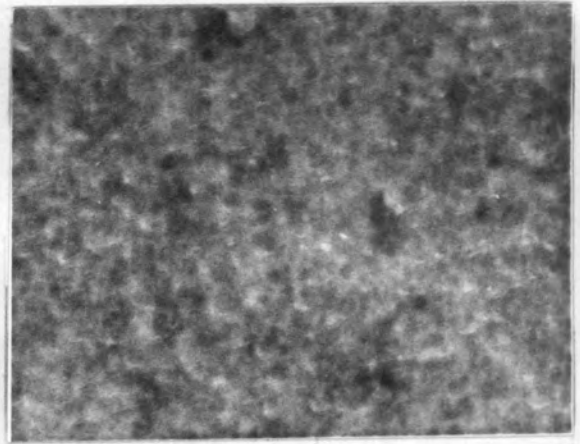
10 / Q   X 35,500

4 / Q   X 35,500

4 / 48   X 13,500

5 / Q   X 13,500
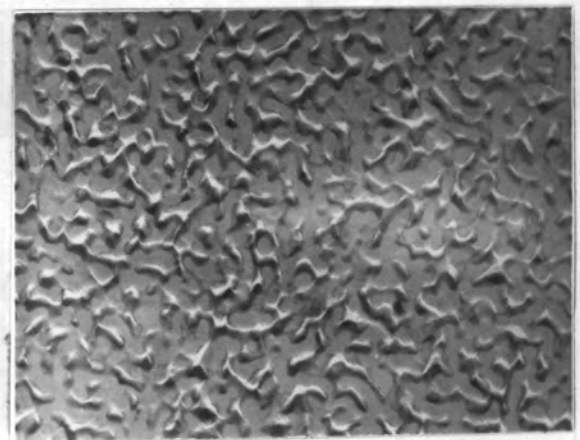
5 / 48   X 13,500

Figure 4.9   Electron   micrographs   of   glasses   in   batches
3, 4, 5 and 10.

Composition 5

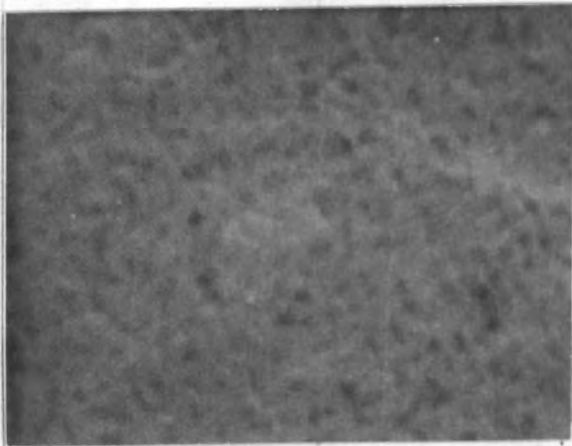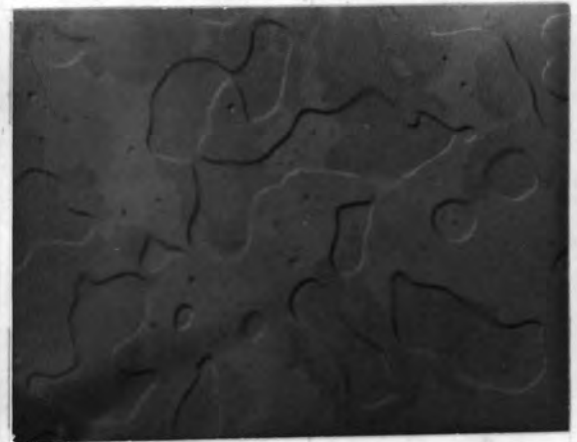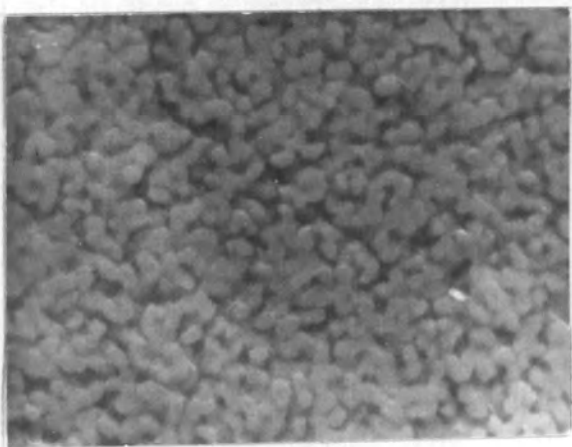Although sampe 5/Q is visibly clear, a very pronounced interconnected structure of approximately 1000 $\overset{o}{A}$ is revealed by the electron microscope. After 48 hours of heat treatment at 550°C the structure has coarsened considerably and the two phases are now distinctively separated by sharp boundaries. This sample has undergone spinodal decomposition and the volume fraction of the B_2O_3 rich etched phase is 0.54. It is difficult to confirm this from the phase diagram of Charles (1970) as the distances of the ends of the tie-lines to the starting composition are nearly equal.

Compositions 6 and 7

These two binary glasses show separation on a fine scale in the quenched condition. Sample 6/Q evidences heterogeneities between 200 $\overset{o}{A}$ and 500 $\overset{o}{A}$ in size, and for 7/Q these distinct regions are 500 $\overset{o}{A}$ to 1000 $\overset{o}{A}$ in size. Both glasses are optically clear.

Composition 8

The composition of this glass places it on the 550°C isotherm of metastability proposed by Charles. The quenched sample of this glass evidences some phase separated character on a scale of 2000 $\overset{o}{A}$ to 4000 $\overset{o}{A}$ and must be regarded as phase separated although it is optically clear.
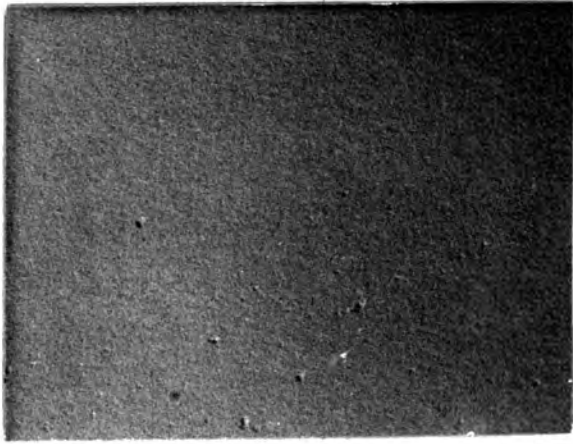
6 / Q   X 35,500

7 / Q   X 35,500
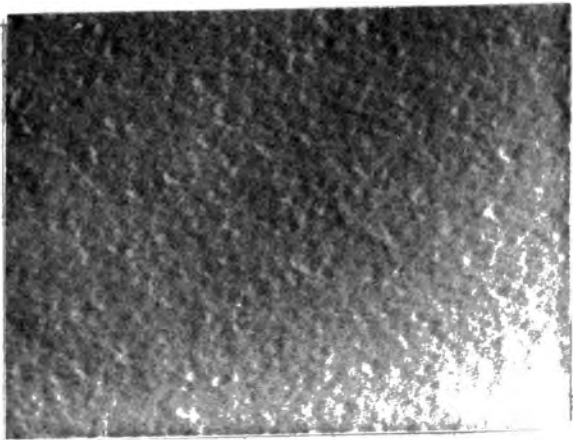
8 / Q   X 35,500

9 / Q   X 35,500

Figure 4.10 Electron micrographs of glasses in batches
6, 7, 8 and 9.

Composition 9

The composition of this glass was chosen to lie outside the area indicated in all the previous studies where sub-liquidus immiscibility occurs in the $Na_2O-B_2O_3-SiO_2$ system. Thus we do not expect any phase separation to be exhibited in this sample, and as such it should be unique amongst all the glasses of this present study. However, the micrographs of this quenched sample evidence a degree of heterogeneity in the structure on a small scale of about 2000 Å. The metastable dome proposed by Charles is based on opalescence and clearing observations; glass 9/Q would thus be judged as homogeneous, yet if the criteria of phase separation is whether the electron microscope reveals heterogeneity, this glass is separated.

Composition 10

A very distinct two phase structure is seen in the electron micrograph of sample 10/Q on a coarse scale of 1000 Å to 3000 Å. The exact morphology of this visibly clear glass is not discernable.

The more general conclusions to be drawn from the electron micrographs of the $Na_2O-B_2O_3-SiO_2$ glasses of this work are two in number. Firstly, all the glasses of this study whether quenched or heat treated are heterogeneous, and must be considered as phase-separated. Secondly, where the phase-separation morphology has been

discernable in the quenched sample of each glass
composition, the same morphology results on heat treat-
ment at 550°C. This is surprising as the thermal history
of a quenched glass is very indeterminate, and the phase-
separation occurring must be characteristic of the
separation processes over a large range of temperatures.
Such a function is further evidence that the micro-
structural characteristics of a phase-separated glass
are determined not only by the temperature of heat-
treatment, but also by the thermal history of the sample.

CHAPTER   FIVE

<u>THE EXPERIMENTAL METHOD</u>

Introduction

This chapter is concerned with the experimental methods involved in the measurement of ultrasound attenuation and velocity. A description of the electronic systems and the operating procedures involved in the determination of the ultrasound propagation characteristics of the $Na_2O-B_2O_3-SiO_2$ glasses are included with full details of the errors in measurement. Particulars of the quartz transducers used in the generation and detection of the ultrasound are found here, and the technique of transducer-sample acoustic bonding is outlined. The chapter concludes with specifications of the cryostats and furnace and the methods of thermometry and temperature control.

5.1.1   The Pulse-Echo Technique

The Pulse-Echo technique is used for the measurement of ultrasound velocity and attenuation, and involves the introduction of a pulse of ultrasound into a sample, observing the echoes as they reflect off two flat and parallel faces normal to the propagation direction of the stress wave. The delay between successive echoes is the transit time of the stress wave in the sample, and the decrease in pulse amplitude is a measure of the attenuation.

Ultrasound generation is achieved by applying a high voltage pulse of r.f. from a pulsed oscillator to a quartz transducer acoustically bonded to one of the sample faces. As a consequence of the converse piezo-electric effect, a stress wave is induced which travels at the velocity of sound to the opposite face. Reflection occurs at the discontinuity in the medium; the stress wave then returns to the initial face where a small amount of sound energy is transferred back to the quartz transducer. Here, as a result of the direct piezoelectric effect, a voltage pulse is induced in the transducer. The cycle of reflection is subsequently repeated to give a diminishing echo train which results in a series of voltage pulses from the transducer.

These received pulses are detected and displayed on an oscilloscope screen, the echo heights decrease exponentially with time, and the time between is the transit time of the sound in the sample. Deviations

from ideality of the transducer and sample system give rise to errors which will be dealt with later in this chapter.

5.1.2   Details of the Measuring System

Two experimental systems have been used for the measurement of ultrasound velocity and attenuation by the pulse-echo technique. Both are essentially the same: a Matec 9000 Attenuation Comparator, a complete system alone, and a Matec 6000 Pulse Modulator and Receiver which, when combined with a 1204A Master Synchronizer and Exponential Generator, and a suitable oscilloscope, form an equivalent circuit.

The basic circuit layout and principle of operation is shown in Figure 5.1. High voltage, high frequency pulses are generated by tunable pulsed oscillator plug-in units, ranging in r.f. frequency from 10 to 800 MHz which are connected into the 9000 or 6000 main frames. Amplitudes of up to 3KV are generated at the lowest frequencies, falling off a little at the highest. These pulses are transmitted by a matching 50Ω coaxial line to the quartz transducer by the T-R junction circuit shown in Figure 5.2. This circuit has the function of protecting the receiving amplifiers from the high-voltage initial pulses, directing them to the transducer. The low voltage pulses received from the transducer on excitation by the echoes force a high resistance in the direction of the oscillator, but only a low resistance towards the receiver, thus gaining maximum efficiency in the small
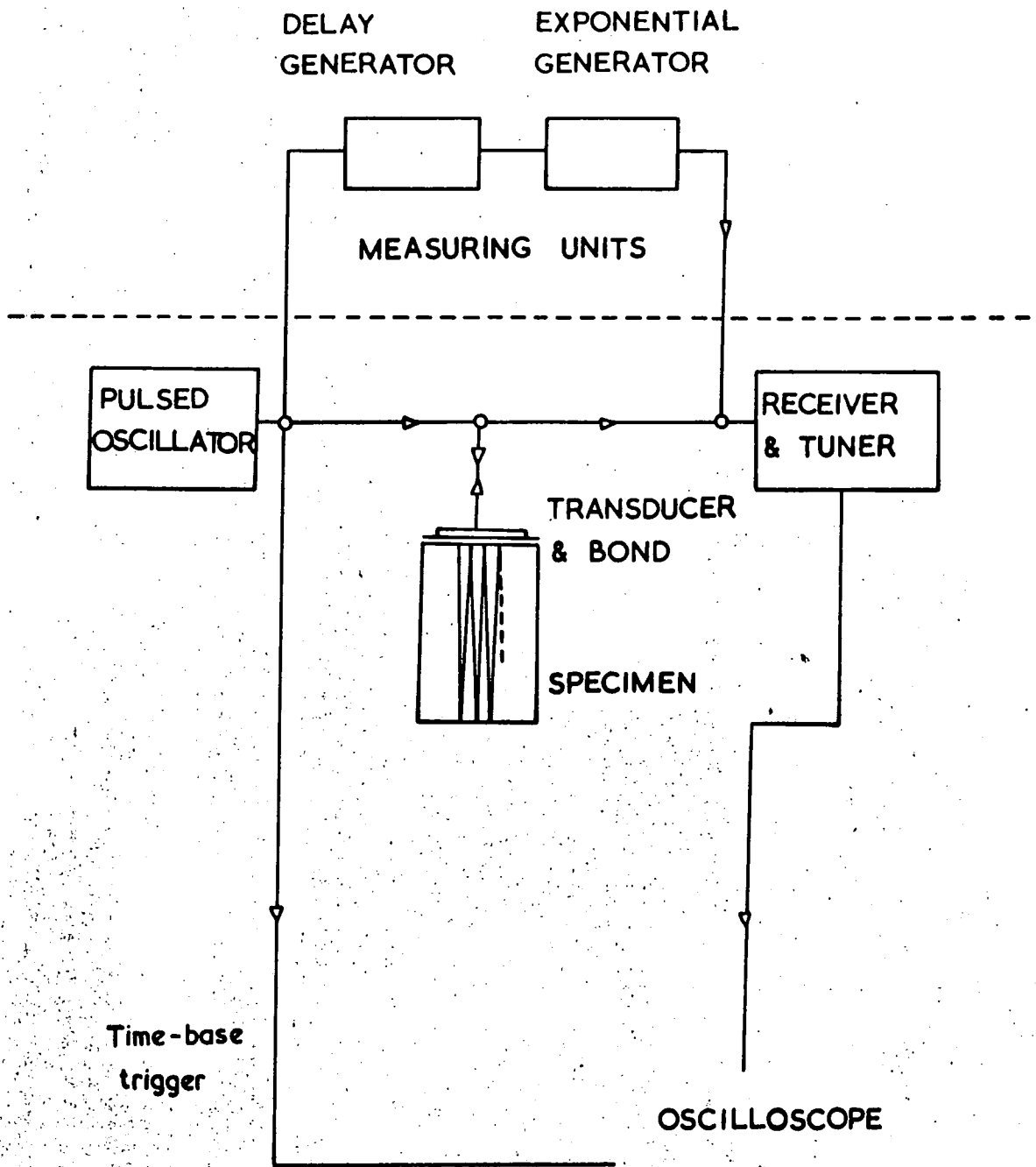
Figure 5.1 The basic circuit and principle of operation of the pulse-echo technique.

signal detection. Pulse lengths, variable between 0.5 and 3 μsec ensure that the oscillator has turned off before the first echoes arrive; pulse repetition frequencies are continuously variable from 10 to 1000 Hz, allowing complete decay of the ultrasound in the sample before initiation of the next r.f. pulse.

A tunable receiver of bandwidth 4MHz mixes the received pulse with a variable oscillator, connecting the signal to a 60MHz intermediate frequency. This is fed to a narrow-band amplifier and is followed by display on an oscilloscope screen. Synchronizing pulses trigger alternately the pulsed oscillator and an exponential generator, and with high pulse repetition rates, these traces appear to be simultaneous.

Method of Operation

With the output of the pulsed oscillator connected to the transducer and sample system, the oscillator and receiver are tuned to the resonant frequency of the transducer, or an odd harmonic if the overtone mode of operation is desired. Small adjustments of oscillator and receiver frequencies are made until a minimum in attenuation is observed. This may be a few percent from the nominal transducer resonance frequency as mechanical and electrical coupling perturb the resonance condition. The exponential decay pattern is then fitted to the tops of the echoes by adjustment of a pre-calibrated multi-turn potentiometer. A delay generator allows movement of the exponential trace, and the fitting of the thin vertical

leading edge gives a measure of the time between the echoes to within ±1%.

5.2.1 The Pulse-Superposition Technique for velocity measurement

Although the pulse-echo technique furnishes velocity measurements to ±1%, often velocity changes three orders of magnitude smaller are required to be investigated. One approach is to use an adaptation of the above method called the Pulse-Superposition technique, and is due to McSkimin (1961).

Basically, the method is to increase the repetition frequency of the r.f. pulses applied to the transducer until their period is a small integral multiple of the sound transit time in the sample. When this condition is reached, the echoes will add, and superposing on each other, a maximum in received signal will follow.

The equation describing the relationship between transit time (δ) and pulse repetition period (T) leading to a maximum in observed signal is

$$T = p\delta - p\gamma/360f + n/f \qquad\qquad 5.1$$

where p is an integer corresponding to the number of transits of the sound in the sample per applied pulse, γ is the phase angle between reflected and incident waves at the sample-bond interface, and n is an integer describing whether the r.f. echoes are adding in phase (n=0) or 360n degrees out of phase. This last condition
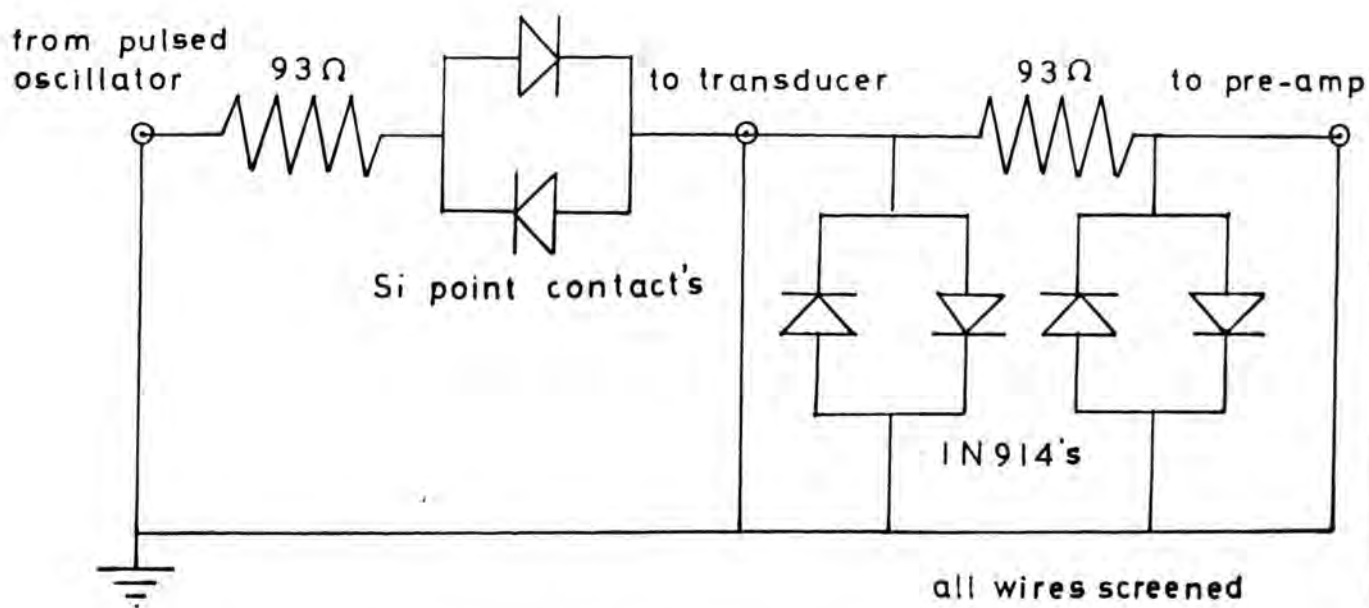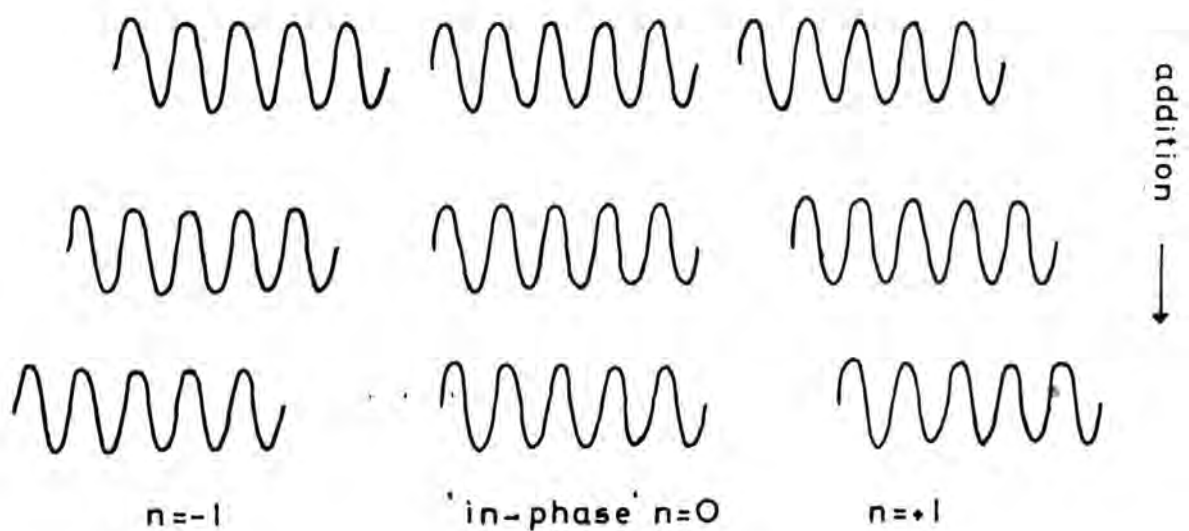
Figure 5.2   T–R junction circuit

Figure 5·3   Addition of pulse-echoes: the in-phase condition

is shown diagramatically in Figure 5.3. The greatest problem associated with the pulse-superposition technique is the evaluation of the n values of the observed maxima; Section 5.2.4 is devoted to this problem.

5.2.2   Description of the System

The layout of the circuit is reproduced in Figure 5.4. The accuracy of the technique is dependent on the ability to detect a maximum in received signal which is itself reliant on the maintenance and measurement of a stable pulse repetition frequency. For this function a Codasyn CS201S frequency synthesizer with digital readout was selected. This piece of equipment generates a sinusoidal wave of 0 to 3V in amplitude at frequencies of 0.1Hz to 2MHz with long term stability 1 part in 10^7 and short term stability 1 part in 10^9. Accuracy of readout is ±0.1Hz, suitable for the function in question.

The sine wave output triggers a General Radio 1217C Pulse Generator on the negative going part of the cycle at a preset signal level. The resultant negative square pulse of variable length from a minimum of 0.1 μsec, and nano-second rise time, is used to modulate the Arenberg PG650C Pulsed Oscillator. A pulsed rather than a blocking oscillator must be used as it is essential in the technique that the pulses produced are coherent with respect to their initiation. Power for the oscillator is provided by an Arenberg PS-660 external supply giving 2KV amplitude at repetition frequencies up to 30KHz, and 1KV
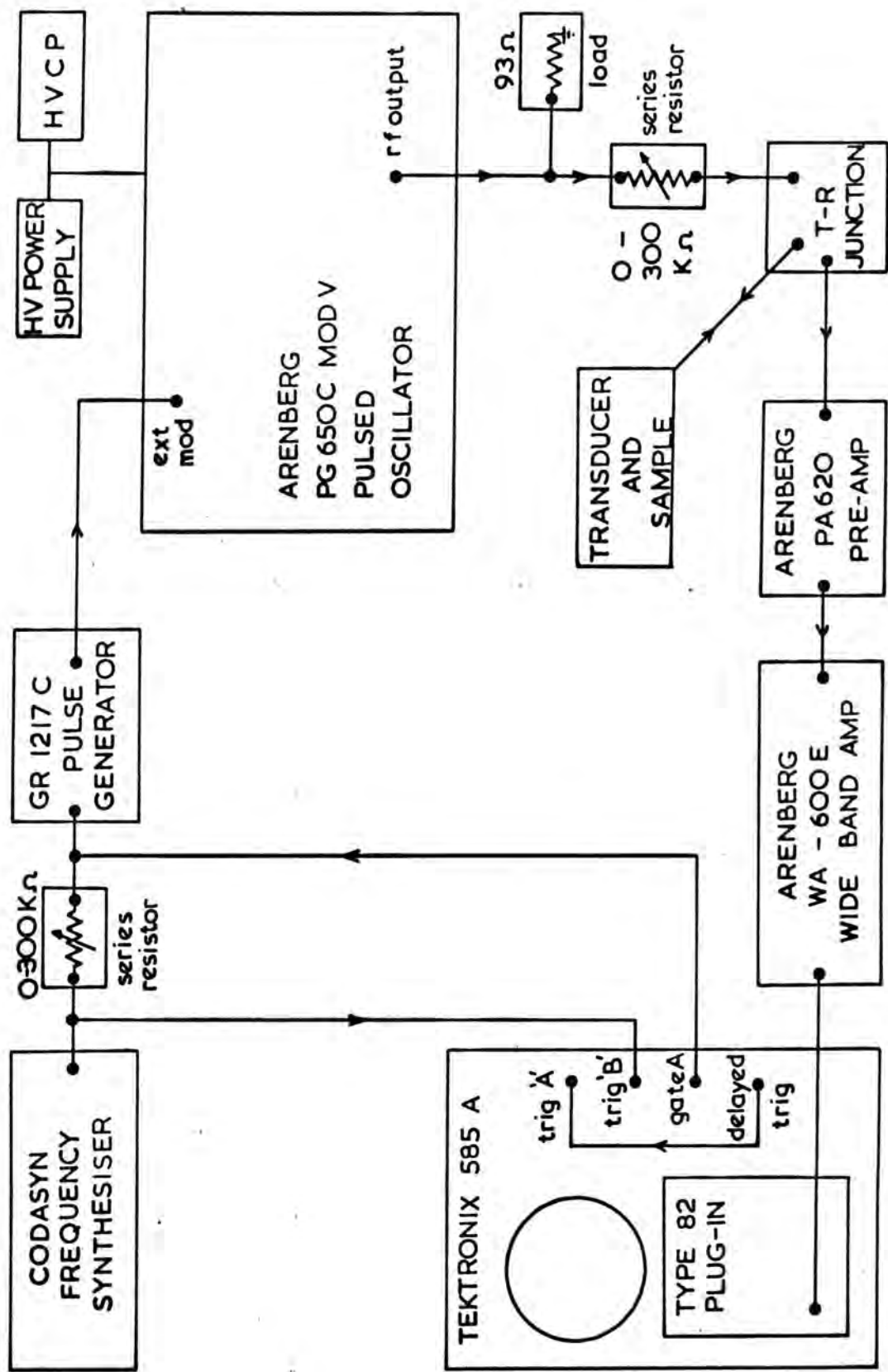
Figure 5.4 The circuit arrangement of the pulse-superposition technique.

amplitude at the more usually necessary repetition frequencies in the 30 to 300KHz range. Care has to be taken in choosing pulse lengths; square pulses are generally desired containing enough cycles for the r.f. frequency to be well defined yet a duty cycle of 25% must not be exceeded or overloading of the oscillator ensues.

A constant resistive loading of 93 Ω in the form of a heat shunt is placed in parallel with the pulsed oscillator output. The pulses are then attenuated by a 680 Ω resistor to allow pulses of considerable magnitude to be applied to the transducer without overloading the amplifier with too large received echoes. A T-R junction protects the Arenberg PA-620 pre-amplifier from the high-voltage pulses supplied to the transducer. The output from this tunable low band-pass amplifier is connected to the Arenberg WA-600E wide band amplifier, capable of 90db gain overall. A Tektronix 585A oscilloscope with a type 82 plug-in is used to display the video output from the wide band amplifier, and is triggered from the positive output terminals of the pulse generator.

5.2.3   Operation Procedure

Firstly, the frequency synthesizer is set to a low value (1KHz) and the pulsed oscillator to the resonant frequency of the transducer. The output level of the pulse generator is maximized, and with the B time-base of the 585A oscilloscope adjusted to a suitable sweep speed, the pulses and echoes are detected on the screen.

Peaking of the echoes is achieved by tuning the input and output stages of the pre-amplifier, small corrections being made in the r.f. frequency of the pulsed oscillator until a maximum in signal intensity is observed. This corresponds to a resonance in the transducer and sample system, the condition required for the most accurate results. The sequence of operation from this point is best represented by Figure 5.5.

The pulse repetition frequency required for pulse superposition can be approximately found by a prior pulse-echo measurement, and the synthesizer is adjusted to this value. The B time base is now changed to give about 50 pulse and echo systems in the x direction of the screen, and the horizontal display selector is turned to the 'B intensified by A' position. Intensification of about 5 pulse and echoes is achieved by selection of a suitable time base speed, the delay being adjusted until they appear central on the screen.

In this mode, a pulse of -40v appears at the 'A gate out' terminal of the oscilloscope for the duration of the A time base operation, and is connected via a 1.5KΩ current limiting resistor to the trigger input terminal of the pulse generator. This depresses the floating sine wave voltage from the synthesizer to below that required to trigger the pulse generator, inhibiting the generation of the r.f. pulses during the time that the time-base is operative. Protection of the output stage of the synthesizer is achieved by incorporating
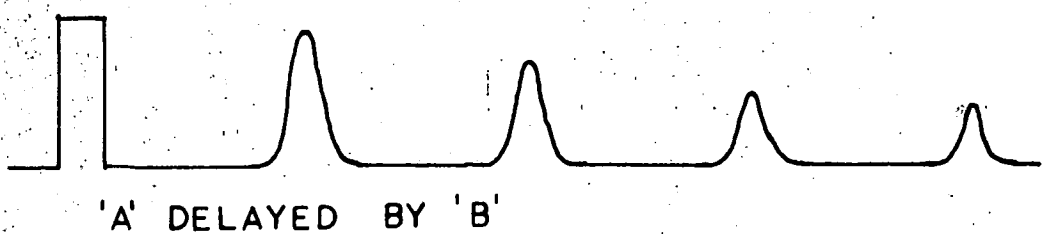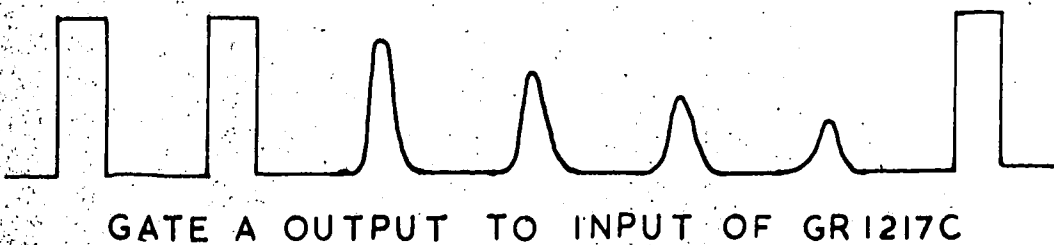
TIME BASE 'B'   P.R.F. LOW

INCREASE P.R.F.

'B' INTENSIFIED BY 'A'

GATE A OUTPUT TO INPUT OF GR1217C

'A' DELAYED BY 'B'
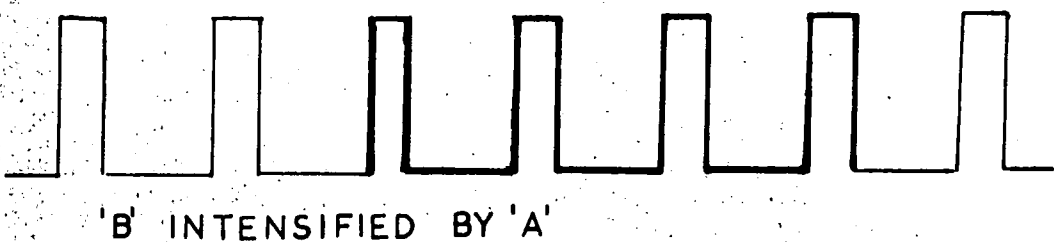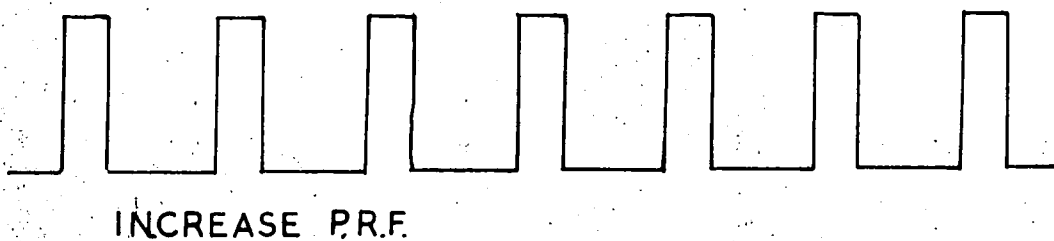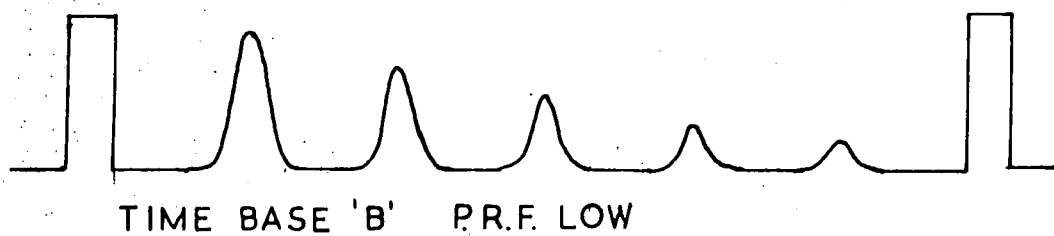
Figure 5.5 The sequence of operation of the pulse – superposition technique.

a 680 Ω series attenuator between the synthesizer and the pulse generator.

If the operation at the p equal to or greater than 2 . condition in equation 5.1, is desired, the last step may be ignored as the superposed echoes occur in the time slow between the applied pulses, but for clarity of display this procedure of allowing the superposed echoes to be observed is normally followed.

On selecting the 'A delayed by B' horizontal display mode, the intensified part of the trace is displayed. The procedure followed next is to adjust the pulse repetition frequency until a maximum in received signal is obtained, the result of the addition of the echoes from successive pulses. If the specimen is flat, parallel and homogeneous in character, sharp maxima will occur; only those corresponding to the different n and p values should be seen. For materials with high attenuation, adjustment of the fifth figure of pulse-repetition frequency will be necessary, sixth figure accuracy is available for those with low attenuation. However, lack of specimen ideality will result in many spurious maxima which are difficult to identify.

5.2.4   Indentification of the 'in-phase' maximum

Indentification of the n equal to zero condition is one of the greatest problems associated with this technique. Measurements by the pulse-echo method are only accurate enough to predict the pulse-repetition

frequency to ±1%, usually leaving some doubt as to
whether the maximum observed is the n equal to -1, 0
or +1 condition.

McSkimin (1961) has produced an analytical
method for determination of the n value associated with
an observed maximum. From equation 5.1 we can determine
the change (ΔT) in repetition period T required to main-
tain superposition as the r.f. frequency is changed from
f_H to f_L:

$$\Delta T = \frac{1}{f_L}\left(n - \frac{p\gamma_L}{360}\right) - \frac{1}{f_H}\left(n - \frac{p\gamma_H}{360}\right) \qquad 5.2$$

The angle by which the reflected wave is out
of phase with the incident wave (γ) is a function of wave
frequency, and it is necessary to evaluate this angle at
frequencies f_H and f_L. Figure 5.6 shows a plan of bond,
transducer and sample, with mechanical impedances
z_1, z_2 and z_3 respectively, equal to the ultrasound
velocity multiplied by the density for each medium. The
reflection phase angle is obtained from the relationship

$$\gamma = -2 \tan^{-1} Zd/jZs \qquad 5.3$$

where $Zd = jZ \dfrac{(Z_1/Z_2) \tan B_1 l_1 + \tan B_2 l_2}{(Z_1/Z_2) - \tan B_2 l_2 \tan B_1 l_1}$

and $B_{1,2} = \dfrac{2\pi \cdot \text{frequency}}{\text{velocity}}$ for bond (1) and transducer (2).

Thus a graph of ΔT versus bond thickness for a specific
change in wave frequency may be drawn.
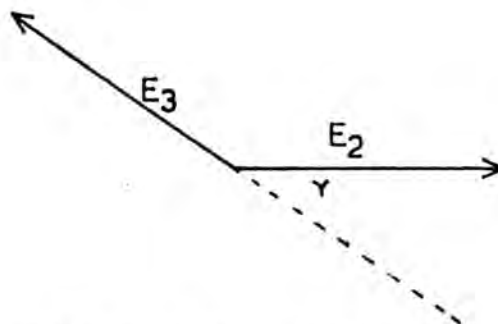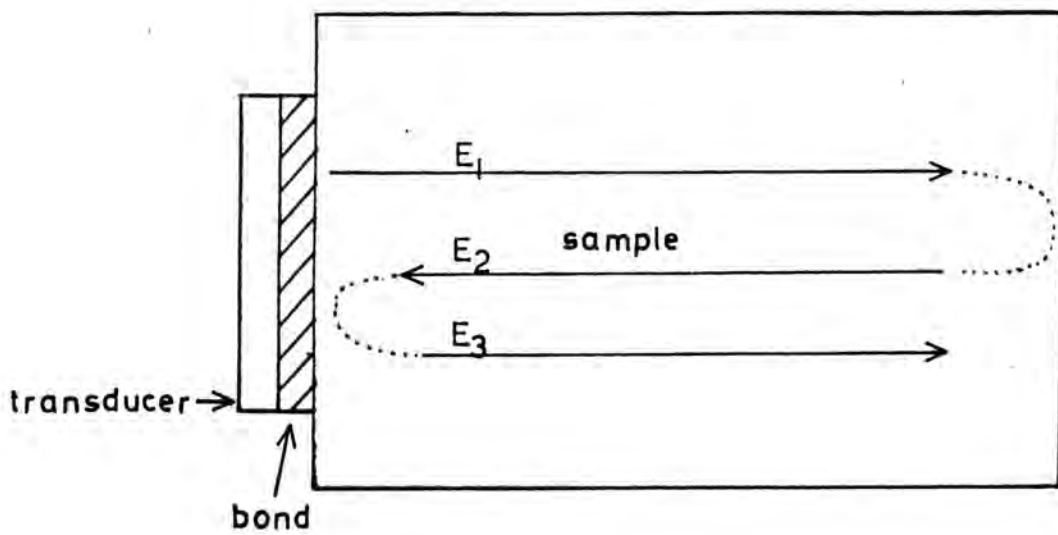
Figure 5.6 Plan of transducer, sample and bond, and phase
relations for reflected waves

By measuring the ΔT's for the superposition maxima in the locality of that predicted from the pulse echo measurements, it should be possible to assign the measured points to the different n and p curves on the graph. Bond thicknesses are not measurable to any appreciable degree of accuracy, but are approximately 3 to 5μ, giving at B1 value of 10 to 20 degrees. However, little success was gained by this method using nonaq as the bonding material.

Private communication with Dr. H.J. McSkimin resulted in his suggestion that the failure of the method when using nonaq as the transducer to sample bond may be due to the ' lossy' nature of the seal. Subsequent experiments using mannitol as the seal proved much more successful, although they could only be carried out at room temperature as the mannitol bond failed at about $-30^{\circ}C$.

Figure 5.7 is a graph of ΔT versus bond thickness in degrees of wavelength of the ultrasound. This set of curves is drawn for sample I /48, using a 12.0MHz shear wave transducer with a mannitol bond, considering a change in wave frequency of 10%; that is, from 12.0MHz to 10.8MHz. The mechanical impedance of mannitol when subjected to a shear stress was measured to be 5.4×10^5 g/cm^{2}sec, and 9.0×10^5 g/cm^{2}sec for a longitudinal stress.

A later experiment executed to determine the apparent sound attenuation due to a nonaq bond is

$\Delta T = (T_f - T_{fr})\ \mu\,secs$

2/48   SHEAR 12·00 MHz

Y-CUT QUARTZ TRANSDUCER

MANNITOL BOND

SEAL THICKNESS BL
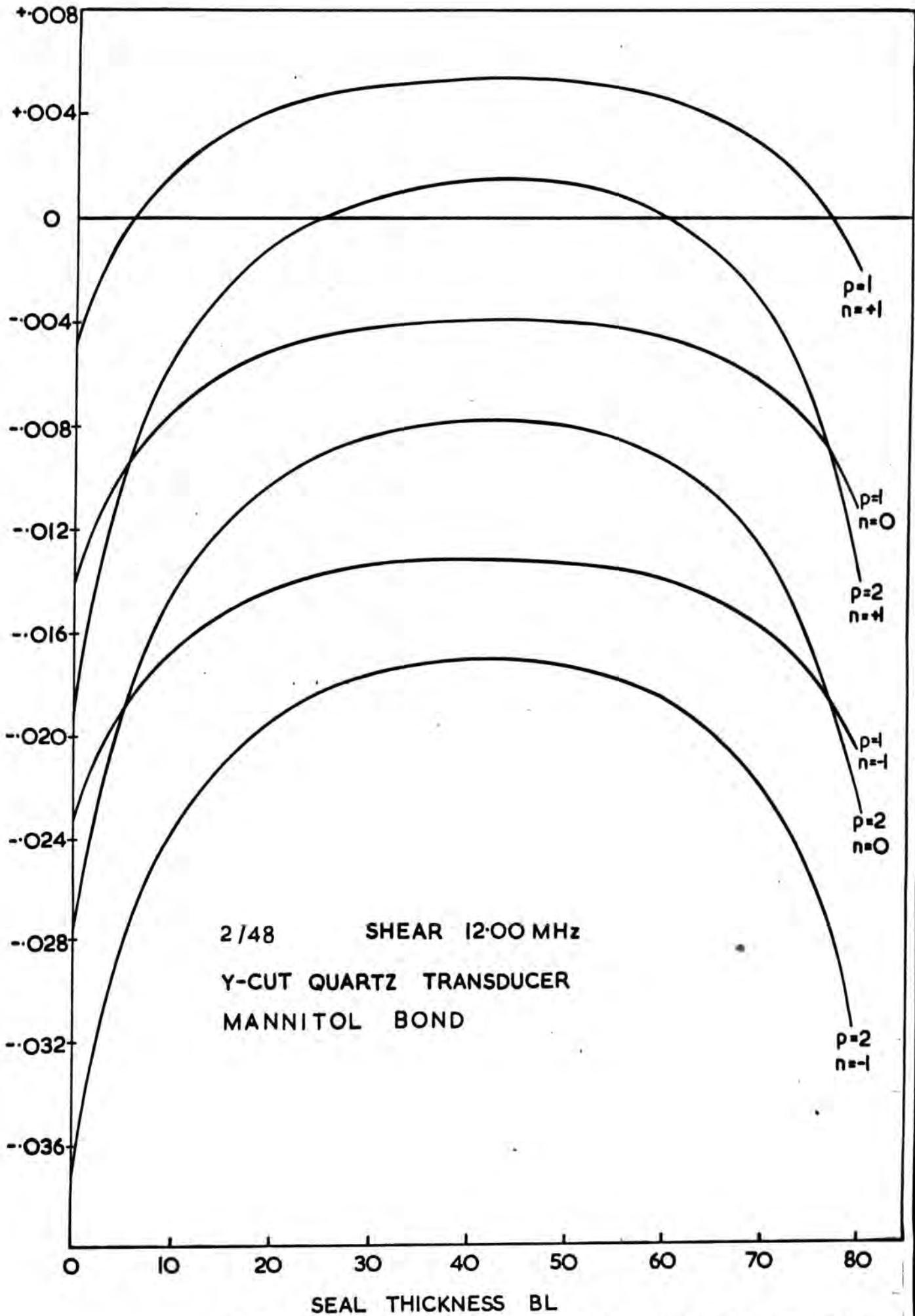
detailed later in Section 5.6.4. This experiment con-
cluded that nonaq did not prove to be an extremely loosy
bonding agent; further reasons for the failure of this
method for this particular seal remain obscure.

5.3   Quartz Transducers

The conversion between electrical and mechanical
energy by the converse and direct piezoelectric effects
is found use in the generation and detection of ultra-
sound. Only non-centrosymmetric materials may be
piezoelectric; although many crystals such as Rochelle
salt, tourmaline and quartz exhibit this property, the
latter is usually chosen for its high physical strength
despite its lower piezoelectric coefficients.

As the piezoelectric properties of a crystal
are anisotropic, consideration of the direction of the
applied electric field must be made to produce the
desired acoustic mode. To produce an ultrasonic trans-
ducer operating in the longitudinal mode, a quartz
crystal is cut so that a slice in the y-z plane with its
thickness in the x direction results. The thickness of
this 'x-cut' crystal is chosen to correspond to one-half
the wavelength of sound at the frequency at which it is
to be operated, thus describing the resonant frequency
of the transducer. A shear mode may be excited by using
a slice cut perpendicular to the y direction, and is
termed the 'y-cut' transducer. These cuts are demonstrated
in Figure 5.8. Both types of transducer are co-axially
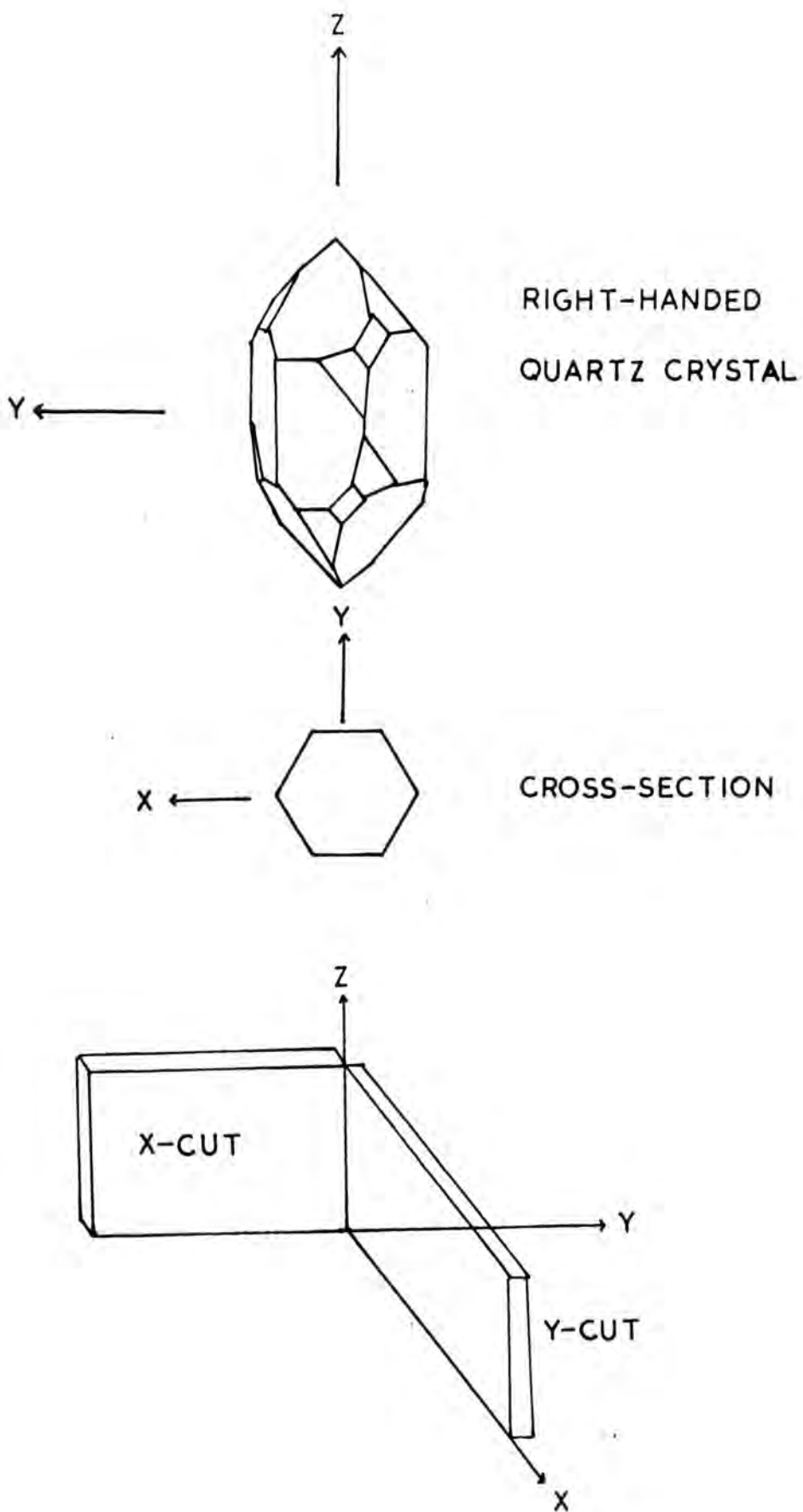
Figure 5.8 Quartz crystal and demonstration of quartz transducer cuts.

gold-plated to produce an electric field parallel to
the thickness axis.

A transducer may be driven at a harmonic
of its fundamental frequency, the nth harmonic producing
n/2 acoustic wavelengths in its thickness direction.
Only if n is odd will any net strain result; odd
harmonic operation is the only possible operation
condition.

5.4   Transducer to Sample Bonding

To obtain good acoustic coupling between the
transducer and sample, it is necessary to use a bonding
agent. This seal should be uniform, and parallel to
the same tolerance as the sample, and it is preferable
that the acoustic properties of this seal do not change
appreciably over the temperature range of the experiment
in question. The efficiency of the bond varies with
sample material for any one bonding agent, and a process
of trial and error indicates the best agent to use.

Silicone fluids of 250,000 and 1,000,000
centi-stoke provide adequate seals to sodium-
borosilicate glasses for both longitudinal and shear
waves between 100 and 280°K, while Dow 279-V9 Resin
proves efficient between 130 and 300°K. Solid bonds
such as phenyl salicylate and mannitol, which require
melting before use tended to powder at low temperatures,
resulting in a failure in acoustic coupling. Nonaq
Stopcock Grease, manufactured by the Fisher Scientific

Company gives excellent characteristics for both waves between 1.5 and 280°K. The bonding agents eventually chosen for this work were Nonaq for below room temperature experiments, and mannitol for experiments between room temperature and 400°K.

To form a transducer to sample bond when using Nonaq, a small drop of the agent is applied to one of the flat sample faces, and the transducer is placed on top. Using a pair of tweezers and a small ball of tissue, the transducer is moved in a circular direction until an increase in the frictional force required to execute the movement evidences the expulsion of most of the agent, leaving a thin transducer to sample seal. The excess agent is then carefully removed from the transducer perimeter. Silver-dag conducting paint is then applied to the outer coaxial gold ring of the transducer and to the remainder of the sample face to enhance a good earth contact.

A mannitol bond is made in much the same method; preheating of the sample and transducer to the melting point of mannitol at 169°C is required, and a small weight placed on the transducer whilst cooling improves the seal homogeneity.

Measurements with a dial guage generally evidence a bond thickness of about 3 to 5 μ, with the desired parallelicity. Preparation by this method is shown to give a homogeneous efficient acoustic bond as shown by decay patterns of an exponential character.

5.5.1 Errors in Velocity Measurement

Errors in velocity measurement can be divided into three categories; an error due to phase changes at the sample-bond interface, errors due to diffraction caused by beam divergence, and an error due to uncertainty in the path length of the ultrasound wave. In a crystalline system, angular misorientation leads to an error in measured ultrasound velocity for a particular direction of propagation, but is redundant for an isotropic system.

5.5.2 Phase Changes at the Sample-Bond Interface

The angle between incident and reflected waves at the sample-bond interface is the constant, γ , of equation 5.1, and its method of evaluation has been outlined in equation 5.3. For a bond of thickness 5 μ having an ultrasound velocity of 5×10^5 cms/sec, γ is calculated to be approximately 5° when the transducer is operated at within 1% of its resonant frequency. This leads to an error of 0.001 μsec in transit time, 0.03% of the typical transit times observed in this work. This error will be smaller for a shear wave of lower velocity, and is calculated as 0.02% for a shear velocity of 3×10^5 cms/sec.

5.5.3 Beam Divergence

Papadakis (1966) has produced an analysis of velocity error due to the transducer acting as a

piston source of finite area. In this analysis, a graph of phase advance of the stress wave versus distance of the echoes from the source into the elastic half-space for various anisotropies is produced. The pulse-superposition effectively adds many echoes of various phase advance weighted by the attenuation in the sample. On materials with low attenuation, such as $CaWO_4$, this effect may be seen by different echoes maximizing at slightly different pulse repetition frequencies, but on the relatively high attenuation glasses used in this work, no such phenomena was observed.

Referring to the graph of Papadakis, an error of negligible magnitude in velocity is calculated for a transducer of 7 mm active area at 12MHz for an isotropic system.

5.5.4   Path Length of the Ultrasound Wave

The path length of the ultrasound wave is defined by the dimensions of the specimen. A correction for thermal expansion must be made for a velocity versus temperature determination, which involves knowledge of the width of the sample at a fixed temperature and the coefficient of thermal expansion throughout the whole temperature range.

The measurement of sample width in this work was made by a dial guage at room temperature. Random errors of measurement are estimated at about 0.05%, while the systematic error due to the absolute calibration

of the instrument is unknown, but is assumed to be small.
Thermal expansion coefficients of the glasses have been
measured only in the range 300 to 750°K and are reported
in Chapter 4, and are of the order 6 x 10^{-6}/°C. This
coefficient is expected to decrease at lower temperatures,
and may possibly be negative below 30°K (Krause and
Kurkjien, 1968), reaching zero at 0°K. The fractional
change in path length can thus be estimated as
approximately 0.1% from 1.5 to 300°K, and 0.06% from
300 to 400°K, though thermal expansion measurements below
room temperature would resolve this problem and allow
accurate correction for velocity to be made.

5.5.5   Total Error

The largest error in velocity is that produced
by the uncertainty in the coefficient of thermal expansion.
For this reason, the velocity curves have been left
uncorrected, but the maximum error may be concluded to
be 0.18% at 1.5°K, 0.08% at 300°K and 0.14% at 400°K.

5.6.1   Errors in Attenuation Measurements

A measurement of ultrasonic attenuation by the
pulse-echo technique is composed of two contributions;
the losses due to the intrinsic attenuation in the
specimen which are the losses of physical significance,
and apparent losses due to the lack of ideality of the
sample, bond and transducer system. Either elimination
of these latter losses, or their calculation and

subtraction from the total measured loss leaves the intrinsic sample attenuation. These apparent losses may be defined intothree categories; diffraction losses, non-parallelism losses, and losses due to the acoustic bond and associated electrical system.

5.6.2   Diffraction Losses

Because of the finite size of the ultrasonic transducer, the sound beam will diverge and have a diffraction field. A non-planar wave results, and an error occurs as the planar transducer integrates the stress wave across its complete surface. The beam divergence may also result in a sidewall reflection, as shown in Figure 5.9. Acoustic mode conversion can also take place at the medium discontinuity. Interference at the transducer between these waves of longer path length also distorts the observed echo pattern. Diffraction effects are most important at the low megahertz frequencies and for small transducers.

These effects are most obvious in materials of low intrinsic attenuation and cause a non-exponential decay pattern even under the most ideal situation of no sidewall reflection, high sample homogeneity, and perfect sample geometry. A small maximum in the attenuation pattern occurs at a distance a^2/λ from the transducer, where a is the radius of the active area of the transducer, generally equal to radius of the area of the overalpping electrode plating, and λ is the
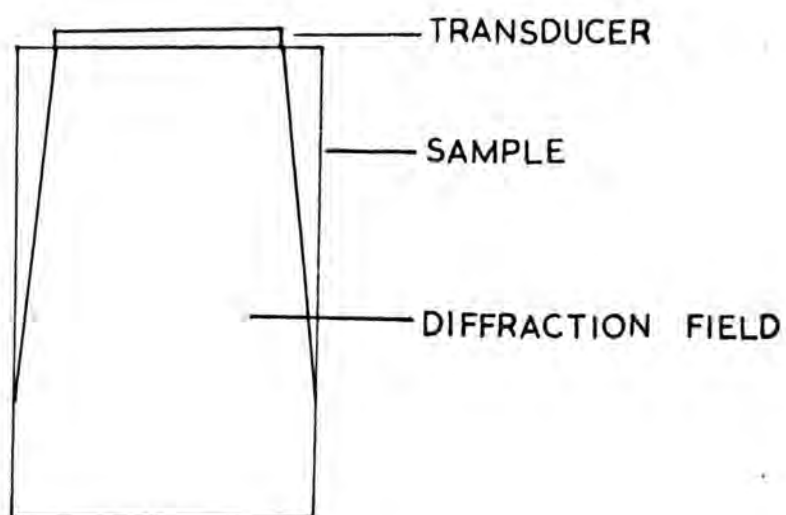
Figure 5.9 The diffraction field and sidewall reflections in an incorrectly sized sample.
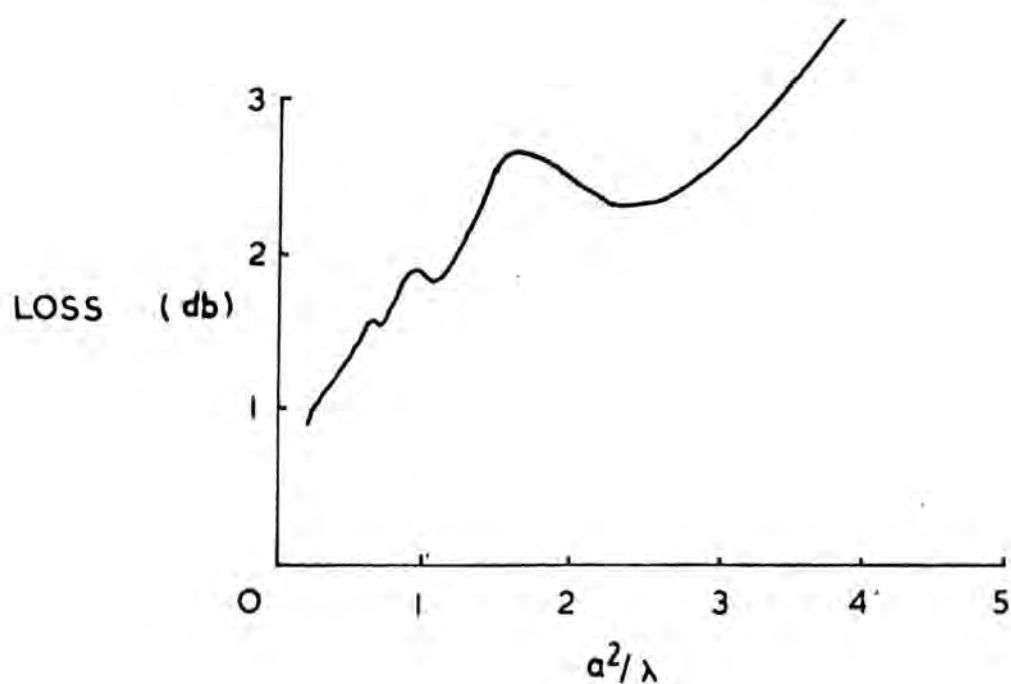
Figure 5.10 Diffraction field loss as a function of $\frac{a^2}{\lambda}$

ultrasound wavelenth. A theoretical analysis (Truell,

Elbaum, Chick, 1969) shows a number of different maxima

resulting from the diffraction field of the transducer;

a graph of loss versus distance from the transducer-

sample interface is shown in Figure 5.10. Thus by

fitting the pre-calibrated exponential decay to identi-

fiable maxima on the echo pattern, a correction for the

diffraction effect may be made.

The sodium borosilicate samples used were of

size 13 x 13 x about 7 mm., large enough to eliminate the

possibility of sidewall reflection with a transducer of

7 mm active radius. At a wave frequency of 12MHz,

a^2/λ is approximate 13 cms for a longitudinal wave of

velocity 4.5 x 10^5 cms/sec. Measuring between echoes

2 and 5 and referring to the graph evidences approximately

0.1 db in diffraction loss in 7 μsecs, the equivalent of

0.014 db/μsec. This is extremely small in comparison

with the experimentally measured attenuations of between

0.5 and 1.5 db/μsec, an error of less than 3%. A shear

wave, with longer wavelength than a longitudinal wave of

the same frequency however produces, in terms of db/μsec,

an approximately equal diffraction loss, again no greater

than 3% at all experimental attenuations.

5.6.3 Non-parallelism

Figure 5.11 shows successive reflections of

an ultrasound beam in a sample with wedge angle θ between

the two opposite flat faces. The planar wave, when

Figure 5.11 Successive reflections of an ultrasound wave in a sample with wedge angle between the opposite faces.

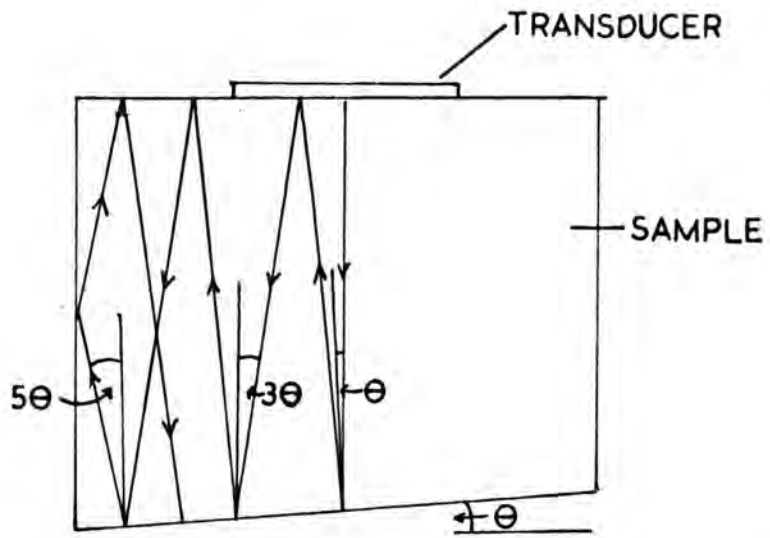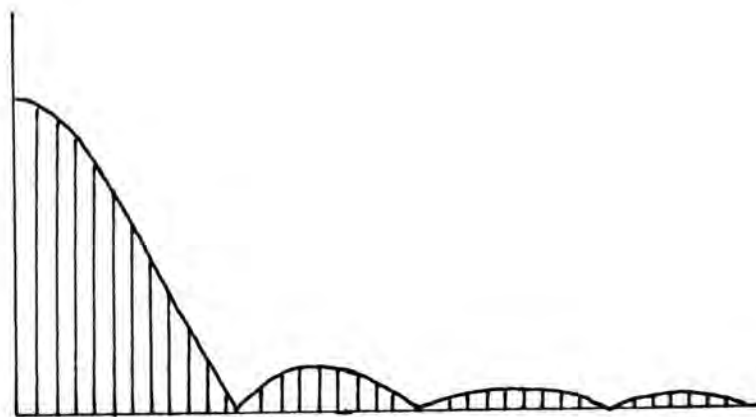**Figure 5.12** The appearance of the pulse-echo train in a sample with non-parallel faces.

reflected from a surface not normal to its direction of
propagation, meets the transducer at an angle θ to the
perpendicular; the consequent phase difference across
the transducer is the cause of a non-exponential echo
pattern. An analysis of the situation (Truell and
Oates, 1963) results in the theoretical modulation of
the echo pattern by a Bessel function, as shown in
Figure 5.12. This curve is an accurate representation
of the observed pattern in a non-parallel sample.

If the sample attenuation is of sufficiently
high attenuation, only the first part of the modulating
curve will be seen, as in the case of the glasses studied
in this work. A good approximation to the apparent
attenuation, α^1, thus seen is

$$\alpha^1 = \frac{8.68 \ \pi^2 \ f^2 \ a^2 \ \theta^2 n}{v \ L} \quad \text{db/unit time} \qquad 5.4$$

where f is the ultrasound frequency, a is the radius of
the active area of the transducer, v is the ultrasound
velocity, L the sample length, with the measurement of
the attenuation made over n echoes.

Substitution of values corresponding to glass
samples used in these experiments, which have a
parallelicity between faces of 10^{-4} radians, shows a
calculated attenuation of 0.001 db/μsec at 12MHz, only
0.25% of the experimental attenuation, and hence negligible.
However, a wedge angle only five times larger leads to
a 6% error in attenuation; great care in sample pre-
paration had to be exercised to achieve the high degree
of parallelicity required.

5.6.4 Coupling losses

Losses arising from the transducer to sample bonding and from the electrical system contribute to the apparent losses in the pulse-echo technique. With a sample of length L and intrinsic attenuation α per unit length, estimation of these losses may be made by the following procedure.

1.   The attenuation for one round trip is made using one transducer as normal. This is equal to $2L\alpha + \alpha_1$, equal to κ_1, where α_1 is the loss due to the coupling and electrical system.

2.   The measurement is repeated with an identical transducer, bond and electrical loading applied to the opposite face. The single round trip attenuation is then $2L\alpha + \alpha_1 + \alpha_2$, equal to κ_2, with α_2 the apparent attenuation due to the addition of the second transducer.

3.   Using the second transducer as the ultrasound generator and receiver, a further measurement of attenuation is made which should be equal to that measured in step 2. Agreement of the two values shows sample homogeneity and alignment of the two transducers.

4.   A further measurement is then made following the removal of the first transducer and associated bonding material. This attenuation is $2\alpha L + \alpha_2$, equal to κ_3.

Thus, by simple elimination between the three

equations

$$\alpha = \frac{\kappa_1 + \kappa_3 - \kappa_2}{2L} \qquad\qquad 5.5$$

and $\qquad \alpha_1 = \kappa_2 - \kappa_3 \qquad\qquad \alpha_2 = \kappa_2 - \kappa_1 \qquad\qquad 5.6$

Attenuation measurements on sample 978/2/Q using 12.0MHz, 10 mm, Y-cut transducers and a nonaq bond, using a double-ended 50 Ω sample-holder at 77°K were as follows:

$$\kappa_1 = 4.74 \text{ db}$$

$$\kappa_2 = 4.76 \text{ db}$$

$$\kappa_3 = 4.74 \text{ db}$$

This shows an apparent attenuation due to each bond and an associated electrical system of 0.02 db, only a small figure in comparison with the intrinsic attenuation in the sample.

5.7 The Sample Holder for use at Low Temperatures

The sample holder for use between 1.5^{O}K and 300°K is designed to produce a continuous matching coaxial transmission line to the transducer while holding the sample in position in the cryostat. A diagram of the sample holder is shown in Figure 5.13. A stainless steel tube with a copper wire inner core form the coaxial line. It terminates in a spring and a silver steel plunger which makes a pressure contact with the inner transducer electrode. This termination is surrounded

THIN-WALLED
STEEL TUBES

CO-AXIAL LINE

THERMOCOUPLES

BRASS BLOCK

SPRING AND
PLUNGER

SAMPLE

SPRINGS

PLATFORMS

COLUMNS

SCREW
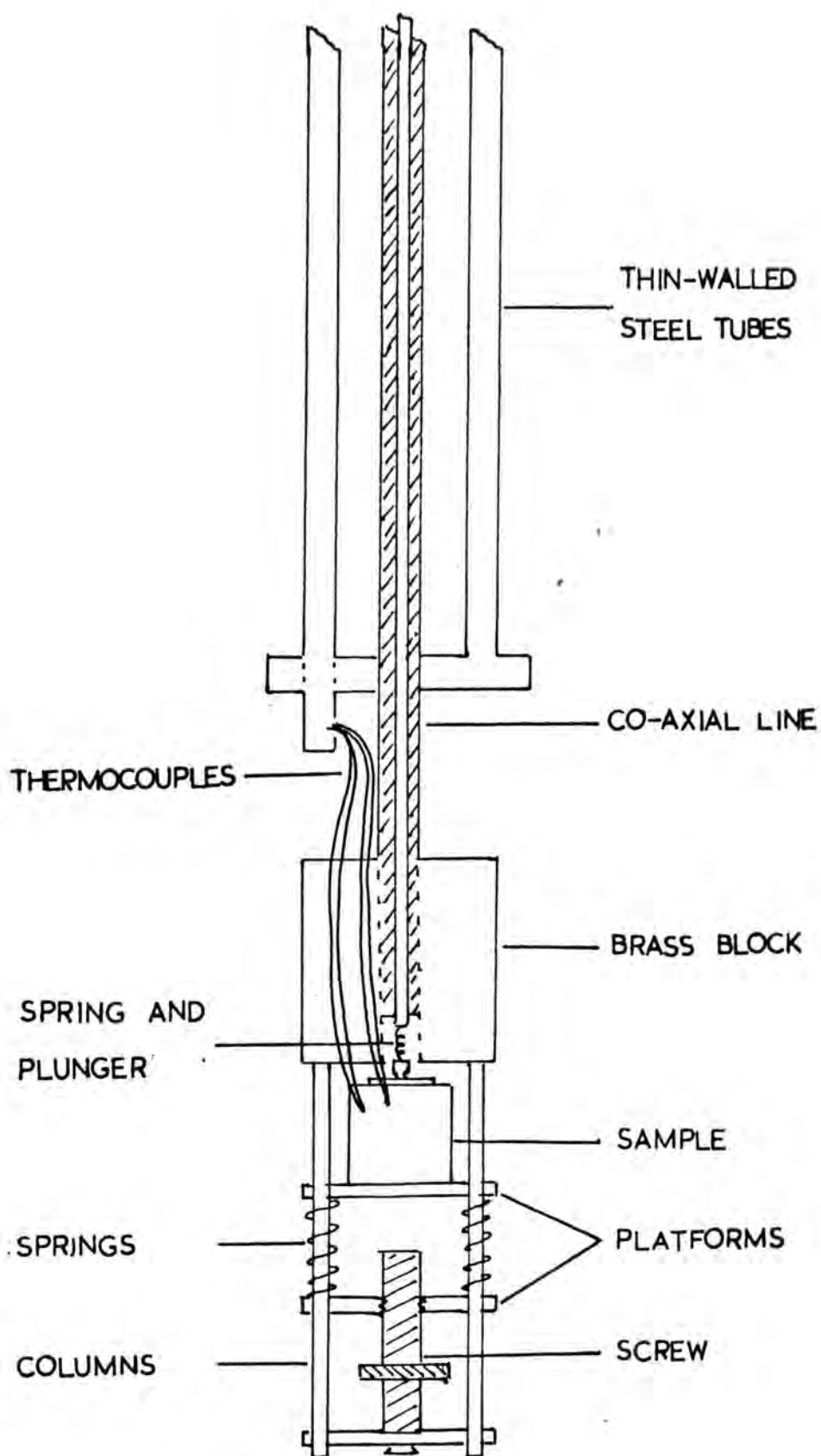
Figure 5.13 The sample holder for use between 1·5°K and 300°K

by a solid brass cylindrical block of high thermal
capacity for minimisation of temperature gradients.
The sample and transducer are mounted on a brass platform
and held in contact with the plunger and block by three
springs wound concentrically around three brass columns.
These springs are in turn adjustable in position by a
moving platform mounted on a screw thread which turns
on a third brass platform. This third platform also
serves to stabilise the columns.

This sample anchoring device is itself
connected to a set of thin-walled stainless steel tubes
strengthened by circular cross-members. The tubes are
attached to a solid vacuum-tight brass disc which fits
into the top of the cryostat. The vacuum seal is made
with the assistance of a rubber O-ring. The thermo-
couples and heater leads pass inside the stainless tubes
and out through a vacuum seal to the potentiometer and
temperature controller.

5.8   The Helium Cryostat

The helium cryostat consists essentially of
two concentric double-walled glass dewars, each with a
vertical window to allow observation of the helium
level, and the associated vacuum systems. Evacuation
of the interspace is performed between experiments
to expel any helium that may have diffused in, while
the interspace of the outer dewar is a permanently
sealer vacuum.

To the inside of the inner dewar is connected
a 150 litre-atmosphere/min rotary pump to evacuate the
dewar and to pump on the liquid helium. A constant
pumping pressure can be maintained by a Cartesian
Manostat, allowing a maximum fluctuation in pressure of
$\pm\frac{1}{2}$ mm of mercury under most pumping conditions. These
pressures are measured by a combination of a mercury
and an oil manometer. Using liquid helium refrigerant,
temperatures down to 1.5^{O}K can be reached. In certain
experiments the range 45°K to 77°K can be conveniently
covered by pumping on liquid nitrogen. In both cases
the sample temperature may be obtained by comparing
measured gas pressures with standard vapour pressure
tables.

Sample temperatures are measured between
4.2^{O}K and 30°K by using a gold-iron versus chromel
thermocouple, and from 30°K to 300°K by using a copper
versus constantan thermocouple. Each thermocouple is
fixed to the sample by low temperature varnish.
Calibration of these thermocouples is performed by taking
e.m.f. measurements at three fixed points and fitting
these to an equation of the form (White, 1959):

$$E = at + bt^2 + ct^3 + d \qquad\qquad 5.7$$

where d is the residual e.m.f. with both thermocouples
at the reference temperature.

For the gold-iron versus chromel thermocouple,
the reference temperature is liquid helium at 4.2^{O}K, with

calibration points at 1.5^{O}K (pumped He), 63.15^{O}K (triple point of N_2) and 77.36^{O}K (boiling point of N_2 at 760 mm pressure). A liquid nitrogen reference at approximately 77.4^{O}K, taking account of this temperature variation with pressure, and calibration points at 4.2^{O}K, 63.15^{O}K and 273.16^{O}K (ice point) are used for the copper versus constantan thermocouple. Good agreement was found in experiments reported here between the e.m.f's. of the two thermocouples between 20°K and 40°K; the temperatures indicated usually agreed to within $\pm 1/3^{O}$K. Measurements of these e.m.f's. are made with either a Tinsley 3387B potentiometer or a Harwell Temperature Controller, both capable of 1 μV resolution.

The Harwell Temperature Controller is also electrically connected to a heater element consisting of a constantan wire of resistance 300 Ω wound on a vermiculite frame surrounding the sample. Power is automatically supplied to the heater when the sample temperature falls below that indicated and set on a front mounted dial, and adjustment of the time constants of internal circuits to match the thermal inertia of the system allows temperatures steady to $1/10$th^{O}K to be maintained. However, most of the experiments executed in the helium cryostat were performed under conditions of rising temperature. At no time did the temperature increase at a rate greater than $1/3^{O}$K per minute, enabling measurements of velocity and attenuation to be made under virtually static conditions.

Cooling of the system is achieved by introduction of liquid nitrogen into the outer dewar. The presence of helium gas in the inner dewar prevents condensation of vapours on the sample and thermocouples. The sample is thus cooled to $80^{\circ}K$ in approximately 12 hours. Liquid helium is then transferred into the inner dewar using a double-walled transfer tube with pre-evacuated interspace. Approximately 1 litre of liquid helium is necessary to reduce the sample temperature to $4.2^{\circ}K$ and a further 2 litres are added if it is desired to reduce the sample temperature to $1.5^{\circ}K$ by pumping.

5.9   The Nitrogen Cryostat

A second cryostat for use between $45^{\circ}K$ and $300^{\circ}K$ is also available. This cryostat is of metal construction and has the usual facilities for evacuation of both interspace and dewar. The sample holder used in this cryostat is similar to that used in the helium cryostat, the only difference being the smaller size needed for accommodation in the smaller system. Copper versus constantan thermocouples are used for temperature measurement. When the Harwell Temperature Controller is in use during a cooling cycle, temperatures can be held for long periods with less than $1/20th^{\circ}K$ fluctuation. A small auxiliary heater is also mounted underneath the sample holder to boil off any excess liquid nitrogen between pumping and heating cycles.

5.10   The High Temperature Sample Holder and Furnace

To examine the acoustic properties of the samples above room temperature it was necessary to construct a compatible sample holder and furnace system. This is considered superior to an oil-bath system for two reasons. Firstly, higher temperatures are attainable, and secondly, damping of the transducer by the oil and conduction of sound at the oil-sample interface produces erroneous results in velocity and attenuation measurements.

The sample holder was designed so that the springs clamping the transducer to the electrical contacts are out of the furnace. This design is shown in Figure 5.14, and ensures that no loss of tension and loss of electrical contact occurs at the high temperatures where the springs would normally lose their elasticity. The main body of the sample holder is stainless steel of consequent high thermal inertia. A 50 Ω matching coaxial line consisting of a copper rod and aluminous porcelain tube of appropriate dimensions inside a stainless steel tube form the transmission line to the transducer.

A platinum versus platinum-13% rhodium thermo-couple in contact with the sample is used as the temperature sensor, and is connected to a Eurotherm PID/SCR stepless temperature controller which supplies power to the furnace windings.

The furnace is made of sindanyo, an asbestos compound, with a mullite core 1¼" in diameter and

ALUMINOUS

PORCELAIN INSULATION

STAINLESS STEEL
COLLAR

SCREWS

SPRING

SINDANYO
COLLAR

ALUMINOUS
PORCELAIN TUBES

CO-AXIAL LINE

STAINLESS-
STEEL BLOCKS
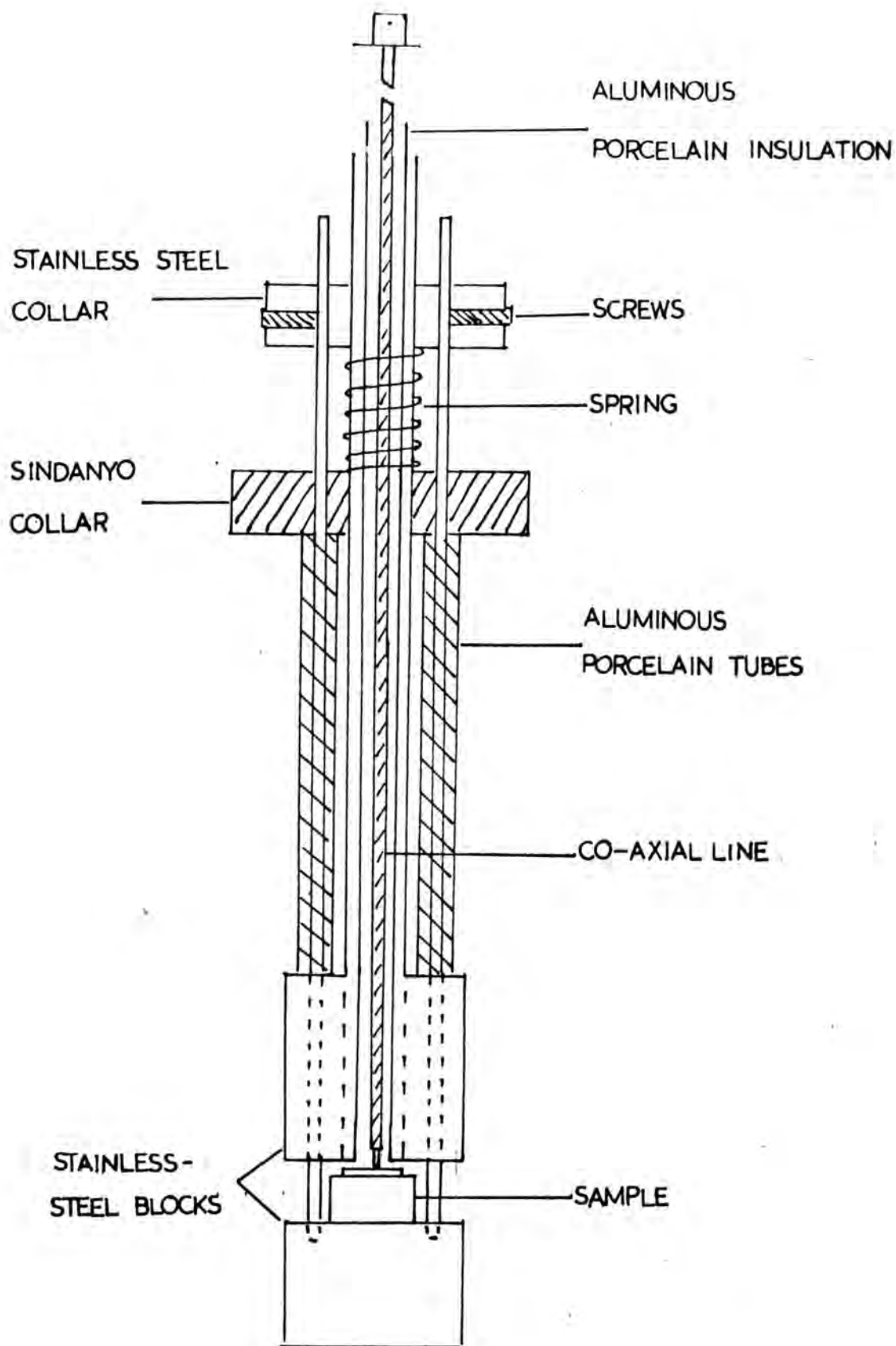
SAMPLE

Figure 5.14   The sample holder for use above 300°K.

12" in length. Vermiculite packing forms the thermal insulation. The furnace winding is Kanthol wire of total resistance 26 Ω to match the output of the Eurotherm temperature controller. This winding of 100 turns is made in such a way as to produce only the minimum of temperature gradients. On introduction of the sample holder, this ideal condition is somewhat perturbed, but thermocouples placed at both ends of the sample evidenced temperature differences no greater than $1.5^{\circ}K$ across the sample.

The maximum operating temperature of about $1000^{\circ}C$ is defined by the materials of construction, but limitations of transducer, bond and sample precluded use above about $400^{\circ}K$.

CHAPTER SIX

RESULTS OF THE ULTRASOUND
ATTENUATION AND VELOCITY MEASUREMENTS

6.1.1   The temperature dependence of ultrasound

attenuation and velocity between 4.2^{O}K and 400°K

To assess the effects of composition and phase separation on the acoustic properties of the Na_2O-B_2O_3-SiO_2 glasses of this work, a programme of measurement of the temperature dependence of ultrasound attenuation and velocity between 4.2^{O}K and 400°K has been undertaken on a variety of samples.

The temperature dependences of ultrasound at 12.0 MHz for samples 1/Q, 1/48, 2/Q, 2/48, 3/Q, 4/Q, 5/Q, 7/Q and 8/Q are shown in Figures 6.1 to 6.9. Both longitudinal and shear wave characteristics are presented for the first seven of these samples, and only the shear wave attenuation for the last two. The feature common to all the attenuation characteristics is a broad loss peak that extends over the whole range of temperature covered. This peak is similar in nature to the acoustic loss peak observed in SiO_2 and other inorganic glasses. In the Na_2O-B_2O_3-SiO_2 glasses the intensity and position of the maximum acoustic loss is a function of both glass composition and heat treatment; for sample 8/Q the peak has become so broad and low that the actual peak position is difficult to determine. Another noticeable finding is that the loss for the longitduinal wave is less than that for the shear wave. Similar behaviour has been observed in vitreous SiO_2.

Also necessary for a comprehensive investigation is the measurement of ultrasound attenuation in glasses

of the same composition but with a range of times of heat treatment. Figure 6.10 illustrates the acoustic shear loss between 45°K and 300°K in glasses 1/96, 1/168, 2/96 and 2/168, with the dashed lines representing data from Figures 6.1 to 6.4 for samples 1/Q, 1/48, 2/Q and 2/48. These results depict the rise in maximum acoustic loss and upward shift in peak temperature as the time of heat treatment at 550°C is increased. A small subsidiary peak of increasing amplitude from sample 2/96 to 2/168 appears at about 280°K, and is also seen in the acoustic attenuation characteristic of sample 8/Q.

If an acoustic loss peak is due to a relaxation mechanism it is usual to study its positional dependence upon frequency and so find the activation energy and attempt frequency of the process responsible. For the $Na_2O-B_2O_3-SiO_2$ glasses of this present study it is found that the peak temperature and maximum acoustic loss increase with increasing acoustic frequency. Examples of this effect are illustrated in Figures 6.11 and 6.12 which show the temperature dependence of acoustic shear loss for the heat treated sample 1/48 at 12.0 MHz, 20.0 MHz and 36.0 MHz acoustic frequencies, and for the quenched sample 2/Q at 12.0 MHz, 15.0 MHz and 20.0 MHz acoustic frequencies. An attempt to measure the acoustic loss for sample 2/Q at 36.0 MHz was made, but the loss at the peak maximum was too high to be reliably measured. The maximum losses are approximately linearly dependent to the acoustic wave frequency and the shift in peak

temperature is small; once again similar behaviour has been noted in vitreous SiO_2.

To further investigate the mechanism responsible for the large acoustic loss peak, measurements of loss at several acoustic frequencies were made at different temperatures in the range $1.4^{\circ}K$ to $400^{\circ}K$. Losses higher than 4 db/µsec were measured from chart recordings of the echo pattern. A Box-Car detector system and an X-Y recorder connected into the video circuit of the attenuation comparator allowed accurate reproduction of the echo display. A typical result is shown for sample 1/48 in Figure 6.13 where ultrasound attenuation is plotted against $\log_{10}$ (frequency). Assuming loss is proportional to (frequency)^n, this plot allows evaluation of the exponent n at each temperature.

A mechanism which attenuates an ultrasound wave should also produce an accompanying change in elastic modulus and hence ultrasound velocity. It is important to measure the ultrasound velocity as a function of temperature in the same samples used for the measurement of attenuation; throughout the work ultrasound attenuation and velocity have been measured simultaneously. Figures 6.14 to 6.19 show the temperature dependence of longitudinal and shear wave velocities in samples 1/Q, 1/48, 2/Q, 2/48, 4/Q and 5/Q between $4.2^{\circ}K$ and $400^{\circ}K$. Shear wave velocities only between $45^{\circ}K$ and $400^{\circ}K$ for samples 7/Q and 8/Q are presented in Figure 6.20. The

velocities have been corrected for phase shift effects
at the transducer-sample interface as detailed in
Section 5.2. All velocities show smooth variations with
temperature and evidence a relaxation in elastic modulus.
The velocities decrease to a minimum value at a temperature
higher than the position of maximum acoustic loss, but
rise again to reach a steady rate of increase by 400°K.
Absolute values of velocity, the fractional relaxation
in velocity and the fractional change in velocity with
temperature dV/VdT at 400°K vary both with sample
composition and time of heat treatment.

In Table 6.1 are collected ultrasound shear and
longitudinal velocities at 280°K for all the samples
studied. A wide range of ultrasound velocities is
exhibited by the $Na_2O-B_2O_3-SiO_2$ glasses of this work.

6.1.2   The temperature dependence of ultrasound
        attenuation and velocity below 4.2°K

To gain information about the low temperature
vibrational properties of $Na_2O-B_2O_3-SiO_2$ glasses,
measurements of ultrasound attenuation and velocity were
made from 4.2°K to as low temperatures as could be reached
in the cryostat, about 1.4°K. Figures 6.21 to 6.23 show
the temperature dependence of ultrasound attenuation of
both shear and longitudinal waves in selected samples
of the glasses at 12.0 MHz and 36.0 MHz acoustic frequencies.
These results are plotted from data originally intended
for the study of attenuation-frequency dependences below

4.2^OK, an example of which is shown in Figure 6.24.
Measurements were made by tuning the pulsed oscillator
to each frequency at each temperature. Figures 6.21
and 6.23 include information taken from the 4.2^OK to
400^OK measurements, and Figure 6.22 incorporates data
from the attenuation versus temperature experiments at
36.0 MHz on sample 1/48.

There is a small peak in the acoustic attenuation
at a temperature below 4.2^OK for all the samples studied,
and for both longitudinal and shear waves. This peak
is in a similar position to the peak observed in other
inorganic glasses (Krause and Kurkjian, 1968), about
which much interest has been recently centred. As such,
this anomalous property of the $Na_2O-B_2O_3-SiO_2$ glasses
is of great importance. The peak is superimposed on the
side of the much larger acoustic absorption which
maximizes at 100^OK to 130^OK, and the total measured attenua-
tion falls rapidly below 2^OK. An increase in the acoustic
frequency has the effect of shifting the maximum of the
small peak to a higher temperature, but an exact determina-
tion of the peak temperature is complicated by the
existence of the larger acoustic loss on to which it
is imposed.

To try to ascertain the activation energy and
attempt frequency of this low temperature absorption
mechanism, careful attenuation and velocity measurements
were repeated on samples 4/Q, and 2/Qii; this latter
sample is a second glass prepared from batch 2. These

experiments were undertaken with the pulsed oscillator of the attenuation comparator fixed at each frequency throughout a complete cooling cycle. It is better to avoid returning the oscillator between measurements and this approach fulfills this requirement. That the sample reached equilibrium in about 4 minutes after each temperature change was evidenced by constant velocity and attenuation readings. However, to make certain of steady state conditions the system was allowed to stabilise for 15 minutes before each measurement was made. Use of the cartesian manostat for pressure control while pumping on the liquid helium ensured good temperature control during the measurements, temperature drift over the 15 minute period did not exceed $1/30th^{\circ}K$.

Figures 6.25 to 6.29 show the results of these experiments. The features of acoustic attenuation are much the same as those of Figures 6.21 to 6.23. A much smaller activation energy is associated with the smaller peak mechanism than with the larger peak on to which it is imposed (a point to be discussed in greater detail later), and the smaller peak thus suffers a larger shift in temperature with increasing acoustic frequency. Thus, between 12.0 MHz and 60.0 MHz, the small peak appears to climb up the steep rise in acoustic attenuation and consequently the attenuation at its maximum is not a simple function of acoustic frequency.

Ultrasound velocities are also reported as a function of temperature for each acoustic frequency in

Figures 6.25 to 6.29, and have been corrected as detailed in Section 5.2. These velocities are linearly dependent on temperature down to about 2^{O}K, where they then flatten out. The scatter of results is largest at 60.0 MHz where the increase in attenuation and decrease in number of echoes available for superposition reduces the sensitivity of the measurement. Ultrasound shear velocities change by less than 0.1% over the temperature range 4.2^{O}K to 2^{O}K, and equal temperature gradients are exhibited at different acoustic frequencies by the same sample.

TABLE 6.1   DENSITY, VELOCITIES AND ELASTIC MODULI OF GLASSES AT 280K   UNITS G/CM3, CM3, CM/SEC, DYNES/CM2

GLASS	DENSITY	VL	VS	BULK	SHEAR	YOUNGS	POISSONS
1/0	2.149	4.9148E 05	2.8221E 05	2.909E 11	1.712E 11	4.293E 11	0.2541
1/24	2.148	4.7900E 05	2.9040E 05	2.513E 11	1.811E 11	4.392E 11	0.2094
1/48	2.145	4.9040E 05	2.7948E 05	2.925E 11	1.675E 11	4.220E 11	0.2595
1/96	2.142	4.8071E 05	2.8585E 05	2.616E 11	1.750E 11	4.293E 11	0.2265
1/168	2.143	4.8940E 05	2.9160E 05	2.703E 11	1.822E 11	4.464E 11	0.2249
1/504	2.140	4.7134E 05	2.8243E 05	2.478E 11	1.707E 11	4.165E 11	0.2190
2/0	2.060	4.4410E 05	2.5730E 05	2.244E 11	1.364E 11	3.402E 11	0.2474
2/24	2.058	4.3358E 05	2.5523E 05	2.081E 11	1.341E 11	3.311E 11	0.2349
2/48	2.058	4.5115E 05	2.6205E 05	2.304E 11	1.413E 11	3.520E 11	0.2454
2/96	2.055	4.3931E 05	2.6707E 05	2.012E 11	1.466E 11	3.538E 11	0.2069
2/168	2.053	4.3210E 05	2.5499E 05	2.055E 11	1.334E 11	3.290E 11	0.2331
2/504	2.054	4.3751E 05	2.6035E 05	2.075E 11	1.392E 11	3.413E 11	0.2259
3/0	2.162	4.8900E 05	2.8923E 05	2.758E 11	1.800E 11	4.453E 11	0.2310
4/0	2.069	4.5341E 05	2.6785E 05	2.347E 11	1.429E 11	3.565E 11	0.2459
4/48	2.066	4.3080E 05	2.5427E 05	2.053E 11	1.336E 11	3.293E 11	0.2327
5/0	2.120	4.7472E 05	2.7081E 05	2.705E 11	1.655E 11	3.914E 11	0.2588
5/48	2.120	4.7164E 05	2.7700E 05	2.545E 11	1.627E 11	4.023E 11	0.2365
6/0	2.042	4.5300E 05	2.5831E 05	2.374E 11	1.363E 11	3.431E 11	0.2591
7/0	1.970	3.0457E 05	2.3272E 05	1.646E 11	1.067E 11	2.632E 11	0.2335
8/0	2.264	5.2460E 05	3.0640E 05	3.307E 11	2.125E 11	5.276E 11	0.2411
9/0	2.400	5.6462E 05	3.4090E 05	3.934E 11	2.787E 11	6.766E 11	0.2134
10/0	2.181	4.9249E 05	2.9164E 05	2.817E 11	1.855E 11	4.563E 11	0.2300
ERROR	#.002	#.0040	#.0020	#.012	#.010	#.012	#.0010

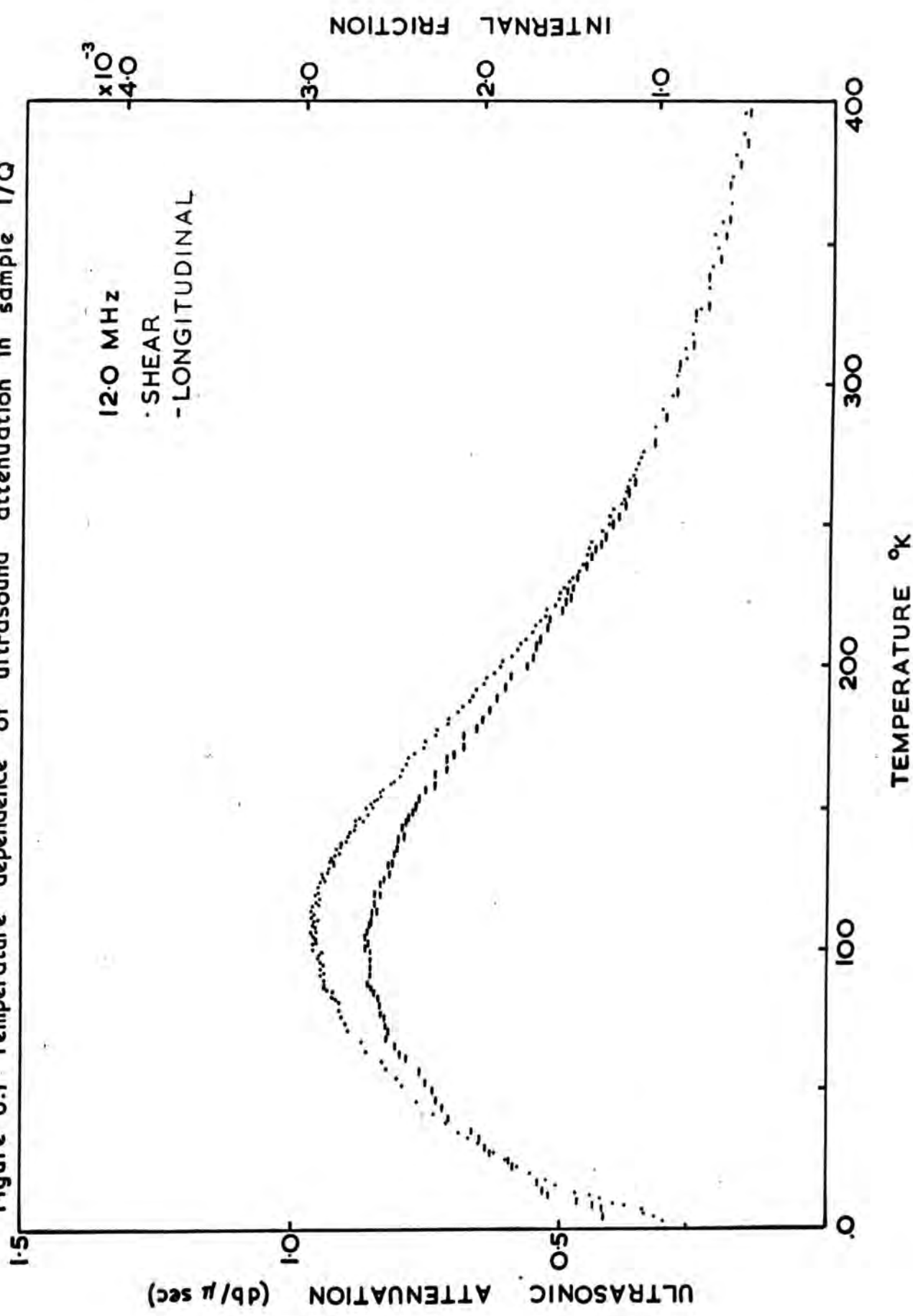Figure 6.1 Temperature dependence of ultrasound attenuation in sample I/Q

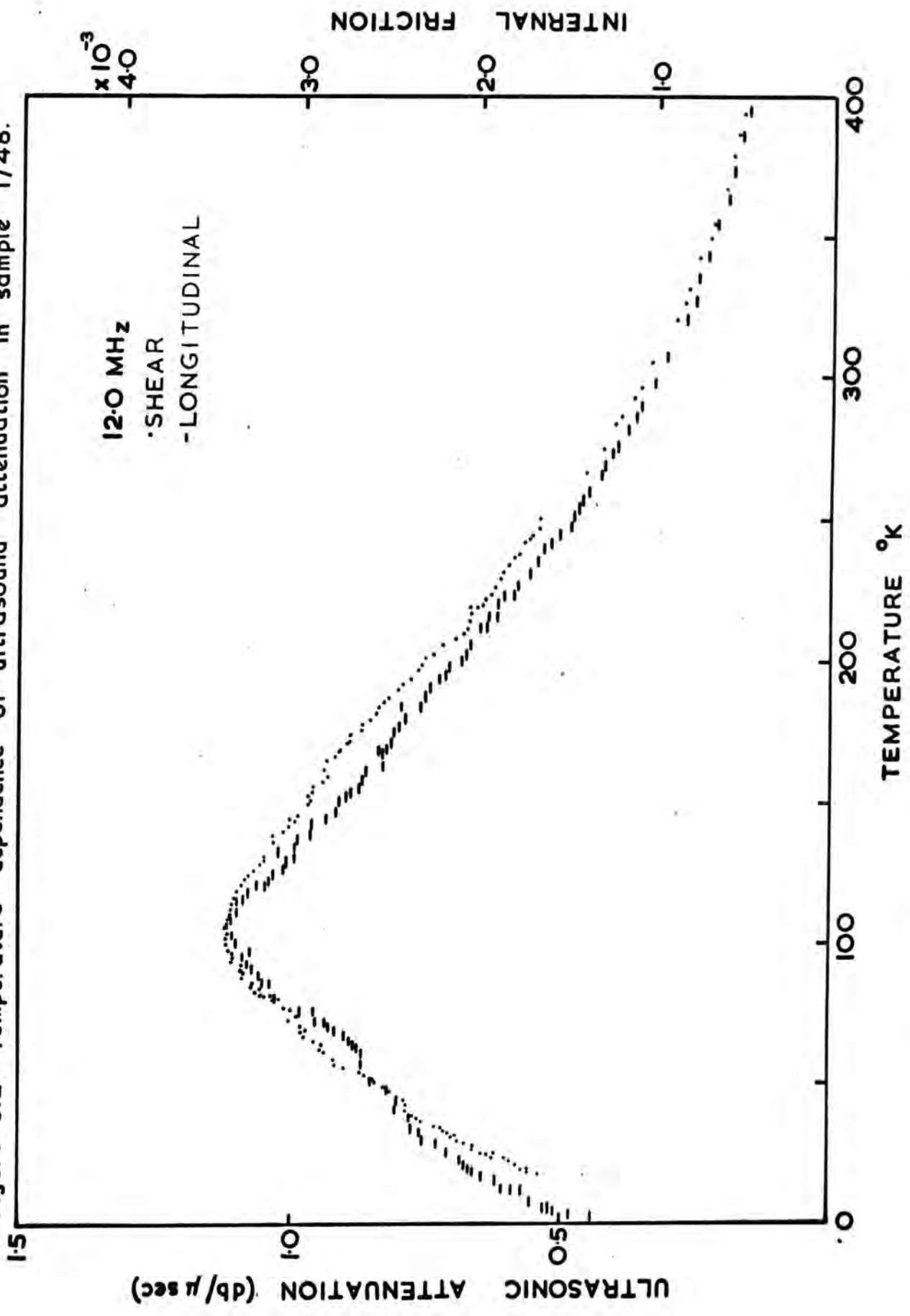Figure 6.2 Temperature dependence of ultrasound attenuation in sample 1/48.

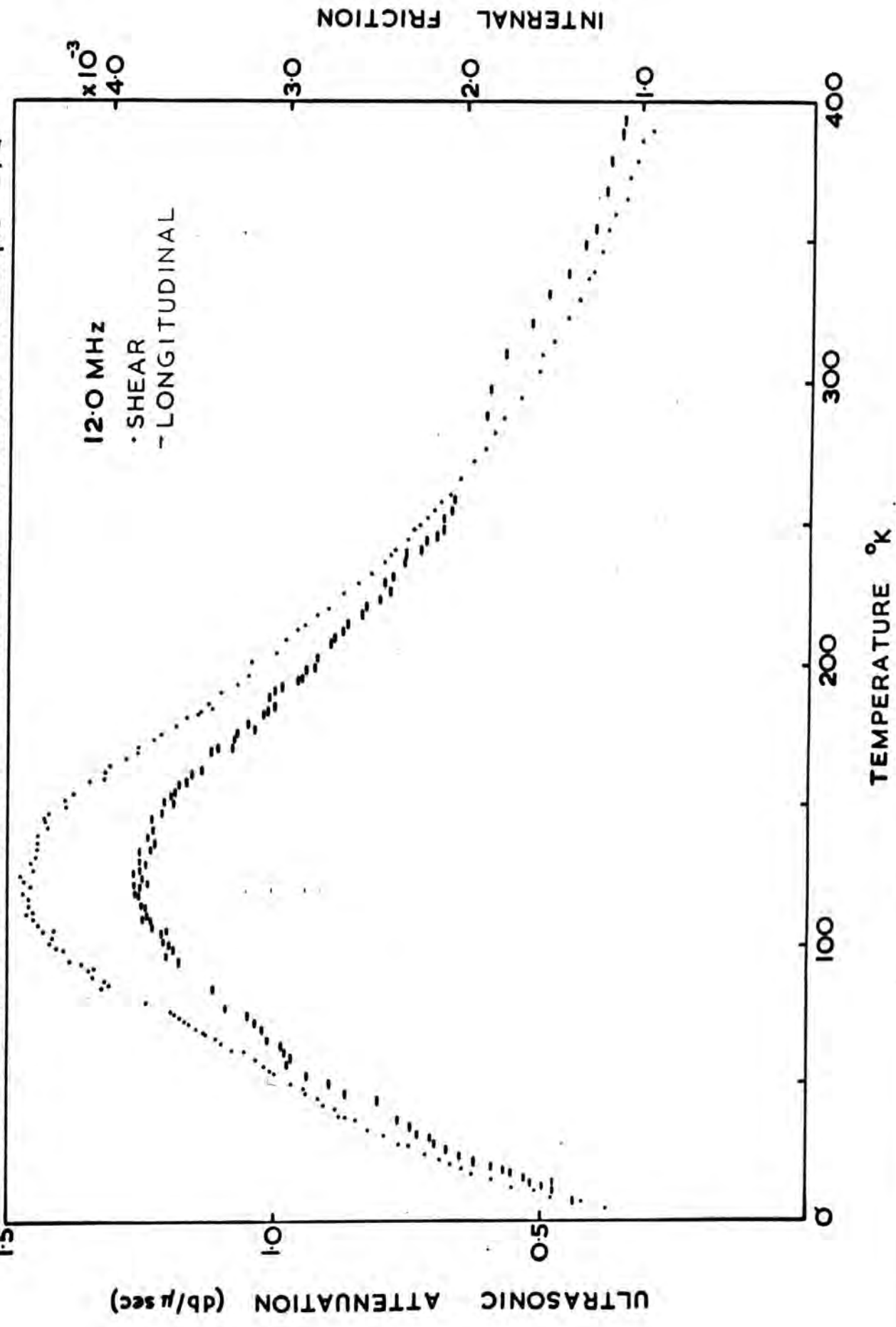Figure 6.3 Temperature dependence of ultrasound attenuation in sample 2/Q.

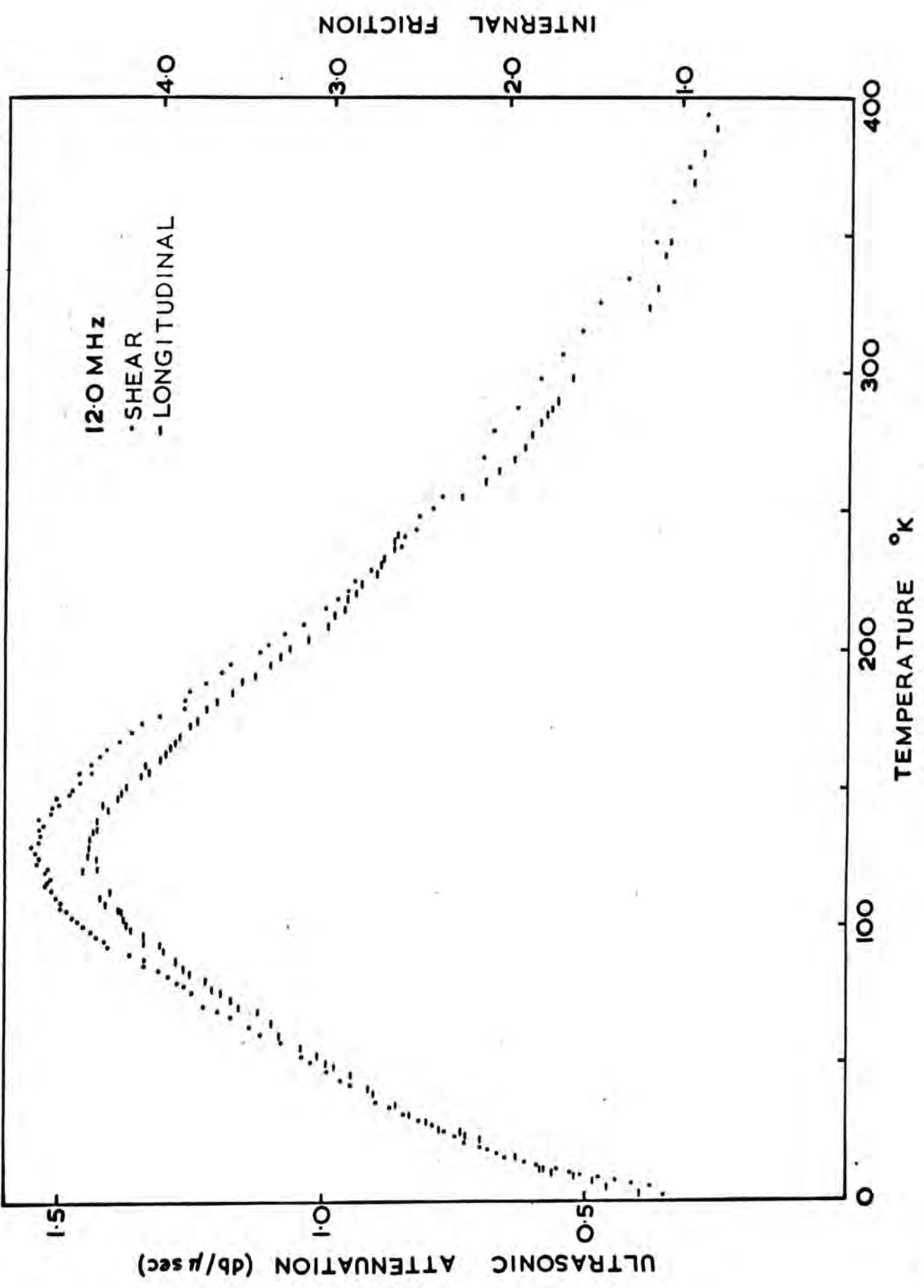Figure 6.4 Temperature dependence of ultrasound attenuation in sample 2/48.

Figure 6.5 Temperature dependence of ultrasound attenuation in sample 3/Q

12·0 MHz

·SHEAR
-LONGITUDINAL

TEMPERATURE °K

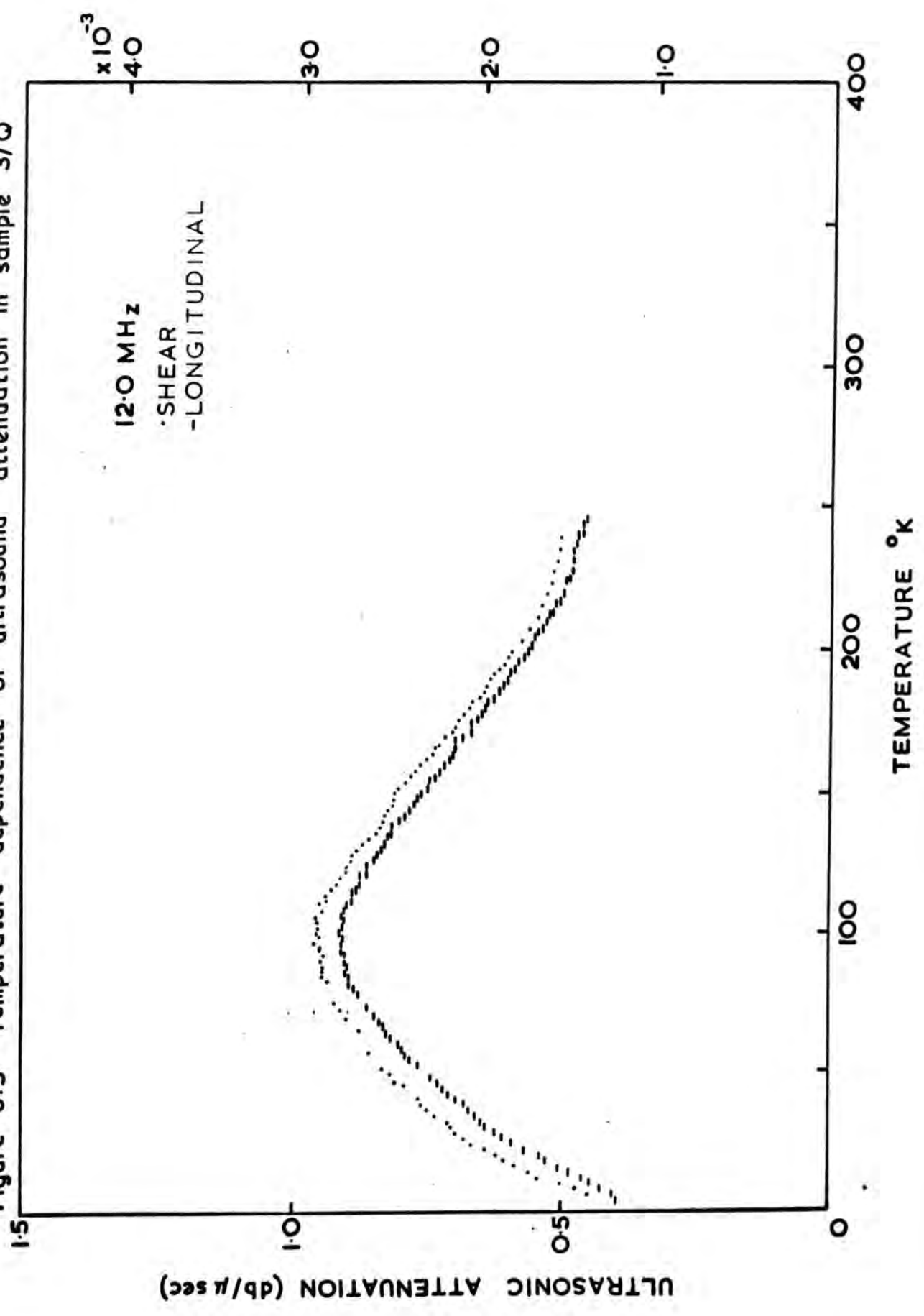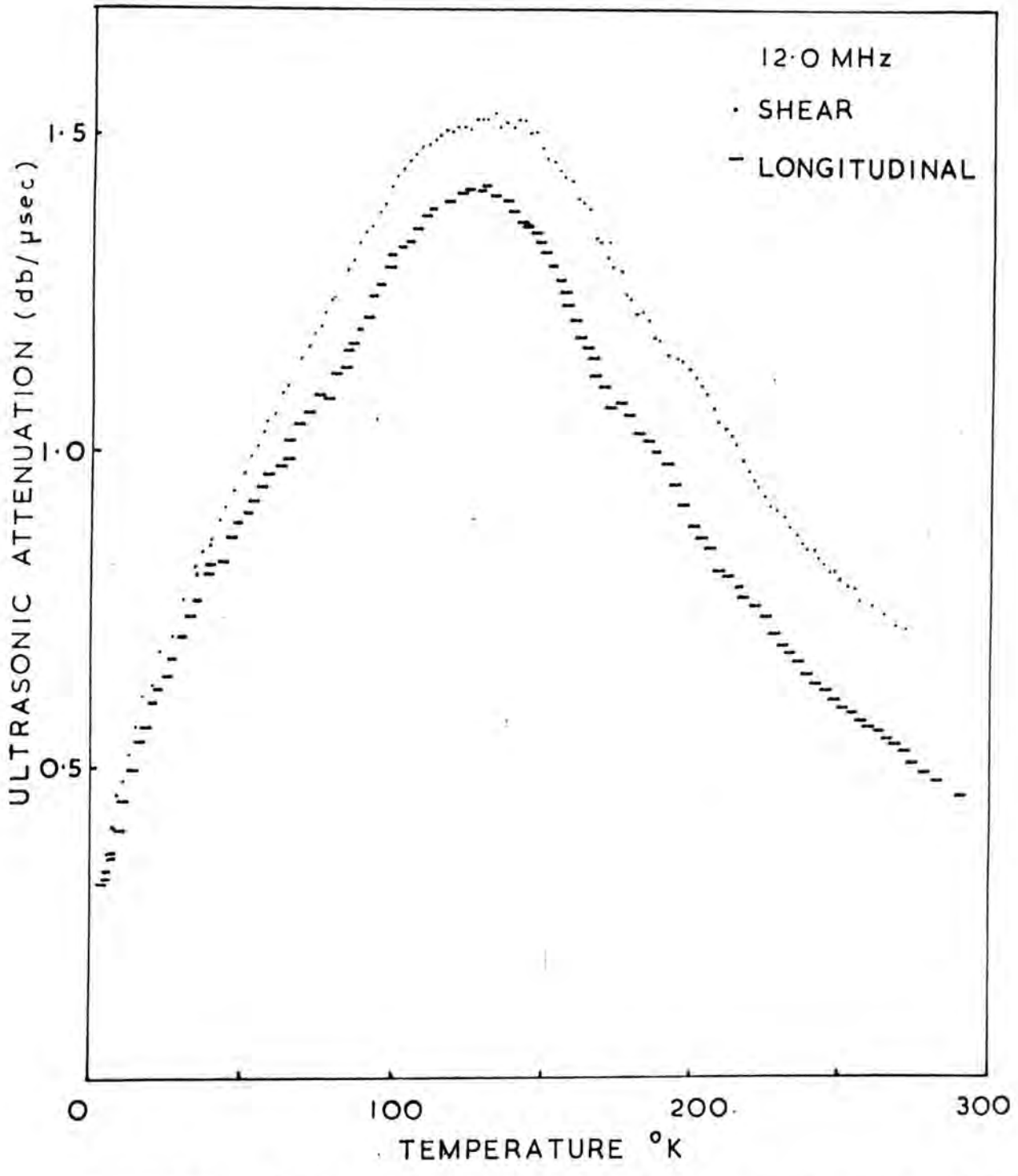ULTRASONIC ATTENUATION (db/μ sec)

Figure 6.6   Temperature dependence of ultrasound attenuation

in sample 4/Q

Figure 6.7 Temperature dependence of ultrasound attenuation in sample 5/Q.

Figure 6.8 and 6.9 Temperature dependence of ultrasound attenuation in samples 7/Q & 8/Q
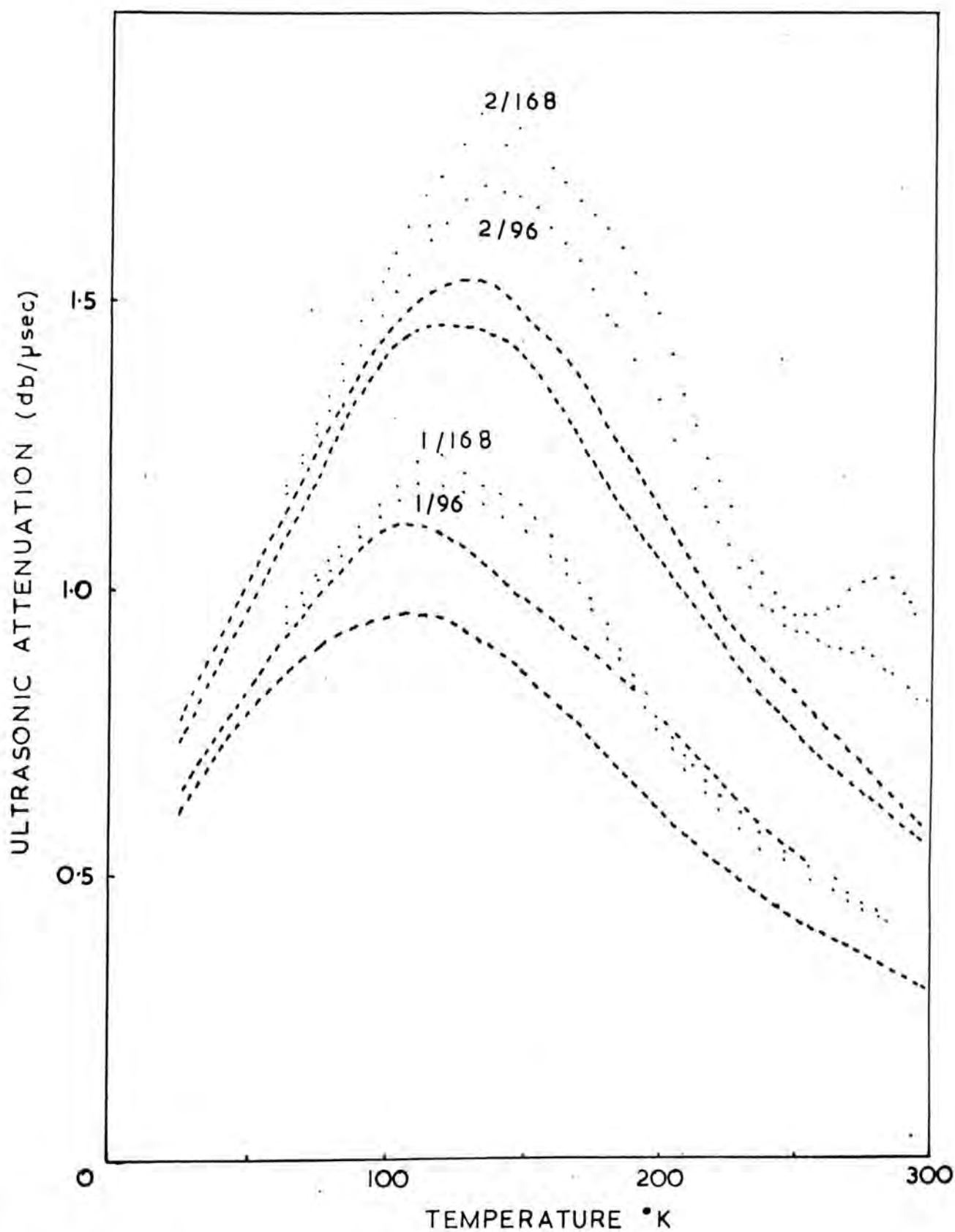
Figure 6.10   Temperature dependence of ultrasound attenuation in samples 1/96, 1/168, 2/96 and 2/168.
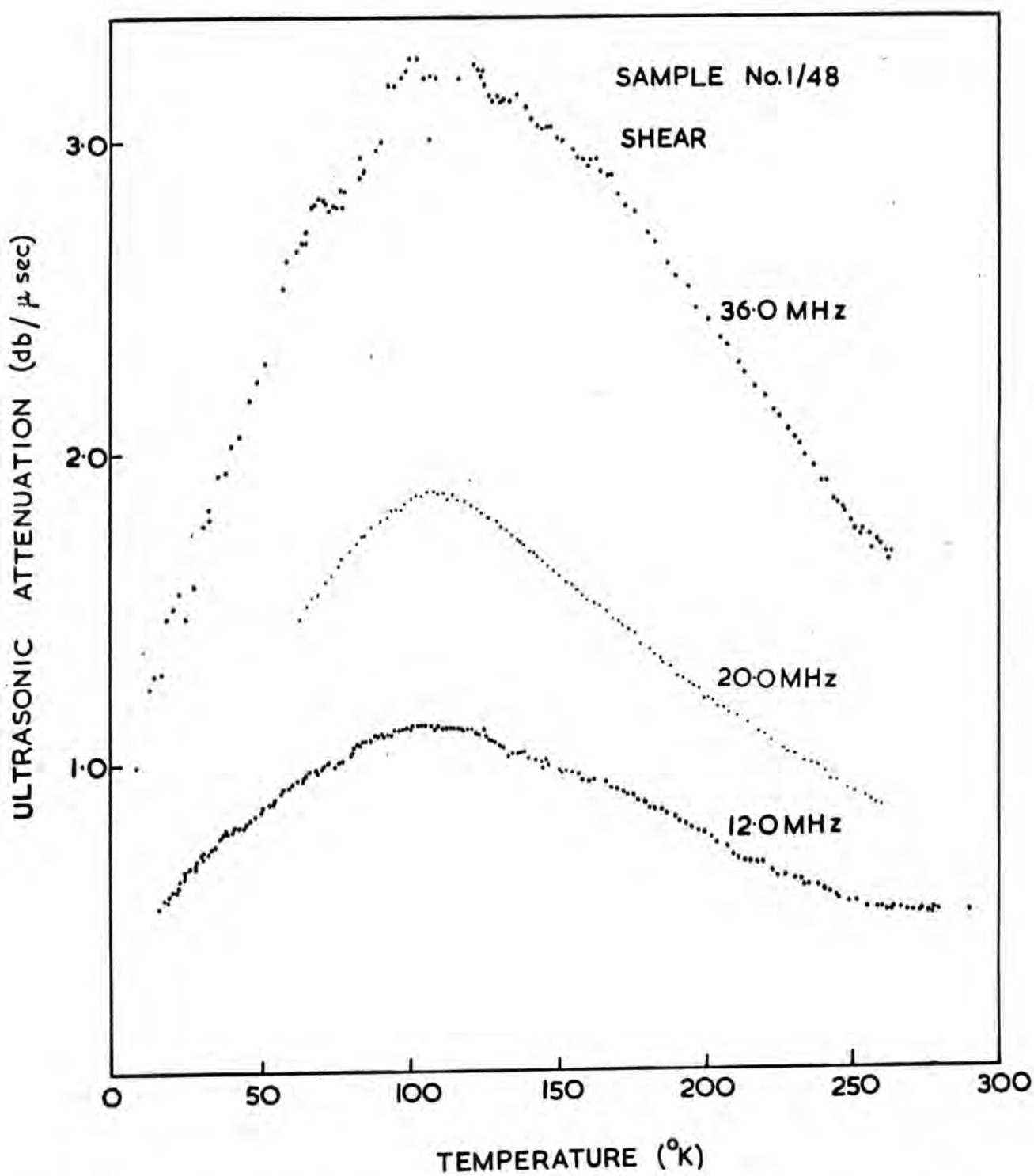
Figure 6.11 Temperature dependence of ultrasound attenuation in sample 1/48 at 12·0 MHz, 20·0 MHz and 36·0 MHz.

Figure 6.12 Temperature dependence of ultrasound attenuation in sample 2/Qii at 12·0MHz, 15·0MHz & 20·0MHz
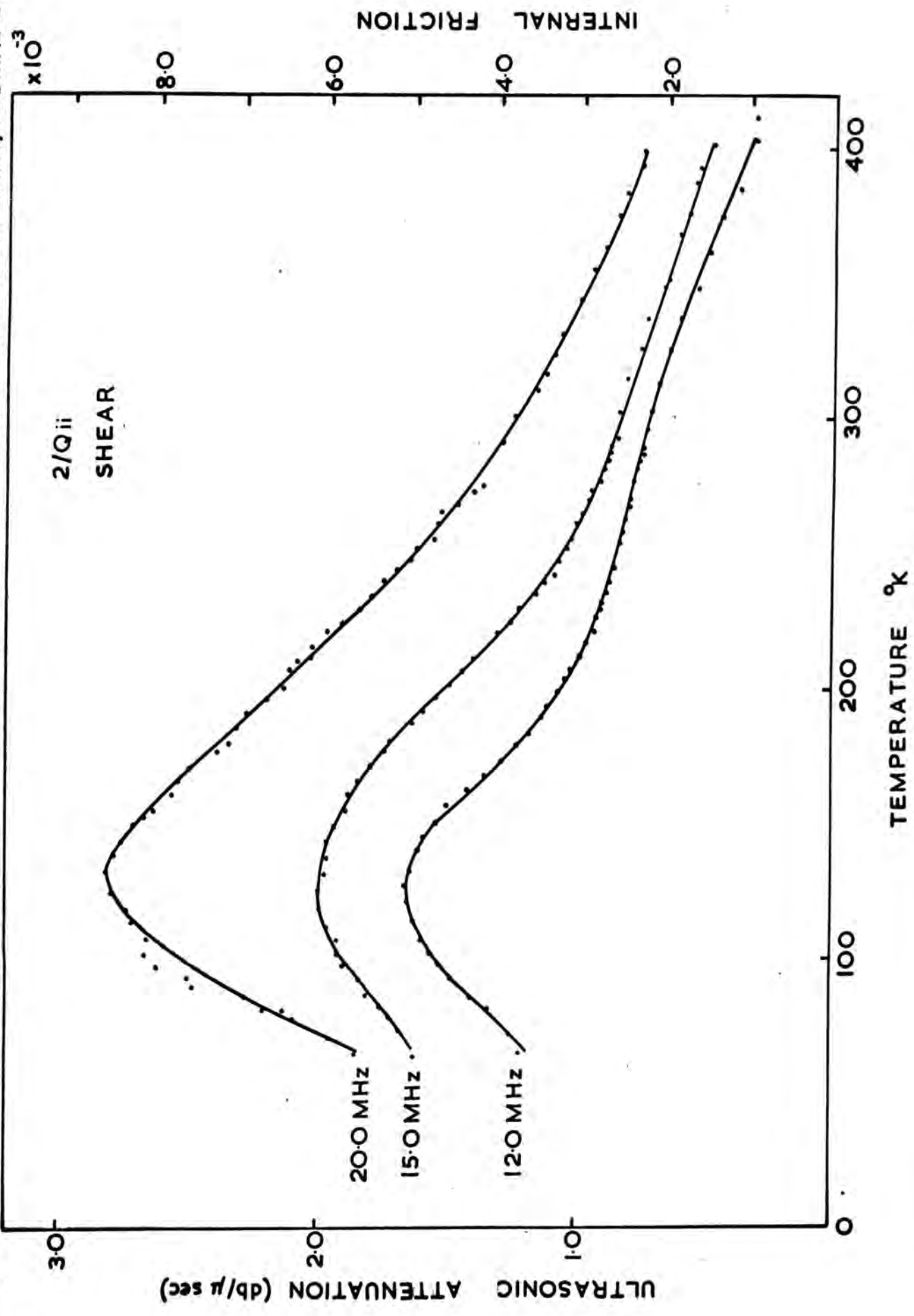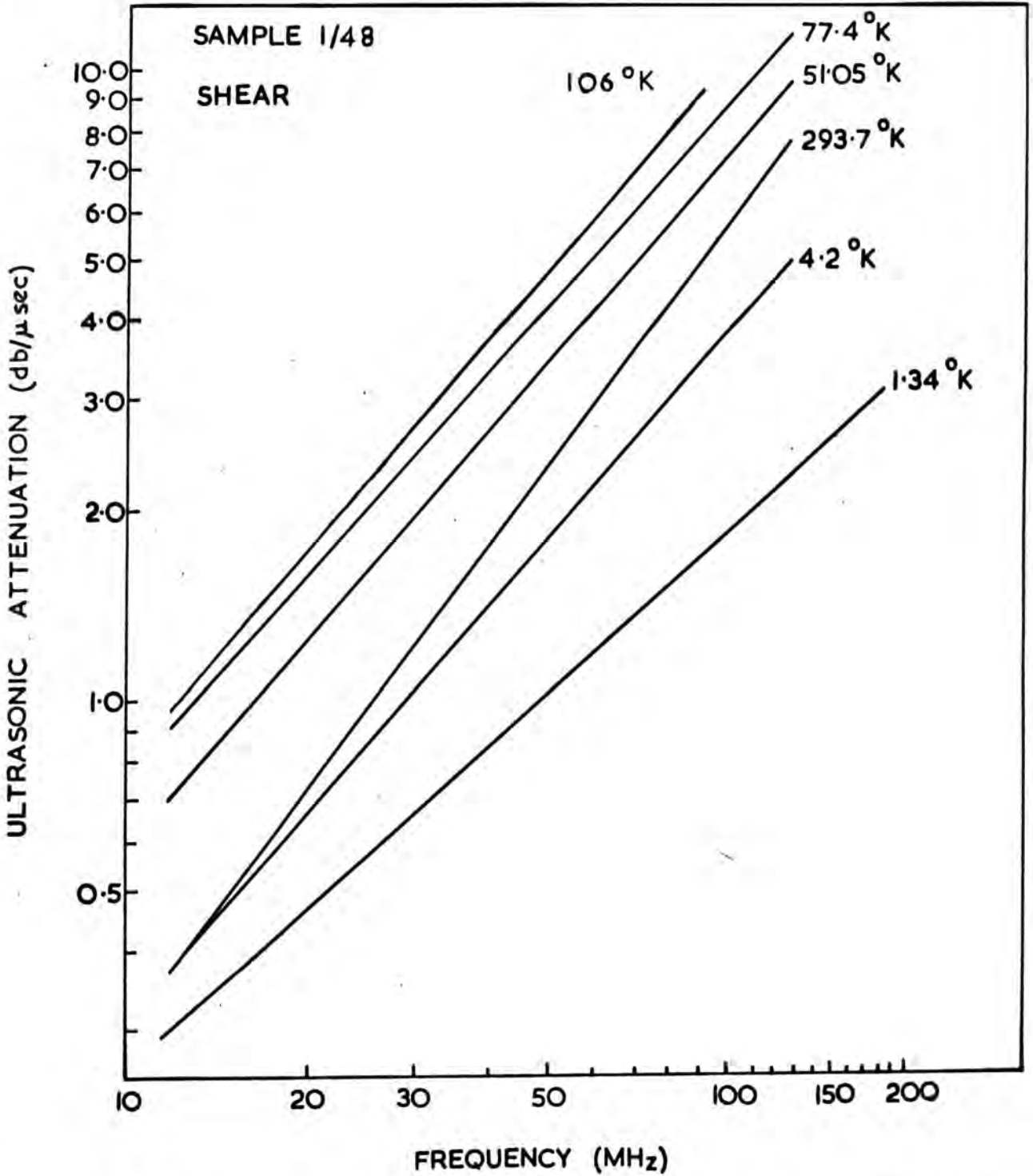
Figure 6.13 Frequency dependence of shear attenuation in sample 1/48.

Figure 6.14 Temperature dependence of ultrasound velocity in sample I/Q.
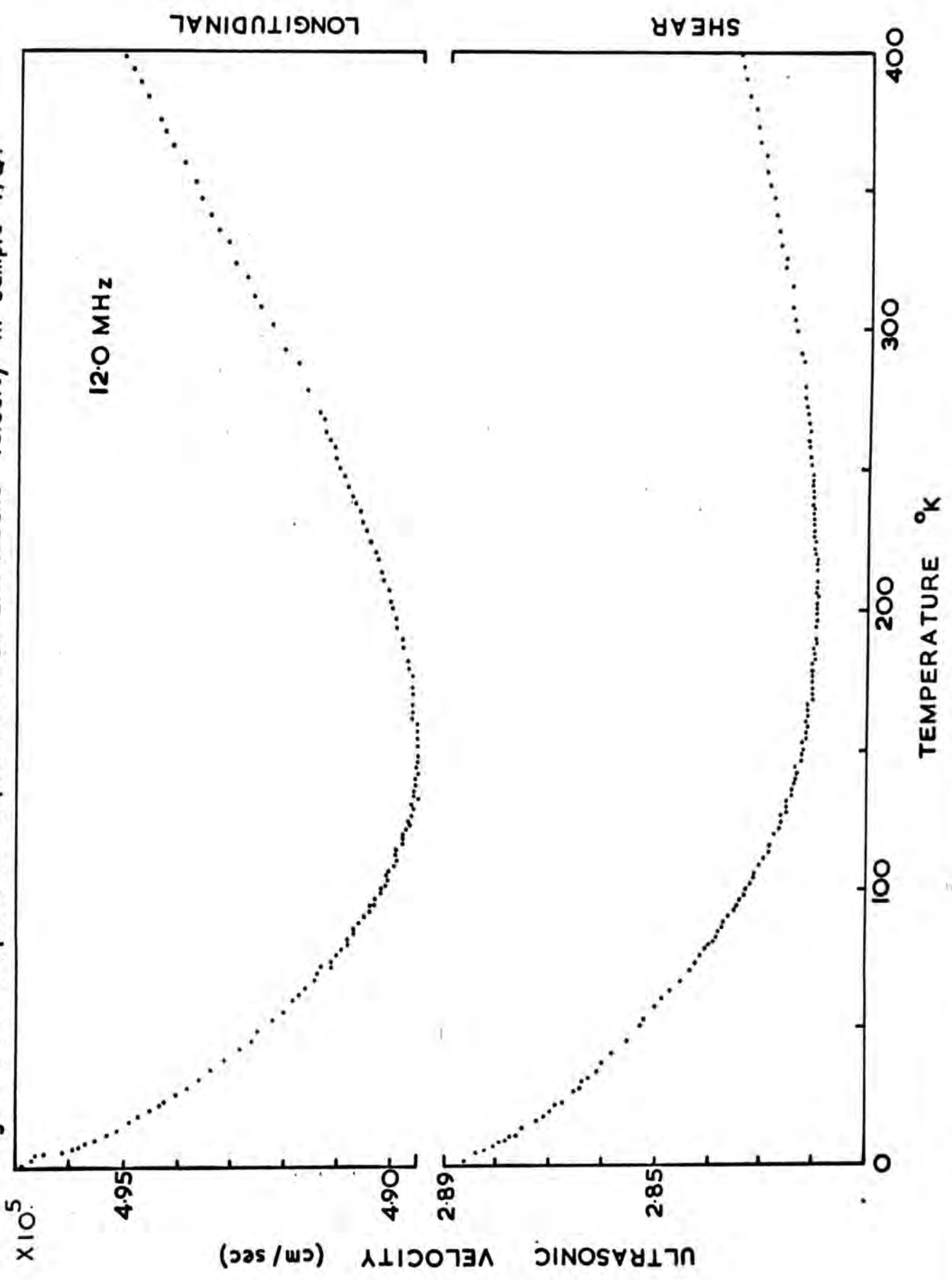
Figure 6.15 Temperature dependence of ultrasound velocity in sample 1/48
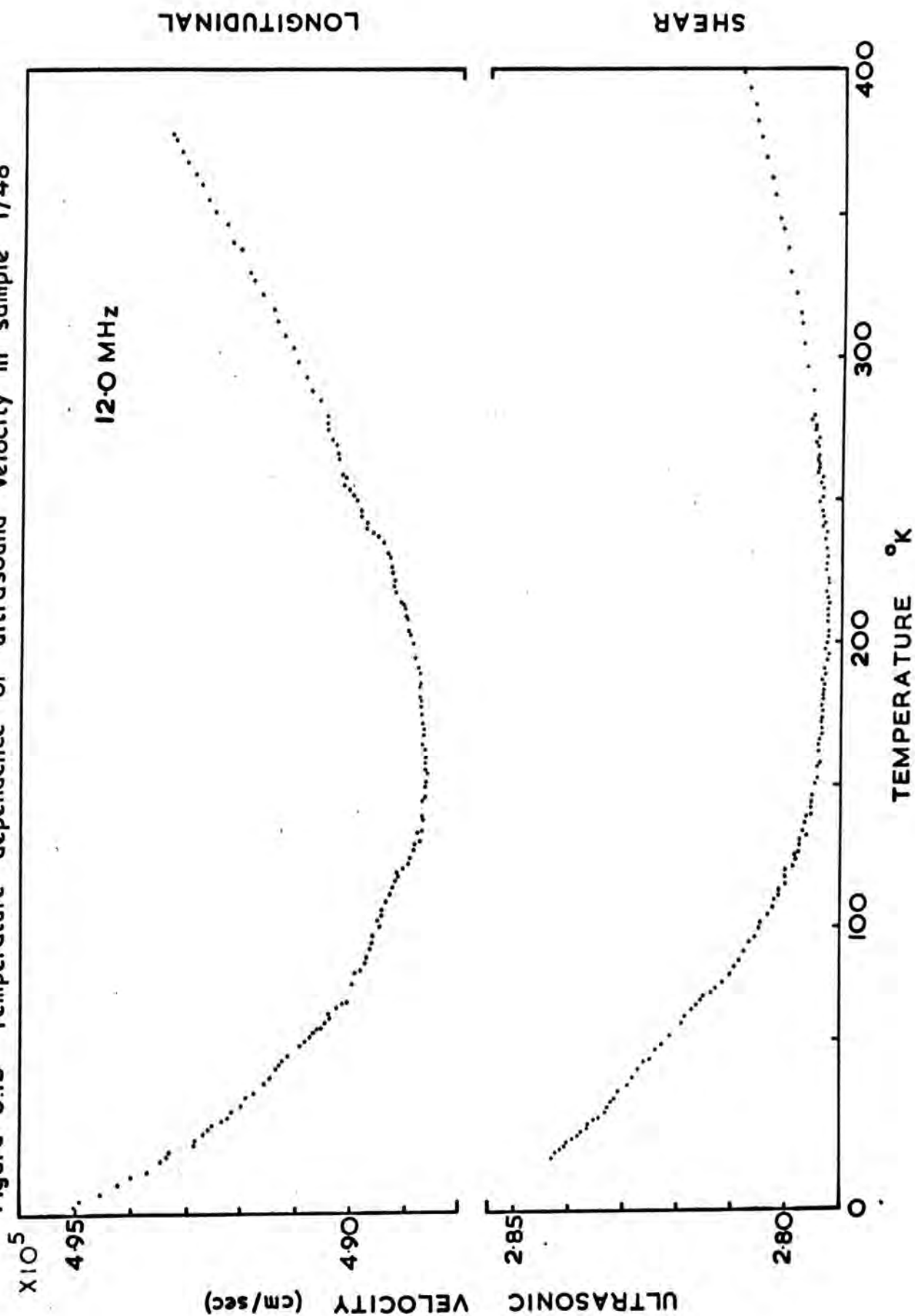
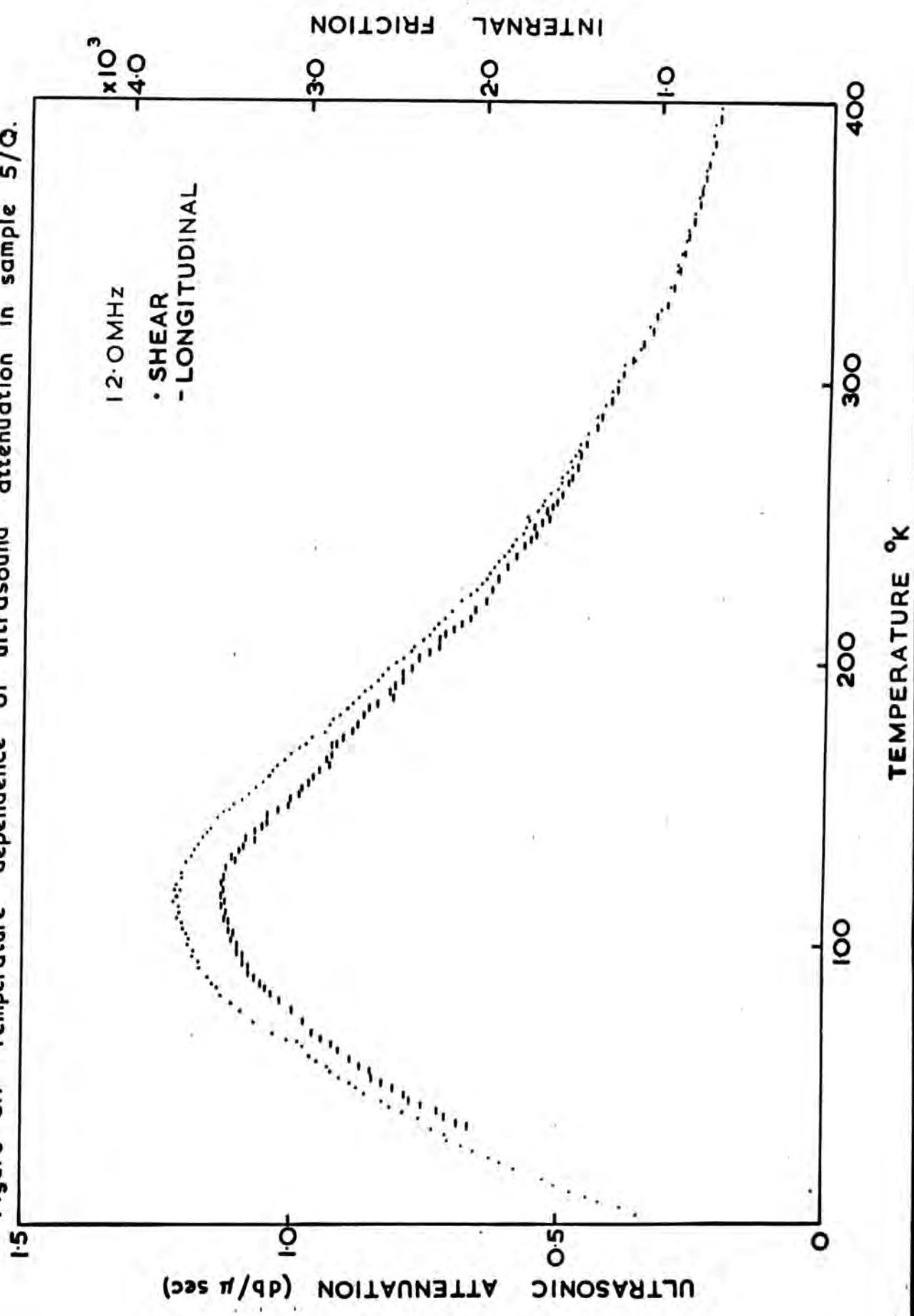Figure 6.16 Temperature dependence of ultrasound velocity in sample 2/Q.
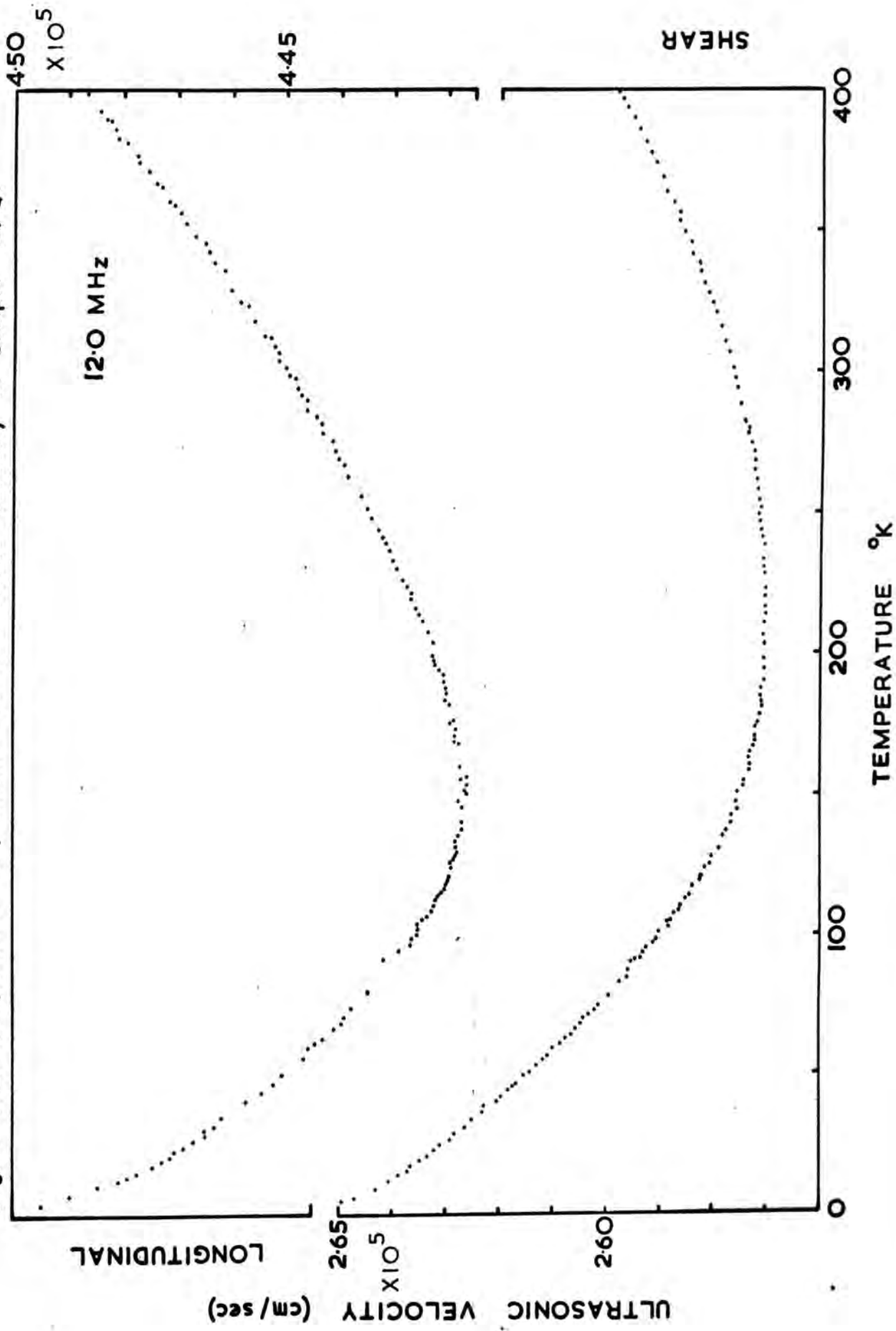
Figure 6.17 Temperature dependence of ultrasound velocity in sample 2/48
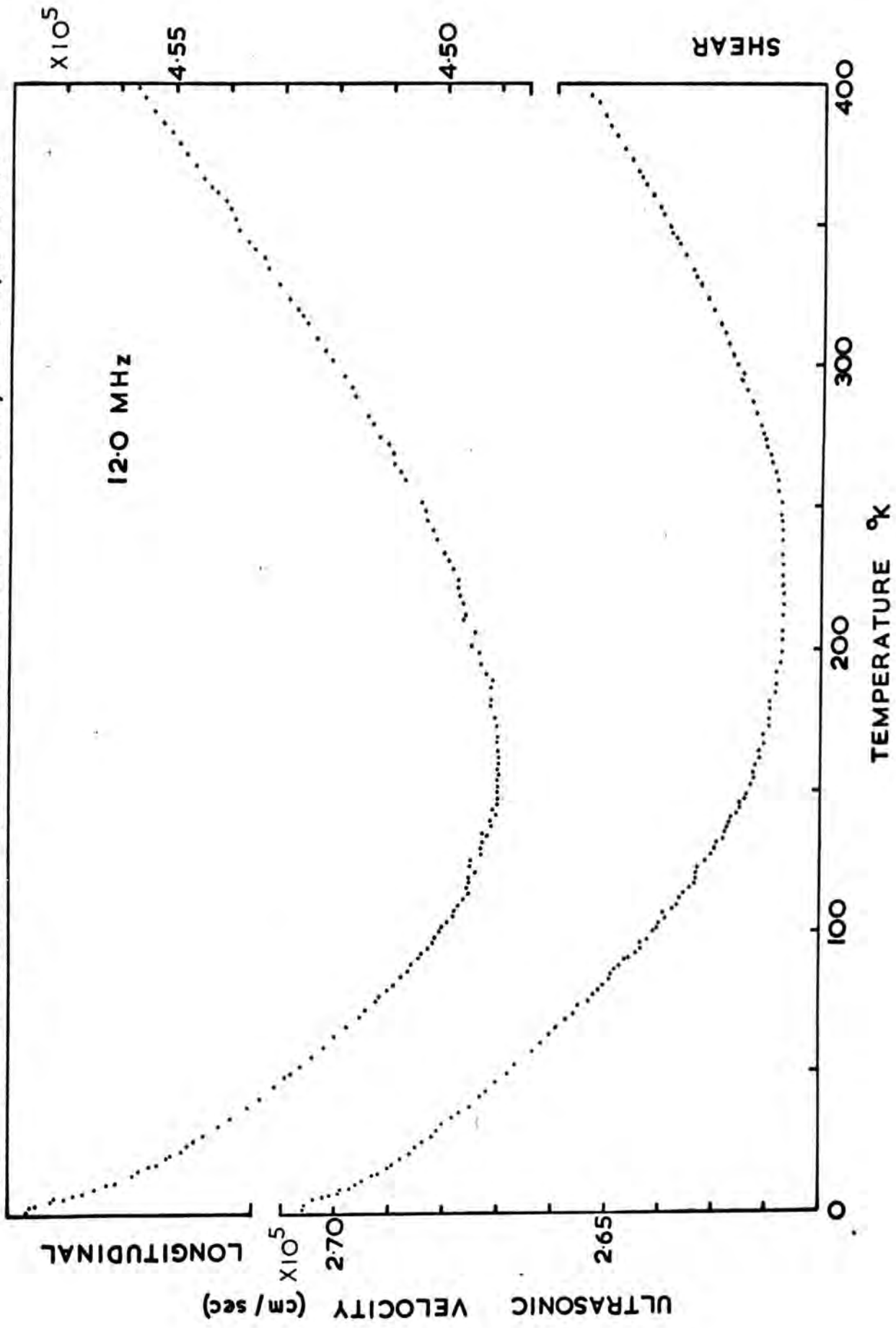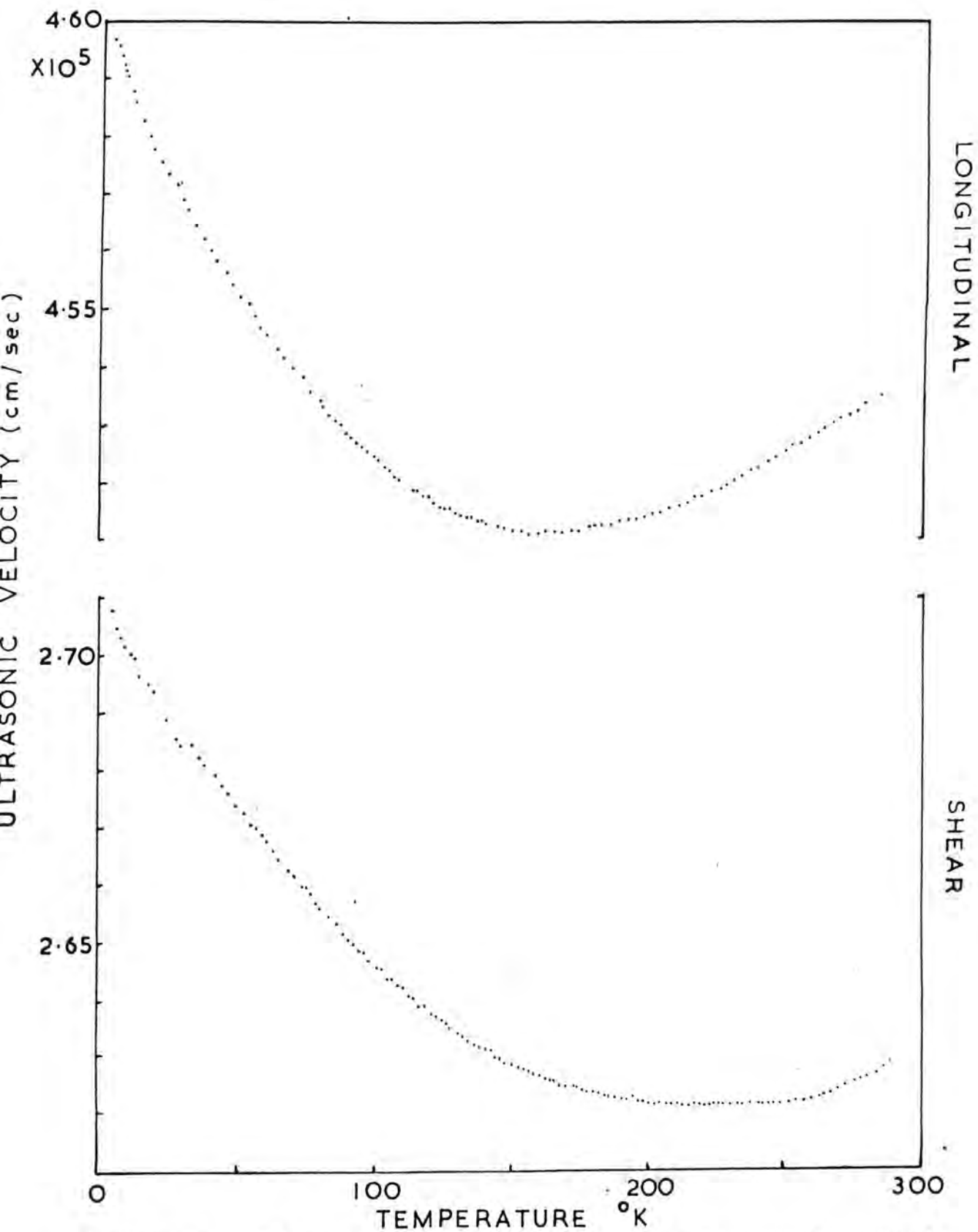
Figure 6.18   Temperature   dependence   of   ultrasound   velocity

in   sample   4/Q

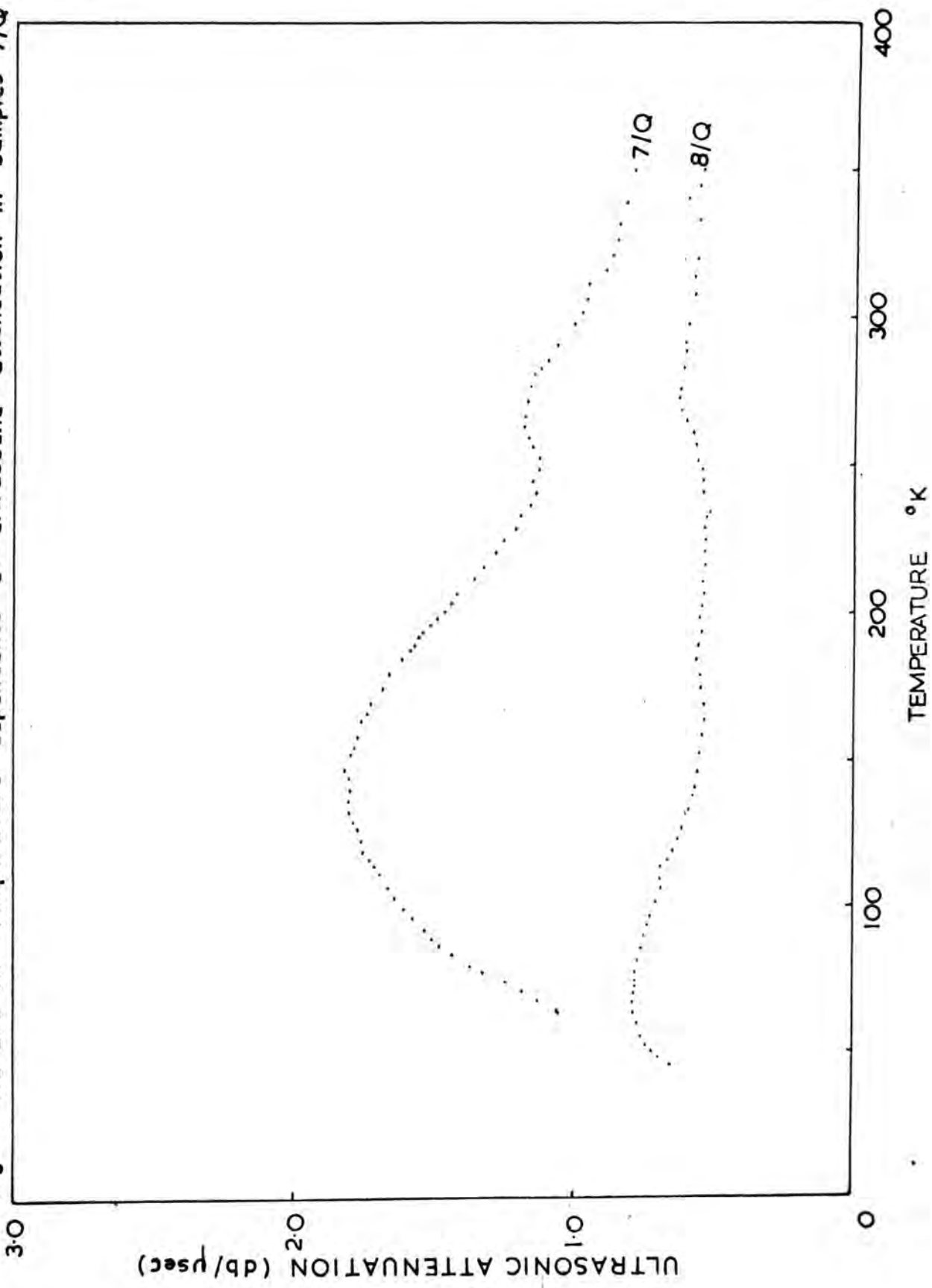Figure 6.19 Temperature dependence of ultrasound velocity in sample 5/Q
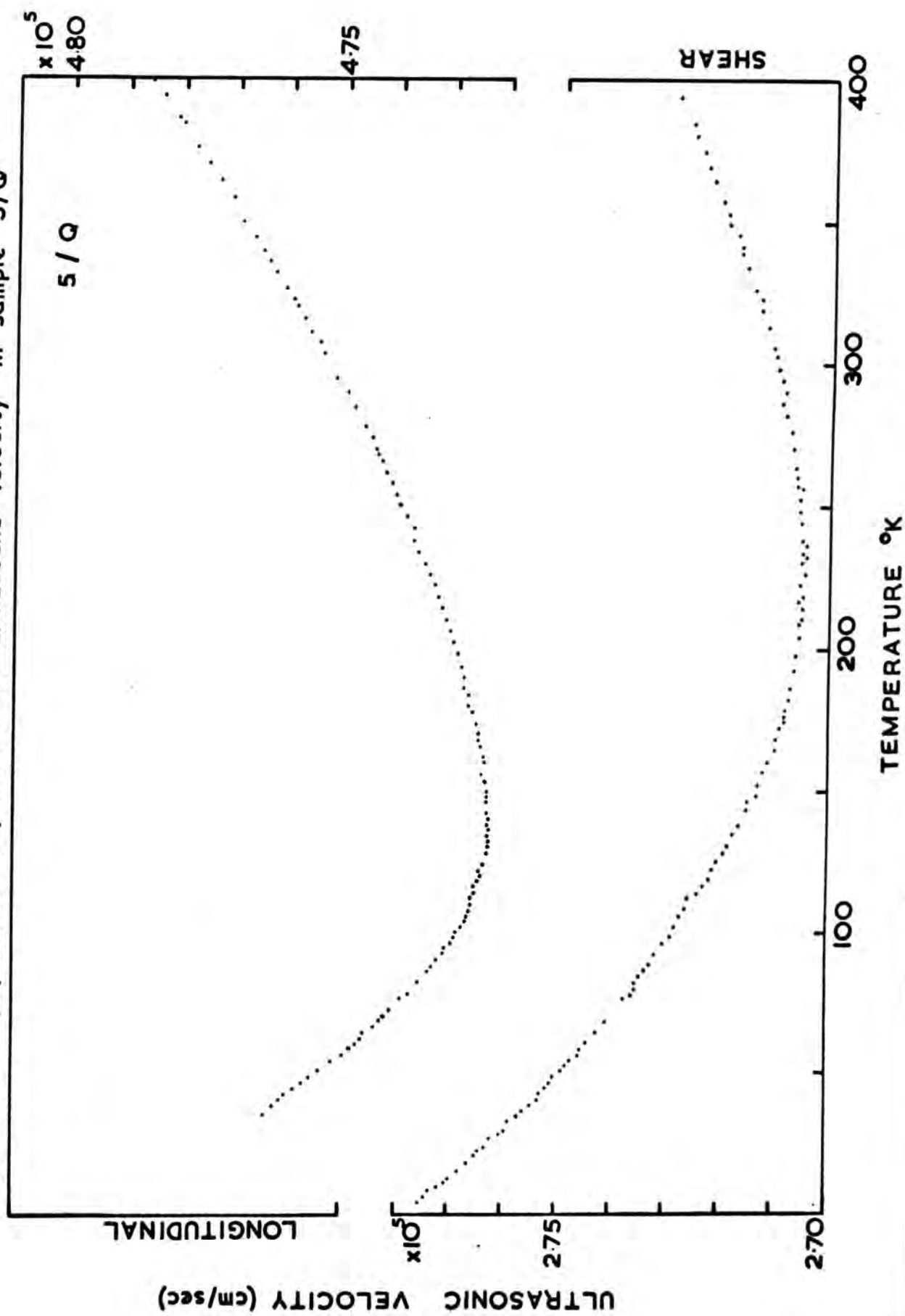
Figure 6·20 Temperature dependence of ultrasound velocity in samples 7/Q and 8/Q

SHEAR

8/Q

7/Q

ULTRASONIC VELOCITY (cm/sec)
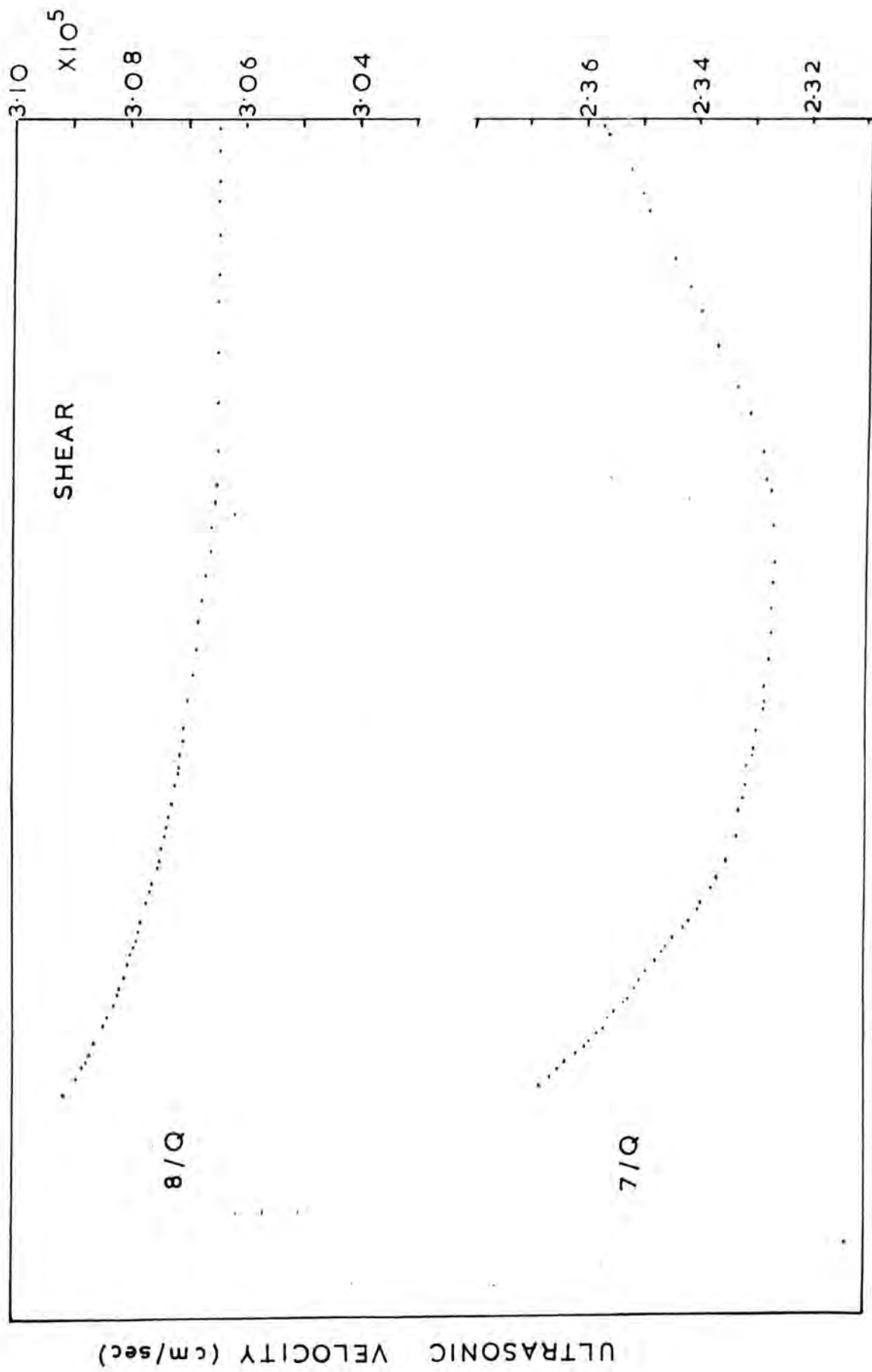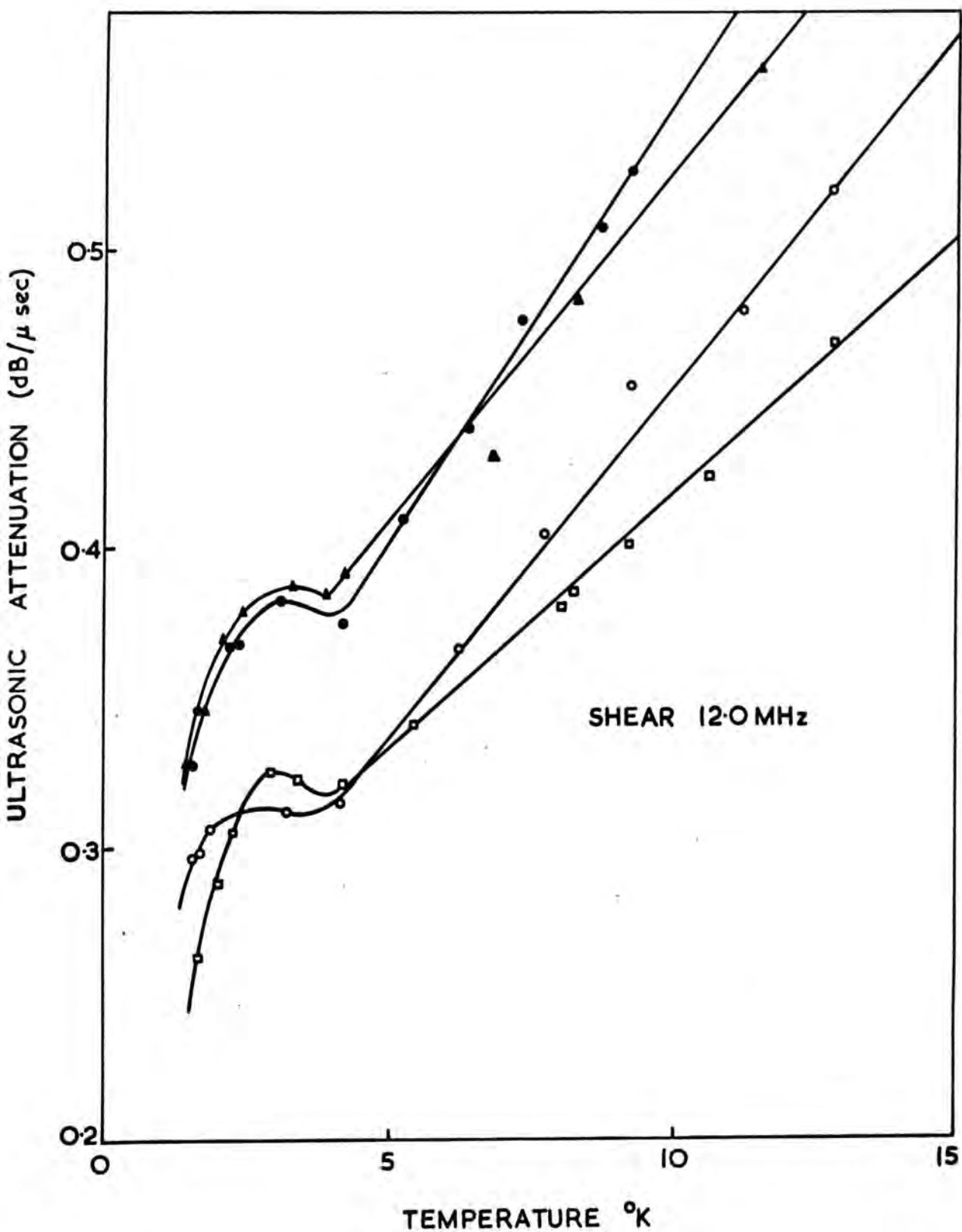
Figure 6.21 Ultrasound attenuation below 4·2°K in samples 1/Q □, .
2/Q ▲, 2/48 ● and 4/Q ○ at 12·0 MHz.
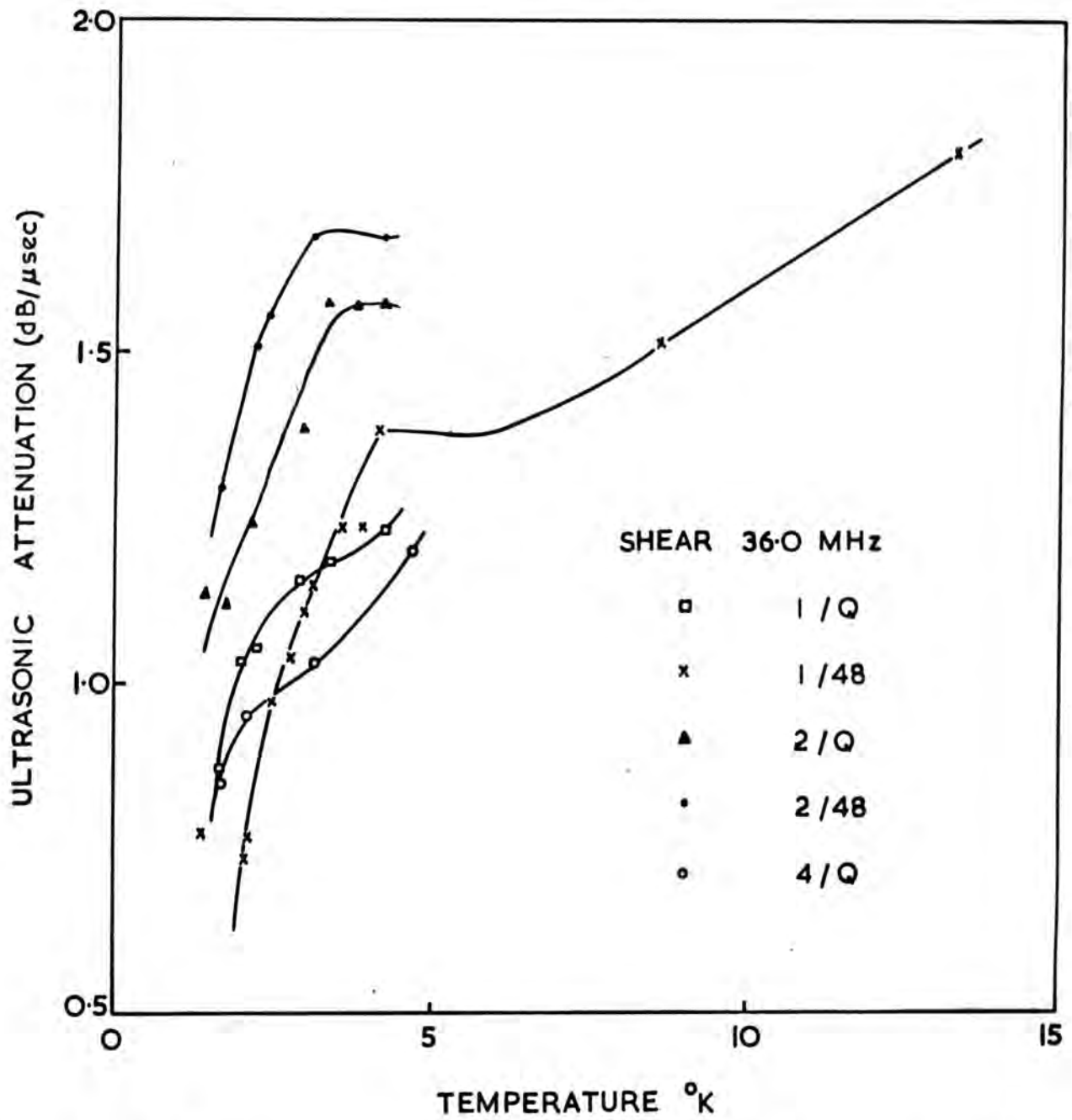
Figure 6.22 Ultrasound attenuation below 4·2°K in samples 1/Q □,
1/48 ×, 2/Q ▲, 2/48 ● and 4/Q ○ at 36·0 MHz
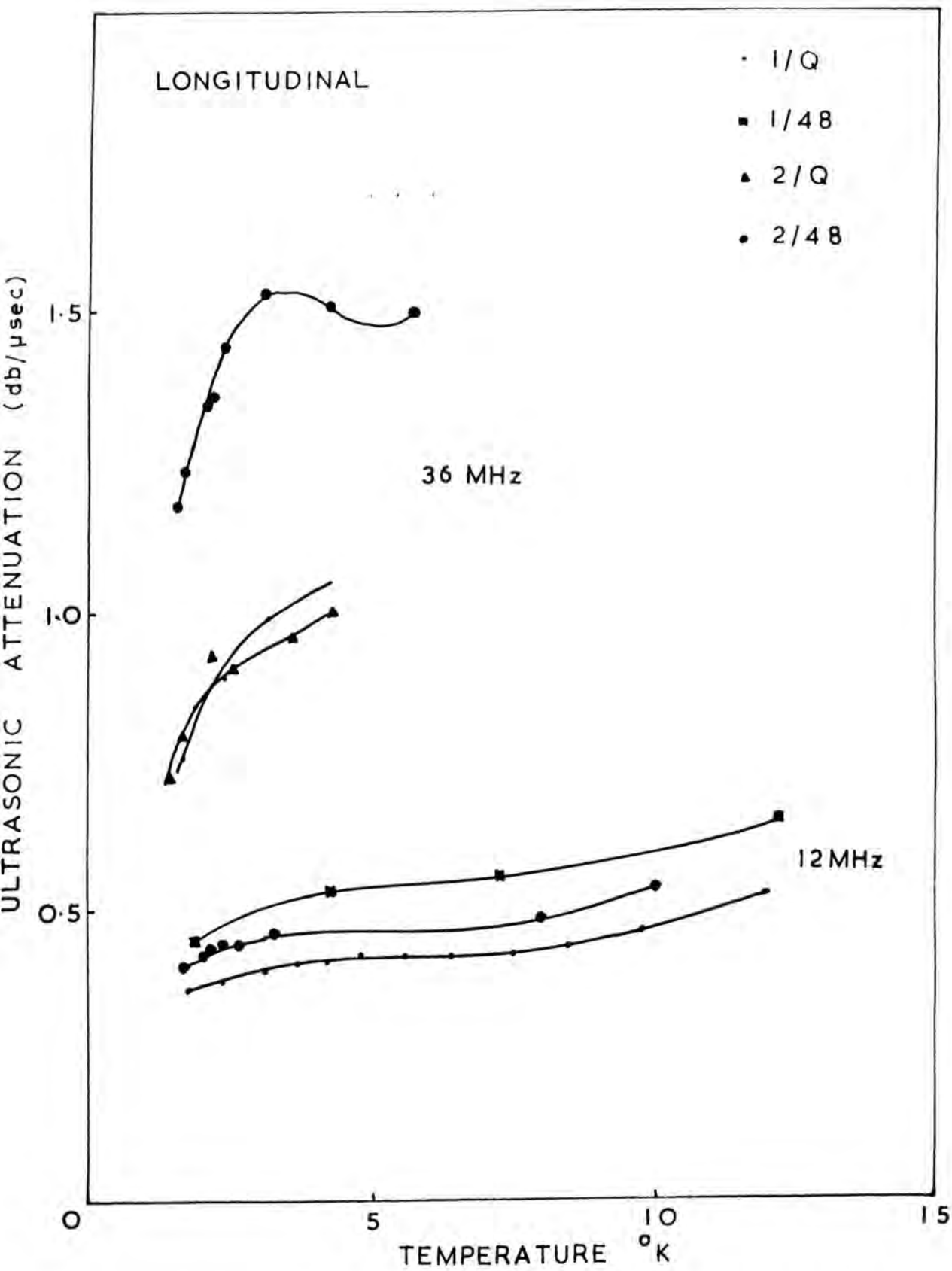
Figure 6.23 Ultrasound attenuation below 4.2°K in samples 1/Q, 1/48, 2/Q and 2/48
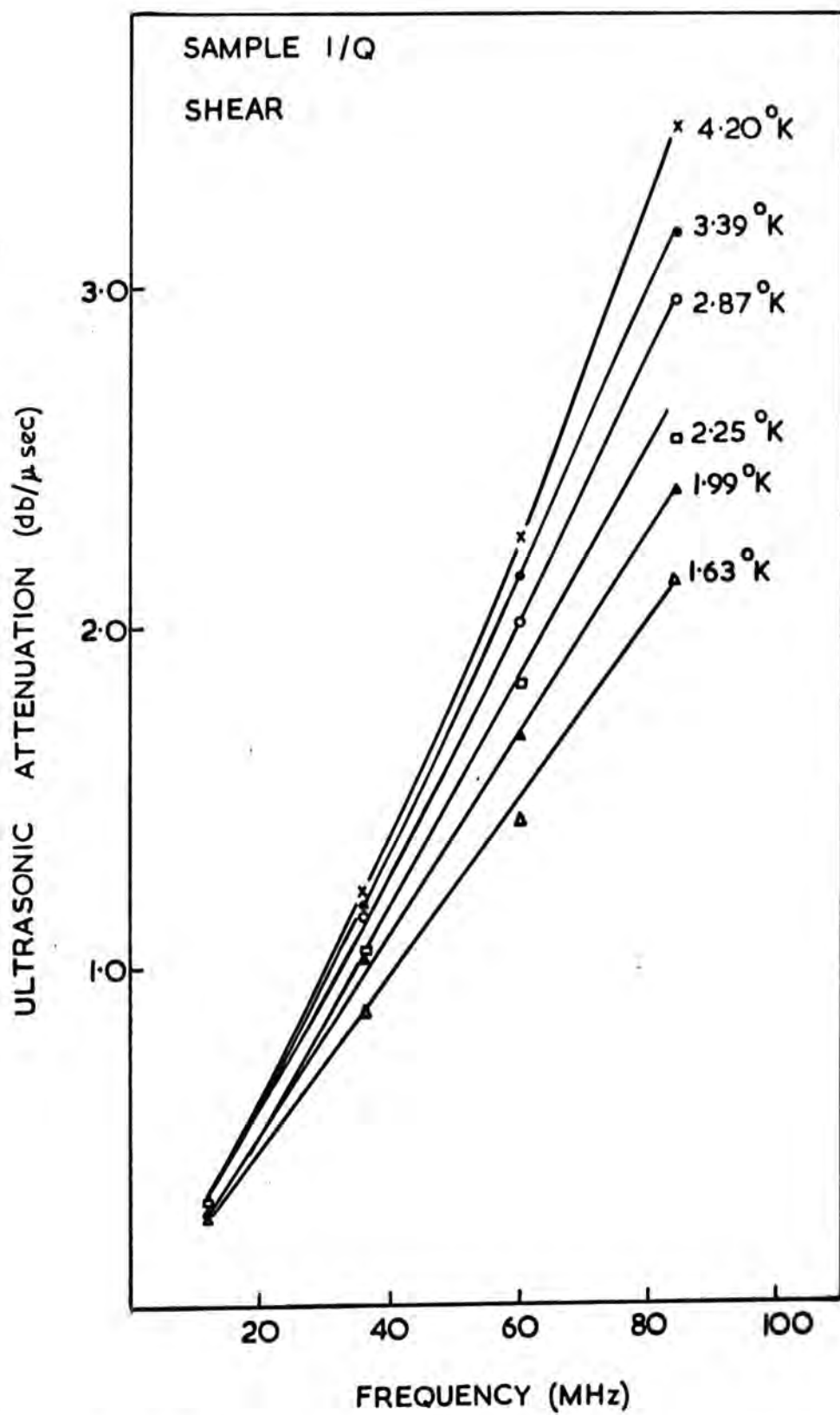
Figure 6.24 Frequency dependence of ultrasound attenuation below 4.2°K in sample 1/Q.
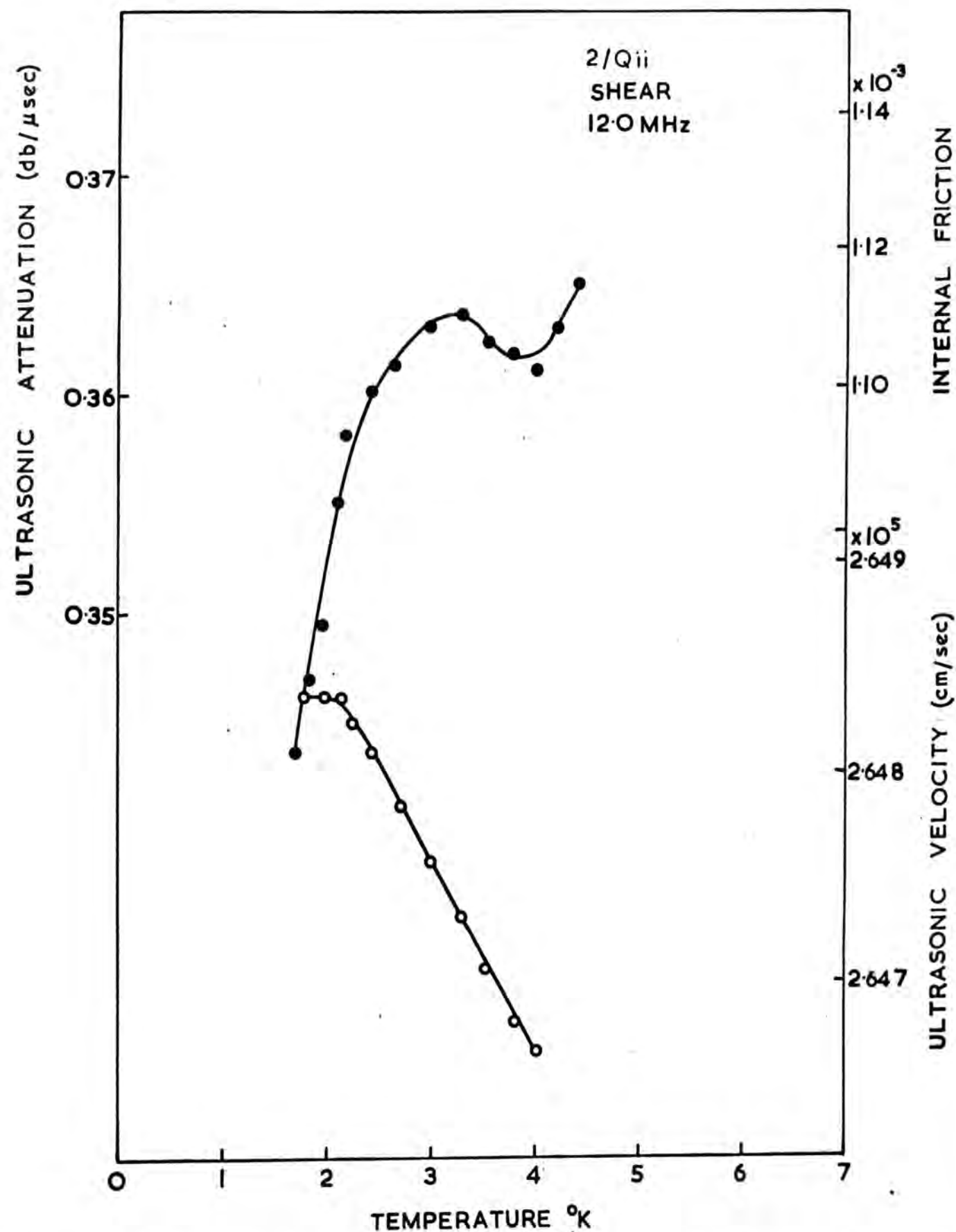
Figure 6.25   Temperature   dependence   of   ultrasound   attenuation   and
velocity   below   4·2°K   at   12·0 MHz   in   sample   2/Q ii.
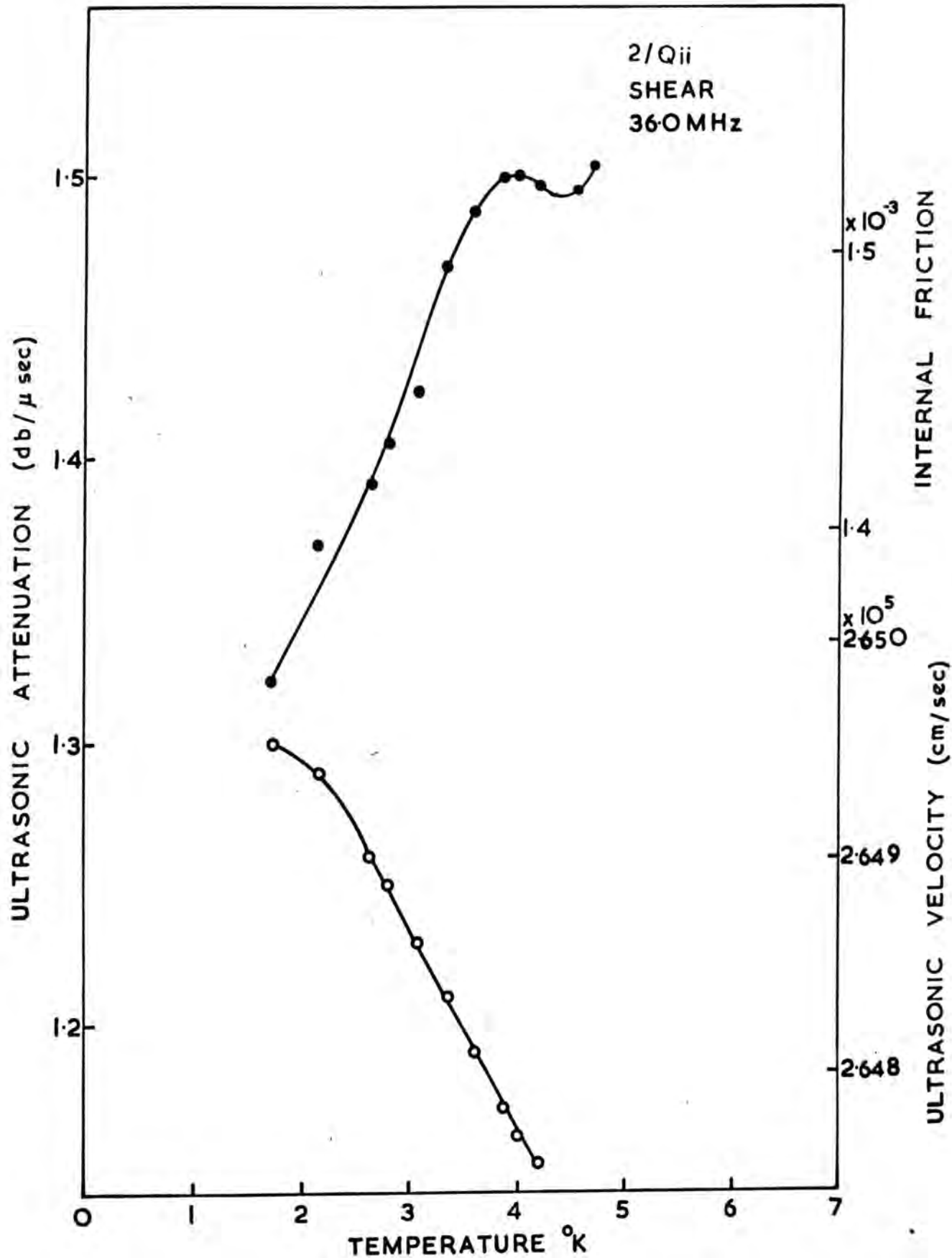
Figure 6.26 Temperature dependence of ultrasound attenuation and velocity below 4·2°K at 36·0 MHz in sample 2/Q ii.
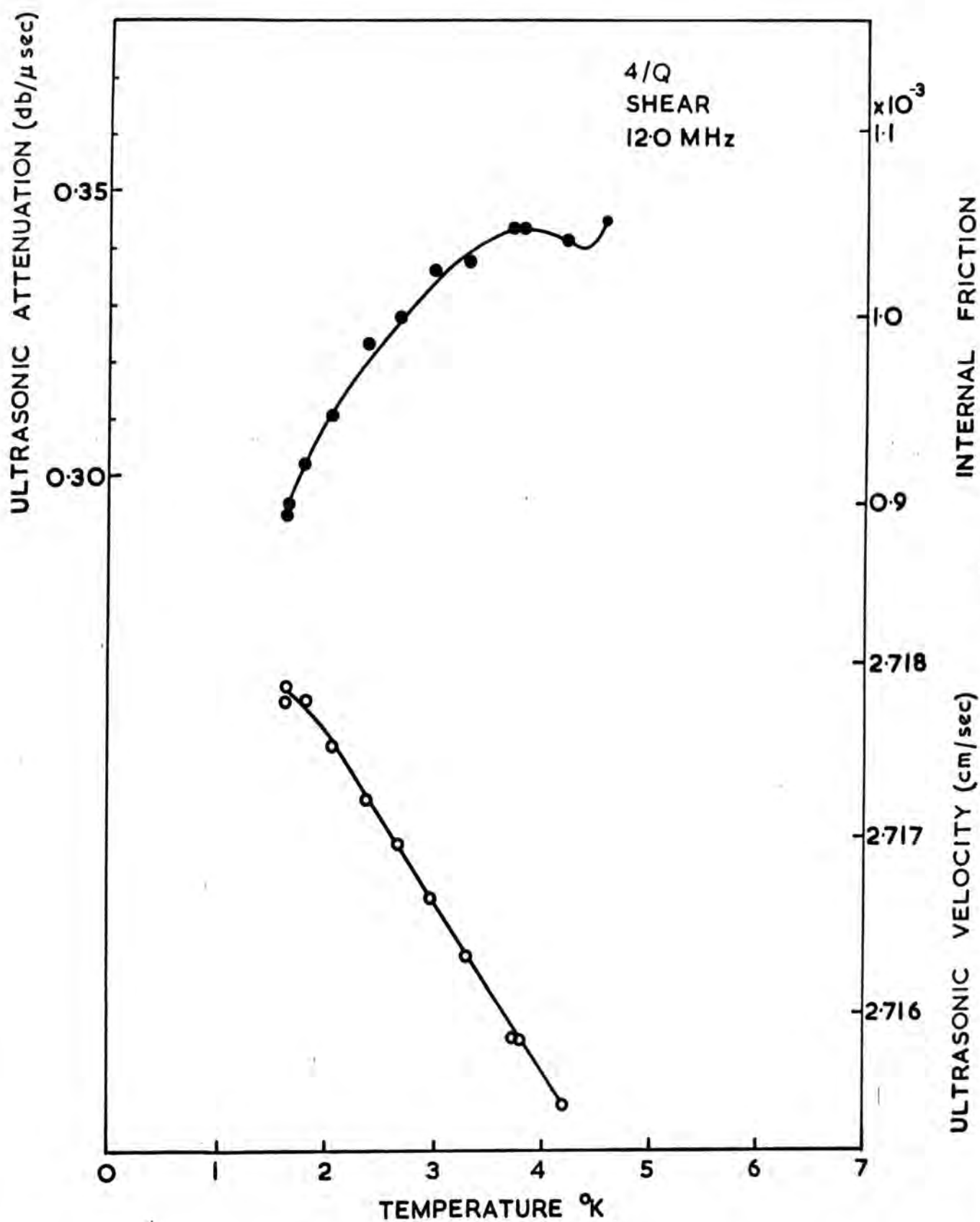
Figure 6.27 Temperature dependence of ultrasound attenuation and velocity below 4·2°K at 12·0 MHz in sample 4/Q
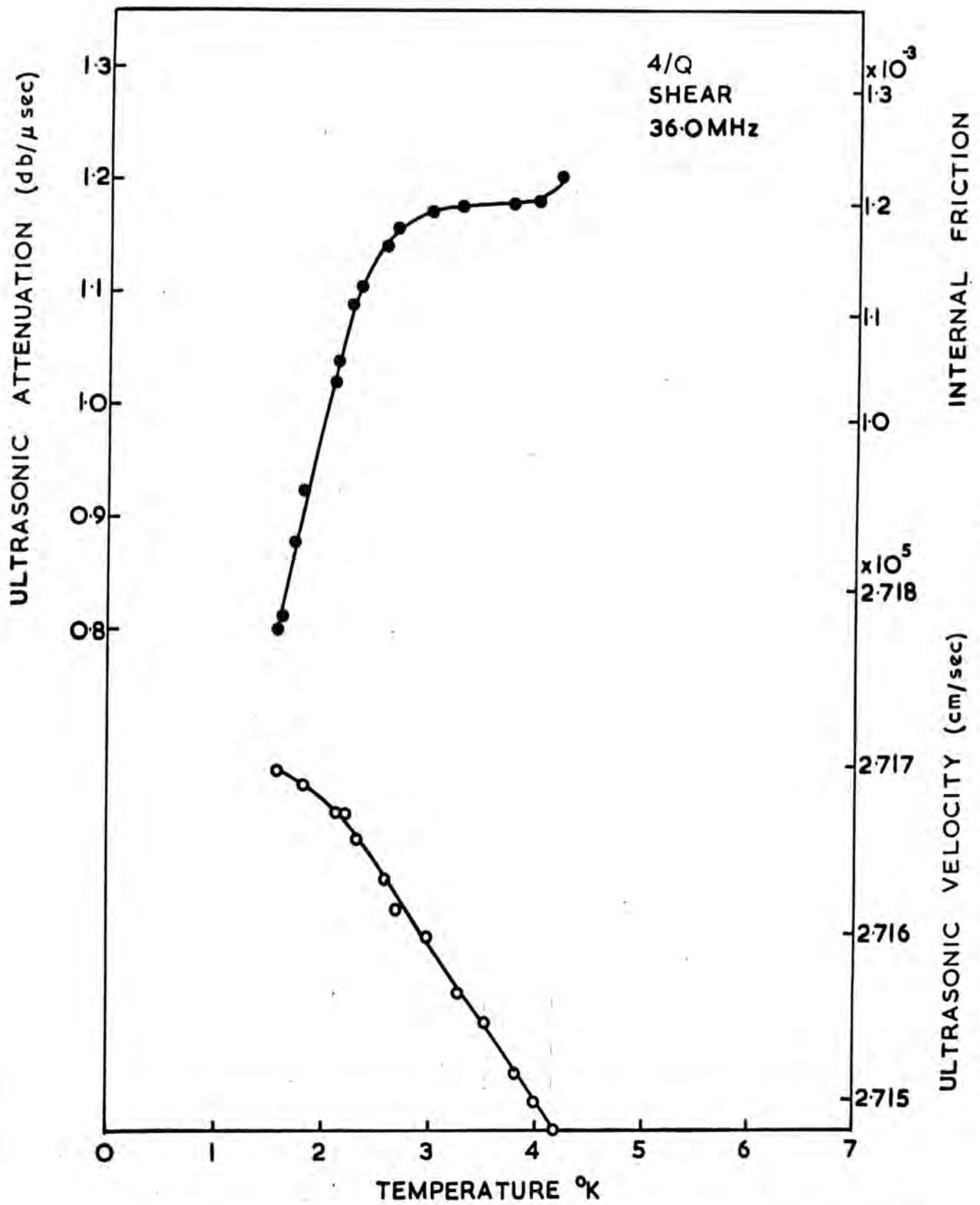
Figure 6.28 Temperature dependence of ultrasound attenuation and velocity below 4·2°K at 36·0 MHz in sample 4/Q.
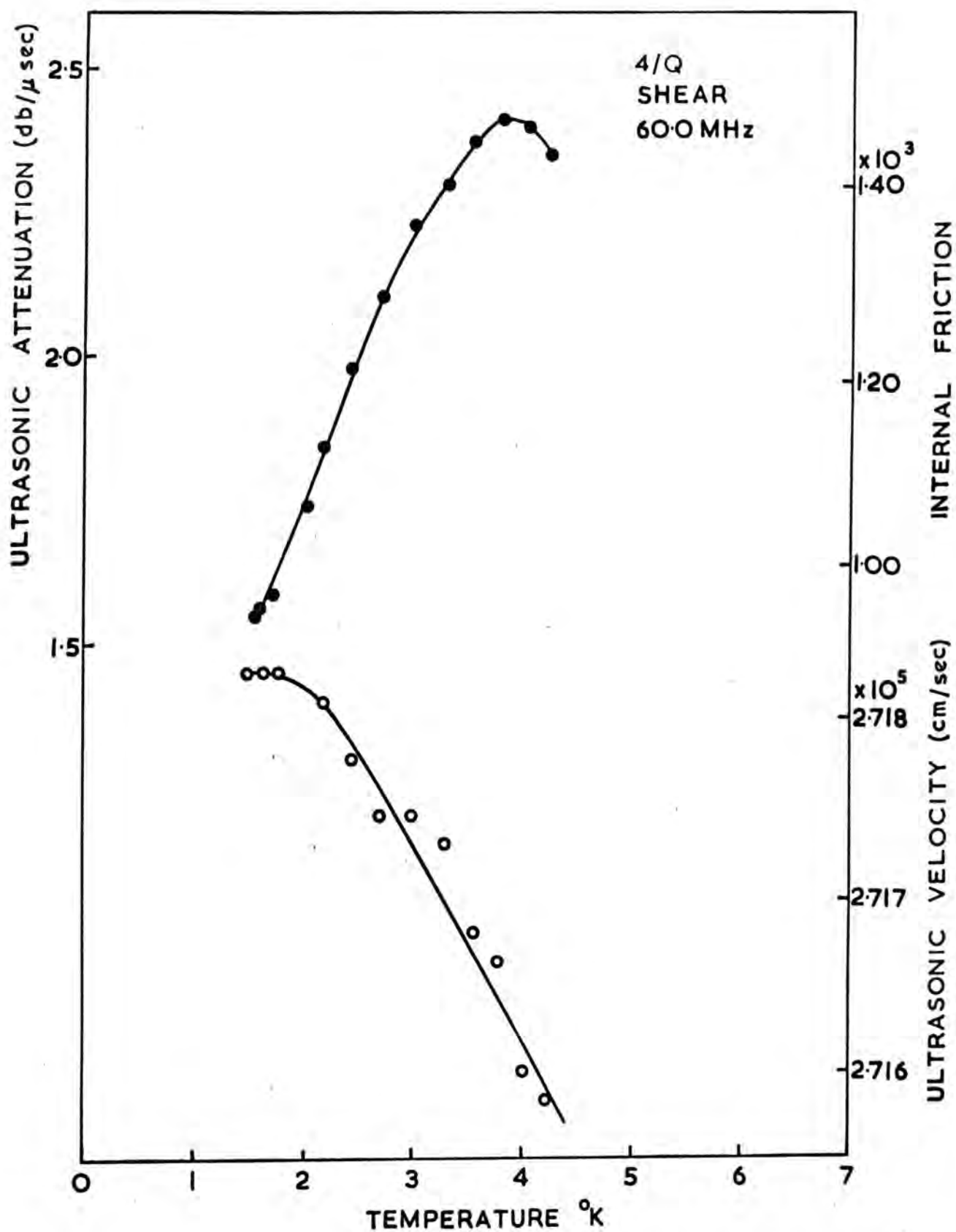
Figure 6.29   Temperature dependence of ultrasound attenuation and velocity below 4·2°K at 60·0MHz in sample 4/Q

CHAPTER   SEVEN

DISCUSSION OF THE RESULTS

Introduction

This chapter is devoted to a discussion of the results from the measurements of acoustical and other physical properties of the $Na_2O-B_2O_3-SiO_2$ glasses made in the course of this study. This discussion is conducted with reference to previous studies of other vitreous materials. The chapter commences with an examination of the densities of the $Na_2O-B_2O_3-SiO_2$ glasses, and some preliminary conclusions are drawn as to their structure. In Section 7.2 the acoustic loss mechanism in both $Na_2O-B_2O_3-SiO_2$ and SiO_2 glasses is investigated in detail. Also included in this section is an enquiry into the more general effects of sample composition upon the ultrasound propagation characteristics. The third section of this chapter contains a survey of the effect of advancing phase separation on the acoustic properties of $Na_2O-B_2O_3-SiO_2$ glasses, and a proposal is made to account for the observed behaviour. Chapter 7 closes with a scrutiny of the small acoustic loss peak which occurs in these and other inorganic glasses in the liquid helium range of temperature. Some possible causes of this low temperature feature of the ultrasound propagation characteristics are reviewed in the context of recent advances in the understanding of the vibrational properties of glassy materials.

7.1.1 The density of the $Na_2O-B_2O_3-SiO_2$ glasses

Much information about the structure of a solid may be gained from one of its most fundamental properties, the density. Before entering into a detailed discussion of the results from the ultrasonic measurements of the $Na_2O-B_2O_3-SiO_2$ glasses we will examine the compositional dependence of the densities and draw some initial conclusions about the packing of the atoms.

Both SiO_2 and B_2O_3 are glass formers, that is they can readily form a glass lattice. Na_2O is a network modifier; while not capable of forming a glass alone it can enter a glass lattice composed of one of the glass forming series of compounds, and modifies the structure. Therefore the density of a glass will be determined largely by the glass forming molecules but will be adjusted by the addition of a modifier. We can calculate a theoretical density for the $Na_2O-B_2O_3-SiO_2$ glasses by consideration of the mole fractions x_i and partial molar volumes v_i of the constituents through the equation

$$\rho_{calc} = \frac{\overset{i}{\underset{i}{\Sigma}} x_i m_i}{\underset{i}{\overset{i}{\Sigma}} x_i v_i} \qquad 7.1$$

where m_i is the molecular weight of each constituent. As choices for the densities of the glass formers we will take that for vitreous SiO_2 as 2.20 g/cm^3 (Fraser, 1968) and that for vitreous B_2O_3 as 1.84 g/cm^3 (Uhlamann and Shaw, 1970), indicating partial molar

volumes of 27.3 cm^3/mole and 37.8 cm^3/mole respectively. Only three significant figure accuracy is used in the following calculations as these densities are dependent on water content and fictive temperature in quite a complex manner. For convenience we will take the partial molar volume of Na_2O as zero, and an interpretation of the results will be made with this fact in mind. Comparison between calculated and experimental values of density for the glasses of this work is made in Figure 7.1 where the densities of each composition is plotted against wt% Na_2O.

The first important feature shown by these results is that the calculated and experimental densities for the binary glasses 6/Q and 7/Q agree to within about 1.5%. They are also close to the values of density reported for glasses in this particular binary system in the review paper of Uhlmann and Shaw (1971) which are shown in comparison to the theoretical densities calculated from the partial molar volumes in Figure 7.1. It is most probable then that the structure of B_2O_3-SiO_2 glasses is locally very similar to the single-component parent compounds, and is mainly SiO_4 tetrahedra and BO_3 triangles with very little modification in terms of cation-oxygen-cation bond lengths. No conclusions may be drawn as to the clustering of the species in the structure but it is well known that glass-in-glass phase separation occurs in the B_2O_3-SiO_2 system (Charles and Wagstaff, 1968).
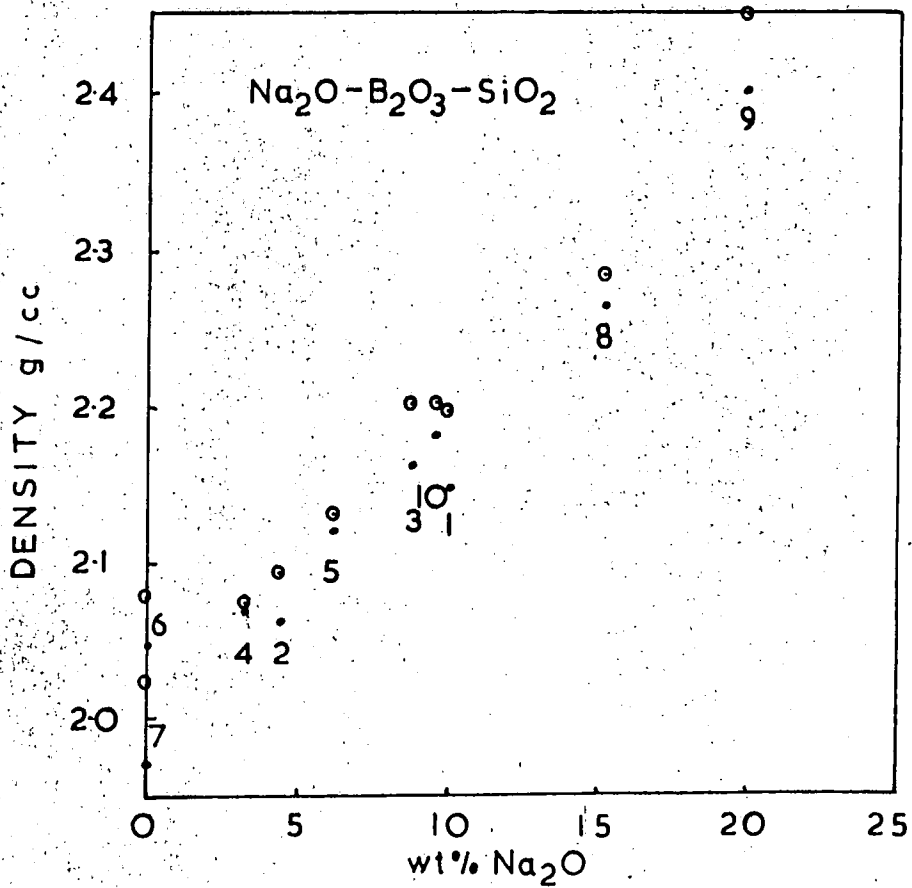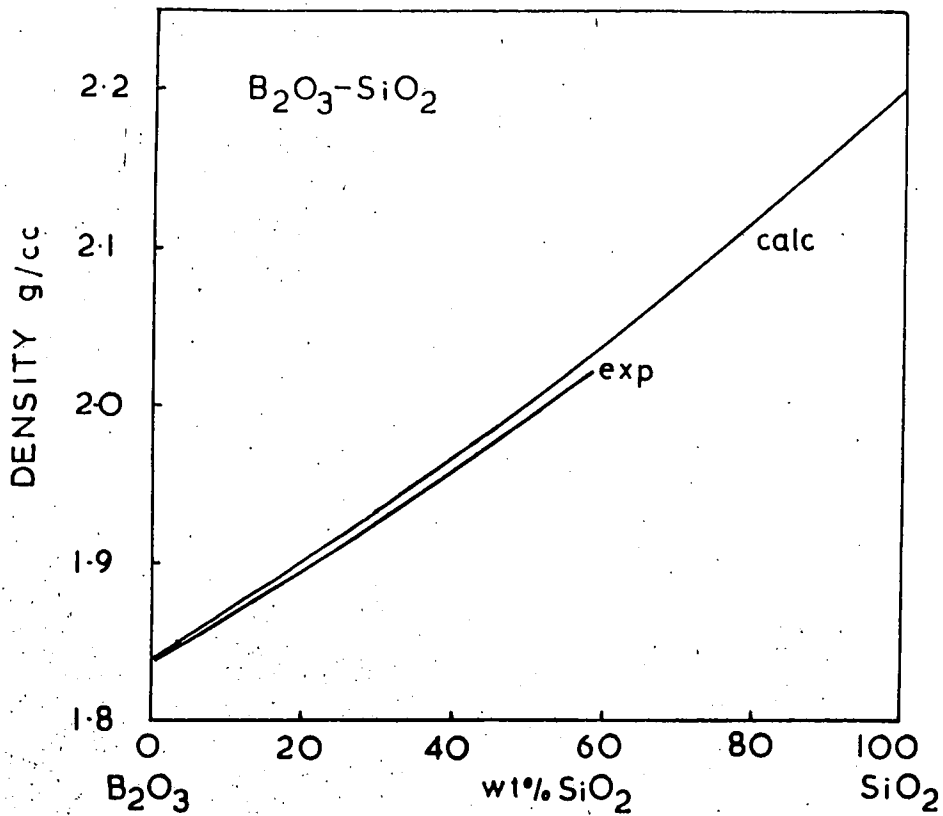
Figure 7.1   Calculated(o) and experimental(·) densities for
B₂O₃ − SiO₂ and Na₂O − B₂O₃ − SiO₂ glasses.

For the glasses which contain from 3.3 wt%
to 19.8 wt% Na_2O the calculated values of density are
only slightly larger than the experimental values
evidencing that the partial molar volume of the Na_2O
species is very small. Thus the Na_2O molecules enter
the B_2O_3-SiO_2 glass network and reside at holes or
vacancies in the lattice. For further elaboration on
this point it is necessary to digress a little and
examine the densities and structural models for
Na_2O-SiO_2 and Na_2O-B_2O_3 glasses.

7.1.2 The densities and structural models for Na_2O-SiO_2 and Na_2O-B_2O_3 glasses

Robinson (1969) and Kruger (1972) have shown
that for a Na_2O-SiO_2 glass the density is not simply
determined by the partial molar volume of each con-
stituent, but a rather more complicated relationship
prevails. It is thought that when a Na_2O molecule
enters a SiO_2 glass lattice, one bridging oxygen atom
joining two adjacent SiO_4 tetrahedra is replaced by
two non-bridging oxygen atoms facing each other, and
the two Na^+ ions are then located in the structure
near this site (Urnes, 1967). This has the effect of
weakening the network and as discussed in Chapter 3,
the ultrasound velocity decreases. An expansion of
the glass lattice also results, and the Na_2O occupies
a finite partial molar volume.

On addition of Na_2O to vitreous B_2O_3, structural changes of quite a different nature take place. Pure B_2O_3 consists mainly of BO_3 triangles with about 1% BO_4 tetrahedra (Bray, 1967). In the presence of the network modifying Na_2O, the boron atoms change their coordination number from 3 to 4 and a strengthening of the lattice ensues (Bray and O'Keefe, 1963). The sodium ions reside in holes in the lattice and the oxygen atom donates an electron to two boron atoms which then assume a tetrahedral environment by sharing the extra oxygen ion (Silver and Bray, 1958). Biscoe and Warren (1938) have noted that the 'average' B-O distance increases slowly from 1.39 $\overset{o}{A}$ to 1.48 $\overset{o}{A}$ on addition of Na_2O. The lattice still expands in the presence of an alkali oxide network modifier, but not on the same scale as glasses in the Na_2O-SiO_2 system.

To demonstrate that Na_2O occupies a larger partial molar volume in a SiO_2 based than a B_2O_3 based lattice, we may compare the density data on Na_2O-SiO_2 and $Na_2O-B_2O_3$ glasses with the values calculated through equation 7.1, using a zero value for the partial molar volume for Na_2O as before. This comparison is seen in Figure 7.2. We observe that the alkali oxide occupies a larger partial molar volume in the SiO_2 than in the B_2O_3 lattice over the entire compositional range of the diagram as witnessed by the greater difference between calculated and experimental densities in the Na_2O-SiO_2 glasses. In fact, between 0% and 12% (wt) Na_2O there
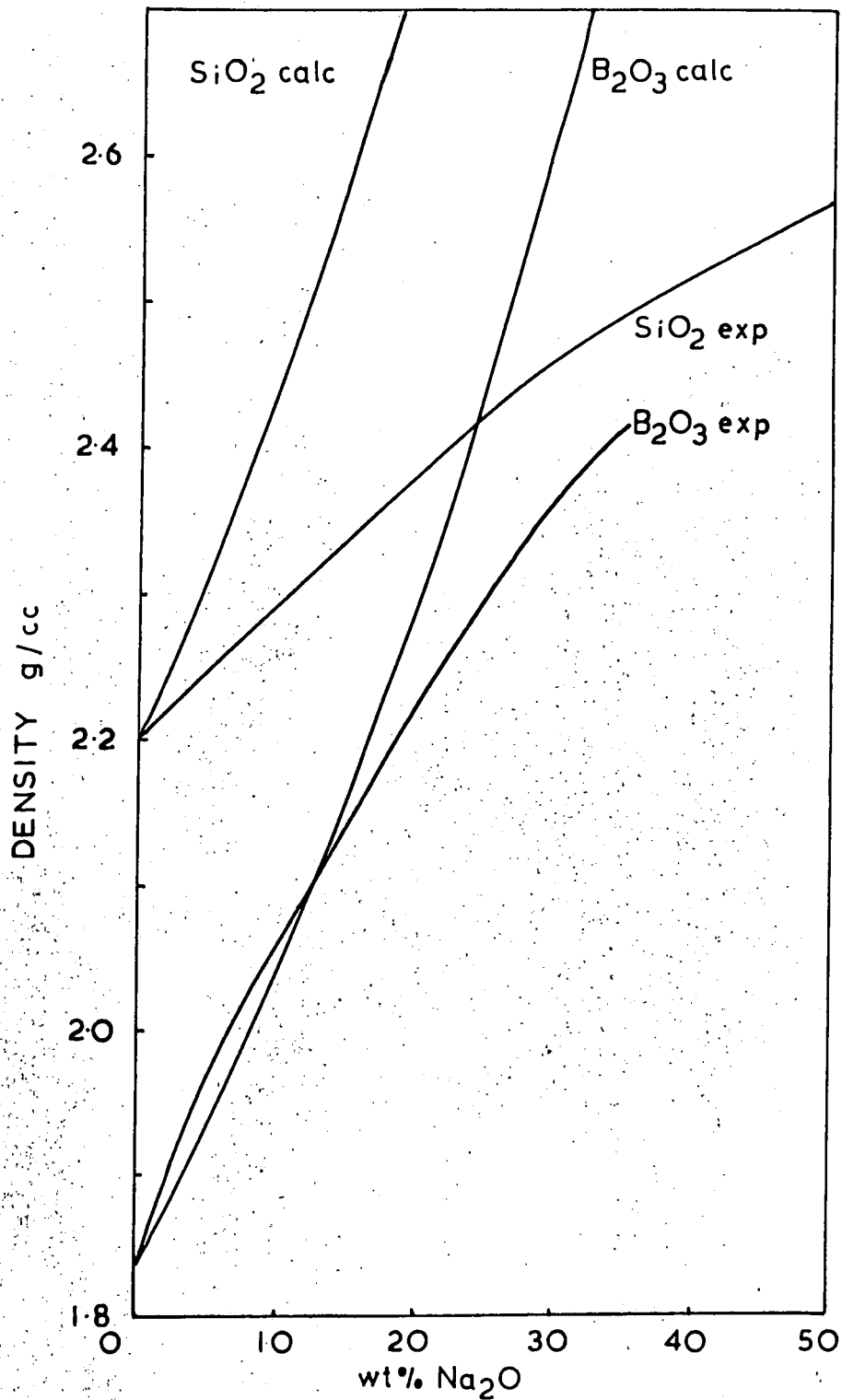
Figure 7.2 Calculated and experimental densities for Na₂O – B₂O₃ and Na₂O – SiO₂ glasses.

is actually a contraction in the B_2O_3 lattice. This is most probably caused by the attraction of the small, charged Na^+ cation and the oxygen atoms in the glassy structure.

In the light of the information on Na_2O-SiO_2 and $Na_2O-B_2O_3$ we can speculate a little on the structure of the $Na_2O-B_2O_3-SiO_2$ glasses of this present concern. From the observation that there is only a small expansion of the $B_2O_3-SiO_2$ glass forming lattice on the introduction of the alkali oxide network modifier we can conclude that most of the Na_2O molecules concentrate in the regions of the structure which are locally high in B_2O_3, where the modifying molecules can take up such positions to cause only small increases in the volume of the lattice. In support of this conclusion the tie-lines on the ternary diagram of the $Na_2O-B_2O_3-SiO_2$ system are such as to indicate that the glass separates into a high B_2O_3-high Na_2O phase and a high SiO_2-low Na_2O phase (see Chapter 4). Thus, in a $Na_2O-B_2O_3-SiO_2$ glass, we can expect, on addition of Na_2O, an increase in the coordination number of the boron atoms from 3 to 4 and hence a general strengthening of the lattice due to further cross linking in the structure. We cannot exclude however the possibility of the collection of Na_2O molecules at Si-O-Si sites though such an occurrence will be less frequent.

7.2   The ultrasound propagation characteristics and

the effects of composition in $Na_2O-B_2O_3-SiO_2$

glasses

7.2.1   Ultrasound attenuation in $Na_2O-B_2O_3-SiO_2$ glasses

The propagation behaviour of an ultrasound stress
wave in a solid is determined by the attenuation and
velocity of the wave. Properties of a solid that are
sufficiently well coupled to the lattice will cause
changes in the attenuation and velocity of the wave, and
an assessment of their individual influences on the propa-
gation behaviour is desirable. We have seen in Chapter 3
how the propagation characteristics of vitreous SiO_2 and
many other inorganic glasses are dominated by a large
acoustic absorption peak that occurs below room temperature.
The $Na_2O-B_2O_3-SiO_2$ glasses too exhibit this large acoustic
loss peak and the associated changes in elastic modulus.
However, in the glasses of this present study there are
two other phenomena which can make a contribution to the
observed acoustic attenuation, namely Rayleigh scattering
at phase-separation boundaries, and thermoelastic loss.
We shall estimate the magnitude of the loss due to each
of these mechanisms to determine the extent of their
effect on the measured attenuation.

Scattering of the phase-separation boundaries

Scattering of stress waves in a solid may be
caused by differences in the elastic properties from
point to point, and the magnitude of the resultant loss

is dependent on the space derivatives of the elasticity
and density. In general, inhomogeneities such as neutron
damaged portions of a solid or voids and bubbles will
give rise to scattering of an ultrasound wave. So too
will the phase separated regions of the glasses of this
study.

The scattering cross section and hence the
acoustic attenuation resulting from the changes in density
and elastic constant between the phases is difficult to
calculate as no exact details of these variables are
available. However, the wavelength of the ultrasound
wave at 12 MHz is approximately 0.5 mm and therefore is
much greater than the dimensions of the phase-separated
regions. It is thus likely that the wave suffers very
little direct Rayleigh scattering. Further evidence for
this assumption is that there is no overall temperature
independent increase in the ultrasound attenuation in the
sequence of glasses from 2/Q to 2/168 where the droplet
structured regions grow from 500Å to 5μ in size. Inspection
of the $Na_2O-B_2O_3-SiO_2$ glasses under both the optical and
electron microscope reveals the absence of any large voids
or bubbles. Thus we can conclude that scattering
mechanisms make negligible contributions to the observed
acoustic attenuation.

Thermoelastic loss

When a longitudinal stress wave propagates
through a solid, there are at any one instant alternate
regions of densification and rarefaction of the material.

These regions suffer changes in temperature, and local temperature gradients are set up. The flow of heat between these regions is accompanied by the production of entropy and a dissipation of energy, which results in the attenuation of the sound wave. Lücke (1956) has derived the equation describing the thermoelastic loss as

$$\alpha = \frac{8.686 \; 2\pi^2}{v\tau} \cdot \frac{\Delta M}{M_O} \cdot \frac{\omega^2 \tau^2}{1+\omega^2 \tau^2} \; db/\mu sec \qquad 7.2$$

where τ is the relaxation time for the flow of heat equal to $\kappa/\rho Cp v^2$. The term $\Delta M/M_O$ is the fractional difference between the adiabatic and isothermal elastic moduli which determine the velocity of the sound wave. Relationships for $\Delta M/M_O$ for isotropic materials are not available in the literature, but for a cubic crystal with longitudinal wave propagation in the <100> direction this ratio is given by

$$\frac{\Delta M}{M_O} = \frac{(C_{11}+2C_{12})^2}{C_{11}} \cdot \frac{\alpha^2 T}{\rho Cp} \qquad 7.3$$

where α is the coefficient of thermal expansion. For an isotropic material C_{11} is equal to ρV_L^2 and C_{12} is equal to $(V_L^2 - 2V_S^2)$, and these values can be substituted into equation 7.3 to calculate the value of $\Delta M/M_O$. Exact values for all the parameters needed to compute the thermoelastic loss for the $Na_2O-B_2O_3-SiO_2$ glass of this study are not known but have been approximated to those of another sodium borosilicate glass, namely Pyrex. For an order of magnitude calculation of the thermoelastic loss at room temperature, the several variables have been taken as follows:

α $\qquad$ $5 \times 10^{-6}/^{\circ}K$

κ (Pyrex: Zeller and Pohl, 1971) 10^5 ergs/cm$^{\circ}$K

Cp (Pyrex: Kaye and Laby, 1971) 7.8×10^6 ergs/g$^{\circ}$K

V_L $\qquad$ 4.5×10^5 cms/sec

V_S $\qquad$ 2.8×10^5 cms/sec

ρ $\qquad$ 2.1 g/cm^2

The calculated thermoelastic loss at 12 MHz acoustic frequency for a longitudinal wave is thus approximately 10^{-8} db/μsec. No thermoelastic loss is expected for the isovolumetric shear wave. The thermoelastic loss can thus produce no measurable contribution to the observed attenuation.

Thus we see that the only intrinsic mechanism that influences the observed acoustic attenuation in the $Na_2O-B_2O_3-SiO_2$ glasses is the structural relaxation mechanism. Following the subtraction of the small apparent losses due to diffraction, coupling and wedging effects which total 0.021 db/μsec (see Chapter 5) the remaining acoustic attenuation is that of direct interest in this study.

7.2.2   Distributional effects in the acoustic loss mechanism in SiO_2 and $Na_2O-B_2O_3-SiO_2$ glasses

Before commencing a detailed investigation of the form of the large acoustic loss peak in the $Na_2O-B_2O_3-SiO_2$ glasses, let us re-examine the data available

on the attenuation in vitreous SiO_2 in order to gain

any extra information which may be of use in the

present study.

It has already been shown in Chapter 3 that

the acoustic loss peak in inorganic glasses such as SiO_2,

GeO_2 and B_2O_3 is much wider than that expected for a

single activation energy (H) and single attempt frequency

(ω_o) process, and that a distribution in activation

energies is necessary to account for this broadening.

However, a distribution in activation energies is not

unique in causing a broadening of a relaxation loss peak;

a distribution in attempt frequencies and a single activa-

tion energy will have a similar effect. To resolve this

point it is advantageous to follow the mathematical

analysis of Niblett (1966). He has shown that where

the internal friction of a relaxation process has been

measured at a number of acoustic frequencies, a graph of

the difference in reciprocal temperatures at the peak

half heights $\Delta(1/T)$ versus the reciprocal temperature

of the peak maximum $1/T_{max}$ should differentiate between

the two possible distributional cases. For a single

H-single ω_o process $(1/T)$ should be constant and equal

to A, where

$$A = \frac{R}{H} \log_e \frac{(2+\sqrt{3})}{(2-\sqrt{3})} \qquad 7.4$$

and R is the universal gas constant. For a single H

and distribution of ω_o, $\Delta(1/T)$ should again be constant

with $1/T_{max}$ but will have a larger value than for the
single relaxation; and for a distribution in H and a
single ω_o the graph will be linear but will have a positive
slope of gradient proportional to the spread in activa-
tion energies. For this latter case, the intercept of
the graph on the $\Delta(1/T)$ axis will be at the value of A
where H is now $\bar{H}$, the average or mean activation energy
obtained from the shift in T_{max} with acoustic frequency
through equation 3.1.

Figure 7.3 shows such a plot for vitreous SiO_2.
The data points are obtained from the 66 KHz results of
Fine (1954), the 20 MHz results of Anderson and Bömmel
(1955), the work 930 MHz of Jones et al (1964) and the
27.5 GHz thermal Brillouin scattering results of
Pine (1969). The value of the intercept A has been
calculated assuming an average activation energy of
1030 cal/mole, and is included on the plot. Uncertainty
in the values of the data points is represented by a
vertical bar. A least mean squares line has been computer
fitted to all 5 points on the graph, and has a positive
gradient of approximately 8.

The scatter of the points from the graph is
typical of that observed in other similar experimental
situations, for example the study of Bordoni peaks
(Niblett, 1966) but it is shown with emphasis from the
gradient of the graph that the broadening of the relaxa-
tion peak in vitreous SiO_2 is due to a distribution in
activation energies rather than a distribution in attempt
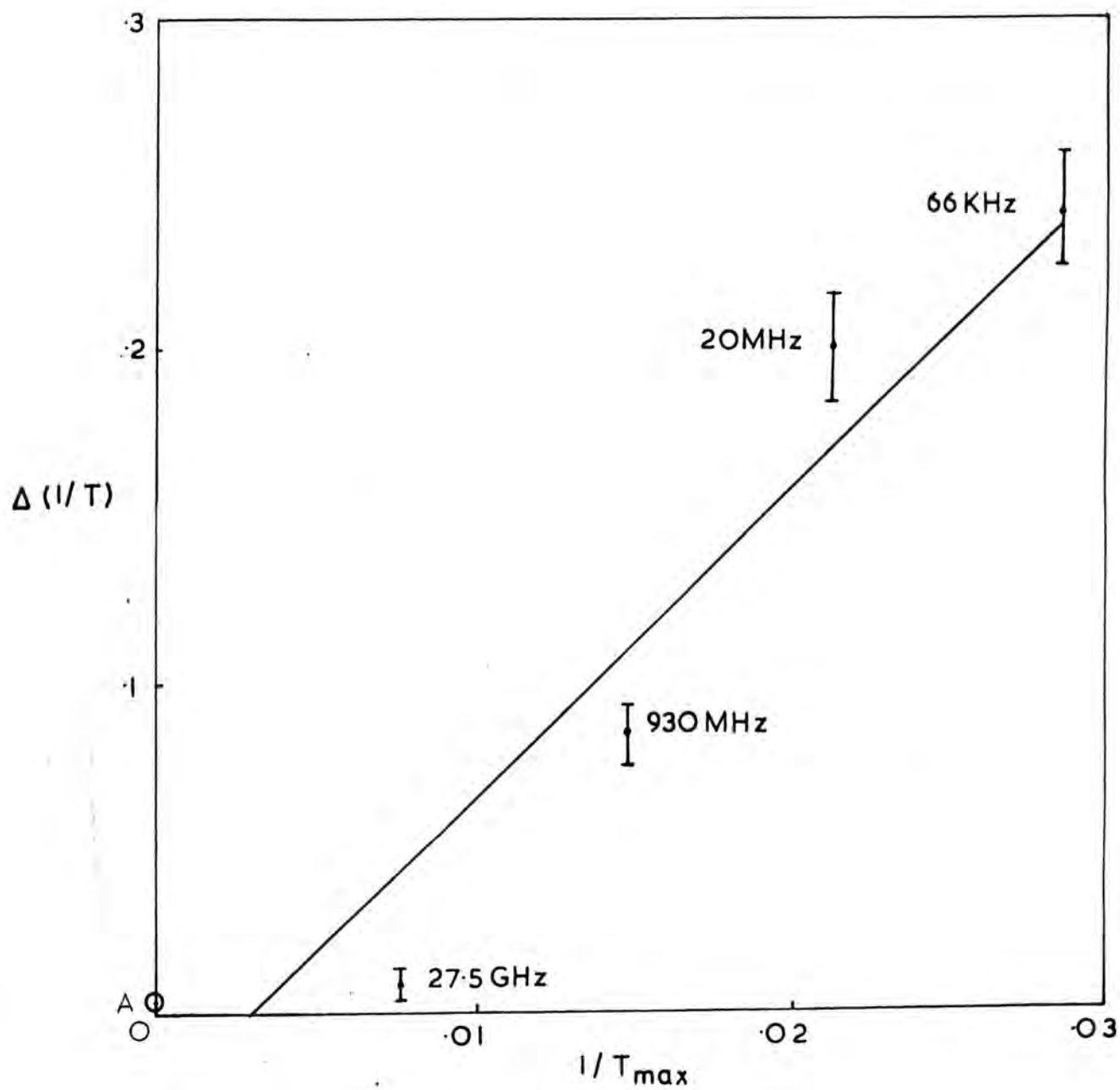
Figure 7.3 Graph of Δ (1/T) against 1/T max for SiO_2 glasses.

frequencies. Further quantitative information is difficult to extract from the graph as the general shape of the activation energy distribution is a complex shape rather than a more simple Gaussian or lognormal distribution. As the general nature of the acoustic loss peak in other inorganic glasses is very similar to that in vitreous SiO_2, it is a very fair assumption that in these glasses too there exists a distribution of activation energies rather than attempt frequencies.

7.2.3   The attempt frequency and mean activation energy of the acoustic loss mechanism in $Na_2O-B_2O_3-SiO_2$ glasses

The acoustic loss peaks in $Na_2O-B_2O_3-SiO_2$ glasses of this study are wider than that of a single τ relaxation with a comparable mean activation energy of about 3K cal/mole (see later) and are broadened on the low temperature side of the peak as shown in Figure 3.6. A comprehensive plot of $\Delta(1/T)$ against $1/T_{max}$ similar to that for vitreous SiO_2 cannot be made as results at such diverse frequencies for the $Na_2O-B_2O_3-SiO_2$ glasses are not available. However, on the assumption that the broadening is due to a distribution in the activation energies of the loss mechanism a similar plot for the $Na_2O-B_2O_3-SiO_2$ glasses has been made using the attenuation results at 12 MHz and the data point A calculated from the average activation energy of the loss process.

The relationship between the angular relaxation frequency and the temperature for an activation process may be calculated through the Arrhenius relationship of equation 3.1. Observation of the peak temperature of maximum loss at two or more acoustic frequencies allows evaluation of both ω_O and $\overline{H}$. In Figure 6.12 it may be seen that the peak temperature in the quenched sample 2/Qii shifts from 128^OK at 12 MHz acoustic frequency to 132^OK at 20 MHz. Ideally a more accurate calculation would be made if the acoustic attenuation had been measured at more diverse acoustic frequencies, but at frequencies above 20 MHz the loss in this sample is too large to be accurately measured, and pulse echo techniques become less powerful at frequencies much below 12 MHz. Solution of equation 3.1 at these two acoustic frequencies yields an attempt frequency of 10^{13} Hz and an average activation energy of 3300 cal/mole.

The heat treated sample 1/48 shows a similar shift in peak temperature, from 104^OK at 12 MHz to 108^OK at 20 MHz, but the peak temperature at 36 MHz cannot be resolved accurately due to the large scatter of results at the high level of attenuation. These results again indicate an attempt frequency of the order of 10^{13} Hz, but with a lower activation energy of about 2800 cal/mole. Although an accurate determination of ω_O is hindered by the absence of results over a much larger range of acoustic frequencies, it is interesting to note that heat treatment which enhances the phase separation in

these glasses and glass composition both have no large
scale effect on the attempt frequency.

We can now complete the plot of $\Delta(1/T)$ versus
$1/T_{max}$ by including the extrapolated point A. This graph
is shown in Figure 7.4, and includes data for glasses
1/Q, 1/48, 2/Q, 2/48 and 5/Q. Mean activation energies
are calculated for the three glasses 1/Q, 2/48 and 5/Q
by assuming an attempt frequency of 10^{13} Hz, and using
the peak temperature through equation 3.1. The extra-
polated point A is extremely close for all the glasses.
The gradients of the lines on the graph vary between
3.5 and 7; this proximity in order of magnitude is taken
to indicate that the distributional widths of the
activation energies are very similar.

The value for the attempt frequency associated
with the acoustic loss mechanism is in agreement with
the findings of both Krause and Kurkjian (1966) and
Strakna and Savage (1964) who have shown that the value
of 10^{13} Hz is reasonably constant for all glasses which
exhibit this acoustic loss peak, including SiO_2, B_2O_3,
GeO_2 and As_2O_3. As both vitreous SiO_2 and B_2O_3 show a
very similar value of ω_o then it is perhaps not surprising
that a borosilicate manifests much the same value too.

7.2.4   Calculation of the distribution in activation
        energy of the acoustic loss mechanism in
        $Na_2O-B_2O_3-SiO_2$ glasses

The total internal friction Q_T^{-1} at a temperature
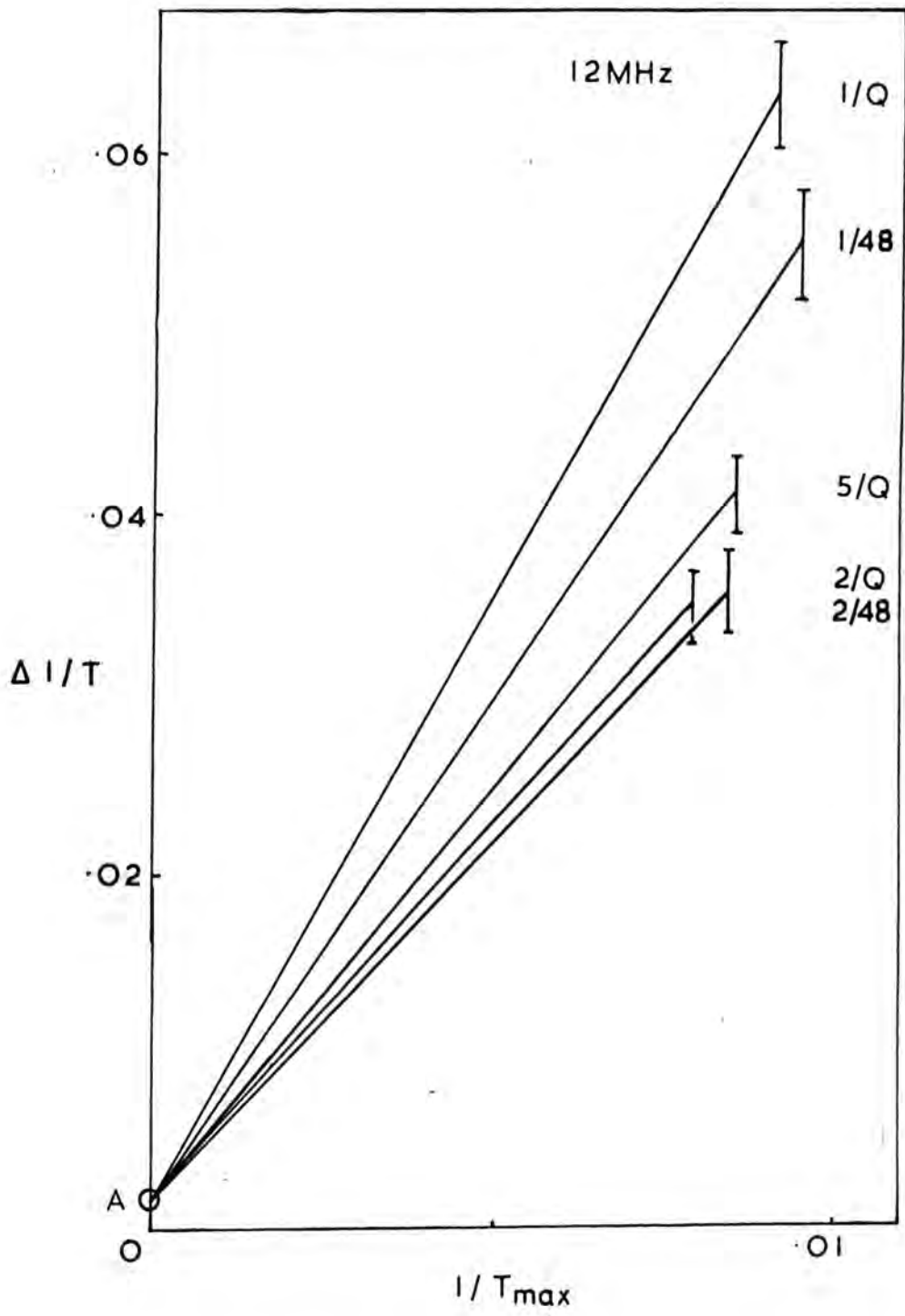
Figure 7.4   Graph of Δ (1/T) against 1/T max for Na₂O – B₂O₃ – SiO₂ glasses at 12 MHz.

T produced by a set of relaxation centres each with a
different activation energy Hi can be represented by a
summation of equations of type 2.46 thus

$$Q_T^{-1} = \sum_i \Delta i \frac{\omega/\omega_i}{1+(\omega/\omega_i)^2} \qquad\qquad 7.5$$

where $\omega_i = \omega_o \exp(-Hi/RT)$ $\qquad\qquad$ 7.6

and Δi is the relaxation strength of the ith loss centre.
The problem in determining the activation energy distri-
bution for the loss mechanism is to calculate the value
of Δi for each Hi from the internal friction data. A
continuous distribution of activation energies can be
represented by a set of discrete equally spaced activation
energies, each with the same attempt frequency ω_o. The
total internal friction is then the sum of the internal
frictions of the single activation centres. When these
single activation energy loss curves are close enough
together a continuum of activation energies is simulated,
as shown in Figure 7.5. The next task is to choose an
appropriate number of activation energies with the correct
spacing and magnitude in energy to represent the distri-
bution in the $Na_2O-B_2O_3-SiO_2$ glasses. Acoustic loss in
all samples is large between $1.3^{\circ}K$ and $400^{\circ}K$ and through
equation 7.6 it can be demonstrated that the activation
energies must range from values of less than 50 cal/mole
to as large as 12,000 cal/mole. An appropriate choice
for the set of discrete energy values is forty equally
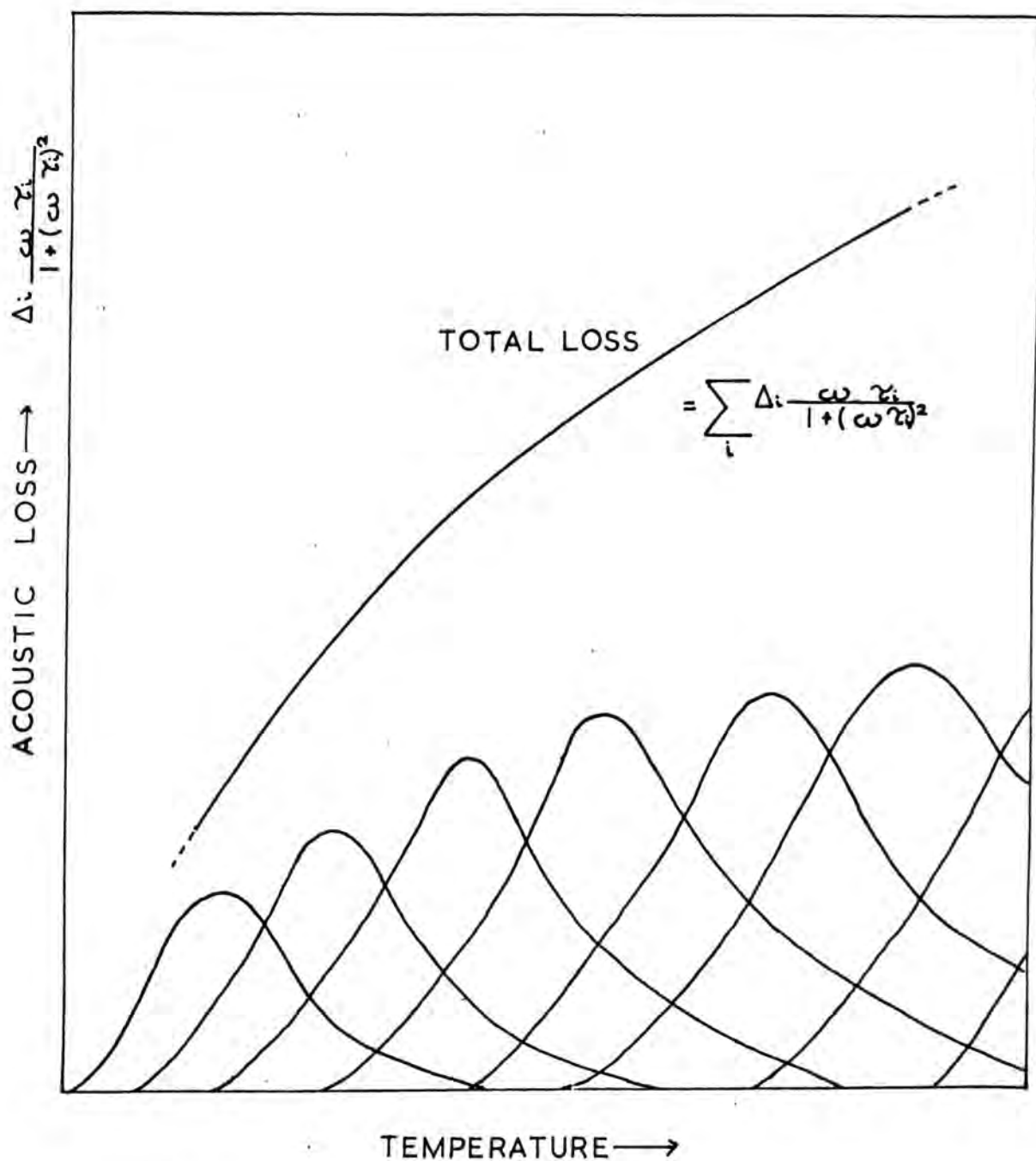
Figure 7.5   The simulation of acoustic loss from a mechanism

with a continuum of activation energies by a series of

single Hi loss curves with good overlap

spaced steps between 300 cal/mole and 12,000 cal/mole.
The overlap of the single Hi loss curves is good down
to 900 cal/mole; an increase in the number of steps to
80 renders only a marginal improvement in the overlap
whilst considerably complicating the calculations to
follow.

The procedure now is to expand equation 7.5 at
forty different temperatures and then solve for the
forty unknown Δi values from the resultant simultaneous
equation system

$$\underline{A} \cdot \underline{x} = \underline{B} \qquad\qquad 7.7$$

where $\underline{A}$ is the square matrix of 1600 elements of type
$(\omega/\omega_i)/(1+(\omega/\omega_i)^2)$, $\underline{x}$ is the matrix of 40 unknown Δi's
to be determined and $\underline{B}$ is the matrix of forty internal
friction measurements at forty temperatures between $10^{\circ}K$
and $400^{\circ}K$ in steps of $10^{\circ}K$.

It would seem that the simplest method of
obtaining the matrix $\underline{x}$ is to multiply the inverse matrix
$\underline{A}^{-1}$ by matrix $\underline{B}$. This method of solution has been
attempted, but results with physical meaning could not
be obtained; values of the elements of $\underline{x}$, both positive
and negative, with orders of magnitude much greater than
expected were acquired by this method. The reason for
this is that the exact solution for the values of the
Δi's found by matrix inversion tolerates no error in the
input data of the internal friction and small changes in
this data result in large numerical changes in the solution.

Thus a different method of solution to equation
7.5 has been formulated which produces a physical result
for the activation energy distribution while allowing for
the presence of random errors in the internal friction
measurements. A set of initially selected set of Δi's
is fitted to the experimentally observed attenuation by
a least mean squares procedure. A Fortran IV programme,
which is reproduced in Appendix I, has been developed
to run on an IBM 360/67 computer. This programme
minimizes a function called SUMSQ equal to

$$\sum_T \left(\frac{Q_M^{-1} - Q_C^{-1}}{Q_M^{-1}} \right)^2$$

where Q_M^{-1} is the measured internal friction at temperature
T and Q_C^{-1} is the internal friction calculated from
equation 7.5 and the initial set of Δi's, each with
corresponding Hi's. Each Δi is incremented or decremented
within preset limits by a supplied step to minimize the
value of SUMSQ. Multiplication of the step by 0.5
followed by further adjustment of the Δi's is then under-
taken to continue the minimization procedure. This
complete process is cycled a number of times until SUMSQ
falls below 0.005. Subroutine programmes are called to
calculate the matrix $\underline{A}$ and also to calculate the value
of Q_C^{-1} after each adjustment of Δi. The final set of
Δi is that obtained when the value of SUMSQ has fallen
to this required level. Another subroutine is then
called to calculate the expected relaxation in elastic

modulus through a modification of equation 2.50

$$\frac{\mu_o - \mu_T}{\mu_T} = \sum_i \frac{\Delta_i}{1+(\omega/\omega_i)^2} \qquad 7.8$$

The expected relaxation can then be compared with the observed relaxation (see Section 7.2.9).

The programme takes about 200 seconds CPU time to reduce SUMSQ below 0.005, where the measured and calculated internal frictions at each temperature then agree to about 1%, which is approximately the random error in measurement at the highest acoustic loss. Here too the value of SUMSQ reaches a minimum; to make SUMSQ exactly zero, a set of Δ_i's similar to that obtained from the matrix inversion method has to be substituted for the set with the correct order of magnitude. The final set of Δ_i are then printed out together with the ratios of the calculated to the measured internal frictions. Also included in the output is a table of the expected relaxation in elastic modulus at each temperature computed from the final distribution in activation energies.

In Figure 7.6 are shown the results of the computation of the distribution of activation energies for the acoustic loss mechanism. The value of the relaxation strength Δ_i per 300 cal/mole interval is plotted against H_i for glasses 1/Q, 1/48, 2/Q, 2/48 and 5/Q. A very similar shape for the activation energy distribution is revealed in all five glasses, and the
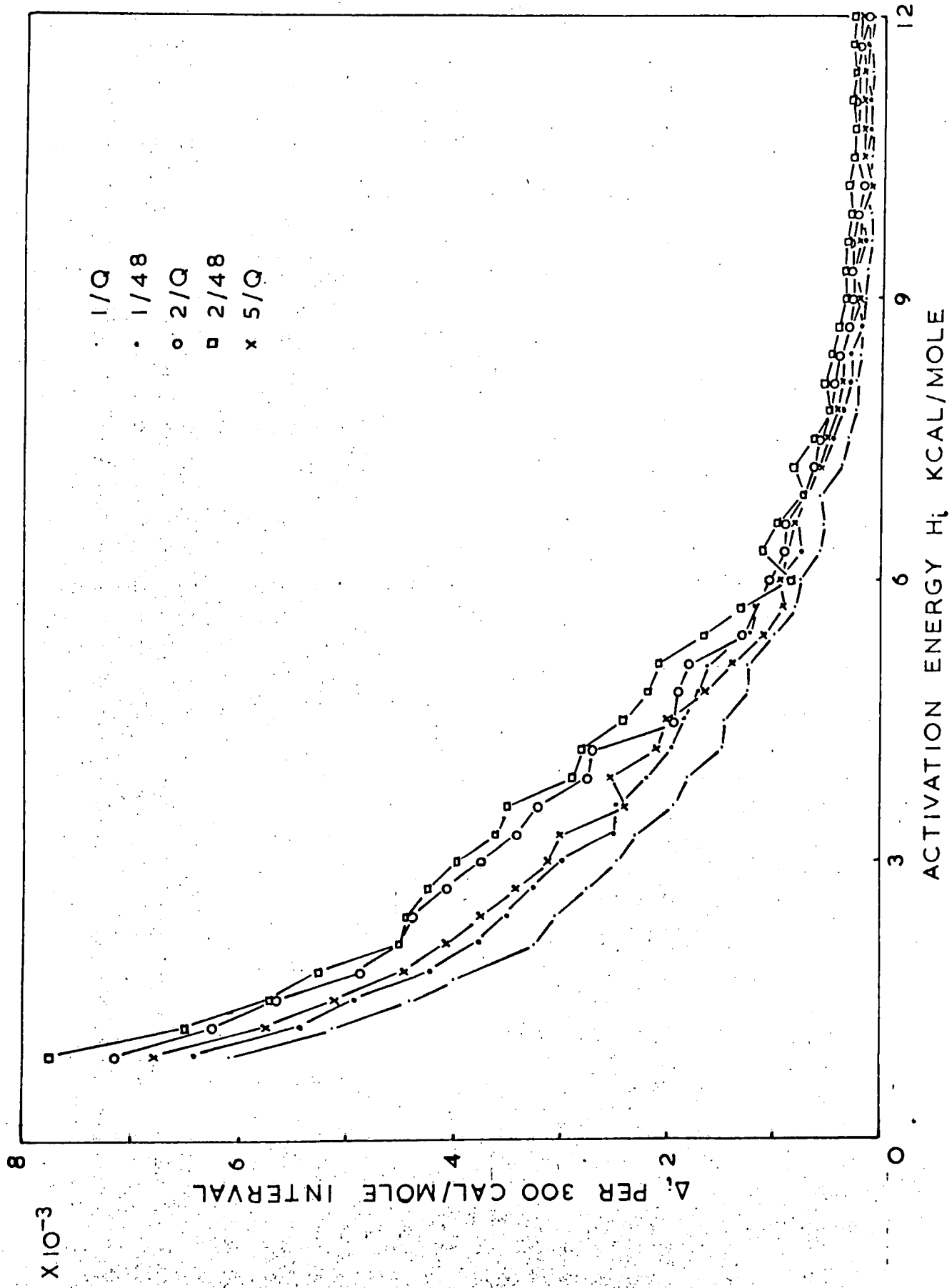
Figure 7.6 The activation energy distribution for the loss mechanism in $Na_2O - B_2O_3 - SiO_2$ glasses.

magnitudes of the Δi's are proportional to the amplitudes
of the observed acoustic loss as expected. A tail in each
distribution is seen as far out as 12000 cal/mole; this
tail is much longer than that for vitreous SiO_2 which
effectively ends at about 4000 cal/mole. This feature
demonstrates the presence of acoustic loss centres with
very high associated activation energies, a point which
will be discussed in greater depth in Section 7.2.5.
No distinctive peaks are seen in the shape of the
distribution which indicates that the average activation
energies $\bar{H}$ calculated from the shift in peak temperature
with acoustic frequency are only a mean in the spread of
Hi and do not correspond to any particular feature of the
loss mechanism in these glasses. The curves take the
form of an exponential decay and can be shown to be
represented by the curve.

$$\Delta i = \Delta o \exp (-Hi/5000)$$

with Hi in units of cals/mole, though the significance
of this exponent is not fully understood.

If we assume that each loss centre exhibits
an equal relaxation strength independent of the activa-
tion energy associated with it, then the graph represents
the relative number of absorption centres with each Hi.
From the observation that the acoustic attenuation falls
sharply below $1.4^{\circ}K$ it seems likely that there is a
maximum in the activation energy distribution at low
values of Hi which is not shown on the graph, and therefore

lies below 900 cal/mole. It is also of interest here to remark that the shape of the activation energy distribution does not alter in any significant degree between samples of the same composition but with different times of heat treatment, excepting that the relaxation strengths at high activation energies undergo greater fractional changes than those at low values of activation energy.

7.2.5 The frequency dependence of acoustic loss

The frequency dependence of ultrasound attenuation at any fixed temperature provides much information on the mechanisms of acoustic absorption at that temperature. A plot for this dependence in sample 1/48 has been introduced in Chapter 6 and shows results typical of all the $Na_2O-B_2O_3-SiO_2$ glasses in this study. Straight lines have been computer fitted to the data points by a least mean squares method, and the calculated exponents n assuming a frequency dependence of $\alpha = af^n$ are as follows

T^OK	n
1.34	0.86 ± 0.03
4.2	1.14
51.1	1.10
77.4	1.08
106.0	1.16
293.7	1.30

The calculated exponents agree well with the hypothesis of a structural relaxation as the mechanism of the acoustic attenuation. For a single activation energy - single attempt frequency the exponent at the peak maximum

should be unity. The complication of a distribution of activation energies and the measurements at constant temperature rather than at corresponding points on the loss curve for each frequency perturb the value of the exponent from unity. The presence of the small low temperature peak disturbs the exponent at $1.34^{O}K$ and $4.2^{O}K$ which should and does have values of less than and greater than 1.0 respectively when astride the loss peak that shifts upwards in temperature with increasing acoustic frequency.

To compare the frequency dependence of the acoustic loss with that in vitreous SiO_2, we can calculate the frequency exponent of this latter glass from the results of Fine (1954) and Anderson and Bömmel (1955). At the peak maximum Q^{-1} is 0.84×10^{-4} at 66 KHz and 18.8×10^{-4} at 20 MHz. These values show a value for n equal to 1.14 which is very similar to the corresponding number in $Na_2O-B_2O_3-SiO_2$ glass. This indicates the great similarity in the nature of the acoustic loss in the two glasses and is further evidence of a common loss mechanism.

7.2.6   The general nature of the large acoustic loss
        peak in the $Na_2O-B_2O_3-SiO_2$ glasses

The value of the attempt frequency associated with the relaxation loss peak of 10^{13} Hz in the $Na_2O-B_2O_3-SiO_2$ glasses is no exception to the common value found for all the inorganic glasses which exhibit this

feature in their acoustic propagation characteristics. This again illustrates the similar nature of the mechanism present in these vitreous materials. We have seen in Chapter 3 that the most probable cause of the loss in vitreous SiO_2 is the transverse motion of oxygen atoms in non-linear oxygen-cation-oxygen bonds; therefore we expect the source of the loss in the Na_2O-B_2O_3-SiO_2 glasses to be a similar oxygen motion in Si-O-B, Si-O-Si and B-O-B non-linear bonds.

The intensity of the acoustic loss peak in the Na_2O-B_2O_3-SiO_2 glasses of zero and low Na_2O content is much greater than that in both SiO_2 and B_2O_3, as can be seen by the direct comparison in Figure 3.1. This important detail evidences a higher concentration of ultrasound absorption centres in the multicomponent than in the single component glasses. A greater incidence of non-linear bonds is presumably necessary for the mutual accommodation in a glassy structure of both BO_3 triangles and SiO_4 tetrahedra and also a small number of BO_4 tetrahedra, all with different cation-oxygen bond lengths. In a crystallographic sense, a greater defect nature is present in the multicomponent glasses.

A second outstanding point is that the average activation energy $\bar{H}$ associated with the loss mechanism in the Na_2O-B_2O_3-SiO_2 glasses (3000 cal/mole) is larger than that in either vitreous SiO_2 (1030 cal/mole) or vitreous B_2O_3 ($\sim$1350 cal/mole). The tail of the distribution in activation energies for the loss mechanism in

the $Na_2O-B_2O_3-SiO_2$ glasses extends out as far as
12000 cal/mole, to much greater value than the cor-
responding distance in the single component SiO_2 glass
of about 4000 cal/mole. It is unlikely that a greater
activation energy will be associated merely with the
presence of non-linear Si-O-B bonds and we conclude
that the cation-oxygen-cation bridging bonds are distorted
through larger angles in the compound glasses. This
phenomenon is again most probably the consequence of the
multicomponent nature of the $Na_2O-B_2O_3-SiO_2$ glass forming
lattice.

The small peak in the acoustic attenuation
which appears at about $300^{\circ}K$ in samples 7/Q, 2/96 and
2/168 is thought to be a similar feature to that seen in
the acoustic absorption spectrum of 'wet' B_2O_3 (Krause
and Kurkjian, 1966b). Its smaller magnitude in the
$Na_2O-B_2O_3-SiO_2$ glasses is due to the lower concentration
of water. As in vitreous B_2O_3, the addition of Na_2O
removes the peak.

7.2.7   The effect of sample composition on the acoustic
        loss characteristics

The addition of Na_2O in the $Na_2O-B_2O_3-SiO_2$ glasses
of this study serves to decrease both the intensity and
the temperature of maximum loss of the large acoustic
absorption peak. The effect on the intensity is clearly
seen in Figure 7.7 where the peak height is plotted
against the molar percentage of Na_2O in the quenched
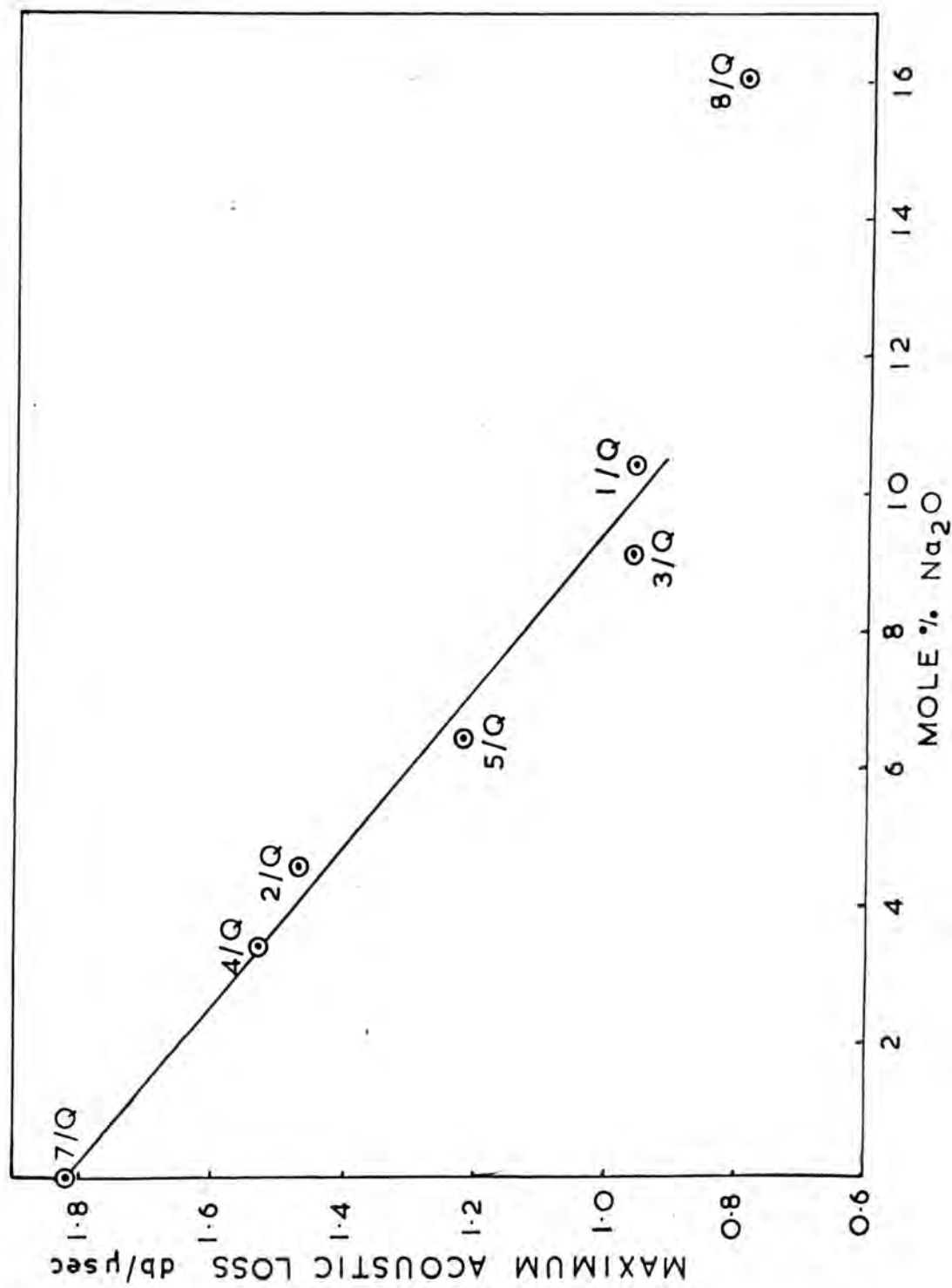
Figure 7.7 The variation of maximum acoustic loss with Na_2O content in quenched $Na_2O-B_2O_3-SiO_2$ glasses.

glasses of the series. Although the water concentration
varies between these samples by a factor of 4, no
systematic behaviour in the acoustic loss which can be
ascribed to the presence of OH ions is indicated and
therefore we can conclude that the changes in the observed
loss characteristics are an intrinsic compositional effect.
A linear dependence of maximum acoustic loss exists out to
at least 10 mole% Na_2O; the data point for the broad and
diffuse loss peak is the only evidence of deviation from
this linear behaviour. The general effect on addition of
Na_2O is similar to that observed in the Na_2O-GeO_2 system
as reported in Chapter 3.

An interpretation of the behaviour in the Na_2O-
$B_2O_3-SiO_2$ glasses can be made through a local structural
model where the alkali oxide molecule modifies the glass
lattice at the cation-oxygen-cation bridging sites, the
non-linear members of which are responsible for the
acoustic loss. We have already seen in Section 7.1.2
how Na^+ ions modify B-O-B bridges by increasing the
coordination number of the boron atoms from 3 to 4 and
create an extra bridging oxygen bond. The proximity of
the Na^+ cations to this site then acts to impede the
movement of the oxygen atoms, and decreases the intensity
of the acoustic loss. Any Si-O-Si bonds which come into
contact with Na_2O molecules result in two non-bridging
Si-O bonds which again make no further contribution to
the acoustic loss. The sequel of addition of an alkali
oxide molecule to a Si-O-B bond is difficult to predict.

An extra bridging oxygen bond will not be produced as the silicon atom cannot increase in coordination number beyond 4, and the most likely result is one Si-O and one B-O non-bridging bond, neither of which will act as an acoustic absorption centre.

We will see in the following section how the ultrasonic velocities rise as the Na_2O content of the glasses increases, and how this may only be explained by the concentration of the alkali oxide molecules at B-O-B sites. Consequently we can infer that the decrease in ultrasonic attenuation is due to the elimination of this type of cation-oxygen-cation bond rather than any other.

The average activation energy for the acoustic loss mechanism is lower in sample 1/48 (2800 cal/mole) than in sample 2/Qii (3300 cal/mole) which suggests that glasses with a higher Na_2O content have a lower associated $\bar{H}$. If we assume a constant attempt frequency for the loss mechanism throughout all the glasses of this work, the general decrease in peak temperature on addition of Na_2O further evidences the effect of alkali oxide on the average activation energy. This effect is again borne out by the greater fractional decrease in magnitude of Δi at higher than lower activation energies in the series 1/Q − 2/Q − 5/Q (see Figure 7.6). It thus follows that the Na_2O molecules concentrate at the B-O-B bonds of highest activation energy for movement of the oxygen atom, which are the most non-linear in nature. Here,

where the boron atoms are closest together, the addition
of an extra oxygen bridging atom can bring about the most
energetic advantage.

7.2.8   Ultrasound velocities : the compositional dependence

The ultrasound velocities of the $Na_2O-B_2O_3-SiO_2$
glasses at any given temperature vary quite considerably
between the samples of different composition. It is of
value to examine the dependence of velocity upon composition
to gain information about the structure of these glasses.
For the purpose of comparison we will choose the velocities
at the convenient temperature of $280^O K$. Firstly, however,
it is pertinent to compare the results of this present
study with those from the only other previous similar
work, that of Gladkov and Tarasov (1960) (see Figure 3.2).

Away from the binary edge of the ternary diagram
but within the compositions defined by the 10 wt% Na_2O
limit, the measured longitudinal velocities of the
quenched glasses 2/Q to 5/Q, and 10/Q are in reasonable
agreement with the results of Gladkov and Tarasov. How-
ever the binary glasses 6/Q and 7/Q have ultrasound
velocities that are respectively 10% and 15% too low.
Proceeding to compositions of higher Na_2O content we
find that the longitudinal velocity of glass 1/Q is 4%
too high to agree with the previous work, and glasses
8/Q and 9/Q have velocities exceeding those indicated

by the previous study by 14% and 12% respectively. The reasons for the discrepancy between the present results and those of Gladkov and Tarasov are as follows:

(a) Gladkov and Tarasov report longitudinal ultrasound velocities of the pure SiO_2 and B_2O_3 glasses 6% and 13% lower than the accepted values found by many other workers and consequently must be regarded as being in error,

(b) they failed to measure the velocity in any binary B_2O_3-SiO_2 glass and assumed a straight line dependence between their (erroneous) values for SiO_2 and B_2O_3; any deviation from this linear behaviour would considerably alter the position of the iso-velocity lines along this edge of the diagram,

(c) they do not report the temperature at which the measurements were made, or comment on the purity and water content of the samples or state their thermal history.

Further comparison between the present study and that of Gladkov and Tarasov is made difficult due to the absence of details of the experimental method of the earlier work.

To collect the information on the effect of the alkali oxide modifier Na_2O on the ultrasound velocity in the glasses of the present work, both longitudinal and shear wave velocities of quenched glass samples are plotted as a function of mole% Na_2O in Figure 7.8. Also included for comparison are the longitudinal wave velocities
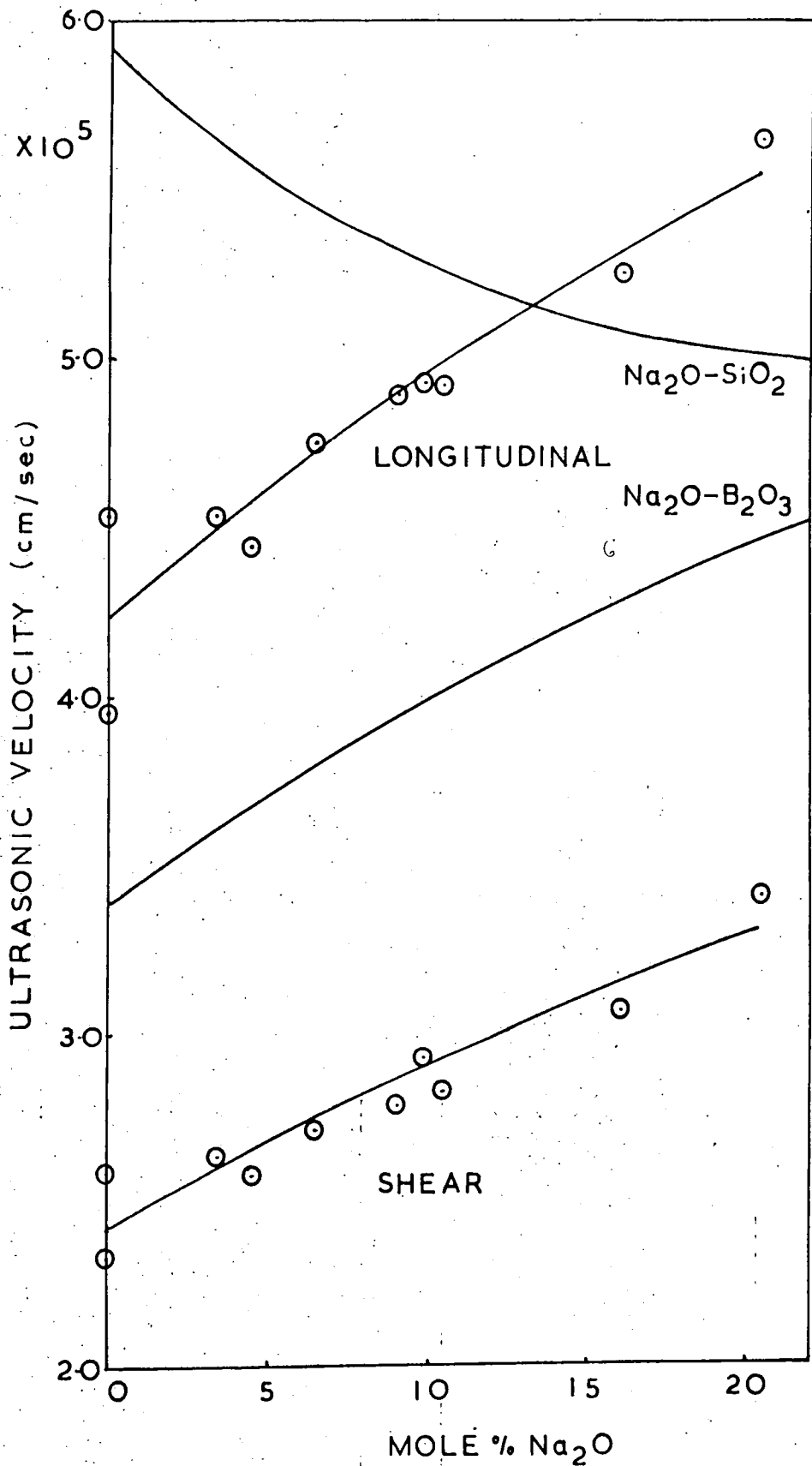
Figure 7.8 Ultrasound velocities for $Na_2O - B_2O_3 - SiO_2$ glasses in comparison with $Na_2O - SiO_2$ and $Na_2O - B_2O_3$ glasses.

for the Na_2O-SiO_2 and $Na_2O-B_2O_3$ glasses (see Chapter 3) but with the value for 100% SiO_2 taken from the results of Fraser (1968) and that for 100% B_2O_3 from Uhlmann and Shaw (1971). The $Na_2O-B_2O_3-SiO_2$ glass compositions all lie near a line on the ternary diagram satisfied by the relationship (wt%) $(n)Na_2O.(40+n)B_2O_3.(60-2n)SiO_2$ which indicates that both Na_2O and B_2O_3 content are increasing from left to right across Figure 7.8. The solid line drawn on this figure for $Na_2O-B_2O_3-SiO_2$ glasses are an interpolation of the velocities for compositions described by this relationship. It should be stressed however that a plot of ultrasound velocity versus actual B_2O_3 or SiO_2 content does not exhibit the essential simplicity of Figure 7.8. The mechanical properties - shear modulus, bulk modulus and Young's modulus - also become progressively larger on addition of alkali oxide in the series of glasses, and evidence an increasing resistance to shear, hydrostatic compression and tension as the Na_2O content is raised. Poissons ratio, however, displays no general trend with sample composition.

The longitudinal and shear ultrasound velocities increase smoothly on addition of Na_2O even though the accompanying increment in B_2O_3 content would be expected to decrease the stiffness of the glass lattice. This behaviour is qualitatively similar to that observed in the $Na_2O-B_2O_3$ system but is opposite to that in glass of the Na_2O-SiO_2 system. An increase in the ultrasound velocity in the $Na_2O-B_2O_3-SiO_2$ glasses as the Na_2O content

is raised evidences growth in the strength of the lattice
and is almost certainly caused by a rise in the coordination
number of the boron atoms from 3 to 4. Association of the
Na^+ ions with SiO_4 tetrahedra would produce singly bonded
oxygen ions and hence decrease the cross-linking in the
structure.

A very important point to note here is that the
Na_2O molecules are apparently associated with the B_2O_3
species in the glass lattice whether the glass compositions
are within (glasses 1 to 8 and 10) or without (glass 9)
the area reported by Charles (1970) as that where
metastable immiscibility is manifested. No sharp change
in ultrasound velocity and hence by implication change
in structure, especially boron coordination number, is
observed anywhere in the series of glasses as would be
expected on the change from a glass of a B_2O_3 and Na_2O
rich phase and a SiO_2 rich phase to a glass of structural
homogeneity. It is reasonable to suppose that there are
regions of high B_2O_3 and Na_2O concentration over all the
area of the ternary diagram bounded by the compositions
of this work; a proposal which is supported by evidence
of phase separation in the electron micrographs of every
glass studied.

Another interesting detail arises from inspection
of Figure 7.8; the longitudinal ultrasound velocity in
the Na_2O-B_2O_3-SiO_2 glasses increases to larger values
compared with glasses in the Na_2O-B_2O_3 system (Gladkov
and Tarasov) even allowing for the suspected error in

the results. The maximum velocity for Na_2O-B_2O_3 glasses

is 4.95 x 10^5 cm/sec at 35 mole% Na_2O, where approximately

45% of the boron atoms are 4 fold coordinated (Bray and

O'Keefe). A plausible reason for the high ultrasound

velocity in the higher Na_2O content Na_2O-B_2O_3-SiO_2 is

that a larger proportion of the boron cations in the

lattice can become 4 coordinated in the Na_2O-B_2O_3-SiO_2

glasses than in the binary Na_2O-B_2O_3 glass.

7.2.9   The temperature dependence of the ultrasound

         velocities

An ultrasound damping mechanism has an associated

change in elastic modulus and hence ultrasound velocity,

as detailed in Chapter 2. The characteristic minima in

both the shear and longitudinal ultrasound velocities

in the Na_2O-B_2O_3-SiO_2 glasses are directly connected with

the large acoustic loss peak which occurs below room

temperature in these materials. After the minimum, the

ultrasound velocity becomes quite linear with temperature;

this form of velocity-temperature curve is very similar to

those for many other inorganic glasses such as SiO_2, GeO_2,

BeF_2 and Zn $(PO_3)_2$ (Krause and Kurkjian, 1968).

The two Láme constants μ and λ, which are related

to the ultrasound velocities through equation 2.12 provide

an alternative way of looking at the ultrasound velocities.

The temperature dependence of these constants for samples

1/Q, 1/48, 2/Q and 2/48 are shown in Figures 7.9 and 7.10

from which it is evident that there is a relaxation in the
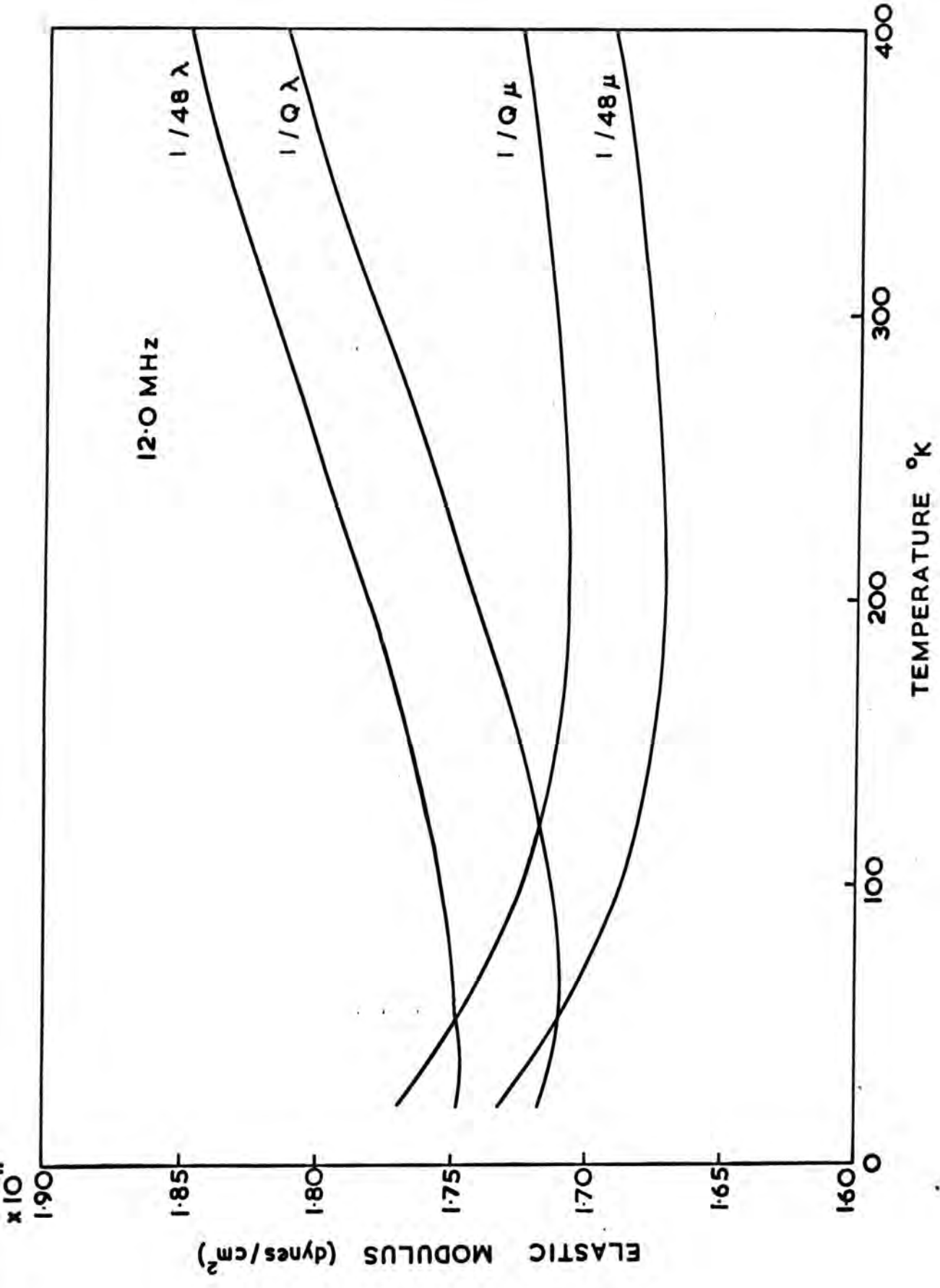
Figure 7.9 The temperature dependence of the Lamé constants for glasses 1/Q and 1/48
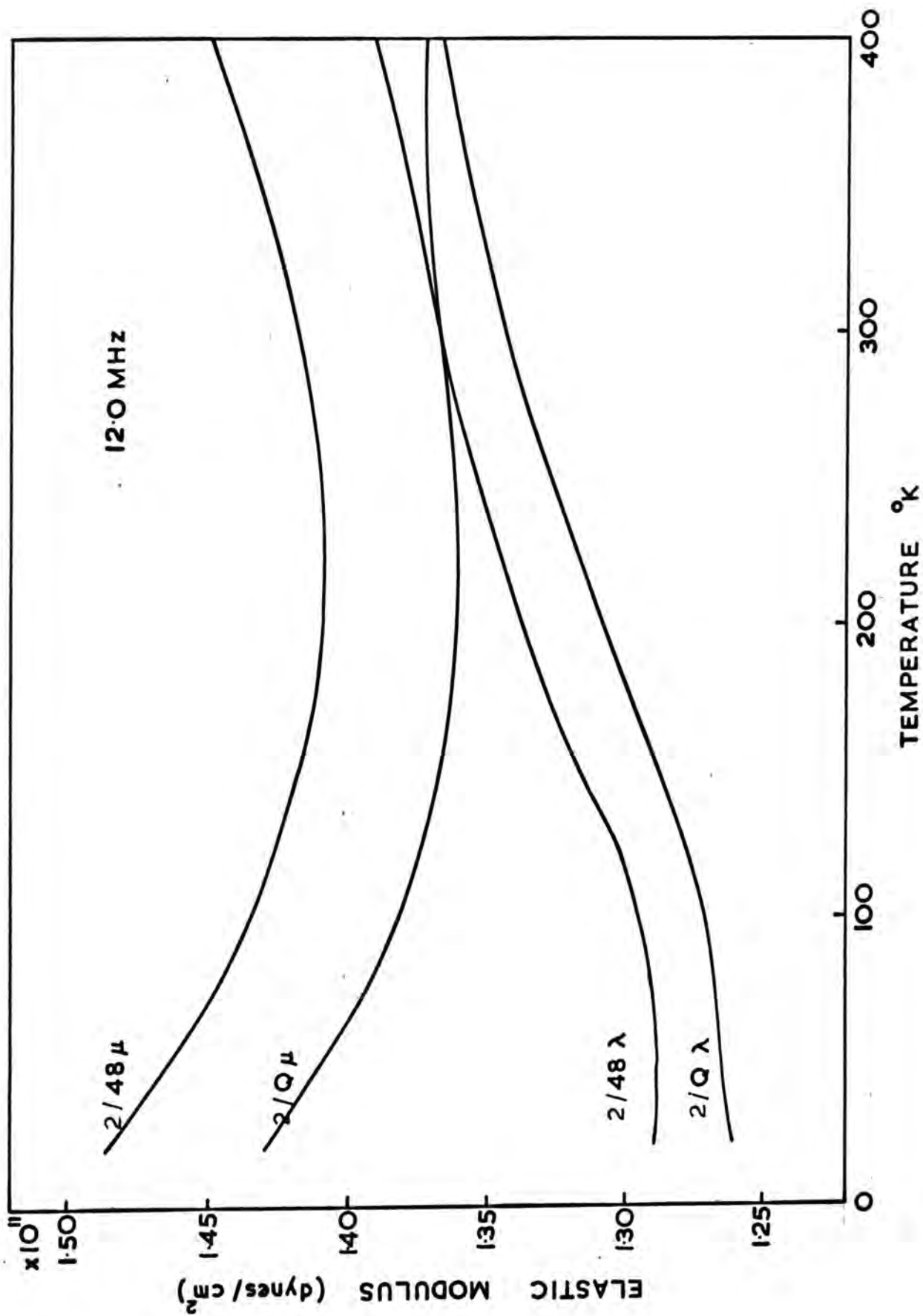
Figure 7.10 The temperature dependence of the Lamé constants for glasses 2/Q and 2/48

modulus μ but not in λ. The value of λ remains fairly
constant over the range 10^OK to 80^OK and then slowly
rises to 400^OK, the upper limit of measurement. On the
other hand, μ decreases to a minimum value at approximately
220^OK and then rises and attains a linear temperature
dependence by 350^OK to 400^OK. The relaxation of the
elastic modulus μ is thus within the temperature range of
the acoustic loss peak, as predicted from the relaxation
theory of Zener. From this approach we see that the
acoustic loss is associated with the stress-strain com-
ponent μ rather than λ.

It is of interest to determine the contributions
to the temperature dependence of μ, which is identically
equal to the shear modulus, from sources other than that
which is associated with the large acoustic loss peak.
To do this, the contribution to the temperature dependence
of μ due to the structural relaxation is calculated from
the computed distribution of the acoustic loss mechanism
as detailed in Section 7.2.4. This has been undertaken
for samples 1/Q, 1/48, 2/Q, and 2/48 and the results are
presented in Figures 7.11 to 7.14. The line connecting
the small circles is the experimentally determined
fractional change in μ normalized to the extrapolated
value at 0^OK, the line connecting the open triangles
is the calculated relaxation in modulus associated with
the large acoustic loss peak, and the solid line is their
difference, which gives the temperature dependence of
the elastic modulus μ, normalized to 0^OK, due to other

Figure 7.11 Separation of the contributions to the change in shear modulus for sample I/Q
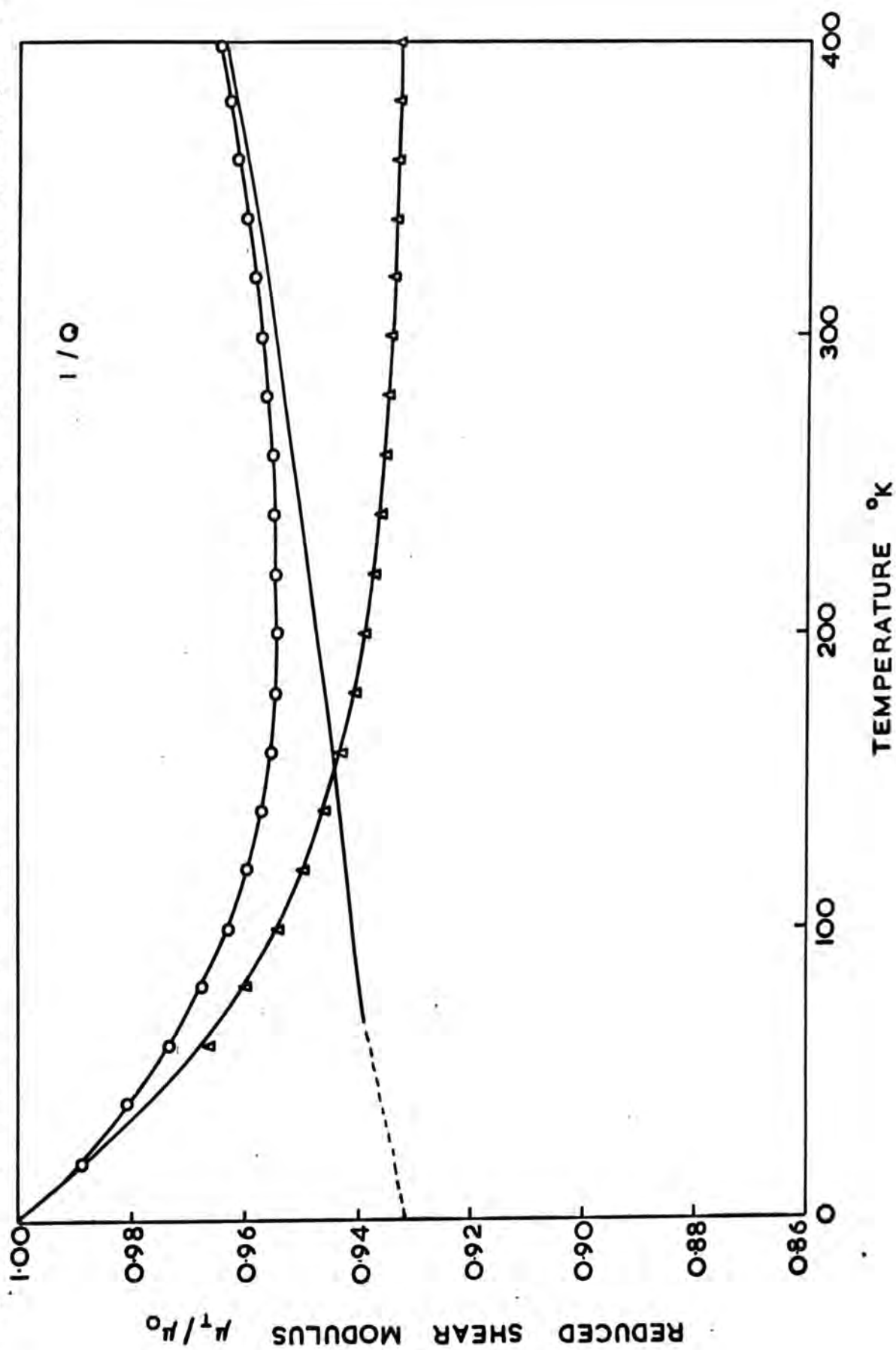
Figure 7.12 Separation of the contributions to the change in shear modulus for sample 1/48
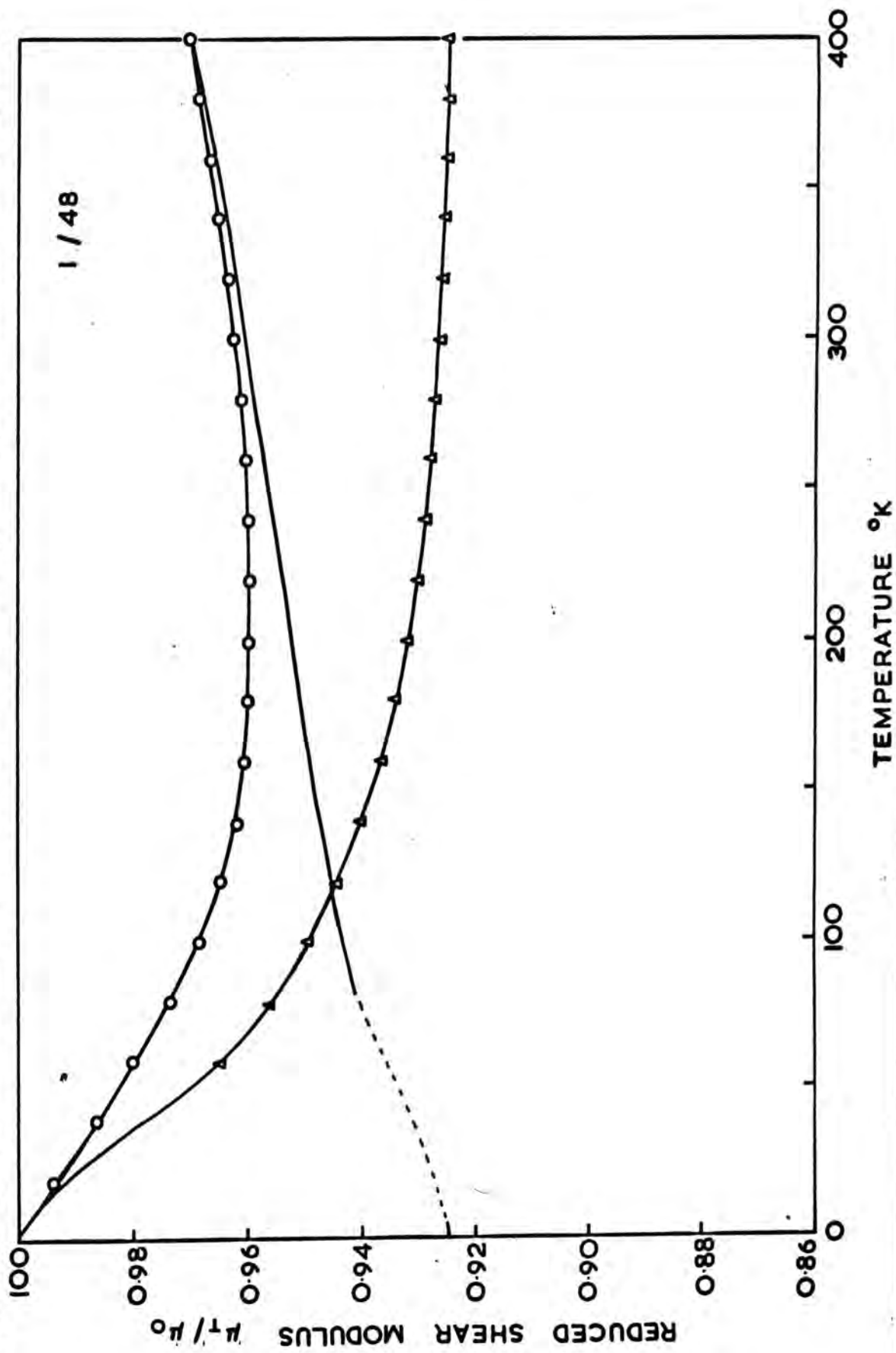
Figure 7.13 Separation of the contributions to the change in shear modulus for sample 2/Q

2/Q

TEMPERATURE °K

REDUCED SHEAR MODULUS μ_T/μ_0
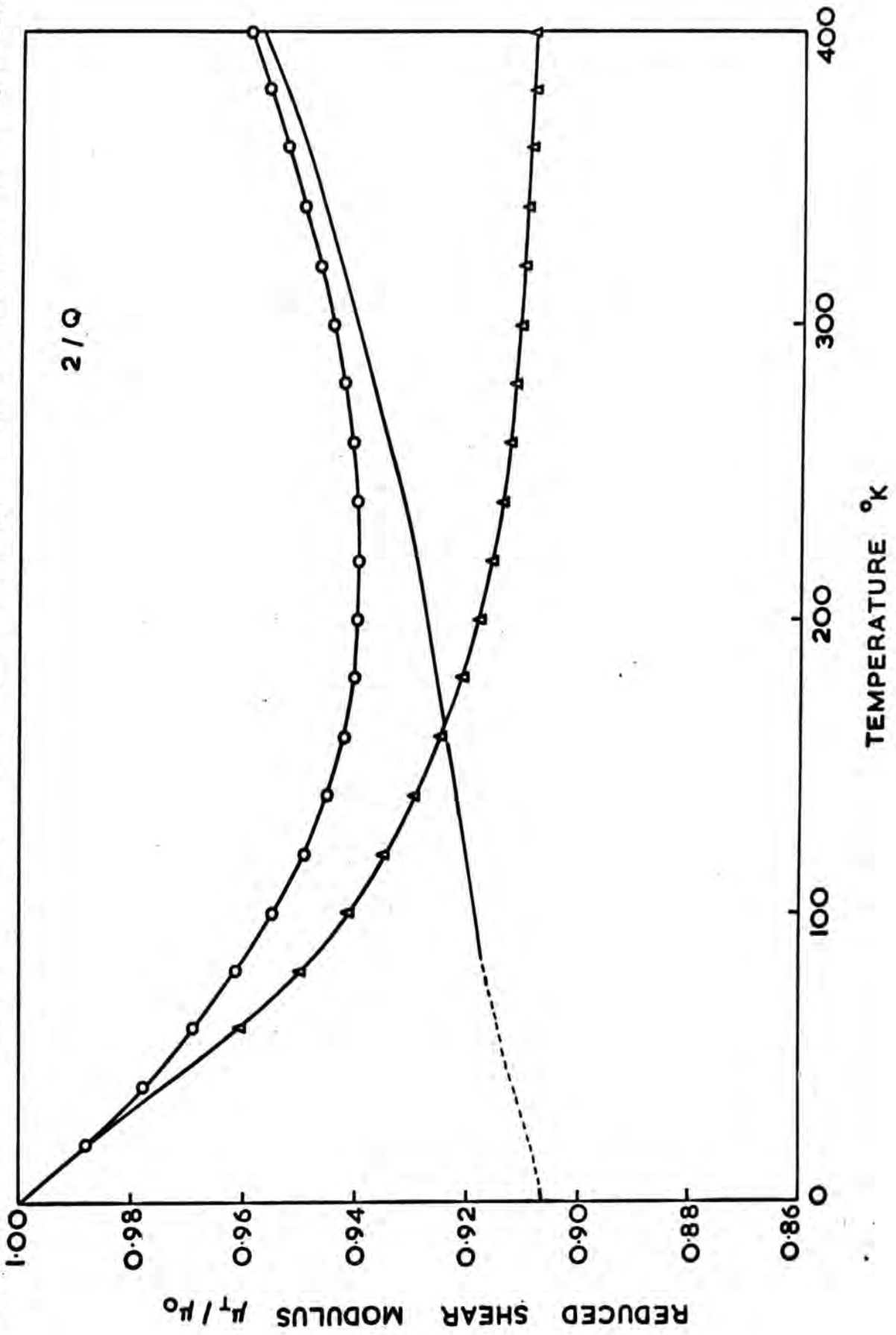
Figure 7.14 Separation of the contributions to the change in shear modulus for sample 2/48
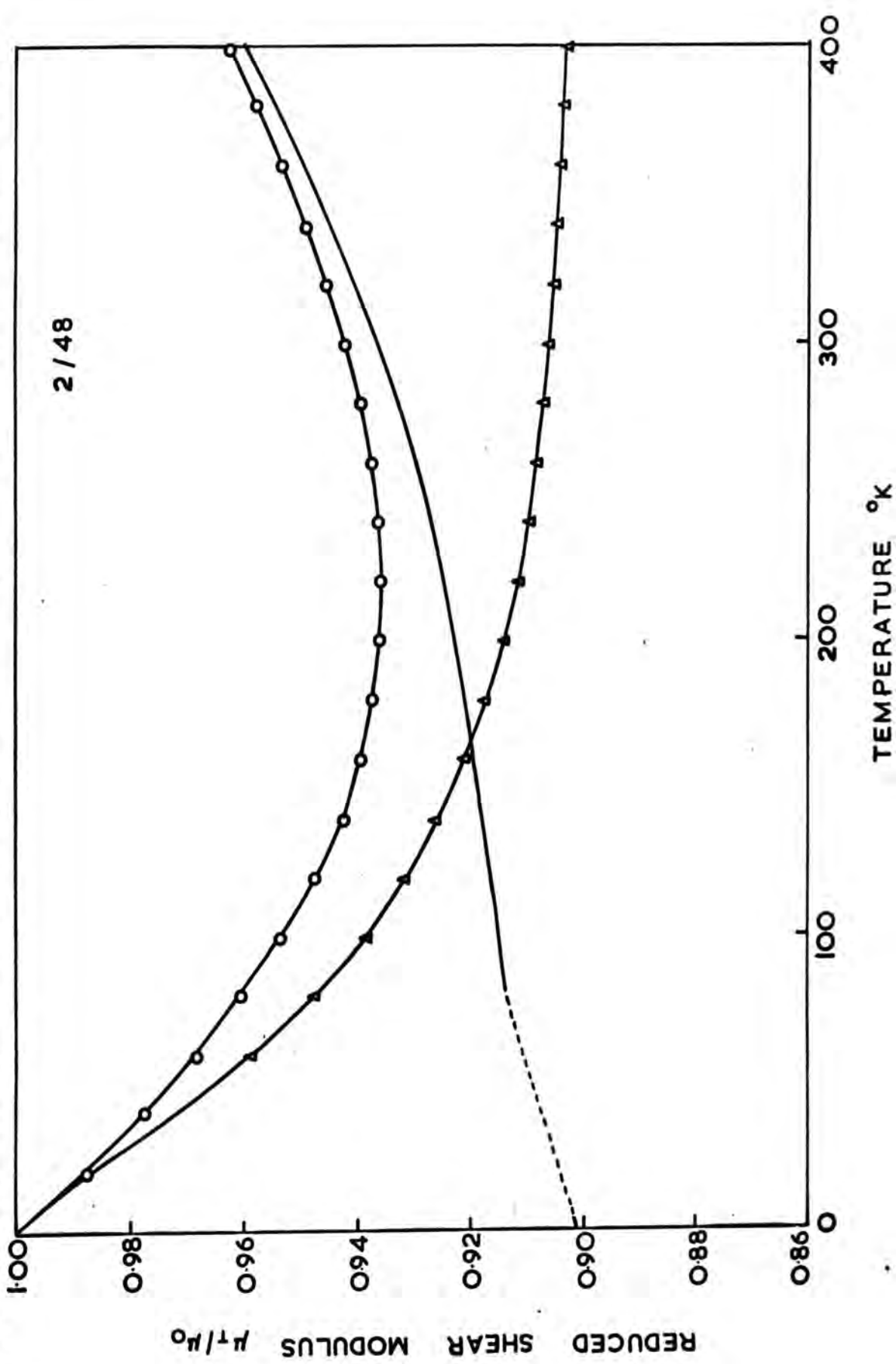
sources. The calculated change below $80^{\circ}K$ is unreliable as the distribution of activation energies below about 900 cal/mole is not accurately obtained, so this portion of the solid line is shown dashed. However, the value for the unrelaxed modulus at $0^{\circ}K$ is precisely indicated.

The first point to notice is that both the experimental and calculated relaxation in elastic modulus, indicated by the total fractional change in these moduli, increase in the order 1/Q, 1/48, 2/Q to 2/48 (see Figures 7.11 to 7.14) in agreement with the magnitude of the observed acoustic loss peaks. This is exactly as expected from the theory of the standard linear model of anelasticity. Secondly, the calculated relaxation in μ is larger than that observed experimentally. This is a very similar situation to that for vitreous SiO_2 (Anderson and Bömmel, 1955) and indicates, as seen in Figure 7.11 to 7.14, that the contributions to the change in elastic modulus from these other sources are such as to increase the modulus μ with increasing temperature.

Once we have removed the contribution to the temperature dependence of the elastic moduli due to the structural relaxation process we see that the changes in both μ and λ with temperature have a very similar shape. Fundamentally, there is a positive temperature coefficient of ultrasound velocity at temperatures higher than where the structural relaxation dominates the propagation velocity. This is itself in complete contrast to the negative temperature dependence of ultrasound

velocity usually shown by crystalline materials. In
this respect there is completely different behaviour
between glasses and crystalline solids. Possible reasons
for this unusual performance, which is characteristic
of many inorganic glasses, will now be investigated.

7.2.10 The positive temperature coefficient of ultrasound
        velocity and the coefficient of thermal expansion
        in $Na_2O-B_2O_3-SiO_2$ glasses

        Krause and Kurkjian (1966a) have demonstrated
that addition of 2 mole% Na_2O to vitreous GeO_2 has the
effect of changing the sign of the temperature coefficient
of ultrasound velocity at 300^oK from positive to negative;
the same authors (1968) have found that at this same
temperature the sign of the coefficient in vitreous B_2O_3
is also negative. In contrast, certain of the materials
of this present study, which contain large amounts of
both Na_2O and B_2O_3, have a positive temperature coefficient
of velocity at temperatures above the minimum associated
with the structural relaxation (glasses 1/Q, 1/48, 2/Q,
2/48, 5/Q and 7/Q), while glass 8/Q exhibits a coefficient
equal to zero, within experimental error.

        The reason for the anomalous positive temperature
coefficient of ultrasound velocity in inorganic glasses
is not well understood. Anderson and Dienes (1960) have
considered that the positive coefficient of ultrasound
velocity in vitreous SiO_2 is phenomenologically related
to the very low coefficient of thermal expansion.

(α = $5.10^{-7}/^{\circ}$K at 300°K). Starting from the supposition of Lazarus (1949) that an elastic modulus M is a function of both volume and temperature, it can be shown that

$$\frac{dM}{dT} = -3\alpha K \frac{\partial M}{\partial P}_T + \frac{\partial M}{\partial T}_V \qquad 7.9$$

where K is the bulk modulus of the solid. The argument is then that if α is small enough then $\frac{dM}{dT}$ is governed by the sign of $\frac{\partial M}{\partial T}_V$. Anderson and Dienes have shown that from considerations of the Born-von Karman model for a solid that $\frac{\partial M}{\partial T}_V$ is positive for a small coefficient of thermal expansion at high temperatures (for example, 300°K).

A similar argument holds for a Grüneisen solid in which

$$\mu = \frac{3\alpha K \overline{V}}{C_V} = \text{constant} \qquad 7.10$$

The differential of this equation is

$$\frac{d\ln\frac{1}{K}}{dT} = 3\alpha + \frac{d\ln\alpha}{dT} - \frac{d\ln C_V}{dT} \qquad 7.11$$

Ordinarily both α and C_V increase with temperature, and the temperature coefficient of the compressibility $^1/K$ depends on the balance of the first two and the last terms. But if α and $\frac{d\ln\alpha}{dT}$ are small enough, then $\frac{d\ln^1/K}{dT}$ can be negative, which results in a positive temperature coefficient for the bulk modulus K and also for the ultrasound velocities.

Krause and Kurkjian (1968) have pointed out that such glasses as GeO_2, BeF_2 and $Zn(PO_3)_2$ have a coefficient of thermal expansion and order of magnitude larger than that in vitreous SiO_2, yet still exhibit a positive temperature coefficient of ultrasound velocity. The same is also true of the $Na_2O-B_2O_3-SiO_2$ glasses of this study. Glassy B_2O_3 has, however, a coefficient of thermal expansion only 2 to 3 times larger than these other inorganic glasses, yet displays a negative temperature coefficient of ultrasound velocity. These facts led Krause and Kurkjian to conclude that the hypothesis of Anderson and Dienes is not correct.

Let us now re-examine that data on the fractional temperature coefficients of longitudinal ultrasound velocity in inorganic glasses which are available in current literature. In Figure 7.15 is shown $\frac{1}{V_L} \cdot \frac{dV_L}{dT}$ for a number of inorganic glasses, including those of this work, plotted against their coefficients of thermal expansion. Data points for the shear velocities of $Na_2O-B_2O_3-SiO_2$ glasses 7/Q and 8/Q, for which the temperature variation of longitudinal velocity has not been measured, are included with the justification that the fractional temperature coefficients of velocity for both shear and longitudinal velocities are usually almost equal. Apart from the data point for the non-oxide BeF_2 which lies off the diagram ($\frac{1}{V_L} \cdot \frac{dV_L}{dT} = +250 \times 10^{-6}$, $\alpha = 7.5 \times 10^{-6}$) there is a clear correlation between the
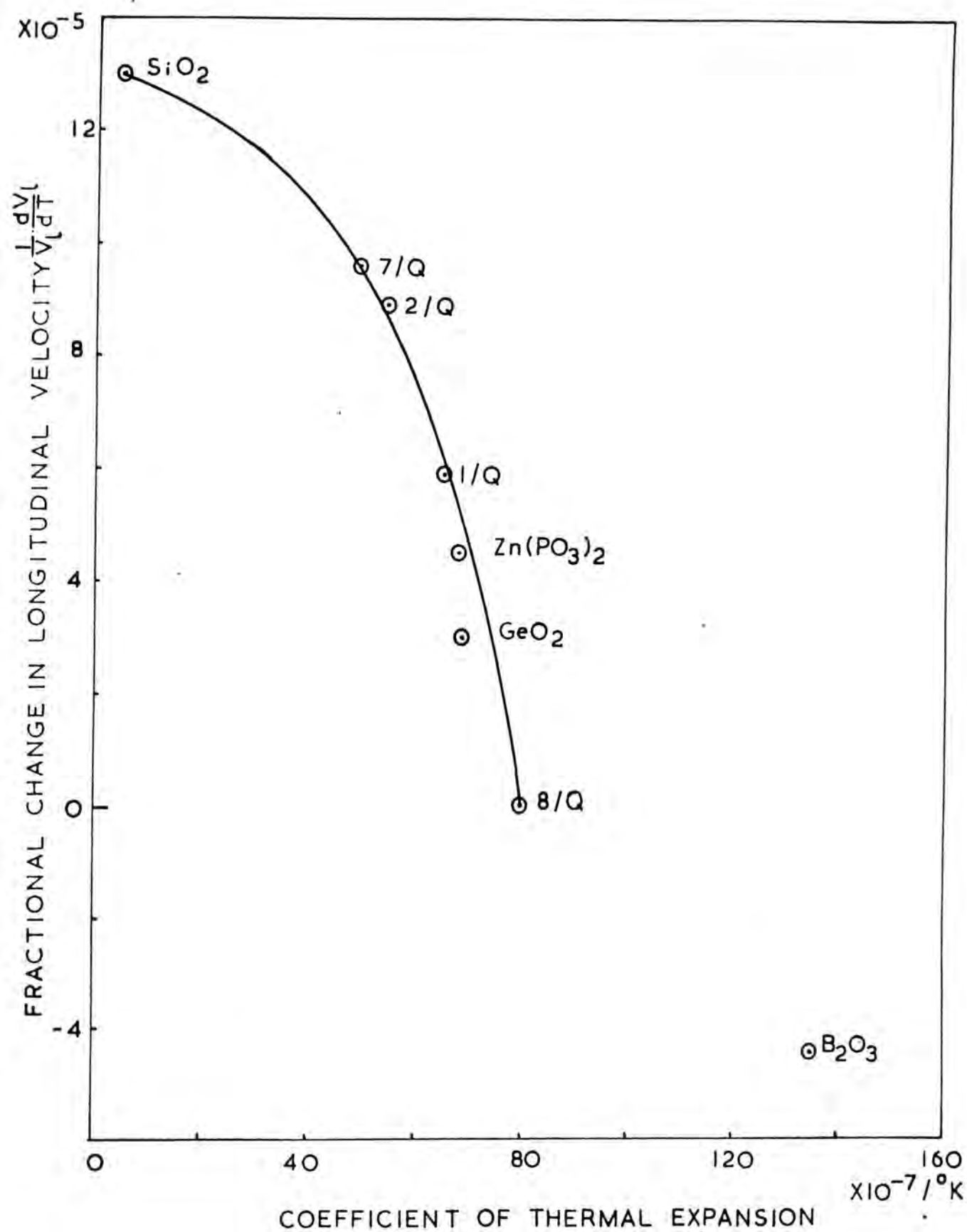
Figure 7.15 The correlation between $\frac{1}{V_L}\frac{dV_L}{dT}$ and α in inorganic glasses at 300°K.

two variables. The failure of the data point for B_2O_3 to lie near the extrapolated curve may be the result of the different bonding character in this glass. The other inorganic glasses mentioned here are tetrahedral in character while B_2O_3 consists chiefly of planar BO_3 triangles in which structure greater amplitude of vibration perpendicular to the triangles is possible.

It is now necessary to look at the magnitude of the terms in equation 7.11 to gain more information on the relationship between the temperature coefficient of ultrasound velocity and the coefficient of thermal expansion. The terms $\frac{d \ln 1/K}{dT}$ and 3α have been calculated for the Na_2O-B_2O_3-SiO_2 glasses 1/Q and 2/Q and also for vitreous SiO_2 from the data of Anderson and Dienes (1960). These results are as follows, in units of $^{\circ}K^{-1}$

	1/Q	2/Q	SiO$_2$
$\frac{d \ln 1/K}{dT}$ (300-400°K)	-6.5×10^{-5}	-7.2×10^{-5}	-1.1×10^{-4}
3α (300°K)	1.95×10^{-5}	1.64×10^{-5}	1.5×10^{-6}

Substituting these numbers into equation 7.11 we can calculate the value of the term $\frac{d \ln \alpha}{dT} - \frac{d \ln C_V}{dT}$ assuming that the Grüneisen model is valid. Then, it can be shown that to render the glass 'normal', that is to have a positive temperature coefficient of compressibility, if all the other terms in equation 7.11 remain constant, the coefficient of thermal expansion in all three glasses would have to be as large as 3×10^{-5}. This value is

much larger than that for α-quartz ($\alpha = 7.5 \times 10^{-6}$ parallel
to the z-axis, 1.37×10^{-5} perpendicular to the z-axis)
which has a negative temperature coefficient of ultrasound
velocity, and is also larger than that for many metals.
It thus appears that factors other than a small coefficient
of thermal expansion cause the anomaly in the behaviour
of the ultrasound velocity. The failure of equation 7.11
to explain satisfactorily the anomaly is most probably
due to the limitations of the single parameter Grüneisen
theory.

The presence of other anomalies in the vibrational
behaviour of vitreous SiO_2 and other inorganic glasses,
such as a negative coefficient of thermal expansion at
low temperatures, excess specific heat over that expected
from the Debye theory, and a negative pressure coefficient
of shear and bulk moduli are considered to result either
from low lying transverse vibrations which are possible
in open tetrahedrally coordinated structures (Krause and
Kurkjian, 1968; White, 1964) or from vibrations connected
with defects such as oxygen vacancies (Leadbetter, 1968).
A network filling alkali oxide decreases the low temperature
expansivity of vitreous SiO_2 (White, 1964) and increases
the coefficient of thermal expansion (Robinson, 1969)
evidencing the suppression of these modes by the alkali
oxide molecules. If these low-lying modes are also
responsible for the positive temperature coefficient of
ultrasound velocity in inorganic glasses, then it is
expected that addition of Na_2O would decrease the magnitude

of this unusual effect. However, no such information on alkali-oxide SiO_2 glasses is available.

The variation of the temperature coefficient of ultrasound velocity with sample composition for Na_2O-B_2O_3-SiO_2 glasses are directly obtainable from the results of this present work. In Figure 7.16 is plotted the fractional temperature coefficient of shear velocity at $400^{\circ}K$ for glasses 1/Q, 2/Q, 5/Q, 7/Q and 8/Q against the molar % Na_2O content of the glass. All the data points lie on or very near a smooth curve, indicating that there is a strong correlation between the two variables, and that the magnitude of the ultrasound velocity anomaly decreases with increasing Na_2O content.

A corresponding increase is also seen in the coefficient of thermal expansion with increasing Na_2O content in the Na_2O-B_2O_3-SiO_2 glasses (see Figure 7.17). It is interesting to observe that the data points lie on a smooth curve even though the glasses are of varying SiO_2:B_2O_3 ratio; the alkali oxide content dominates the thermal expansion behaviour. Although the coefficients of thermal expansion cannot be considered as anomalously low, even at zero Na_2O content, the coefficient of thermal expansion does increase on addition of the network modifying alkali oxide.

In conclusion it appears that on inspection of the results from this present study and the data available on vitreous SiO_2 and other inorganic glasses, that the positive temperature coefficient of ultrasound
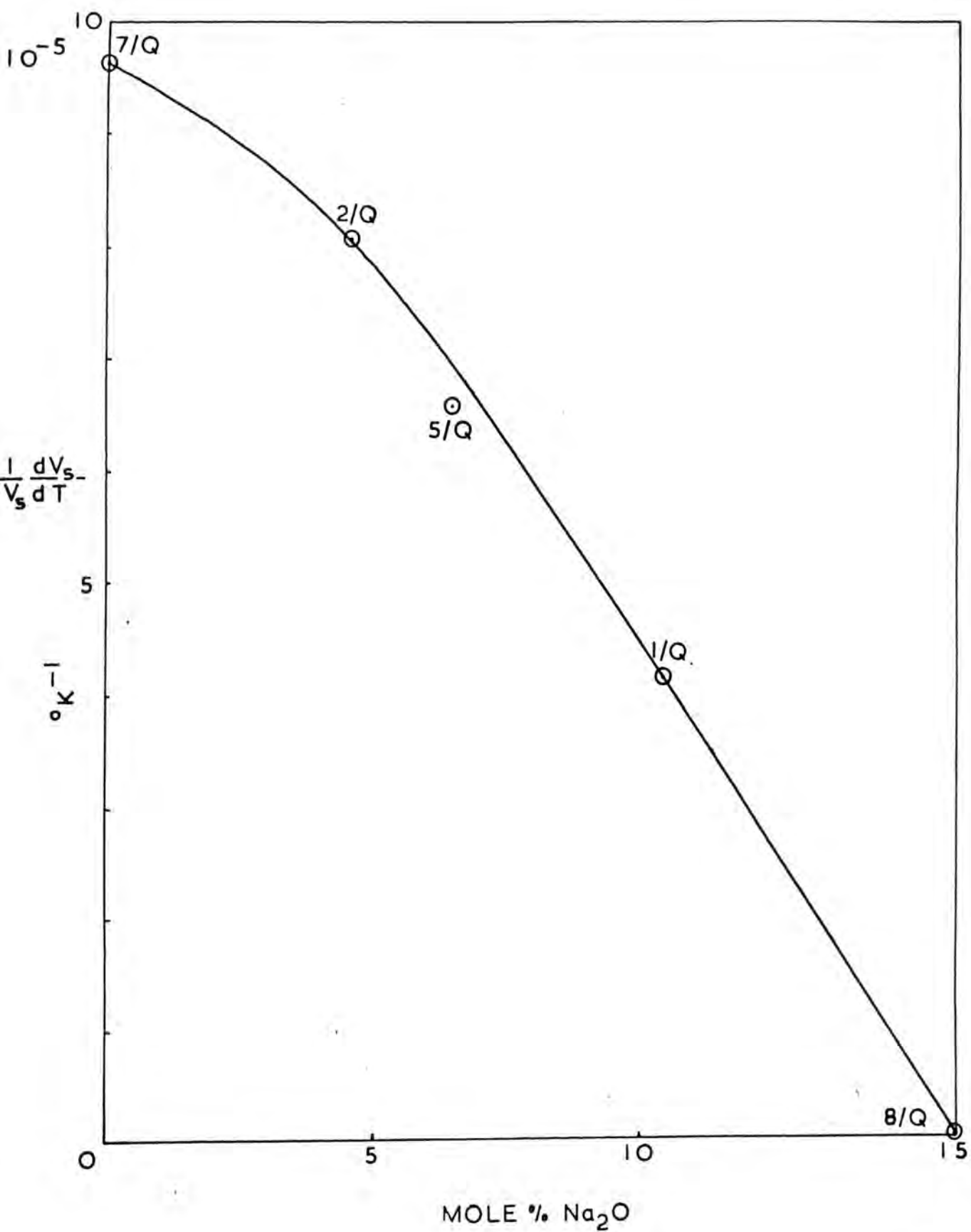
Figure 7.16 The variation of $\frac{1}{V_s}\frac{dV_s}{dT}$ at $400^\circ K$ with Na_2O content for $Na_2O - B_2O_3 - SiO_2$ glasses.
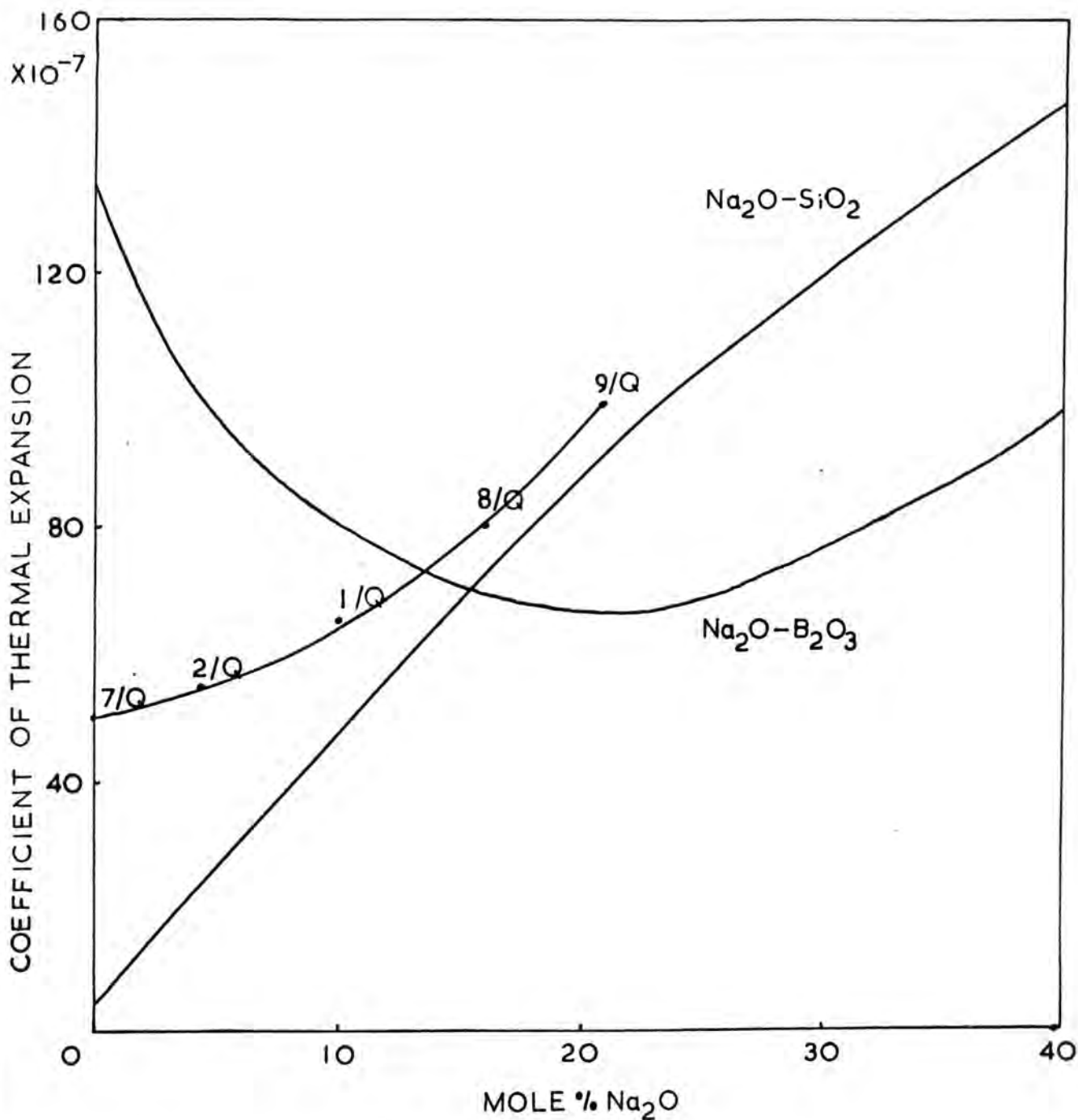
Figure 7.17 The coefficient of thermal expansion in $Na_2O - B_2O_3 - SiO_2$, $Na_2O - SiO_2$ and $Na_2O - B_2O_3$ glasses.

velocity is not the consequence of a small coefficient of thermal expansion. The two properties appear to be related to the existence of a third phenomenon, which is most likely the low-lying vibrational modes of the type proposed by White or Leadbetter.

7.2.11   The complex parts of the elastic moduli μ' and λ'

We have seen in Chapter 2 that the internal friction exhibited by a material is given by the ratio of the imaginary part to the real part of the complex elastic modulus which governs the velocity of the acoustic wave. That is, for a complex elastic modulus $c + ic$,

$$Q^{-1} = \frac{c'}{c} \qquad 7.12$$

Both the real and imaginary parts of the elastic moduli of a solid can be calculated from the attenuation and velocity data, and the out-of-phase stress-strain relationship for the acoustic loss identified. For an isotropic material, for example a glass,

$$Q_S^{-1} = \frac{\mu'}{\mu} \quad \text{and} \quad Q_L^{-1} = \frac{\lambda'+2\mu'}{\lambda+2\mu} \qquad 7.13$$

where Q_S and Q_L are the internal frictions exhibited for a shear and a longitudinal ultrasound wave. The models of Anderson and Bömmel and Strakna for the loss mechanism in vitreous SiO_2 and other inorganic single-component glasses predict more loss for a shear vibration, and only when the potential wells, between which the oxygen atom

moves, are of initially unequal depth will a longitudinal wave be attenuated. This is reflected in the imaginary parts of the elastic constants for vitreous SiO_2, which are calculated from the results for the attenuation of both shear and longitudinal waves at 21.5 MHz as

$$\mu' = 5.45 \times 10^8 \text{ dynes/cm}^2, \quad \lambda' = 2.17 \times 10^8 \text{ dynes/cm}^2$$

at the peak maximum (47°K). Thus the loss in both the shear and longitudinal waves is mainly accounted for by the shear vibrational term μ'. This finding is in agreement with that of McSkimin (1953) who has compared the μ' and λ' terms in vitreous SiO_2 down to 70°K at 20 MHz acoustic frequency.

If we now envisage a mixed cation-oxygen-cation bond, for example an Si-O-B bond, then we expect that on application of Anderson and Bömmel's model that the potential wells perpendicular to the Si-B direction will be of equal depth. We then anticipate that the shear vibrational term μ' will be greater than the dilational term λ'. However, on application of the elongated bond model of Strakna to an Si-O-B bridging unit the potential wells will be of unequal depth and we thus expect a larger term in λ'. The $Na_2O-B_2O_3-SiO_2$ glasses of this work must contain mixed cation-oxygen-cation bonds; a comparison of the magnitudes of the imaginary parts of the elastic moduli may provide some valuable information about the mechanism of ultrasound absorption. The moduli μ' and λ' have been calculated at the maximum of

the acoustic loss for various Na_2O-B_2O_3-SiO_2 samples
and are as follows, in units of 10^8 dynes/cm^2.

	μ'	λ'
1/Q	5.04	3.33
1/48	5.77	6.06
2/Q	6.14	3.21
2/48	6.71	4.88
4/Q	5.83	4.66
5/Q	6.70	4.77

Thus we see that λ' is greater in relation to
μ' than in vitreous SiO_2, and in most Na_2O-B_2O_3-SiO_2
glasses is almost as large as μ'. This gives support
for the elongated as opposed to the non-linear bond model
for the acoustic loss mechanism.

The multicomponent nature of the Na_2O-B_2O_3-SiO_2
glasses may, however, have the effect of disturbing the
symmetry of the potential wells between which the oxygen
atoms vibrate and thus change the ratio of μ' to λ' that
is found in the single component SiO_2 material. A
puzzling aspect of a relatively large term in λ' is that
there is no corresponding relaxation minima in the
temperature dependence of λ. This point at present
remains unexplained.

It is also of note that the presence of the
relatively large λ' term is the most notable way in which
the anelastic properties of Na_2O-B_2O_3-SiO_2 glasses differ
from those in vitreous SiO_2. Further comparisons with
other inorganic glasses cannot be undertaken at the

present time due to the unavailability of concurrent ultrasound velocity and attenuation measurements; a comparison of the complex elastic constants in different glasses would be a study worth undertaking by future workers.

7.2.12 The ultrasound velocities below $4.2^{\circ}K$

In the liquid helium temperature range the ultrasound shear velocities show a linear dependence on temperature to about $1.5^{\circ}K$ where the dependence then flattens off. The increase in sound velocity with decreasing temperature is associated with the rapid fall in the magnitude of the acoustic attenuation of the higher temperature peak. A relaxation in velocity associated with the $4^{\circ}K$ peak is not seen as this feature is relatively small.

Extrapolation of the ultrasound velocities from $4.2^{\circ}K$ to the limit of $0^{\circ}K$ is simplified by the smooth temperature dependences. Thus, an accurate calculation of the Debye temperature and the parameter A of equation 3.5, which describes the value of C/T^3 in the low temperature limit, can be made. The values of this latter parameter are calculated here with the purpose of finding use in future comparisons with the values determined from measurements of the specific heat of glasses in the $Na_2O-B_2O_3-SiO_2$ system. In Table 7.1 is collected the data of the number of atoms per unit volume (N), the Debye temperature calculated through equation 3.6

Table 7.1

The atomic density (N), C/T^3 in the low temperature limit, Debye temperature (θ_D) and Debye frequency (ν_D) for $Na_2O-B_2O_3-SiO_2$ and other inorganic glasses. The asterisk denotes glasses for which the parameters have been calculated from the $280^\circ K$ values of ultrasound velocity.

Glass	$Nx10^{22}$ no.atoms/cc	$C/T^3_{T=0}$ ergs/$^\circ K^4$mole	θ_D $^\circ K$	ν_D sec^{-1}
1/Q	7.88	$1.12x10^3$	409	$8.51x10^{12}$
1/48	7.86	$1.16x10^3$	405	$8.42x10^{12}$
2/Q	7.52	$1.51x10^3$	369	$7.68x10^{12}$
2/48	7.51	$1.42x10^3$	377	$7.84x10^{12}$
3/Q	7.75	$1.10x10^3$	407	$8.47x10^{12}$
4/Q	7.52	$1.40x10^3$	378	$7.86x10^{12}$
5/Q	7.71	$1.27x10^3$	391	$8.13x10^{12}$
6/Q*	6.95	$1.59x10^3$	352	$7.32x10^{12}$
7/Q*	7.10	$2.33x10^3$	318	$6.61x10^{12}$
8/Q*	8.52	$9.05x10^2$	445	$9.27x10^{12}$
9/Q*	8.75	$6.19x10^2$	498	$1.04x10^{13}$
10/Q*	8.24	$1.02x10^3$	418	$8.71x10^{12}$
SiO_2	6.62	$4.96x10^2$	495	$1.03x10^{13}$
B_2O_3*	7.95	$2.83x10^3$	276	$5.75x10^{12}$
Pyrex	7.05	$7.07x10^2$	449	$9.34x10^{12}$
GeO_2	6.36	$4.9 x10^2$	309	$6.43x10^{12}$

assuming that the atom is the fundamental vibrational unit, $C/T^3_{acoustic}$ in the low temperature limit and the Debye frequency equal to $k\theta_D/h$. These parameters are presented for the Na_2O-B_2O_3-SiO_2 glasses of this study and also for vitreous SiO_2 (Flubacher, 1959), GeO_2 (Antoniou and Morrison, 1965), Pyrex 7740 (Zeller and Pohl, 1971) and B_2O_3 (calculated from data collected by Uhlmann and Shaw, 1971). Data for the Na_2O-B_2O_3-SiO_2 glasses for which the ultrasound velocities have not been measured as a function of temperature are denoted by an asterisk, and there each parameter has been calculated from the $280^{\circ}K$ value of ultrasound velocity.

The Debye temperatures of the Na_2O-B_2O_3-SiO_2 glasses lie between those of vitreous SiO_2 and B_2O_3 which is to be expected of a compound of these two materials. There is also a correlation between the Debye temperatures of the Na_2O-B_2O_3-SiO_2 glasses and their total Na_2O content, a correspondence which carries over to the low temperature limit of C/T^3. Thus we can expect a strong dependence of the thermal properties upon the Na_2O content, and the important role that the alkali metal take in determining the vibrational character of the Na_2O-B_2O_3-SiO_2 glasses is again accentuated.

A further point of importance to notice from the table is that the Debye frequency for each of the glasses is of the order of the attempt frequency

associated with the activation energy process that is the cause of the large acoustic loss peak. Anderson and Dienes (1960) interpret this fact as indicating that there is zero entropy of activation which infers that the relaxation proceeds with no reorganisation of the structure around the relaxing species. This conclusion is perfectly in accord with the proposed models for the acoustic loss mechanism of Anderson and Bömmel. The common value for Debye frequency and attempt frequency of the loss process further indicates that the vibrational frequency of the relaxing unit is of the order of highest lattice frequency that contributes to the specific heat. This strongly points to a single atom as the relaxing species, and adds weight to the propounded acoustic loss mechanism.

7.3   The effect of phase separation on the elastic and anelastic properties of $Na_2O-B_2O_3-SiO_2$ glasses

7.3.1   Elastic properties

The elastic constants of shear modulus, bulk modulus, Young's modulus and Poisson's ratio at $280^\circ K$ for the $Na_2O-B_2O_3-SiO_2$ glasses in the different stages of heat treatment are presented in Table 6.1. An important feature to notice is that the ultrasound velocities and elastic constants vary with the time of heat treatment at $550^\circ C$ in glasses in batches 1 and 2 in a complex manner; a smooth or simple variation is not found. To help understand this behaviour it is useful to utilise

previous theoretical treatments of the elastic properties of two-phase materials.

Many investigators have endeavoured to find a way of expressing the elastic properties of a two-phase composite in terms of the elastic constants of the individual phases. The majority of these attempts have been concerned with the properties of a material having the morphology of regions of one phase isolated in a matrix of the other. However, it has proved difficult to find an expression which takes into account such factors as second phase shape and distribution. It has been found more useful to derive formulae for the upper and lower numerical limits to the elastic properties of the composite material.

The first (Voigt) model for the investigation of the elastic behaviour of a two-phase system assumes constant strain throughout all the regions of the solid. The results from this model are formulae for the upper limit to the bulk modulus K, shear modulus μ and Young's modulus E thus

$$K_u = (1-V_2)K_1 + K_2V_2 \qquad 7.14$$

$$\mu_u = (1-V_2)\mu_1 + \mu_2V_2 \qquad 7.15$$

$$E_u = (1-V_2)E_1 + E_2V_2 \qquad 7.16$$

where the subscripts 1 and 2 refer to the matrix and dispersed phases respectively, and V_2 is the volume fraction of the dispersed phase. A second (Reuss) model

assumes constant stress throughout the solid, and yields

formulae for the lower limits to the elastic moduli

$$\frac{1}{K_L} = \frac{1 - V_2}{K_1} + \frac{V_2}{K_2} \qquad 7.17$$

$$\frac{1}{\mu_L} = \frac{1 - V_2}{\mu_1} + \frac{V_2}{\mu_2} \qquad 7.18$$

$$\frac{1}{E_L} = \frac{1 - V_2}{E_1} + \frac{V_2}{E_2} \qquad 7.19$$

Hashin and Shtrikman (1963) have formulated

improved upper and lower bounds for these elastic constants

using more modern mathematical techniques. These bounds

are the most restrictive possible for the bulk modulus

in terms of only the volume fractions of the phases and

their elastic constants, and assume arbitrary phase

geometry. Hashin and Shtrikman consider that further

information on the second phase distribution is necessary

before an exact solution can be obtained, though exactly

how this information can be used is at present not known.

The upper limits to the bulk and shear moduli are given

through this treatment by

$$K_u = K_2 + \frac{1 - V_2}{\dfrac{1}{K_1 - K_2} + \dfrac{3V_2}{3K_2 + 4\mu_2}} \qquad 7.20$$

$$\mu_u = \mu_2 + \frac{1 - V_2}{\dfrac{1}{\mu_1 - \mu_2} + \dfrac{6(K_2 + 2\mu_1)V_2}{5\mu_2(3K_2 + 4\mu_2)}} \qquad 7.21$$

and the lower limits are obtained by interchanging

subscripts 1 and 2. These equations and their derivatives

are those which have been found by Uhlmann and Shaw (1971)
to describe quite well the variation in elastic properties
of a number of two component, phase-separated glasses over
known or suspected two-phase regions of composition.

We are now in a position to see if the variation
in the elastic constants of the $Na_2O-B_2O_3-SiO_2$ glasses
with time of heat treatment is due to changes in the
shape and distribution of the second phase morphology or
whether it is due to changes in the elastic constants of
the individual phases themselves. To do this we need the
information on the elastic constants of the individual
phases within the heat treated glasses. The tie lines
on the ternary phase diagram for glasses in batch 2 end
at compositions very nearly corresponding to those of
glasses 7 and 8. We will assume that the elastic constants
of the individual phases of glasses in batch 2 are equal
to those of glasses 7/Q and 8/Q although some error is
introduced from estimating the tie line position from
volume fractions obtained from electron-micrographs and
from the further complication that both these latter
glasses are seen to be inhomogeneous under the electron
microscope. For the purposes of the calculations to
follow the approximation is quite adequate. The tie line
for glasses in batch 1 after heat treatment at $550^{\circ}C$
terminate at compositions other than those of any of the
glasses of this study but not too far away from the
compositions of glasses in batches 7 and 8. Again we
will assume that the individual phase elastic constants

are similar to those in glasses of batch 2.

The Voigt upper and Reuss lower bounds, and the Hashin-Shtrikman bounds to the bulk and shear moduli of a hypothetical phase-separated glass of varying volume fraction but with individual phases of compositions the same as those of glasses 7/Q and 8/Q is shown in Figure 7.18. On the diagram are plotted the shear and bulk moduli of the glasses in batches 1 and 2, with B_2O_3 rich phases volume fractions of 0.62 and 0.28 respectively. The data points are labelled with the time of heat treatment at 550^OC. The vertical displacement of these points is relatively unimportant as some error has inevitably been introduced in selection of the elastic constants of the individual phases, but the expected and experimental spread in the constants is well illustrated.

The important feature of this graph is that the experimental shear and bulk moduli for the glasses in batches 1 and 2 heat treated at 550^OC exhibit a large spread in values. The shear moduli for glasses in batch 2 cover a range of values within the vertical distance described by the separation of the Voigt and Reuss limits, but the bulk moduli have a much larger range than expected. We do not anticipate that the experimental values for the moduli of glasses in batch 1 will be limited by the Voigt and Reuss bounds as the interconnected phase morphology of the heat treated samples of this composition are not accounted for in
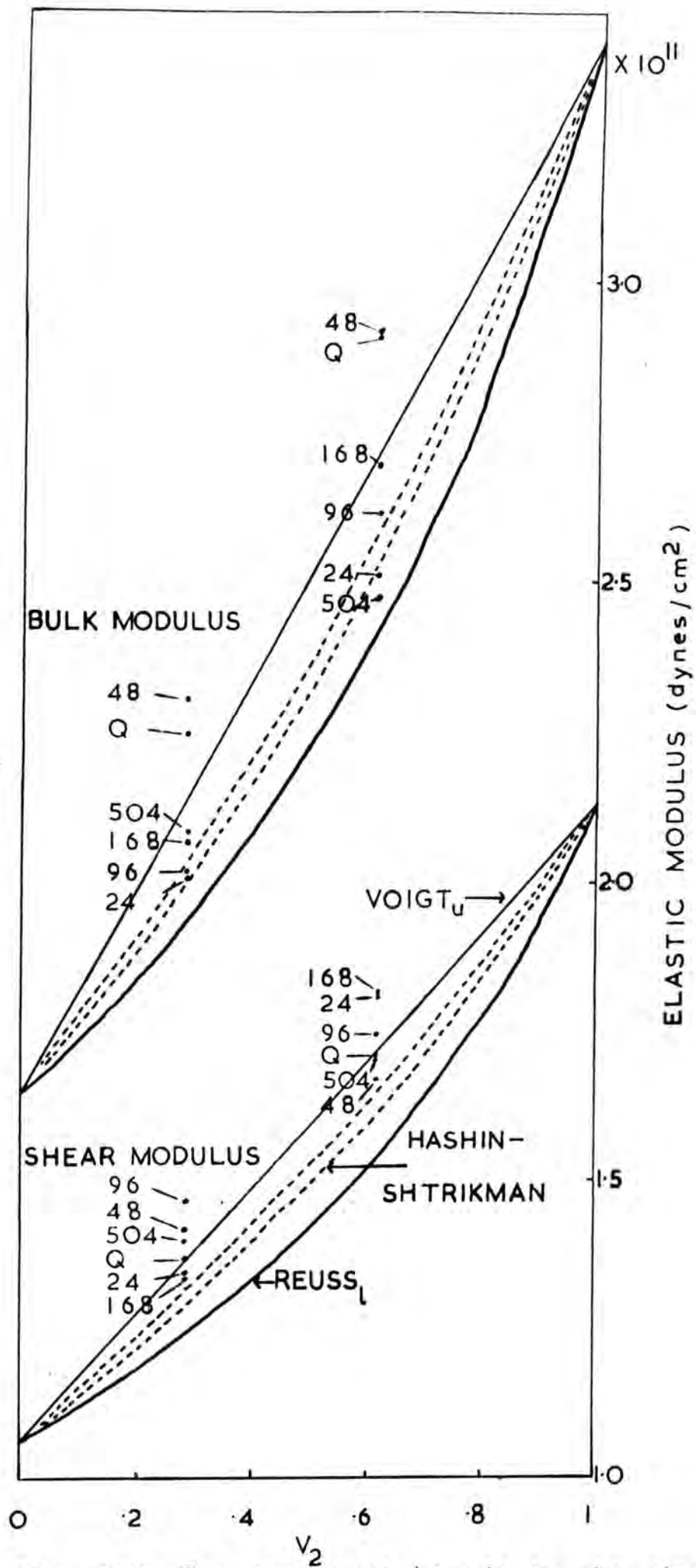
Figure 7.18 The theoretical bounds to the elastic moduli of a two-phase composite with individual phase compositions the same as glasses 7/Q and 8/Q, and moduli of glasses in batches 1 and 2.

these theoretical models. However, we do expect them to
be bounded by the narrower Hashin-Shtrikman limits which
are for arbitrary phase geometries. The shear moduli for
glasses in batch 1 also show a smaller spread in values
than the bulk moduli but both sets of elastic constants
are greater in range than expected from the Hashin-
Shtrikman bounds. These latter bounds fit the experimental
data very well over the range of immiscibility in
composition of both $Na_2O-B_2O_3$ and Na_2O-SiO_2 glasses
(Uhlmann and Shaw, 1971); for the $Na_2O-B_2O_3-SiO_2$ glasses
of this present study they do not.

We can conclude that the elastic constants of
the individual glassy phases in the phase-separated
$Na_2O-B_2O_3-SiO_2$ glasses do not remain constant throughout
the time of heat treatment of the glass at $550^{\circ}C$. The
added complication of the change in size and shapes of
the individual phases , especially those in samples of
batch 2, puts further calculations beyond the scope of
any mathematical treatment of two-phase composites yet
provided. Reasons for the change in the elastic constants
of the phases can only be speculative at the present time.
Plausibly the cause is a change in the internal structure
of the phases connected with a redistribution of the
Na^+ ions, a smaller scale process of that which dominates
the elastic constants over all the compositions of the
glasses in this work.

7.3.2   Anelastic properties

The ultrasound attenuation characteristics of glasses in batches 1 and 2, unlike the ultrasound velocities, vary in a simple way with time of heat treatment at $550^{\circ}C$. In Figure 7.19 is shown the dependence of the loss at the peak maximum on the time of heat treatment; the peak **loss rises** smoothly with treatment time. This behaviour is of great interest and has not been previously reported upon in the MHz range of acoustic attenuation.

Firstly, we must ask whether the increase in peak height is associated with phase separation processes or with the more general fictive temperature effects that have been observed for example in vitreous SiO_2 (see Chapter 3). Let us explore this second possibility more thoroughly. The temperature of heat treatment, $550^{\circ}C$, is well above the Tg point of the glasses in the quenched state, and is also above that of both phases in the interconnected structured glasses of batch 1, and above that of at least the continuous phase of glasses of batch 2, as witnessed by deformation of the glass samples upon heat treatment. Any macroscopic structural relaxation effect would have ample time to come to equilibrium within the shortest time of heat treatment and we expect a common fictive temperature amongst all the heat treated samples of $550^{\circ}C$. Although a change in fictive temperature has a large effect on the maximum acoustic loss in vitreous SiO_2, from 0.98 db/μsec at $\overline{T}=980^{\circ}C$ to
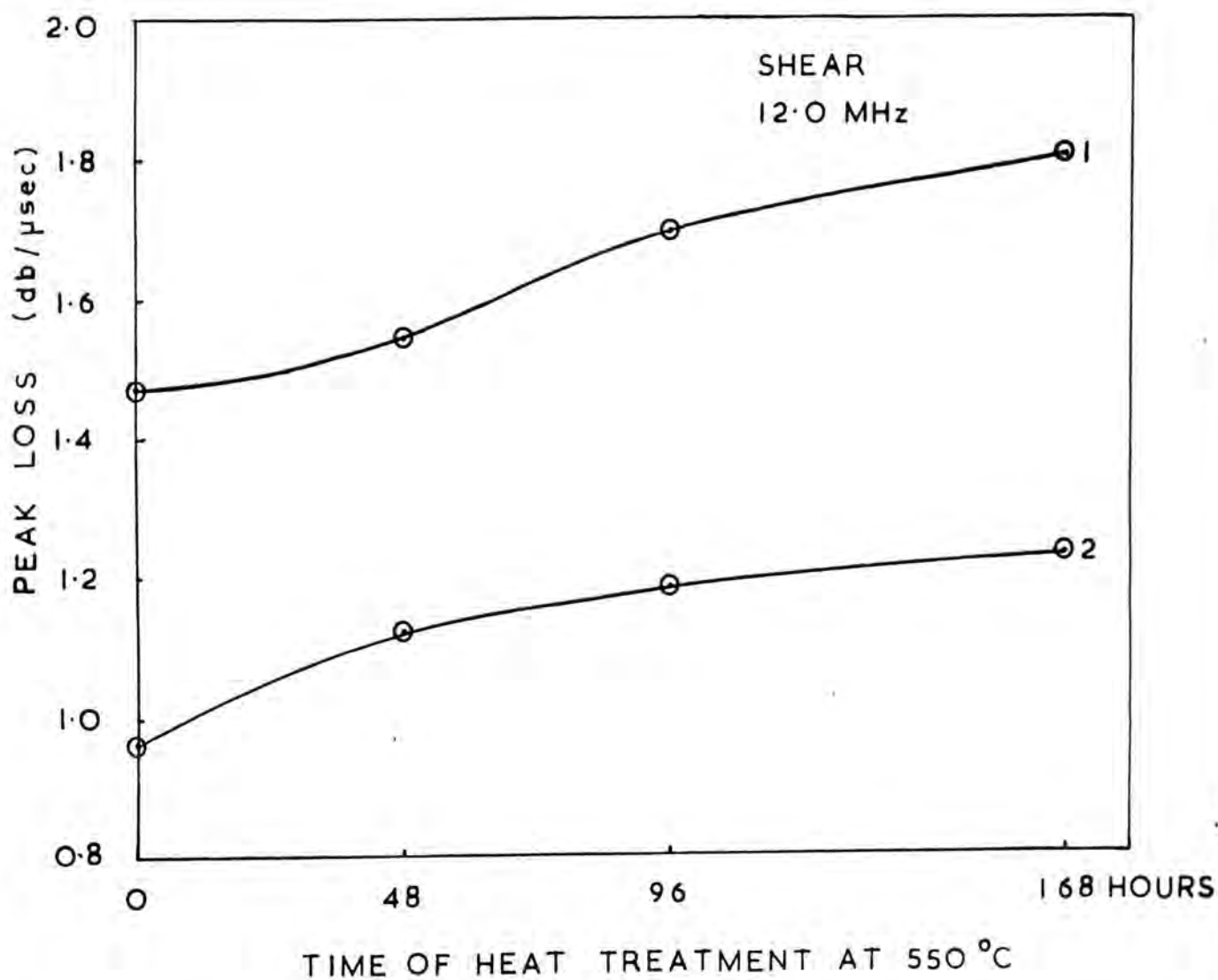
Figure 7.19 The effect of time of heat treatment at 550°C on the maximum acoustic loss in $Na_2O - B_2O_3 - SiO_2$ glasses.

0.84 db/μsec at $\bar{T}$=1400°C at 20 MHz (Krause, 1971) such a process is not active here. A second factor to mention briefly is the effect of hydroxyl ion content on acoustic loss. The OH content has only been assessed for the Na_2O-B_2O_3-SiO_2 glasses in the quenched state but it is not possible that a bulk diffusion of water either in or out of the glass samples can occur within the time of heat treatment. The pulse echo displays observed during the measurements of ultrasound velocity and attenuation did not evidence any gradient in elastic or anelastic properties as would be expected if any long range diffusional processes were operative during the heat treatment of the samples.

Therefore, the changes in acoustic attenuation in the Na_2O-B_2O_3-SiO_2 glasses of this work appear to be closely connected with the enhancement of glass-in-glass separation. We can rule out the possibility of a Rayleigh scattering contribution to the acoustic attenuation through the consideration of Section 7.2.1 It seems most likely that the changes in acoustic attenuation characteristics on heat treatment are the result of a re-organisation in the structure of the glass on a sub-microscopic level.

The variation of peak temperature with time of heat treatment is an interesting aspect of the acoustic attenuation characteristics of glasses in batches 1 and 2; the peak temperature rises with time of treatment.

This variation is closely connected with the similarity of the whole family of loss characteristics of the Na_2O-B_2O_3-SiO_2 glasses. Figure 7.20 illustrates the maximum acoustic loss and peak temperature for all the glass samples of this work. A clear correspondence is shown between these two variables, which reflects the general nature of the acoustic loss characteristics be they for glasses with different compositions or different heat treatments. The data points for glasses 5/Q and 1/168 are coincident; a comparison of the temperature dependences of acoustic loss of the two samples evidences almost identical characteristics. It therefore seems that the rise in acoustic attenuation upon heat treatment is due to an increase in the number of loss centres in the same way as this number is also affected by the total Na_2O content in the quenched glasses of different composition.

The constant volume fractions of the individual glassy phases in glasses of batches 1 and 2 have shown that the two phases have reached their terminal chemical compositions early on in the heat treatment; the initial stages of separation are thus complete after a very short time at $550^{\circ}C$. The phase morphology is undergoing the ripening processes subsequent to the initial unmixing. Therefore we do not expect that the change in acoustic attenuation is due to an overall change in chemical composition of the phases, but is the result of atomic re-arrangement within the phases. The
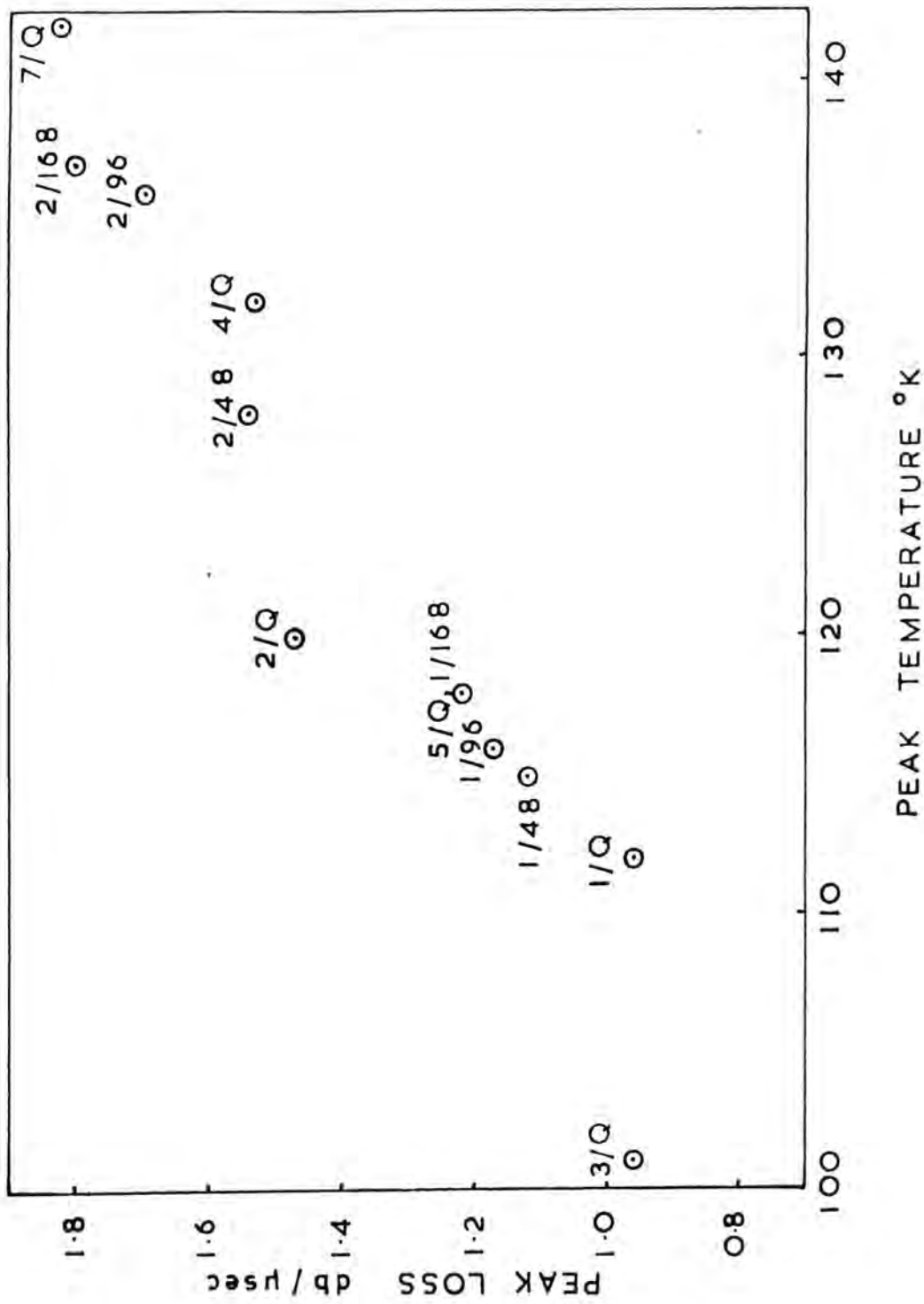
Figure 7.20 The correlation between peak loss and peak temperature in Na₂O – B₂O₃ – SiO₂ glasses.

resemblance between the effects of composition and heat
treatment on the acoustic loss in the $Na_2O-B_2O_3-SiO_2$
strongly suggests that on heat treatment there is a
migration of Na^+ ions away from B-O-B bonds in the high
B_2O_3 phase of the glass.

A comparison of the effects of phase-separation on the acoustic loss mechanism at MHz frequencies to those at lower frequencies

The only other phase-separation dependent
feature of the anelasticity of glasses is the alkali ion
diffusion peak of $Na_2O-B_2O_3-SiO_2$ materials which reduces in
magnitude upon heat treatment, as mentioned in Chapter 3.
Charles (1964) found that the corresponding peak in
dielectric loss due to Na^+ ion migration in one particular
$Na_2O-B_2O_3-SiO_2$ glass also decreases in magnitude upon
heat treatment and has shown that this behaviour is
expected if the spheroidation of the Na_2O rich phase
increases with heat treatment. However, in a later paper
(1970) Charles reports that the separation morphology
of an identical glass at an identical temperature and
time of heat treatment is of the interconnected type.
This casts doubt upon his original hypothesis about the
decrease in dielectric loss upon heat treatment. It is
also difficult to see how such a theory could explain
the observed behaviour of acoustic attenuation. It is
interesting to note however that the changes in
anelasticity at both low KHz and MHz acoustic frequencies

are connected with mechanisms involving Na^+ ions. This strongly suggests that the observed behaviour in acoustic and dielectric loss in the later stages of phase-separation in $Na_2O-B_2O_3-SiO_2$ glasses results from the repositioning of the alkali metal ions in the glass lattice.

7.4   The $4^{\circ}K$ acoustic loss peak in the $Na_2O-B_2O_3-$ SiO_2 glasses

The small acoustic loss peak that occurs at about $4^{\circ}K$ in the $Na_2O-B_2O_3-SiO_2$ glasses of this study has a counterpart in a wide variety of inorganic glass, see Chapter 3. The feature common to all the glasses in which this acoustic anomaly appears is that the cations of the glass forming lattice are tetrahedrally coordinated to either oxygen atoms as in vitreous SiO_2, GeO_2 and $Zn(PO_3)_2$, or in the case of BeF_2 to fluorine atoms. As we have seen in Section 7.2.8, the presence of the network modifier Na_2O increases the tetrahedral character of the $Na_2O-B_2O_3-SiO_2$ glasses by conversion of the boron atoms from 3 to 4 fold coordination. This, and the fact that there are also regions of the lattice of low Na_2O and high SiO_2 content where the tetrahedrally coordinated Si atoms remain relatively undisturbed establishes the tetrahedral nature of many cations in the glass lattice. Thus the coincidence of tetrahedral bonding and the $4^{\circ}K$ acoustic loss peak is also apparent in the $Na_2O-B_2O_3-SiO_2$ glasses of this study.

It has been suggested by Krause and Kurkjian (1968) that the 4°K acoustic loss peak and the positive temperature coefficient of ultrasound velocity have a common cause in certain vibrational modes which can occur in tetrahedrally coordinated structures. In the Na_2O-B_2O_3-SiO_2 glasses of this study, the temperature coefficient of velocity is strongly dependent on the total Na_2O content, evidencing suppression of the cause of this effect by the alkali oxide network modifier. However, the intensity of the 4°K acoustic loss peak does not vary appreciably between the glasses of this study with differing Na_2O content, but to conclude that Krause and Kurkjian's hypothesis is wrong would be hazardous as the source of the loss may occur in the relatively undisturbed SiO_2 rich regions of the glass lattice.

The mechanism for the loss remains so far unresolved. In the light of recent theoretical treatments and experimental observations on vibrational properties of vitreous materials we will now examine processes which could be responsible for the 4°K acoustic loss.

Phonon-phonon interactions

If low-lying modes of vibration exist in a solid, then they can have effects in the thermal conductivity and ultrasound attenuation which will be most discernable at low temperatures where higher frequency modes have been frozen out. A possible cause for the

$4^{\circ}K$ peak in the $Na_2O-B_2O_3-SiO_2$ glasses is then an acoustic phonon-low frequency thermal phonon interaction. Before any detailed calculations of the acoustic loss can be made it is necessary to know the thermal phonon relaxation time. This is obtained directly from the thermal conductivity, specific heat and mean sound velocity in the manner described in Section 3.3.1. The former two parameters have not been measured for the $Na_2O-B_2O_3-SiO_2$ glasses, but will again be approximated by those of Pyrex. Zeller and Pohl (1971) have measured the specific heat and thermal conductivity of Pyrex 7740 down to $0.1^{\circ}K$, and have shown that these parameters are very similar for all SiO_2 based glasses. At $4^{\circ}K$ their results show that

$$C_V = 4 \times 10^3 \text{ ergs/g}^{\circ}K \qquad \kappa = 1 \times 10^4 \text{ ergs/cm}^{\circ}K$$

and hence, through equation 3.15, $\tau = 4 \times 10^{-11}$ secs.

The Akhieser type phonon-phonon damping loss can now be calculated through equation 3.10. On the assumption that the Grüneisen parameter is equal to unity, the calculated loss for sampe 2/Q is 1.2×10^{-4} db/cm. and that for sample 4/Q is 1.7×10^{-4} db/cm. These values are too small to account for the experimentally observed peak intensities of 7×10^{-2} db/cm and 8×10^{-2} db/cm respectively. A similar calculation for vitreous SiO_2 using values of $C_V = 3 \times 10^{-3}$ ergs/g$^{\circ}K$ and $\kappa = 1 \times 10^4$ ergs/cm$^{\circ}K$ indicates a phonon-phonon damping contribution to the acoustic loss at $4^{\circ}K$ of 1.2×10^{-4} db/cm compared to the observed value of 8×10^{-2} db/cm. Thus it is seen that the

low temperature peak in $Na_2O-B_2O_3-SiO_2$ and SiO_2 glasses, and by inference other inorganic glasses, is not connected with an acoustic phonon-thermal phonon interaction.

An activation energy process

From the upward shift in peak temperature with increasing acoustic frequency, it is evident that the 4^OK loss is consistent with the operation of an activation energy process. Figure 7.21 shows the relaxation frequency versus reciprocal temperature plot of the data points for the 4^OK loss peak in vitreous SiO_2 taken from the results of Krause (1964). Data points for $Na_2O-B_2O_3-SiO_2$ glasses 2 and 4 are included on the plot and lie in close proximity to the solid line for vitreous SiO_2 represented by

$$f = 1.4 \times 10^{11} \exp(-60/RT)$$

which indicates, for SiO_2, an attempt frequency of 1.4×10^{11} Hz and an activation energy of 60 cal/mole for the loss mechanism. The point A is taken from the dielectric loss data for vitreous SiO_2 of Jaeger (1968); a similar small peak in the dielectric loss in vitreous SiO_2 appears below 4^OK.

A certain amount of error is introduced in the identification of the peak temperature in the $Na_2O-B_2O_3-SiO_2$ glasses due to contributions to the acoustic attenuation from the higher temperature loss mechanism and appropriate error bars are included for each data point. An attempt frequency of 10^{10} Hz to 10^{12} Hz and an
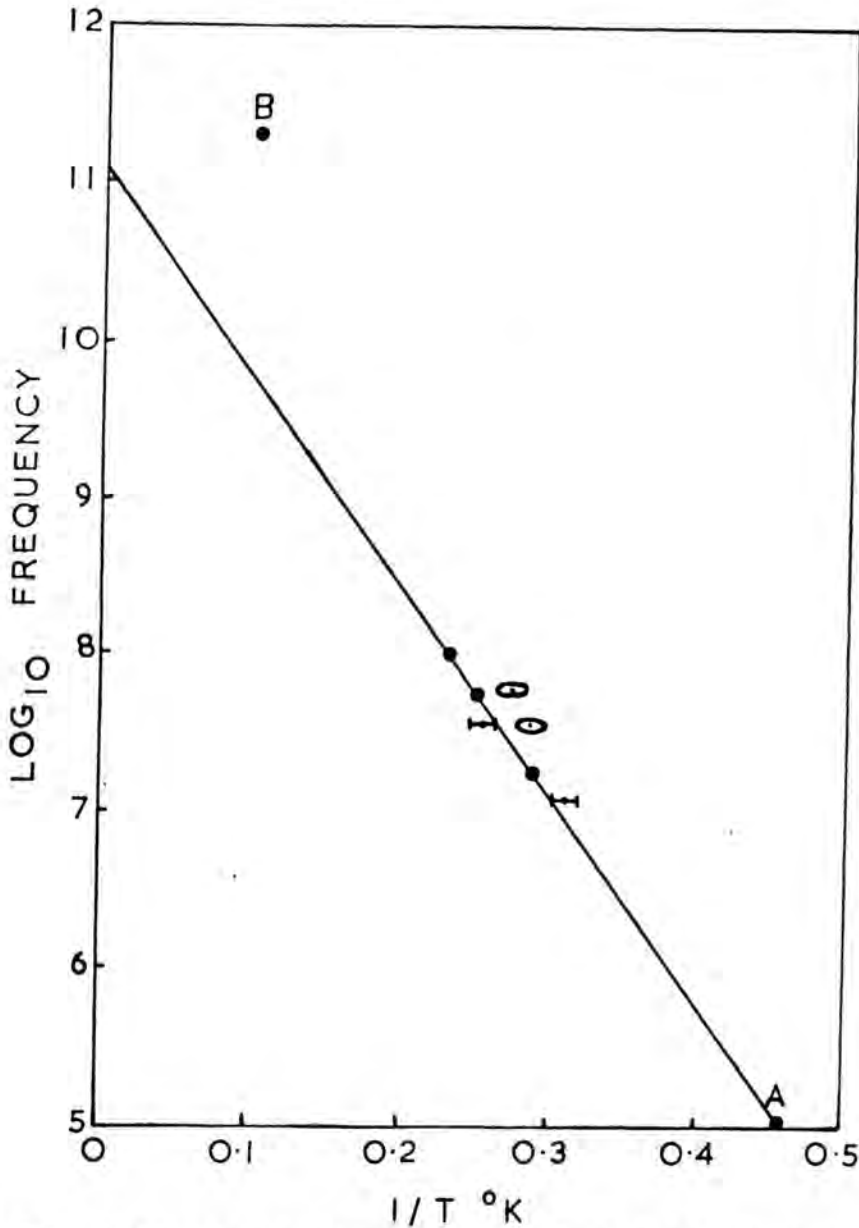
Figure 7.21   Relaxation frequency plot for the low temperature
loss peak in glasses 2/Q(⊙) and 4/Q(↦). The solid line
is for vitreous SiO₂ ; point A is from dielectric loss data
and the point B represents the knee in thermal conductivity.

activation energy of 60 ± 15 cal/mole is indicated for the $Na_2O-B_2O_3-SiO_2$ glasses.

Assuming that an activation energy process is responsible for the $4^{\circ}K$ acoustic loss peak, it is difficult to conject on the member responsible. The low attempt frequency suggests that if it is a structural relaxation then the relaxing unit is of large mass or is constrained by weak forces. This unit must also be polarizable or it would not affect the dielectric loss. The low activation energy for the process indicates a very small barrier to the motion of the member and precludes any translational or rotational movement of the active member.

An interesting point arises here on inspection of the thermal conductivity data for vitreous SiO_2 and Pyrex from the results of Zeller and Pohl (1971). There is quite a distinctive 'knee' in the temperature dependence at about $10^{\circ}K$ which is the result of an anomaly in the thermal phonon mean free path rather than in the specific heat. In the dominant phonon approximation, the frequency of the thermal phonons at $10^{\circ}K$ is about 2×10^{11} Hz; in practice this value is the upper limit to the phonon frequency spectrum at this temperature. A point B (see Figure 7.21) corresponding to this frequency and temperature lies fairly near the relaxation plot of Krause for the $4^{\circ}K$ acoustic loss peak in vitreous SiO_2, and also near that for the $Na_2O-B_2O_3-SiO_2$ glasses of this study. It seems a possibility that the acoustic and thermal phonon scattering has a common cause.

Zeller and Pohl have found that at 10^OK the phonon mean free path is proportional to the inverse of the fourth power of the phonon frequency, which indicates that a Rayleigh scattering process may be involved. They suggest that this scattering in a glassy structure is similar to isotopic scattering in a crystal; the vitreous material is approximated in their treatment to a crystal where every atom is displaced from its lattice site. The mean free path of a thermal phonon at 4^OK is 5×10^{-5} cm. Thus with a dependence of mean free path proportional to ω^{-4} that for an acoustic phonon at frequency 12 MHz will be of the order of 10^{13} cms which would result in an attenuation due to this type of scattering mechanism of 10^{-12} db/μsec. Clearly such a mechanism cannot account for the observed acoustic loss peak. Furthermore, it is difficult to envisage how a peak in acoustic loss rather than a constant contribution to the observed attenuation could result from such a process.

To sum up, the knee in the thermal conductivity and the low temperature acoustic loss peak in vitreous Na_2O-B_2O_3-SiO_2 and SiO_2 either have a common cause which is not a Rayleigh scattering process, or they are the result of separate mechanisms.

Phonon assisted tunnelling

More recently, Anderson Halperin and Varma (1971) have shown from general considerations of the

glassy state that at low temperatures there should be a linear temperature contribution to the specific heat and thermal conductivity which is proportional to T^2 and ω^{-1}, and of interest here, an ultrasonic attenuation which increases as T^{-1} and ω^2. Their model is based on the probability of phonon assisted tunnelling of atoms or small groups of atoms between sites of equivalent or nearly equivalent potential energy which are separated by a small energy barrier. The results of Zeller and Pohl agree with this predicted behaviour in specific heat and thermal conductivity in a number of vitreous materials including SiO_2 based glasses, but only in the temperature range $0.1^{\circ}K$ to $1^{\circ}K$. At $4^{\circ}K$, where the small acoustic loss peak is observed in Na_2O-B_2O_3-SiO_2 and SiO_2, the phonon mean free path varies as ω^{-4} and T^{-4}; thus the temperature range of the acoustic experiments is outside that where the phonon-assisted tunnelling mechanism is operating. In addition it is also difficult to foresee a situation where an acoustic loss which varies as T^{-1} would cause a peak in attenuation rather than a steady parabolic rise.

To conclude, the only mechanism presently available to account for the acoustic loss peak in the liquid helium temperature range for Na_2O-B_2O_3-SiO_2 and other inorganic glasses is a thermally activated relaxation mechanism. However, although such a model can be fitted to the ultrasonic data, this cannot be

held as proof of its validity. Further detailed studies of ultrasonic loss in both tetrahedrally and non-tetrahedrally coordinated materials will be needed to help identify the responsible mechanism. Such investigations in the liquid helium temperature range and also those at lower temperatures still will provide valuable information on the character of the glassy state.

CHAPTER   8

S U M M A R Y

Summary

The propagation characteristics of both longitudinal and shear ultrasound waves have been studied in glasses in the $Na_2O-B_2O_3-SiO_2$ system. The temperature dependence of ultrasound wave velocity and attenuation between $1.3^\circ K$ and $400^\circ K$ is dominated by an intense and broad acoustic loss peak; in this respect the acoustic properties of $Na_2O-B_2O_3-SiO_2$ glasses are qualitatively similar to those in many other vitreous inorganic materials such as SiO_2, GeO_2, and B_2O_3. It has been shown that a thermally activated structural relaxation involving the transverse motion of an oxygen atom between two sites of equal or nearly equal energy in a non-linear cation-oxygen-cation bond is the most likely mechanism for the acoustic loss in vitreous SiO_2 $Na_2O-B_2O_3-SiO_2$, and other inorganic glasses. A different mechanism involving an acoustic phonon-thermal phonon interaction has proved unacceptable as an explanation for the observed loss. The intensity of the acoustic attenuation peak and the mean activation energy for the relaxation process are much larger in the $Na_2O-B_2O_3-SiO_2$ than in the single component SiO_2 and B_2O_3 glasses; in the ternary materials there are larger numbers of non-linear bridging oxygen bonds and these bonds tend to be distorted on average through larger angles.

A recurrent theme that has emerged from the results of this work is the strong dependence of the

ultrasound propagation characteristics on the total Na_2O network modifier content of the glasses. The intensity of the large acoustic loss peak and the unusual positive fractional temperature coefficient of ultrasound velocity decrease, and the ultrasound velocity and coefficient of thermal expansion increase as the Na_2O content of the glass is raised. The decrease in maximum acoustic loss and the increase in stiffness of the structure can be accounted for by a local structural model where two adjacent boron atoms linked by a common oxygen atom are converted from 3 to 4 fold coordination. Plausibly the explanation for the observed decrease in the positive temperature coefficient of ultrasound velocity is elimination by the alkali oxide molecules of the low frequency modes of vibration which have been proposed to be responsible for many of the anomalous properties of inorganic glasses. That the Na_2O network modifier plays a vital role in the structure forming processes in the $Na_2O-B_2O_3-SiO_2$ glasses is further demonstrated by the dependence of the phase-separation characteristics upon the amount of alkali oxide present. Results from this study have provided valuable information on the function of Na_2O in determining the acoustical and vibrational properties of the glasses.

In the general field of glass physics it has been found difficult to expose properties which are discriminating enough to provide detailed information about structural processes involved in phase-separation

phenomena. As a technique for the investigation of glass-in-glass phase-separation, ultrasonic studies have proved sensitive to changes taking place in the individual phases of Na_2O-B_2O_3-SiO_2 glasses after long periods of heat treatment. These changes are connected most likely with the redistribution of the Na^+ ions within the separate phases. In the Na_2O-B_2O_3-SiO_2 glasses of this study, which lie in or near the region where metastable immiscibility is observed, it has not been possible to state that any sample is not phase-separated as all samples have proved heterogeneous by the critical inspection of the electron microscope. However, as has been discussed in Chapter 4, the term 'phase-separated' may well be a relative rather than an absolute term especially for glasses that lie very near in composition to the extremities to the immiscibility dome; the ultra-sound propagation characteristics of both optically clear and blue-white large-scale separated Na_2O-B_2O_3-SiO_2 glasses have been systematically studied in the course of this work.

In all the Na_2O-B_2O_3-SiO_2 glasses whose acoustic loss characteristics have been measured in the liquid helium range of temperatures a small attenuation peak has been observed at about 4^OK. This feature is common to the acoustic properties of many tetrahedrally coordinated inorganic glasses. The frequency dependence of the loss peak is consistent with an activation energy process of energy 60 ± 15 cal/mole and attempt frequency

of 10^{10} to 10^{12} Hz; further studies of this acoustic anomaly in other glasses are needed to clarify the mechanism responsible. Indeed, more general investigations of ultrasound propagation characteristics at very low temperatures, perhaps as low as 0.1°K, will provide much information about the vibrational properties of the glassy state.

This present study, as an investigation into the ability of ultrasonic techniques to provide information on the structure of multicomponent glasses, has served to identify the variables of interest in the temperature and acoustic frequency ranges in question. It is anticipated that further similar ultrasonic examinations of the elasticity and anelasticity of both $Na_2O\text{-}B_2O_3\text{-}SiO_2$ and other glasses will be undertaken, especially with reference to the significant and most important effects of advancing glass-in-glass separation.

During the final stages of preparation of this thesis an important paper was published entitled 'Boron coordination in sodium borosilicate glasses,' (Milberg, M.E., O'Keefe, J.G., Verhelst, R.A., Hooper, H.O., (1972) Phys. Chem. Glasses, 13, 79) in which results of N.M.R. studies of boron-oxygen coordination were reported. The major conclusions were as follows:

1. Na_2O-B_2O_3-SiO_2 glasses with a Na_2O:B_2O_3 ratio of less than 0.5 behave with regard to boron coordination as if they were Na_2O-B_2O_3 glasses diluted by SiO_2. They contain essentially no non-bridging oxygen ions and the fraction of the boron atoms in 4 coordination is equal to the ratio of Na_2O to B_2O_3.

2. Na_2O-B_2O_3-SiO_2 glasses with a Na_2O:B_2O_3 ratio greater than 0.5 have a fraction of 4 coordinated boron atoms less than this ratio, but still act as to show a preference of the Na_2O molecules for the B_2O_3 species.

The conclusions of this present study drawn from the compositional dependences of density and ultrasound velocity have emphasised the same basic findings of the N.M.R. study, that the network modifying Na_2O species has affinity for areas of the glass network locally rich in B_2O_3.

Appendix I

This appendix contains a copy of the computer programme used to calculate the distribution of activation energies in the mechanism responsible for the large acoustic loss peak in the Na_2O-B_2O_3-SiO_2 glasses. Further details of this least mean squares minimzation procedure can be found in Chapter 7. The parameters read into the programme are summarized in the following table:

Symbol	Parameter	Value
N	Number of unknown Δ_i	40
WW	Acoustic frequency (Hz)	12×10^6
SMALL	Preset value of SUMSQ	0.005
CYCLE	Cycles of minimization	3
MAX	Upper limit of Δ_i	1
MIN	Lower limit of Δ_i	10^{-10}
S	Initially set values of Δ_i	10^{-2}
STEP	Initial steps of Δ_i	10^{-3}
CO	Measured values of internal friction	variable
IJ	Upper temperature limit of measurements ($^{\circ}K$)	400
KJ	Steps in Hi (cal/mole)	300

```
      DIMENSION S(40),STEP(4 ),SOL(40),CO(40),Q(40),COEFF(1600),WI(1600)
     7,SO(1600),WE(40)
      DOUBLE PRECISION SMALL,SUM(2),Z(40)
      INTEGER CYCLE,H(40),C,U
      REAL MAX(40),MIN(40)
    1 FORMAT(10E8.0)
    2 FORMAT(25X,'INITIAL SOLUTIONS FITTED'/ 25X,'MEASURED COEFF'/(4(10E
     710.3/)))
    3 FORMAT(25X,'FINAL SOLUTIONS'/ (4(10E10.3/)))
    4 FORMAT(25X,'RATIOS'/(4(10E10.3/)))
    5 FORMAT(25X,'SUM'/ (2F30.8))
    6 FORMAT(25X,'MEASURED COEFF'/ (4(10E10.3/)))
    8 FORMAT(1E11.5)
    9 FORMAT(1E10.3)
   10 FORMAT(25X,'CALCULATED COEFF'/ (4(10D10.3/)))
   33 FORMAT(25X,'STEPS'/(4(10E10.3/)))
   59 FORMAT(////25X,'SOLUTIONS',/(4(10E10.3/)))
  101 FORMAT(I3)
  102 FORMAT(F10.0)
  103 FORMAT(I2)
  104 FORMAT(E12.5)
  105 FORMAT(25X,'FREQUENCY=',E12.5)
  302 FORMAT(25X,'MAX',/(4(10E10.3/)))
  303 FORMAT(25X,'MIN',/(4(10E10.3/)))
  304 FORMAT(//'SMALL=',F10.7///)
      READ(5,101) N
      READ(5,104) WW
      READ(5,102) SMALL
      READ(5,103) CYCLE
      READ(5,1) (MAX(I),I=1,N)
      READ(5,1) (MIN(I),I=1,N)
      READ(5,8) (S(I),I=1,N)
      READ(5,1) (STEP(I),I=1,N)
      READ(5,9) (CO(I),I=1,N)
      DO 12 I=1,N
   12 CO(I)=CO(I)*1.0E6/(8.686*3.142*WW)
      WRITE(6,105) WW
      WRITE(6,302) (MAX(I),I=1,N)
      WRITE(6,303) (MIN(I),I=1,N)
      WRITE(6,33) (STEP(I),I=1,N)
      WRITE(6,2) (CO(I),I=1,N)
      WRITE(6,59) (S(I),I=1,N)
      WRITE(6,304) SMALL
   97 CALL CALC(SO,N,COEFF,WI,SCAL,WW)
      DO 7 I=1,N
      SOL(I)=S(I)
      H(I)=0
    7 CONTINUE
      SUM(1)=0
      SUM(2)=0
      CALL DEV(S,Z,SO,N)
      WRITE(6,2) (CO(I),I=1,N)
      WRITE(6,10) (Z(I),I=1,N)
      WRITE(6,59) (SOL(I),I=1,N)
      DO 17 K=1,N
```

```
       Q(K)=(Z(K)/CO(K))
       WE(K)=(Q(K)-1)
       SUM(1)=SUM(1)+WE(K)**2
   17 CONTINUE
       WRITE(6,4) (Q(I),I=1,N)
       WRITE(6,5) (SUM(I),I=1,2)
       DO 16 C=1,CYCLE
       DO 19 U=1,100
       DO 13 I=1,N
       SUM(2)=0
       S(I)=S(I)+STEP(I)
       IF(S(I).GT.MAX(I)) GO TO 15
       IF(S(I).LT.MIN(I)) GO TO 15
       CALL DEV(S,Z,SO,N)
       DO 18 K=1,N
       Q(K)=(Z(K)/CO(K))
       WE(K)=(Q(K)-1)
       SUM(2)=SUM(2)+WE(K)**2
   18 CONTINUE
       IF(SUM(1)-SUM(2))15,14,14
   15 IF(H(I)-10)21,21,22
   21 STEP(I)=-STEP(I)
       S(I)=SOL(I)
       H(I)=H(I)+1
       GO TO 13
   22 STEP(I)=-0.5*STEP(I)
       S(I)=SOL(I)
       H(I)=1
       GO TO 13
   14 IF(SUM(2)-SMALL)99,99,20
   20 SOL(I)=S(I)
       SUM(1)=SUM(2)
   13 CONTINUE
   19 CONTINUE
       WRITE(6,59) (SOL(I),I=1,N)
       WRITE(6,4) (Q(I),I=1,N)
       WRITE(6,33) (STEP(I),I=1,N)
       WRITE(6,5) (SUM(I),I=1,2)
   16 CONTINUE
   99 DO 25 I=1,N
       S(I)=SOL(I)
   25 CONTINUE
       WRITE(6,3) (SOL(I),I=1,N)
       WRITE(6,6) (CO(I),I=1,N)
       WRITE(6,10) (Z(I),I=1,N)
       WRITE(6,4) (Q(I),I=1,N)
       WRITE(6,5) (SUM(I),I=1,2)
       CALL DISP(N,COEFF,SCAL,WI,WW,SOL)
       DO 656 I=1,N
       A=ALOG(SOL(I))
       B=ALOG10(SOL(I))
  656 WRITE(6,655) SOL(I),A,B
  655 FORMAT(E15.3,2F15.5)
   98 STOP
       END
```

```
      SUBROUTINE CALC(A,N,COEFF,WI,SCAL,W)
C     THIS SUBROUTINE CALCULATES THE 1600 TERMS OF TYPE
C     WT/(1+(WT)**2))
      DIMENSION COEFF(1600),WI(1600),A(1600),II(1600)
  151 FORMAT(I4)
  161 FORMAT(25X,'TEMPERATURE 0-',I3)
  171 FORMAT(I5)
      READ(5,151) IJ
      WRITE(6,161) IJ
      READ(5,171) KJ
      WRITE(6,181) KJ
  181 FORMAT(25X,'ACTIVATION ENERGIES 0-',I5)
      NN=N*N
      SCAL=1.0
      ZZZ=1.0E-30
      R=1.987
      Z=1.0E-30
      C=1.0E13
      M=0
      KK=KJ/N
      JJ=IJ/N
      DO 1 I=KK,KJ,KK
      DO 1 J=JJ,IJ,JJ
      M=M+1
      T=J
      H=I
      WI(M)=C*EXP(-H/(R*T))
      IF(WI(M)-1.0)3,4,4
    3 COEFF(M)=WI(M)/W
      GO TO 5
    4 COEFF(M)=(W/WI(M))/(1+((W/WI(M))**2))
    5 SMALL=COEFF(M)/Z
      IF(SMALL-1.0)35,1,1
   35 COEFF(M)=ZZZ
    1 A(M)=COEFF(M)
      RETURN
      END



      SUBROUTINE DEV(A,Z,SO,N)
C     THIS SUBROUTINE CALCULATES THE INTERNAL FRICTION FROM THE
C     INCREMENTED OR DECREMENTED VALUES OF THE RELAXATION STRENGTHS
      DIMENSION A(40),SO(1600)
      DOUBLE PRECISION Z(40)
      DO 1 K=1,N
      Z(K)=0.0
      DO 2 I=1,N
      L=K+(I-1)*N
    2 Z(K)=Z(K)+SO(L)*A(I)
    1 CONTINUE
      RETURN
      END
```

```
      SUBROUTINE DISP(N,COEFF,SCAL,WI,W,X)
C     THIS SUBROUTINE CALCULATES THE EXPECTED RELAXATION IN ELASTIC
C     MODULUS FROM THE DISTRIBUTION IN ACTIVATION ENERGIES
  118 FORMAT(I3,D15.5)
  119 FORMAT(//' TABLE OF DU/U')
  191 FORMAT(//' CHECK TABLE')
  201 FORMAT('Y(',I2,')=',D15.5)
      DIMENSION X(40),WI(1600),COEFF(1600)
      DOUBLE PRECISION DUU(40),Y(40)
      NN=N*N
      WRITE(6,191)
      DO 31 K=1,N
      Y(K)=0.0
      DO 32 I=1,N
      L=K+(I-1)*N
   32 Y(K)=Y(K)+X(I)*COEFF(L)
      WRITE(6,201) K,Y(K)
   31 CONTINUE
      ZZ=1.0E-15
      DO 98 I=1,NN
      SMALL=WI(I)/ZZ
      IF(SMALL-1.0) 97,98,98
   97 WI(I)=ZZ
   98 CONTINUE
      WRITE(6,119)
      DO 13 K=1,N
      DUU(K)=0.0
      DO 14 I=1,N
      L=K+(I-1)*N
   14 DUU(K)=DUU(K)+X(I)*(1/(1+((W/WI(L))**2)))
      WRITE(6,118) K,DUU(K)
   13 CONTINUE
      RETURN
      END
```

Appendix II

For the purpose of further identification of the $Na_2O-B_2O_3-SiO_2$ glasses of this work, a list is included here of the glass code numbers as used in this thesis and the corresponding numbers used at the Advanced Research Unit of James A. Jobling, Brancepeth Castle, Co. Durham. These latter identifiers take the form of the batch or composition number followed by the melt number of the actual samples studied.

Present Code No.	A.R.U. Code No.
1	978/2
2	979/2
3	1217/2
4	1218/1
5	1363/1
6	1373/1
7	1374/1
8	1389/1
9	1394/1
10	626/2

References

Adams, R.V., (1961) Phys. Chem. Glasses, 2, 39

Akhieser, A., (1939) J. Phys. U.S.S.R., 1, 277

Anderson, O.L., Bömmel, H.E., (1955) J. Amer. Ceram. Soc. 38, 125

Anderson, O.L., (1959) J. Phys. Chem. Solids, 12, 41

Anderson, O.L., Dienes, G.J., (1960) "Non-crystalline Solids," Ed. Frechette (John Wiley, New York), 449

Anderson, O.L., (1965) "Physics of Non-crystalline Solids," (North-Holland, Amsterdam), 179

Anderson, P.W., Halperin, B.I., Varma, C.M., (1972) Phil. Mag. 25, 1

Antoniou, A.A., Morrison, J.A., (1965) J. Appl. Phys. 36, 1873

Bell, R.J., Dean, P., (1967) National Physical Laboratory Report Ma. 62

Bell, R.J., Dean, P., (1968) Phys. Chem. Glasses, 9, 125

Bell, R.J., Bird, N.F., Dean, P., (1968) Proc. Roy. Soc. C1, 299

Bell, R.J., Dean, P., (1970) New Scientist, 15, 104

Blackmann, M., (1955) Handbuch der Physik, 7, 325

Bömmel, H.E., Dransfeld, K., (1960) Phys. Rev. 123, 1553

Bray, P.J., (1967) Phys. Chem. Glasses, 8, 125

Bray, P.J., O'Keefe, J.G., (1963) Phys. Chem Glasses, 4, 37

Biscoe, J., Warren, B.E., (1938) J. Amer. Ceram. Soc. 21, 287

Cahn, J.W., (1961) Acta. Met. 9, 795

Cahn, J.W., (1965) J. Chem. Phys. 42, 93

Charles, R.J., (1964) J. Amer. Ceram. Soc. 47, 559

Charles, R.J., Cahn, J.W., (1965) Phys. Chem. Glasses,
6, 181

Charles, R.J., Turkalo, A.M., (1969) G.E.C. Internal
Report No. 69-C-212

Charles, R.J., Haller, W., Blackburn, D.H., Wagstaff, F.E.,
(1970) J. Amer. Ceram. Soc. 53, 34

Clark, A.E., Strakna, R.E., (1962) Phys. Chem. Glasses,
3, 121

Craig, R.S., Massena, C.W., Mallya, R.M., (1965) J. Appl.
Phys. 36, 108

Day, D.E., Rindone, G.E., (1961) J. Amer. Ceram. Soc.
44, 161

Dean, P., (1964) Phys. Chem. Solids, Suppl. 1 , 561

Fine, M.E., (1954) J. Appl. Phys. 24, 81

Flubacher, P., Leadbetter, A.J., Morrison, J.A.,
Stoicheff, B.P., (1960) J. Phys. Chem. Solids, 12, 53

Franz, H., (1966) J. Amer. Ceram. Soc. 49, 473

Fraser, D.B., (1968) J. Appl. Phys. 39, 5868

Galakhov, F. Ya., Alekseeva, O.S., (1969) Liqvatsionne
Yavleniya v Steklakh, p.64

Gibbs, J.W., (1948) "Collected Works" (Yale University
Press, New Haven, Conneticut) p.105

Gladkov, A.V., Tarasov, V.V., (1960) "Structure of
Glass" (Consultants Bureau, New York)

Haller, W., (1965) J. Chem. Phys. 42, 686

Hashin, Z., Shtrikman, S., (1963) J. Mech. Phys. Solids,

    11, 127

Jaeger, R.E., (1968) J. Amer. Ceram. Soc. 51, 57

Jones, C.K., Klemens, P.G., Rayne, J.A., (1964) Phys.

    Lett. 8, 31

Krause, J.T., (1964) J. Amer. Ceram. Soc. 47, 103

Krause, J.T., Kurkjian, C.R., (1966a) J. Amer. Ceram.

    Soc. 49, 134

Krause, J.T., Kurkjian, C.R. (1966b) J. Amer. Ceram.

    Soc. 49, 171

Krause, J.T., Kurkjian, C.R., (1968) J. Amer. Ceram. Soc.

    51, 226

Krause, J.T., (1971) J. Appl. Phys. 42, 3035

Kuhne, K., Skatulla, W., (1959) Silikat. Tech. 10, 105

Lazarus, D., (1949) Phys. Rev. 76, 545

Leadbetter, A.J., Morrison, J., (1963) Phys. Chem. Glasses,

    4, 188

Leadbetter, A.J., (1968) Phys. Chem. Glasses, 9, 1

Leadbetter, A.J., Wycherley, K.F., (1971) Phys. Chem.

    Glasses, 12, 41

Lippincott, E.R., Valkenburg, A.V., Weir, C.E.,

    Bunting, E.N., (1958) J. Res. N.B.S. 61, 61

Lücke, K., (1956) J. Appl. Phys. 27, 1433

Marx, J.W., Sivertsen, J.M., (1953) J. Appl. Phys.

    24, 81

Mason, W.P., (1958) "Physical Acoustics and the Properties

    of Solids," (D. Van Nostrand, New York)

Mazurin, O.V., (1968) Phys. Chem. Glasses, 11, 89

Mazurin, O.V., Streltsina, M.V., Totesh, A.S., (1969)

   Phys. Chem. Glasses, 10, 63

McSkimin, H.J., (1953) J. Appl. Phys. 24, 988

McSkimin, H.J., (1961) J. Acoust. Soc. Am. 33, 12

Meyer, O., (1874) J. rein. v. angew. Math. LXXVIII, 130

Murthy, M.K., Aguayo, J., (1964) J. Amer. Ceram. Soc.

   47, 444

Nemec, L., Götz, J., (1969) J. Amer. Ceram. Soc. 53, 526

Niblett, D.H., (1966) "Physical Acoustics," Ed. Mason, W.P.,

   (Academic Press, New York) p.116

Nye, J.F., (1957) "Physical Properties of Crystals,"

   (Clarendon Press, Oxford)

Papadakis, E.P., (1967) J. Acoust. Soc. Am. 42, 1045

Pine, A.S., (1969) Phys. Rev. 185, 1187

Porai-Koshits, E.A., Andreyev, N.S., (1958) Nature,

   182, 335

Redwine, R.H., Field, M.B., (1968) J. Mat. Sci. 3, 380

Redwine, R.H., Field, M.B., (1969) J. Mat. Sci. 4, 713

Richter, H., Breitlung, G., Herre, F., (1953) Naturnissenschaften,

   40, 621

Rindone, G.E., Ryder, R.J., (1957) Glass Industry, Jan. 29

Rockett, T.J., Foster, W.R., Ferguson, R.G., (1965)

   J. Amer. Ceram. Soc. 48, 329

Scholes, S., Wilkinson, F.C.F., (1970) Disc. Faraday Soc.

   50, 175

Seward, T.P., Uhlmann, D.R., Turnbull, D., (1968) J. Amer.

   Ceram. Soc. 15, 634

Silver, A.H., Bray, P.J., (1958) J. Chem. Phys. 29, 984

Simmons, J.H., Macedo, P.B., Haller, W., (1968) Phys.
Chem. Glasses, 9, 156

Simmons, J.H., Macedo, O.B., Napolitano, A., (1971)
J. Chem. Phys. 53, 1165

Simmons, J.H., Macedo, P.B., (1971) J. Res. N.B.S.
a 75A, 175

Simmons, J.H., Macedo, P.B., (1971) J. Chem. Phys. 54, 1325

Skatulla, W., Vogel, W., Hessel, H., (1958) Silikat
Tech. 9, 51

Srinivasan, G.R., Tweer, I., Macedo, P.B., Sarkar, A.,
(1971) J. Non-Cryst. Solids, 6, 221

Stevels, J.H., Glastechnische Berichte, (1953) 26, 24

Strakna, R.E., (1961) Phys. Rev. 123, 2020

Strakna, R.E., Savage, H.T., (1964) J. Appl. Phys. 35, 1445

Taylor, S.W., Day, D.E., (1970) Phys. Chem. Glasses, 11, 89

Tran, T.L., (1965) Verres Refract. 19, 416

Truell, R., Oates, W., (1963) J. Acoust. Soc. Am. 35, 1382

Truell, R., Elbaum, C., Chick, B.B., (1969) "Ultrasonic
Methods in Solid State Physics" (Academic Press,
New York)

Uhlmann, D.R., Shaw, R.R., (1920) J. Non-Cryt. Solids,
1, 474

Uhlmann, D.R., Shaw, R.R., (1971) J. Non-Cryst. Solids,
5, 237

Urnes, S., (1967) Phys. Chem. Glasses, 8, 125

Vogel, W., Gerth, K., (1962) "Symposium on Nucleation

and Crystallization in Glasses and Melts," (Amer.

Ceram. Soc. Columbus, Ohio) p.21

Vogel, W., (1965) "Struktur und Kristallisation der

Gläser," (V.E.B. Deutscher Verlag für Grundstoffundustrie,

Leipzig), p.73

Voigt, W., (1892) Ann. d. Phys., XLVII, 671

White, G.K., (1959) "Experimental Techniques in Low-temperature
                        Physics" (Clarendon Press, Oxford)
White, G.K., (1964) Cryogenics, 4, 2

White, G.K., Birch, J.A., (1965) Phys. Chem. Glasses,

6, 85

Woodruff, T.O., Ehrenreich, H., (1961) Phys. Rev. 123, 1553

Zachariasen, W.H., (1932) J. Am. Chem. Soc. 54, 3841

Zarzycki, J., Naudin, F., (1967) Phys. Chem. Glasses, 8, 11

Zener, C., (1947) "Elasticity and Anelasticity of Metals,"

(University of Chicago Press, Chicago)

Robinson, H.A., (1969) J. Amer. Ceram. Soc. 52, 392

Krüger, J., (1972) Phys. Chem. Glasses, 13, 9